

University of Alberta

**Validation of Floc Size Measurements Made with Flow Particle Image
Analyzer (FPIA)**

by

Marzieh Saadat

A thesis submitted to the Faculty of Graduate Studies and Research
in partial fulfillment of the requirements for the degree of

Master of Science

in

Chemical Engineering

Department of Chemical and Materials Engineering

©Marzieh Saadat

Spring 2014

Edmonton, Alberta

Permission is hereby granted to the University of Alberta Libraries to reproduce single copies of this thesis and to lend or sell such copies for private, scholarly or scientific research purposes only. Where the thesis is converted to, or otherwise made available in digital form, the University of Alberta will advise potential users of the thesis of these terms.

The author reserves all other publication and other rights in association with the copyright in the thesis and, except as herein before provided, neither the thesis nor any substantial portion thereof may be printed or otherwise reproduced in any material form whatsoever without the author's prior written permission.

Abstract

Clay flocs exist in different streams of the oil sands extraction process and in tailings treatment. The clay fraction in these streams has a significant effect on design and operation of slurry pipelines, flotation efficiency, sludging in the separation vessel, froth treatment and tailings behavior. The size of clay flocs plays an important role in determining the behavior of colloidal suspensions. The Flow Particle Image Analyzer (FPIA) is an image analysis based instrument used for particle size measurement. In this study, floc size measurements are made for suspensions of kaolinite in water. Size analysis results are additionally obtained using the Malvern Mastersizer and microscopy. The results of this study indicate that the Mastersizer is not an appropriate option for floc size measurement. However, the microscopy results were in good agreement with the FPIA measurements.

Acknowledgements

I would like to express my endless gratitude to my family. If it was not for their support, love and inspiration, I would have stopped long ago.

My deepest gratitude and appreciation goes to my supervisor, Dr. Sean Sanders, for his insight, support and guidance throughout my project.

Next, I would like to acknowledge my colleagues in Pipeline Transport Processes research group for their technical support and kind words. Special thanks to Terry Runyon for her invaluable help throughout the process.

Thanks to NSERC Industrial Research Chair in Pipeline Transport Processes for providing financial support. I would also like to express my appreciation to Dr. Zhenghe Xu and Dr. Suzanne Kresta for providing access to their laboratory facilities. I would like to thank Lily Laser for her endless help.

My gratitude is also given to my friends who were like family to me far from home for their encouragement and help.

Table of Contents

1	Problem Statement and Objectives	1
2	Background and Literature Review	12
2.1	Particle Size Analysis Using the FPIA.....	12
2.1.1	How does the FPIA Work?	12
2.1.2	Applications Involving the FPIA Described in the Literature	13
2.2	Complications in Measuring Floc Sizes.....	15
2.2.1	Flocculating Particles and Applications.....	15
2.2.2	Why Measure Floc Size (Instead of Primary Particle Size)?.....	17
2.2.3	Factors Affecting the Behaviour of Aqueous Clay Suspensions (Flocs Formation and Breakage).....	17
2.2.4	Factors Complicating Floc Size Measurement	22
2.3	Standard Particle/Floc Size Measurement Methods.....	23
2.3.1	Sedimentation	25
2.3.2	Individual Particle Sensors (Sensing Zone Techniques).....	27
2.3.3	Microscopy (Direct Optical Methods)	29
2.3.4	Light Scattering.....	31
2.4	Particle Size Measurements in the Oil Sands Industry.....	32
2.4.1	Role of Clays in Oil Sands Mining and Bitumen Extraction.....	32
2.4.2	How are Particle Size Measurements Currently Made?	36
2.4.3	Anticipated Advantages of Utilizing the FPIA in Oil Sands Mining and Bitumen Extraction	37

2.5	Selection of Kaolinite for This Project.....	38
2.5.1	Composition of Oil Sands Fine Clays.....	38
2.5.2	Previous Experience with Kaolinite.....	39
2.5.3	Properties of Kaolinite	39
2.5.4	Parameters Affecting Kaolinite Floc Size Distribution	41
3	Experimental Method.....	44
3.1	Materials.....	44
3.2	Apparatus	46
3.2.1	Sysmex Flow Particle Image Analyzer (FPIA)	46
3.2.2	Malvern Mastersizer	51
3.2.3	Carl Zeiss Microscope	56
3.3	Procedures	59
3.3.1	Mixture Preparation	59
3.3.2	FPIA Tests	64
3.3.3	Mastersizer Tests	67
3.3.4	Microscopy Tests	68
4	Evaluation of Operating Conditions and Development of Test Procedures .	70
4.1	Evaluation of Suspension Properties Affecting Kaolinite FSD	70
4.1.1	Kaolinite Concentration	71
4.1.2	Suspension pH	75
4.1.3	Coagulant Addition	81

4.2	Evaluation of Equipment Configuration and Operating Conditions	83
4.2.1	Sample Mixing	84
4.2.2	Effect of FPIA Operating Parameters	86
4.2.3	Mastersizer Performance Tests	91
4.2.4	Microscope Settings	98
5	Results and Discussion	99
5.1	Measurements Repeatability	99
5.1.1	Latex and Sand Particles	99
5.1.2	Kaolinite Flocs	102
5.2	Comparison of the FPIA and Mastersizer Measurements	113
5.2.1	Latex Suspension	113
5.2.2	Silica Flour Suspension	117
5.2.3	Kaolinite Flocs	120
5.2.4	Comparison of Different Types of Flocs	135
5.3	Comparison of FPIA and Microscopy Measurements	140
5.3.1	Latex Particles	140
5.3.2	Silica Flour	142
5.3.3	Kaolinite Flocs	145
6	Conclusions and Recommendations for Future Work	151
6.1	Conclusions	151
6.2	Recommendations for Future Work	153

References	154
Appendix A: Octave code used for size distribution calculations	168
Appendix B: Microscopy sample size determination	172
Appendix C: Size distribution data used for plotting the graphs in Chapter 4 ...	178
Appendix D: Size distribution data used for plotting the graphs in Chapter 5 ...	192

List of Tables

Table 2.1 The most common equivalent diameters for flocs characterization (Jarvis et al., 2005).....	24
Table 3.1 Properties of silica flour (Asadi, 2012).....	44
Table 3.2 Properties of de-ionized water.....	45
Table 3.3 Polymer microsphere suspension properties.....	46
Table 3.4 FPIA-300 measuring range with high or low magnification lens unit (Sysmex FPIA-3000 Operator's Manual, 2006).....	50
Table 3.5 Legend of Figure 3.4.....	58
Table 4.1 Quantitative comparison of samples with different solid concentration.....	74
Table 4.2 Quantitative comparison of samples with different pHs.....	80
Table 4.3 Quantitative comparison of samples with or without coagulant.....	83
Table 4.4 Quantitative comparison of samples with different mixing times.....	86
Table 4.5 Quantitative comparison of samples with different FPIA mixing speeds.....	89
Table 4.6 Quantitative comparison of samples with different FPIA mixing times.....	91
Table 4.7 Quantitative comparison of samples with different Mastersizer mixing speeds.....	93
Table 4.8 Quantitative comparison of samples diluted with DI water or filtrate...	96
Table 4.9 Quantitative comparison of diluted and non-diluted samples for Malvern Mastersizer measurements.....	98

Table 5.1 Quantitative comparison of the FPIA repeatability measurements....	104
Table 5.2 Quantitative comparison of the FPIA curve fitting parameter.....	106
Table 5.3 Quantitative comparison of the Mastersizer repeatability measurements.....	108
Table 5.4 Quantitative comparison of the Mastersizer curve fitting parameters.	109
Table 5.5 Quantitative comparison of the microscope repeatability measurements.....	111
Table 5.6 Quantitative comparison of the microscope curve fitting parameters.	112
Table 5.7 Comparison of latex measurements with the FPIA and Mastersizer...	115
Table 5.8 Comparison of silica flour measurements with the FPIA and Mastersizer.....	120
Table 5.9 Comparison of primary flocs measurements with the FPIA and Mastersizer.....	122
Table 5.10 Comparison of natural flocs measurements with the FPIA and Mastersizer.....	127
Table 5.11 Comparison of acidic flocs measurements with the FPIA and Mastersizer.....	131
Table 5.12 Comparison of basic coagulated flocs measurements obtained with the FPIA and Mastersizer.....	134
Table 5.13 Comparison of different kaolinite floc measurements with the FPIA.....	138
Table 5.14 Comparison of different kaolinite floc measurements with the Mastersizer.....	140
Table 5.15 Comparison of latex measurements with the FPIA and microscope.	142

Table 5.16 Comparison of silica measurements with the FPIA and microscope 145

Table 5.17 Comparison of basic coagulated flocs measurements with the FPIA
and microscope..... 148

List of Figures

Figure 1.1 Relative viscosity vs. solid volume fraction for kaolinite-water mixtures at pH 4 and 9 (Asadi, 2012).....	4
Figure 1.2 Generalized scheme of water based bitumen extraction process (Masliyah et al., 2011).....	6
Figure 1.3 Schematic of the FPIA experiment.....	9
Figure 2.1 Fluid flow through the FPIA-3000 (Sysmex FPIA-3000 operator's manual, 2006).....	13
Figure 2.2 Attraction, repulsion, and net interaction energy between two charged particles (Masliyah and Bhattacharjee, 2006).....	22
Figure 2.3 Illustration of particle counting and sizing by electrical or optical sensing zone method (Gregory, 2009).....	28
Figure 2.4 The stages of digital image analysis (Jarvis et al., 2005).....	29
Figure 2.5 Characterization of clay minerals in oil sands ore (Masliyah et al., 2011).....	38
Figure 2.6 High resolution SEM micrographs of kaolinite (Zbik et al., 2008).....	39
Figure 2.7 Kaolinite charge distribution at low pH (Nasser and James, 2006)....	40
Figure 2.8 Modes of particle association (a) E-F flocculated and aggregated (b) E-E flocculated and aggregated (c) aggregated but deflocculated (F-F) (d) dispersed and deflocculated (van Olphen, 1977).....	40
Figure 2.9 Kaolinite flocs in (a) card-pack structure (b) card-house structure and (Nasser and James, 2006).....	43
Figure 3.1 Illustration of flat particle flow (Sysmex FPIA-3000 Brochure, 2013).....	48

Figure 3.2 Mechanism of capturing, extracting and analyzing the images (Sysmex FPIA-3000 Brochure, 2013).....	49
Figure 3.3 Mechanism of laser diffraction operation inside the Mastersizer (Mastersizer-2000 Brochure, 2013).....	54
Figure 3.4 Identification of controls and functional elements on the Carl Zeiss Microscope	58
Figure 3.5 Pycnometer used for slurry density measurement.....	62
Figure 3.6 Sample preparation set up.....	63
Figure 3.7 Filtration set up.....	65
Figure 3.8 Large tip opening transfer pipette.....	67
Figure 4.1 Effect of solid concentration on Kaolinite cumulative FSD (natural pH, no coagulant).....	73
Figure 4.2 Effect of solid concentration on Kaolinite FSD (natural pH, no coagulant).....	73
Figure 4.3 Effect of sample concentration on number-based mean and median...	74
Figure 4.4 Kaolinite cumulative FSD at natural and low pH (c=5 g/L, no coagulant).....	76
Figure 4.5 Kaolinite FSD at natural and low pH (c=5 g/L, no coagulant).....	76
Figure 4.6 Kaolinite cumulative FSD at natural and high pH (c=5 g/L, no coagulant).....	77
Figure 4.7 Kaolinite frequency FSD at natural and high pH (c=5 g/L, no coagulant).....	78
Figure 4.8 Effect of pH on kaolinite cumulative FSD (c=5 g/L, no coagulant)....	79
Figure 4.9 Effect of pH on kaolinite FSD (c=5 g/L, no coagulant).....	79

Figure 4.10 Effect of suspension pH on number-based mean and median.....	80
Figure 4.11 Effect of coagulant addition on kaolinite cumulative FSD (pH=9; c=5 g/L).....	82
Figure 4.12 Effect of coagulant addition on kaolinite FSD (pH=9; c=5 g/L).....	82
Figure 4.13 Effect of sample mixing time on kaolinite FSD (c=10g/L, pH=4.9)..	85
Figure 4.14 Particle size versus sample mixing time (c=10g/L, pH=4.9).....	85
Figure 4.15 Effect of FPIA mixing speed on kaolinite cumulative FSD (c=5g/L, pH=4.9).....	88
Figure 4.16 Effect of FPIA mixing speed on kaolinite FSD (c=5g/L, pH=4.9)....	88
Figure 4.17 Effect of FPIA mixing time on kaolinite cumulative FSD (c=5g/L, pH=4.9).....	90
Figure 4.18 Effect of FPIA mixing speed on kaolinite cumulative FSD (c=5g/L, pH=4.9).....	90
Figure 4.19 Effect of Mastersizer mixing speed on kaolinite FSD.....	92
Figure 4.20 Effect of Mastersizer mixing speed on kaolinite cumulative FSD.....	93
Figure 4.21 Effect of dispersing medium in the Mastersizer on kaolinite cumulative FSD.....	95
Figure 4.22 Effect of dispersing medium in the Mastersizer on kaolinite FSD.....	95
Figure 4.23 Effect of dilution on kaolinite cumulative FSD.....	97
Figure 4.24 Effect of dilution on kaolinite FSD.....	97
Figure 5.1 Repeatability of FPIA measurements (cumulative latex PSD, 0.1 wt% aqueous suspension).....	100

Figure 5.2 Repeatability of FPIA measurements (cumulative silica PSD, $c = 2.5$ g/L).....	100
Figure 5.3 Repeatability of Mastersizer measurements (cumulative latex PSD, 0.1 wt% aqueous suspension).....	101
Figure 5.4 Repeatability of Mastersizer measurements (cumulative silica PSD, $c = 2.5$ g/L).....	101
Figure 5.5 Repeatability of FPIA measurements (cumulative kaolinite FSD, $c = 5$ g/L, 0.01 M CaCl ₂ , pH 9).....	103
Figure 5.6 Repeatability of FPIA measurements (frequency kaolinite FSD, $c = 5$ g/L, 0.01 M CaCl ₂ , pH 9).....	103
Figure 5.7 FPIA data curve fitting using Octave code.....	106
Figure 5.8 Repeatability of Mastersizer measurements (cumulative kaolinite FSD, $c = 5$ g/L, 0.01 M CaCl ₂ , pH 9).....	107
Figure 5.9 Repeatability of Mastersizer measurements (frequency kaolinite FSD, $c = 5$ g/L, 0.01 M CaCl ₂ , pH 9).....	108
Figure 5.10 Mastersizer data curve fitting using Octave code.....	109
Figure 5.11 Repeatability of microscope measurements (cumulative kaolinite FSD, $c = 5$ g/L, 0.01 M CaCl ₂ , pH 9).....	110
Figure 5.12 Repeatability of microscope measurements (kaolinite FSD, $c = 5$ g/L, 0.01 M CaCl ₂ , pH 9).....	111
Figure 5.13 Microscope data curve fitting using Octave code.....	112
Figure 5.14 Cumulative particle size distributions for the 2 μ m latex particles obtained using the FPIA and Mastersizer.....	115
Figure 5.15 Frequency particle size distributions for the 2 μ m latex particles obtained using the FPIA and Mastersizer.....	115

Figure 5.16 Some latex particles detected by the FPIA.....	116
Figure 5.17 Cumulative particle size distributions for the silica particles obtained using the FPIA and Mastersizer.....	117
Figure 5.18 Frequency particle size distributions for the silica particles obtained using the FPIA and Mastersizer.....	118
Figure 5.19 Some silica particles detected by the FPIA.....	119
Figure 5.20 Comparison of the FPIA and Mastersizer frequency for silica particles.....	120
Figure 5.21 Cumulative floc size distributions for kaolinite primary flocs obtained using the FPIA and Mastersizer.....	122
Figure 5.22 Frequency floc size distributions for kaolinite primary flocs obtained using the FPIA and Mastersizer.....	122
Figure 5.23 Some of the largest primary kaolinite flocs detected by the FPIA...	124
Figure 5.24 Comparison of the FPIA and Mastersizer frequency for kaolinite primary flocs.....	125
Figure 5.25 Cumulative floc size distributions for kaolinite natural flocs obtained using the FPIA and Mastersizer.....	126
Figure 5.26 Frequency floc size distributions for kaolinite natural flocs obtained using the FPIA and Mastersizer	126
Figure 5.27 Some natural kaolinite flocs detected by the FPIA.....	127
Figure 5.28 Comparison of the FPIA and Mastersizer frequency for kaolinite natural flocs.....	128
Figure 5.29 Cumulative floc size distributions for kaolinite acidic flocs obtained using the FPIA and Mastersizer.....	129

Figure 5.30 Frequency floc size distributions for kaolinite acidic flocs obtained using the FPIA and Mastersizer.....	129
Figure 5.31 Some acidic kaolinite flocs detected by the FPIA.....	130
Figure 5.32 Comparison of the FPIA and Mastersizer frequency for kaolinite acidic flocs.....	131
Figure 5.33 Cumulative floc size distributions for kaolinite coagulated alkaline flocs obtained using the FPIA and Mastersizer.....	133
Figure 5.34 Frequency floc size distributions for kaolinite coagulated alkaline flocs obtained using the FPIA and Mastersizer.....	133
Figure 5.35 Some coagulated alkaline kaolinite flocs detected by the FPIA.....	134
Figure 5.36 Comparison of the FPIA and Mastersizer frequency for kaolinite alkaline coagulated flocs.....	135
Figure 5.37 Cumulative FSDs for different types of kaolinite flocs measured using the FPIA.....	137
Figure 5.38 Frequency FSDs for different types of kaolinite flocs measured using the FPIA.....	137
Figure 5.39 Cumulative FSDs for different types of kaolinite flocs obtained using the Mastersizer.....	139
Figure 5.40 Frequency FSDs for different types of kaolinite flocs obtained using the Mastersizer.....	139
Figure 5.41 Cumulative particle size distributions for the 2 μm latex particles obtained using the FPIA and microscope.....	141
Figure 5.42 Frequency particle size distributions for the 2 μm latex particles obtained using the FPIA and microscope.....	141

Figure 5.43 A micrograph of latex particles (0.1 wt% aqueous suspension, 400x magnification).....	142
Figure 5.44 Cumulative particle size distributions for the silica particles obtained using the FPIA and microscope.....	143
Figure 5.45 Frequency particle size distributions for the silica particles obtained using the FPIA and microscope.....	143
Figure 5.46 A micrograph of silica particles (2.5 g/L silica in DI water, 400x magnification).....	144
Figure 5.47 Comparison of the FPIA and microscope frequency for silica particles.....	145
Figure 5.48 Cumulative floc size distributions for the kaolinite flocs obtained using the FPIA and microscope.....	147
Figure 5.49 Frequency floc size distributions for the kaolinite flocs obtained using the FPIA and microscope.....	147
Figure 5.50 A micrograph of kaolinite flocs ($c = 5$ g/L, 0.01 M CaCl_2 , pH 9, 400x magnification).....	148
Figure 5.51 Some of the largest coagulated basic kaolinite flocs detected by the FPIA.....	149
Figure 5.52 Comparison of the FPIA and microscope frequency for kaolinite flocs.....	150

List of Symbols

a	spherical particle radius, m
A	Hamaker constant
$A(\beta)$	correction factor accounting for advection flow through the floc
c	concentration, g/L
C_p	proportionality constant, $\text{kg}\cdot\text{m}^{-D_f}$
d	floc diameter
D	distance between the particles, m
D_f	fractal dimension
e	elementary charge (1.602×10^{-19} C)
g	acceleration due to gravity, m/s^2
h	separation distance, m
T	absolute temperature, K
V	volume
x	particle diameter, m
z	absolute value of valence of the electrolyte
μ	viscosity, Pa.s
v_s	terminal settling velocity, m/s
ρ_K	kaolinite density, kg/m^3
ρ_l	density of the liquid, kg/m^3
ρ_p	density of the particle, kg/m^3
ρ_{Slurry}	slurry density, g/L
ρ_{Water}	water density, g/L
k_B	Boltzmann constant (1.38×10^{-23} J/K)
n_∞	ionic number concentration in the bulk solution, m^{-3}

ε	dielectric permittivity of medium, F/m
ε_0	permittivity of vacuum (8.854×10^{-12} F/m)
κ^{-1}	Debye length, m
φ	surface potential (zeta potential), V

1 Problem Statement and Objectives

In colloidal particle-fluid systems, particle size plays a governing role in particle-particle and particle-fluid interactions: the ratio of particle surface area to volume increases with decreasing particle size, causing the surface forces to become stronger and more important (Masliyah et al., 2011). The particle size must therefore be known (i.e. measured) before the behaviour of a colloidal system can be predicted or characterized (Masliyah et al., 2011). Adsorptive, magnetic, electric, optical and other dispersion characteristics are also influenced by particle size (Delago and Matijevic, 1991). Fields such as waste water treatment, oil production, medicine and nanotechnology involve colloidal systems and require particle size measurement in order to optimize their processes. For instance, particle size can affect the mobility, reactivity and toxicity of nanoparticles (Jiang et al., 2009; Keller et al., 2010; Jassby, 2011), flotation efficiency in primary separation vessel in the bitumen extraction process (Masliyah et al., 2011), and permeability of dental materials into dentin tubules in dentistry (Komabayashi et al., 2009).

Clay particles are small enough to behave as a colloidal system. Clay particle size and water chemistry (among other factors) are related to behaviours that are detrimental to separation of bitumen; for example, slime coating of bitumen droplets and/or air bubbles and increased suspension viscosities (Masliyah et al., 2004; Liu et al., 2004). Clay suspension behaviour also play an important role in the minimum operating velocity (deposition velocity) in hydrotransport pipelines

and the settling behaviour of slurries in tailings ponds (Adeyinka et al., 2009; Masliyah et al., 2011).

In many industrial colloidal systems, the particles are rarely found as single particles; rather, they form persisting structures known as “flocs” or “aggregates”. The building blocks of these flocs are the primary particles. Michaels and Bolger (1962) suggested that flocs, rather than individual particles cause the flow behavior of the agglomerating particles suspensions. Nasser and James (2008 & 2009) also used kaolinite suspensions in their aggregated state to study their settling and rheological behavior.

In this chapter, the importance of measuring in situ entities rather than primary particle size, the role of clays in different stages of bitumen extraction process and tailings management, and the current practice in the oil sands industry for particle size measurement are discussed. The instrument utilized in this study for floc size measurement, the objective of the research and activities done to achieve the objective are also described.

There are two ways to attempt to understand colloidal suspension behaviour. One way is to look at primary particle size and one is to study the in situ entities that exist. An advantage of utilizing primary particle is that the size measurement analysis can be done without the concern of particle size modification during sample preparation or during measurement. Numerous particle size measurement techniques are available for these particles, as opposed to flocs (as is discussed in Chapter 2). Also, if a suspension is fully dispersed to primary particles, the results

are independent of suspension pH and water chemistry. On the other hand, sonication, which is used in dispersion, can change the primary particle size (Marefatallah, 2013). Besides, measurement of ultrafine particles ($< 0.3 \mu\text{m}$) in their dispersed state is very time-consuming and laborious. Scales et al. (1998) correlated shear yield stress with primary particle size. Adeyinka et al. (2009) also studied the effect of particle size on the viscosity of oil sands slurries.

However, flocs are the entities that actually exist in the suspension, not primary particles. In some cases like flocculant dosed tailings, the dispersed mixture does not correlate to the original suspension properties due to the presence of the flocculant. Nasser and James (2006 & 2008) used coagulated suspensions in their study of the settling behaviour, gel point and rheological behavior of flocculating particles. James and Williams (1982) also stated that clay flocculation is a significant factor affecting the rheological behavior. Asadi (2012) proved that the floc size distribution should be used to infer the viscosity of the carrier fluid instead of individual particle size distribution for ideal clay suspensions. In other words, the aggregates control the viscosity of the carrier fluid. In her research, two samples were made with the same source of material and identical sub-micron sized primary particles. However, the relative viscosity (ratio of the viscosity of the suspension to the viscosity of the suspending medium) of the two mixtures, as depicted in Figure 1.1, is very much dependent on mixture pH. Accordingly, if pH, water chemistry and clay mineralogy are not known, not much information regarding the behavior of a clay-water mixture can be obtained from primary particle size analysis compared with the information provided by

the in situ floc size. In the case of flocculating particles, it is often the floc size distribution (FSD) rather than the primary particle size distribution (PSD) that is related directly to the rheological or settling behavior of the suspension and should be studied, especially if other suspension properties (pH, ion content) are not known or measured.

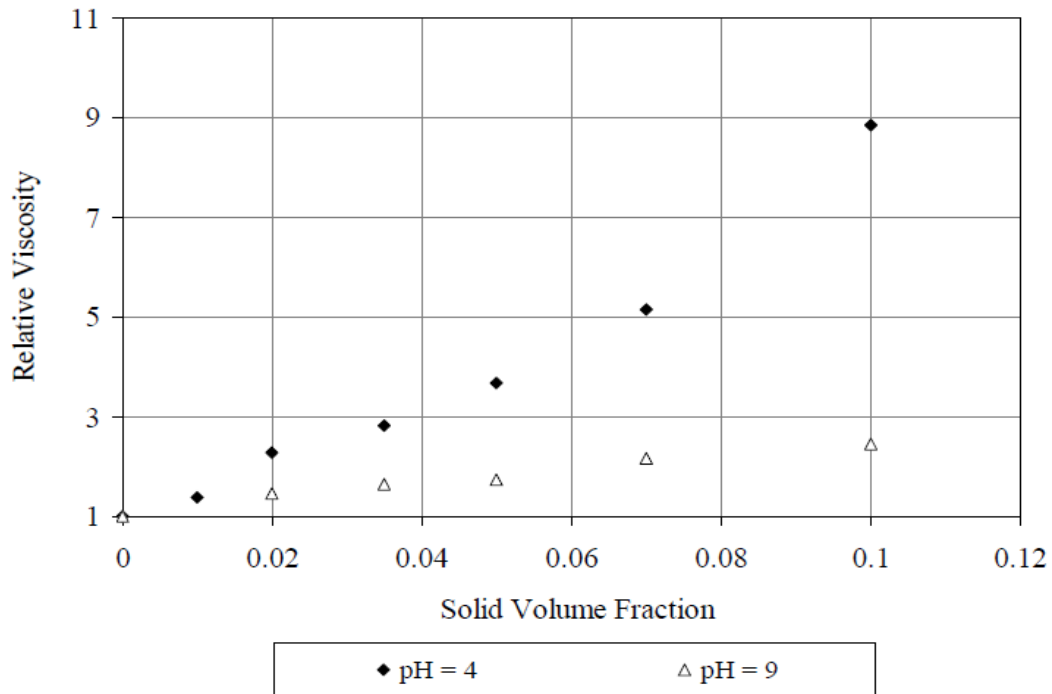


Figure 1.1 Relative viscosity vs. solid volume fraction for kaolinite-water mixtures at pH 4 and 9 (Asadi, 2012)

Flocs can be modified with exposure to mechanical shear or with changes in water chemistry. Different size measurement methods and sample preparation procedures affect and bias the measured floc size distributions (Delago and Matijevic, 1991; Jeeravipoolvarn et al., 2008). Jeeravipoolvarn et al. (2008) showed that characterization of fine flocculating particles in the original physical and chemical field conditions is necessary, since change of the conditions can

result in modification of FSDs. Therefore, floc sizes should be measured as they exist in the process stream.

Process streams found in surface mining and water-based extraction of bitumen consist of a stable mixture of water and fines, also known as “carrier fluid”, and coarse particles. These slurries are involved in different steps of the bitumen extraction process such as oil sands hydrotransport, gravity separation, flotation, froth treatment and tailings (Masliyah et al., 2004). Fine clays extensively impact bitumen extraction from oil sands (Liu et al., 2004) through their effect on carrier fluid rheology, flotation efficiency, bitumen recovery and quality, settling behaviour and degree of partitioning during conditioning (Schramm, 1989; Sparks et al., 2003; Masliyah et al., 2004; Mikula et al., 2008; Kaminsky et al., 2009).

At the beginning of the bitumen extraction process (Figure 1.2), warm water is added to crushed oil sands ore. The slurry is then pumped to the extraction plant through hydrotransport pipelines. The particle size distribution is an important parameter in predicting the deposition velocity (minimum operating velocity) and pressure drop using existing design models (Sanders et al., 2004; Masliyah et al., 2011). The deposition velocity and pressure drop are key factors in design and operation of slurry pipelines (Shook et al., 2002; Gillies et al., 2004). One of the challenges in slurry transport pipelines is sedimentation of solids which is a function of particle size and carrier fluid properties. In order to prevent solids accumulation and avoid pipeline plugging, the pipeline should be operated just above the deposition velocity. Velocities greater than this contribute to excessive power consumption and pipe wear (Wilson et al., 2006).

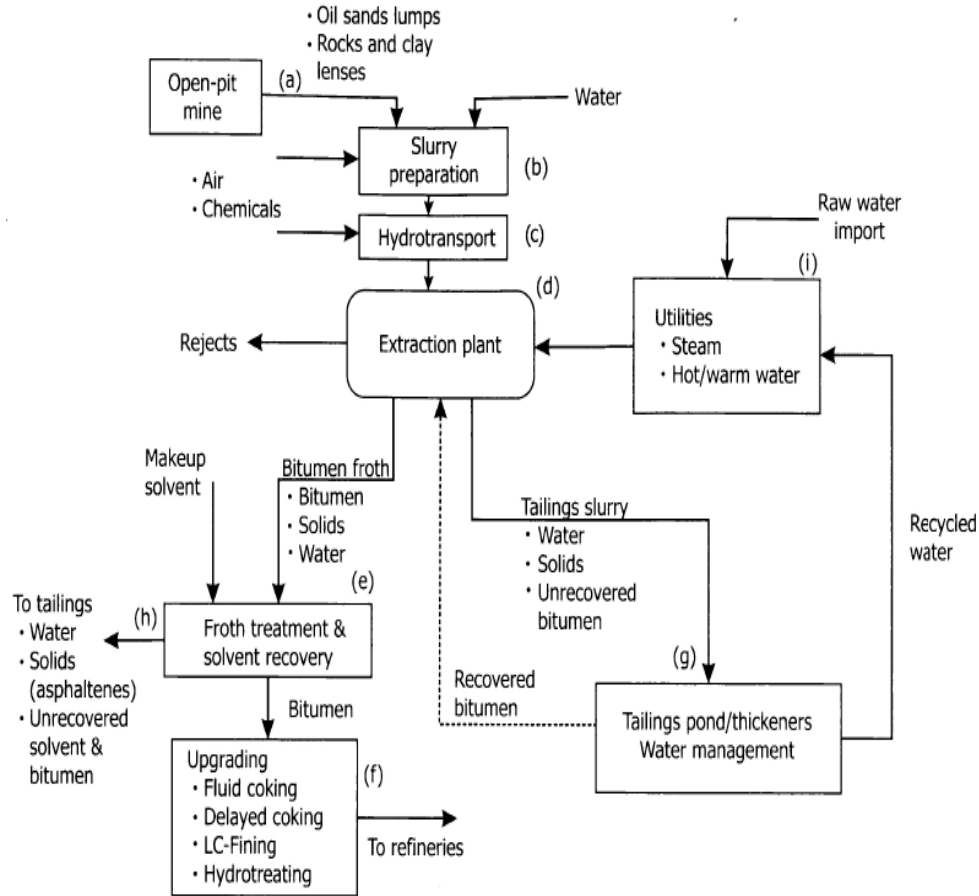


Figure 1.2 Generalized scheme of water based bitumen extraction process (Masliyah et al., 2011)

Slurry characteristics governed by the presence of clay particles are also critical to the performance of separation processes. The separation stage starts when the slurry is introduced to the primary separation vessel (PSV), also known as the primary separation cell (PSC). Based on their density difference, the aerated bitumen droplets rise to the top of the vessel and coarse particles fall to the bottom of the cell. Bitumen froth is then sent to the froth treatment plant to remove water and fine solids (Schramm, 1989; Masliyah et al., 2004; Gray et al., 2009). Fine clay particles can form a viscous suspension in the middlings zone of the PSV (Tu

et al., 2005; Adeyinka et al., 2009). This operational condition is sometimes called sludging. It hinders the rise of aerated bitumen and, therefore, decreases flotation efficiency and oil recovery (Schramm, 1989; Masliyah et al., 2011).

An aqueous stream from the middle of the PSV containing clay and residual bitumen, called middlings, is reaerated to produce secondary froth. The secondary recovery process happens in mechanical or column flotation cells (Masliyah et al., 2011). The rise of reaerated bitumen and bitumen recovery are affected by the viscosity of the slurry inside the flotation cell. The suspension viscosity, in turn, is influenced by clay particle size, mineralogy, water chemistry and pH (Shook et al., 2002; Asadi, 2012).

The tailings streams from the PSV, secondary recovery cells and froth treatment unit are treated in thickeners or directly pumped to the tailings ponds (Kasperski, 1992; Masliyah et al., 2011). A tailings stream contains sand, clay, fugitive bitumen and trace amounts of soluble organic compounds (Kasperski, 1992). In order to reduce the volume of fine tailings in the ponds, the consolidated tailings (CT) process, also known as the non-segregated tailings (NST) process, can be employed. The process uses gypsum or flocculants to consolidate the fines and produces a mixture that does not segregate during transportation, discharge and deposition (Masliyah et al., 2011). Clay particle flocculation or dispersion governs sedimentation and consolidation behavior of fine tailings and the operation of the CT process (Uhlik et al., 2008; Masliyah et al., 2011).

Despite the importance of floc sizes (as previously discussed), the current practice in industry is to fully disperse the flocs and aggregates (down to primary particles) prior to the size analysis measurement, i.e. measure the primary particle size. Although it is the in situ floc size that matters, an ultrasonic probe is employed to de-aggregate the flocs, so that the results are reproducible and independent of sample preparation procedure (Bulmer and Star, 1979; Cowles, 2003).

Many techniques have been used for particle/floc size measurement over the years. Sedimentation, individual particle sensors, microscopy and light scattering are examples of the techniques utilized for particle size measurements that are described in the literature (Wen et al., 2002; Jarvis et al., 2005; Nasser and James, 2006; Yuan et al., 2009). Some of these methods are described in detail in Chapter 2. Depending on the conditions and demands of an experiment, a suitable instrument is chosen for size measurement. The fact that flocs are sensitive and loosely attached structures makes some of the techniques undesirable for floc size measurement. Such constraints on measurement techniques are discussed in the next chapter.

The Sysmex Flow Particle Image Analyzer (FPIA), an image analysis based instrument for automated particle size and morphology measurements, is utilized in this study to measure the size of clay flocs rather than the fully dispersed primary particle size. Recent research (Asadi, 2012; Marefatallah, 2013; Smith, 2013) proved that the FPIA produces reproducible and consistent floc size distribution measurement results. The device processes and provides particle size and shape information in a short time. Up to 300,000 particles are analyzed and

their images are stored in less than 3 minutes (Sysmex FPIA-3000 Operator's Manual, 2006). Despite its advantages, the FPIA has rarely been used for floc size measurements or for characterization of clay materials. Therefore, the FPIA floc size distribution measurement results must be validated.

The objective of the present study is to evaluate the FPIA performance and validate the floc size measurements obtained from the FPIA. The goal is to determine if the floc size measurements obtained from the FPIA are representative of the in situ sample and to determine if the device somehow modifies the floc size. The problem in its simplest form is illustrated in Figure 1.3. Suppose the suspension in the beaker has a given FSD. The FPIA is used to obtain a FSD. The question here is: what FSD does the FPIA give? Is it the same as the FSD of the original sample?

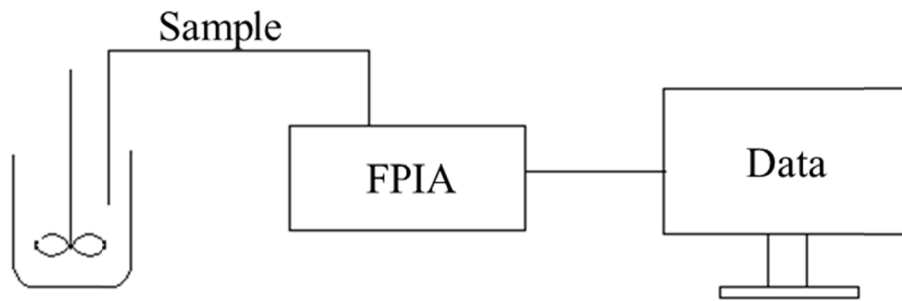


Figure 1.3 Schematic of the FPIA experiment

In this project, the floc size distribution measurement results from the FPIA are compared with the results from other devices, specifically the Malvern Mastersizer and a Carl Zeiss optical microscope. The first stage in the project was

to compare the floc size distribution measurements obtained from the FPIA with the results from the Mastersizer. This stage included the following activities:

- Assess, using the FPIA, the floc size distribution (FSD) of kaolinite samples at different concentrations, at acidic and basic pH values, and in the absence and presence of flocculants. This step is performed to select the desired suspension conditions for further testing.
- Assess the repeatability of the FPIA and Mastersizer particle/floc size distribution measurements.
- Study the effect of mixing and dilution in the FPIA and Mastersizer in order to assess the equipment configuration/conditions and create a test procedure.
- Compare the results of the FPIA and Mastersizer for a sample of standard mono-sized latex beads. The PSD of ideal particles needs to be validated to ensure the agreement of devices before carrying on with more complicated particles.
- Compare the size distribution of sand particles obtained from the FPIA and Mastersizer. The size distribution of sand particles, which are non-flocculating irregular shaped particles, should be compared to determine the agreement/disagreement of the results between the two instruments for this type of particles.
- Assess the size distribution results of kaolinite primary flocs (dense rigid micro-flocs) from both devices (FPIA and Mastersizer). After comparing

results of non-flocclating particles the extent of difference between the FSDs arising from the modification of flocs can be inferred.

- Carry out the FSD comparison using the two techniques with different kaolinite suspensions.

The second stage of the project was to compare the FPIA floc size distribution measurements with results obtained using the microscope. The activities performed in this stage include the following:

- Assess the repeatability of microscope floc size distribution measurements.
- Compare the standard latex particle size distribution from the FPIA with that of the microscope. In this way the standard non-flocculating mono-sized particle measurement is validated and the procedure can be carried on to more complicated type of particles.
- Compare the results for size distribution of irregular shaped non-flocculating sand particles from the FPIA and microscope. This more complicated type of particles also needs to be compared before continuing with flocculating particles.
- Compare the FPIA floc size distribution measurements with those obtained using microscopy for a kaolinite suspension. The extent of FSD changes occurring during the FPIA measurements can hopefully be inferred.

2 Background and Literature Review

2.1 Particle Size Analysis Using the FPIA

The Sysmex Flow Particle Image Analyzer (FPIA-3000) is utilized in this study to measure the floc size distribution of kaolinite suspensions. The FPIA combines flat sheath flow formation and image processing technology. It is hoped that the device can measure the clay flocs in their natural aggregated state without breaking them down or otherwise changing the FSD. Three MSc theses (Asadi, 2012; Marefatallah, 2013; Smith, 2013) showed the reproducibility of the FSD results, but for those studies, the true FSD was not the focus; rather, those studies were based on qualitative comparisons between samples. The operation principles of the FPIA and its applications in the literature are discussed in the following sections.

2.1.1 How does the FPIA Work?

The FPIA measures the size and morphology of particles in size range of 0.8 to 300 μm within suspensions. The device works based on automated image analysis. The fluid flow through the FPIA is illustrated in Figure 2.1. As little as 1 to 5 mL of the dilute sample (in order to capture clear images) is introduced to the mixing unit (1). The sample flows to the transparent flow cell while aligned with the sheath fluid forming a laminar flat flow (2). The narrow stream causes the particles to orient with their largest face toward the camera. The light source illuminates the flat sample (3). The images are then captured with a camera at a rate of 60 frames per second (4) and are automatically analyzed in the image

processing unit producing particle size distribution and morphological parameters. The limitation of 360,000 particles per sample applies. Finally, after the measurement is done, the flow cell is rinsed with the sheath fluid and the waste is collected in the waste chamber (5).

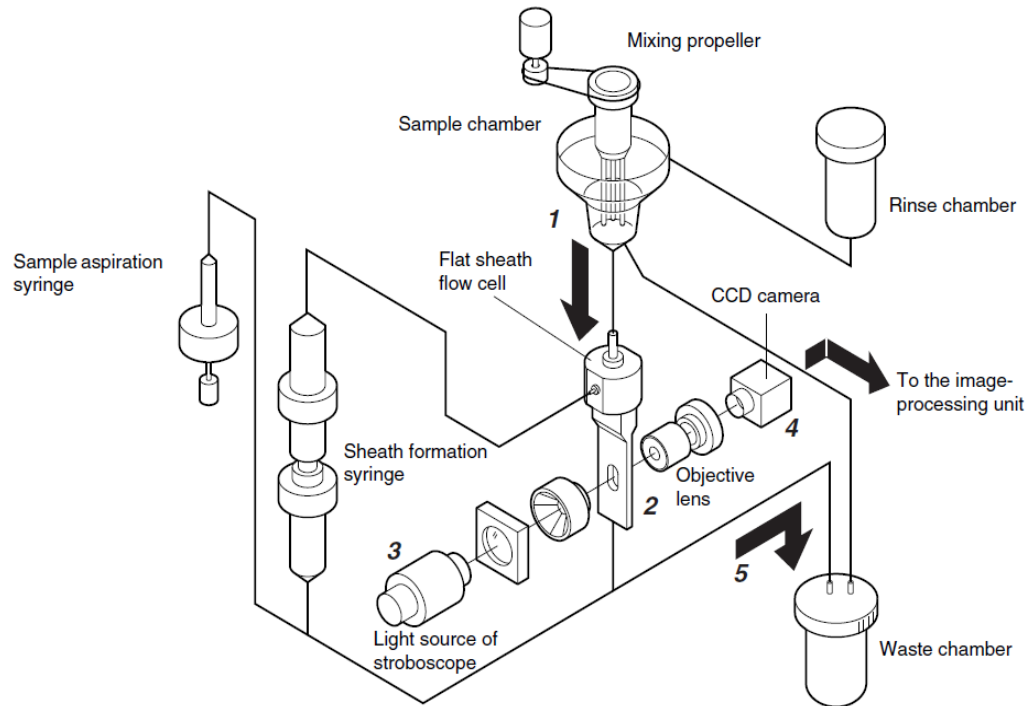


Figure 2.1 Fluid flow through the FPIA-3000 (Sysmex FPIA-3000 Operator's Manual, 2006)

2.1.2 Applications Involving the FPIA Described in the Literature

In recent years, the FPIA has been utilized to study the particle size distribution and shape parameters of different suspensions. Komabayashi and Spanberg (2008a & b) used the FPIA-3000 to characterize the particle size distribution and circularity of mineral trioxide aggregates (MTA) and Portland cement (PC). The reported size of particles range from 0.5 to 40 μm . The size and shape of particles relates to the depth of penetration of MTAs into dentin tubules. They chose the

FPIA for its rapid particle imaging over scanning electron microscopy, spectroscopy and x-ray diffraction that were used for characterization of the same materials (MTA and PC) by many others. Komabayashi et al. (2009) examined the particle length, width, perimeter, and aspect ratio of calcium hydroxide flocs (used as antimicrobial dressing in root canal treatment) in alcohol using the FPIA-3000. The size and shape information by the FPIA can be used to determine the permeability of calcium hydroxide particles into open dentin tubules. Arnold et al. (2003) determined the particle size distribution of newly-synthesized lithium iron phosphate (LiFePO_4) particles in an aqueous suspension with a FPIA-2100. The material is used as positive electrode material in lithium and lithium-ion batteries. As the particles get smaller the capacity of the batteries improves. Tanaka et al. (2008) used the FPIA-2100 to study the shape of toner powder particles. Toner powder consists of polyester resins, carbon blacks and wax. The shape analysis information was used to determine the roughness of particles. The roughness affects the fluidity of the toner which in turn influences the image quality of the printer. The mean diameter of the toner particles ranged from 5.5 to 6.5 μm . Carbon nanotube particles were also studied by Krause et al. (2009) using the FPIA. The circularity distribution of the aggregates measured with the FPIA corresponded to the results obtained from cryofractured analysis. Asadi (2012) used the FPIA-3000 to measure the size and concentration of clay and sand slurries. Marefatallah (2013) used the FPIA to study the effect of sonication on kaolinite flocs by comparing the size distribution of kaolinite particles before and

after sonication. Smith (2013) also used the FPIA as part of a project designed to relate fine-particle slurry rheology to the concentration of aggregates.

Several other size and shape parameters measurement studies using the FPIA were conducted on various other materials such as DNA nanoparticles (Collins et al., 2004), viral suspensions (Langlet et al., 2007), pollen grains (Mitsumoto et al., 2009), protein aggregates (Promeyrat et al., 2010), red cells (Saigo et al., 2005), microgel droplets (Brugger and Richtering, 2007) and LTCC (low-temperature cofired ceramic) powders (Besendorfer and Roosen, 2008).

2.2 Complications in Measuring Floc Sizes

Small particles have the potential to flocculate and form clusters, called flocs or aggregates, due to the inter-particle forces (Jarvis et al., 2005; Masliyah et al., 2011). Due to the sensitive loosely-attached structure of resulting flocs, some complications in size measurement can result.

In the next sections, some examples of flocculating particles and their applications are described. The necessity of measuring flocs instead of primary particles is discussed. Also, colloidal forces that govern the behaviour of particles are explained. Finally, the complications in floc size measurement are specified.

2.2.1 Flocculating Particles and Applications

Flocculating particles, whether natural or synthesized, have attracted much attention in recent years, owing to their unique physical properties and widespread consumer and industrial applications (Pialy et al., 2008; Jassby, 2011;). Flocculating particles are involved in several fields such as water treatment, oil

production, agriculture, medicine, nanotechnology, polymer, paint, paper and ceramic (Stone and Krishnappan, 2003; Borm et al., 2006; Tripathy and Ranjan De, 2006; Pialy et al., 2008). Nanoparticles, polymer latexes, wastewater sludge and clays are examples of flocculating particles. Applications related to sludges and clays are described in this section.

Sludge is made up of agglomerated inorganic and organic particles, and is produced during water treatment and purification processes (Benouali et al., 2010). Removal of sludge and slimes from municipal and industrial wastewater is essential to meet potable, industrial and agricultural water standards (Tripathy and Ranjan De, 2006). In order to optimize the treatment and purification process, detailed knowledge of the flocs and their properties, such as morphology and size distribution, is critical. There are many studies that characterize wastewater sludge (Stone and Krishnappan, 2003; Govoreanu et al., 2009; Yuan et al., 2009; Zeilina, 2011).

Clays are important in numerous applications, including paper, paint, plastic, rubber, pharmaceuticals, cosmetics, chemicals, ceramics, food, fertilizers, pet litter, drilling fluids, filler for polymers and cement (Murray, 1991; Costanza, 2001; Pialy et al., 2008; Silva-Valenzuela et al., 2013). The widespread industrial applications involving clay and clay flocs drive the need to study and characterize clay flocs.

In the oil sands industry, clays play important roles. They influence different stages of the oil sands extraction process. Clay is one of the components of oil

sands ore, along with bitumen, water, sand and silt. Typically, oil sands ore contains 80-85 wt% solids from which 3.1-31 wt% is fine fraction, 0.9-11.8 wt% is clay fraction, and 0.1-5.1 wt% is ultra-fine fraction (Chong et al., 2003; Tu et al., 2005).

2.2.2 Why Measure Floc Size (Instead of Primary Particle Size)?

In order to better understand colloidal suspension behavior, floc size should be measured. In industrial colloidal systems, particles are usually found in their aggregated state instead of as primary particles. Flocs, rather than individual particles, govern the flow behavior of flocculating particle suspensions (Michaels and Bolger, 1962). As previously discussed, Asadi (2012) proved that floc size distribution should be taken into account to infer the carrier fluid viscosity instead of individual particle size distribution for a kaolinite clay suspension. She compared the viscosities of two mixtures made from the same material and identical primary particles at different pH values. The results showed different viscosities for the two samples (Figure 1.1). Additionally, Nasser and James (2008 & 2009) correlated the floc size to suspension behaviour.

2.2.3 Factors Affecting the Behaviour of Aqueous Clay Suspensions (Flocs Formation and Breakage)

Generally, in colloidal suspensions, the force between two particles (F) can be either attractive or repulsive, depending upon the surface to surface separation distance between the particles (D) and the potential energy (V) at that distance. This is the relationship between the force and potential energy (Rhodes, 2008):

$$F = -\frac{dV}{dD} \quad (2.1)$$

Within the appropriate distance, colloid particles apply forces on each other that determine the probability of aggregation, the structure of the aggregates and the final structure of colloidal systems.

There are attractive forces, called van der Waals forces, between particles of any type in a fluid medium. However, inter-particle repulsive forces also usually exist as a result of the overlap of electric double layers. DLVO theory explains the interplay between van der Waals attractive forces and repulsive electrostatic forces (Berg, 2010). These forces govern many important characteristics of the clay suspension that can influence bitumen recovery, froth treatment and tailings management and also directly affect bitumen liberation, bitumen aeration and clay aggregation (Masliyah et al., 2011).

Van der Waals and Electrostatic Forces

Electrodynamic interactions include Keesom, Debye and London dispersion interactions (which has the single highest contribution). They are commonly referred to as van der Waals forces, and exist between atoms of two different particles. In other words, interactions between permanent charge distributions in the molecules (dipole-dipole interaction), permanent charge distributions and induced charge distributions (dipole-induced dipole interactions), and London or dispersion forces (dispersive interactions) form van der Waals forces (Berg, 2010). Equations 2.2a and 2.2b show the simple equations for overall interactions between two identical spherical particles:

$$V_{vdW} = - \frac{Ax}{24D} \quad (2.2a)$$

$$F_{vdW} = - \frac{Ax}{24D^2} \quad (2.2b)$$

where

V_{vdW} : van der Waals interaction energy

F_{vdW} : van der Waals force

D: distance between the particles

x: particle diameter

A: Hamaker constant which determines the sign and magnitude of the interaction for a particular pair of particles

It will be more complicated if the particles are not the same size or their separation distance is greater than their diameter (Rhodes, 2008).

The other dominant forces present in colloidal suspensions are the electrostatic forces, also known as double layer overlapping forces or electrical double layer forces. Due to the surface charge, particles interact with each other when they are in close proximity. Since clay particles carry a net negative charge, the forces between clay particles in a suspension are mainly repulsive. The colloidal particle surface charge is neutralized by an adjacent diffuse layer of counter ions, a “cloud” of ions often called the electrical double layer. The Debye length, κ^{-1} , is the thickness of the double layer and a property of the electrolyte solution. It

impacts the magnitude of the electrostatic forces and can be calculated from (Masliyah and Bhattacharjee, 2006; Berg, 2010)

$$\kappa^{-1} = \left(\frac{\varepsilon T k_B}{2 e^2 z^2 n_\infty} \right)^{1/2} \quad (2.3)$$

where

κ^{-1} : Debye length, m

T: absolute temperature, K

ε : dielectric permittivity of medium, F/m

k_B : Boltzmann constant (1.38×10^{-23} J/K)

z: absolute value of valence of the electrolyte

e: elementary charge (1.602×10^{-19} C)

n_∞ : ionic number concentration in the bulk solution, m^{-3}

The theory of colloidal stability in terms of coagulation and dispersion, or DLVO theory is named after scientists Derjaguin, Landau, Verway and Overbeek. It assumes the net force between particles (F) is a summation of attractive van der Waals forces (F_{vdW}) and the repulsive colloidal double layer overlapping force (F_{DL}) (Masliyah and Bhattacharjee, 2006; Masliyah, 2011):

$$F = F_{vdW} + F_{DL} \quad (2.4)$$

where

$$F_{vdW} = -\frac{Aa_1a_2}{6h^2(a_1+a_2)} \quad (2.5)$$

$$F_{DL} = \frac{2\pi\epsilon\epsilon_0\kappa a_1a_2}{a_1+a_2} \left[\frac{2\varphi_1\varphi_2e^{-\kappa h}}{1+e^{-\kappa h}} - \frac{(\varphi_1+\varphi_2)^2e^{-2\kappa h}}{1-e^{-2\kappa h}} \right] \quad (2.6)$$

where

a: spherical particle radius, m

ϵ : dielectric permittivity of medium, F/m

ϵ_0 : permittivity of vacuum, 8.854×10^{-12} F/m

κ^{-1} : Debye length, m

φ : surface potential (zeta potential), V

h: separation distance, m

Three different net interaction energy curves are shown in Figure 2.2 (U(1), U(2), U(3)). Each curve represents different conditions for two charged particles. Each solid line is the summation of electrostatic repulsion energy ($U_R(n)$) and van der Waals attraction energy (U_A).

A well-stabilized colloidal system and an unstable dispersion are represented by U(1) and U(3), respectively. Curve U(1) has a repulsive energy barrier that prevents the contact of two colloidal particles and aggregation. The system is stable if this barrier is larger than particles' thermal energy ($k_B T$). On the other hand, a repulsive barrier is absent in curve U(3) and particles flocculate rapidly. Curve U(2) is placed somewhere between stability and flocculation

(Masliyah and Bhattacharjee, 2006). It also has a secondary minimum which is responsible for formation of loose flocs that are disrupted by agitation (Berg, 2010). As reported by Masliyah et al. (2011), van der Waals energy is dominant at very small and very large distances between two particles, whereas at average distances the double layer overlapping repulsion is dominant.

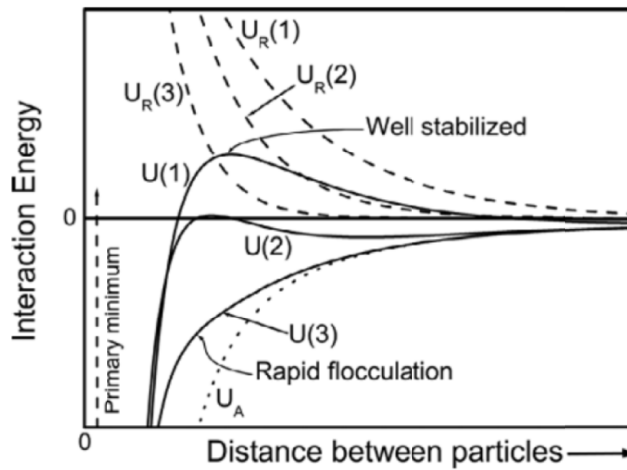


Figure 2.2 Attraction, repulsion, and net interaction energy between two charged particles (Masliyah and Bhattacharjee, 2006)

2.2.4 Factors Complicating Floc Size Measurement

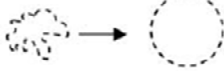

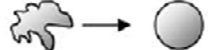
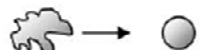
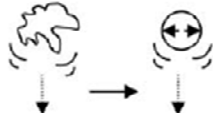
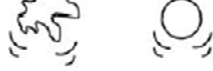
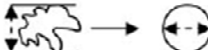
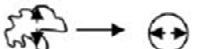
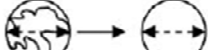
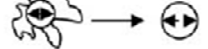
Clay flocs are very sensitive and affected by their environment. Changes in suspension properties and conditions can affect the inter-particle forces and, therefore, result in modification of flocs. Collisions cause flocs to grow and shear forces result in floc breakage (Michaels and Bolger, 1962; Vaezi et al., 2011). Thus, it is desirable to characterize clay flocs in their physical and chemical field condition. However, some size measurement techniques and sample preparation procedures can influence and bias floc size distribution measurements by dilution,

mixing and dispersing (Delago and Matijevic, 1991; Cowles, 2003). Moreover, reproducing the process conditions in an analytical procedure is very difficult to achieve (Cowles, 2003).

2.3 Standard Particle/Floc Size Measurement Methods

Flocs are highly porous clusters of sub-micron primary particles, loosely attached and irregularly structured (Jarvis et al., 2005). However, their size and structure are fundamental to the operation of processes such as settling and dewatering of slurries in oil sands slurries and water treatment and purification (Waite, 1999; Masliyah et al., 2011). Thus, many techniques for structural characterization of flocs and particles of irregular shapes and sizes have been introduced over the years. Due to the irregular shape and three-dimensional structure of flocs, and their sensitive nature, characterizing flocs is challenging (Jarvis et al., 2005). A reported floc size is typically an equivalent diameter that defines the particle as a sphere or circle that is equivalent to the floc in some way. Different diameters are defined and used in the literature. A list of equivalent diameters is shown in Table 2.1 as reported by Jarvis et al. (2005). The comparison between very irregular forms is made possible by using such standard measurements (Jarvis et al., 2005). In the present study, projected area diameter is used for the FPIA and microscopy measurements. The diameters obtained using the Mastersizer are also converted to projected area diameters.

Table 2.1 The most common equivalent diameters for floc characterization (Jarvis et al., 2005)

Floc Diameter	Description	Diagram	Equation for Calculation
<i>Perimeter diameter, d_c</i>	The diameter of a circle with the same perimeter (P) as the measured particle.		$d_c = \frac{P}{\pi}$
<i>Projected area diameter1, d_a</i>	The diameter of a circle with the same projected cross-sectional area (A) as the floc measured in a stable orientation.		$d = 2\sqrt{\frac{A}{\pi}}$
<i>Projected area diameter2, d_p</i>	The diameter of a circle with the same projected area as the floc measured in a random orientation.		
<i>Surface diameter, d_s</i>	The diameter of a sphere having the same surface area (S) as the floc.		$d_s = \sqrt{\frac{S}{\pi}}$
<i>Volumetric diameter, d_v</i> (OR equivalent spherical diameter)	The diameter of a circle with the same volume (V) as the floc measured.		$d_v = \sqrt[3]{\frac{6V}{\pi}}$
<i>Surface-volume diameter, d_{sv}</i>	The diameter of a sphere with the same surface area to volume ratio as the floc.		$d_{sv} = \frac{d_v^3}{d_s^2}$
<i>Free-falling diameter, d_f</i>	The diameter of a sphere having the same density and free-falling speed as the floc in the same fluid at the same density and viscosity.		
<i>Stoke's diameter, d_{st}</i>	The diameter of a free falling particle in the laminar flow range (where $Re < 0.2$).		$d_{st} = \frac{18\mu v}{\rho_f - \rho}$
<i>Feret's diameter, d_F</i>	The (mean) value between pairs of parallel tangents to the projected outline of the particle.		-
<i>Martin's diameter, d_M</i>	The length of the chord parallel to a fixed direction which splits the floc projected area into two equal parts.		-
<i>Circumscribing diameter, d_{sc}</i>	The diameter of the smallest circle that circumscribes the outline of the projected floc.		-
<i>Inscribing diameter, d_i</i>	The diameter of the biggest circle that fits inside the outline of the projected floc.		-

As stated in Chapter 1, it is the objective of the current project to validate the floc size distribution measurements obtained from the FPIA. Accordingly, the floc size measurement results from other techniques should be compared to the FPIA results. In order to choose the suitable techniques, a number of methods, along with their advantages and disadvantages, are described.

2.3.1 Sedimentation

Sedimentation or settling tests provide the equivalent spherical diameter of particles based on their settling velocity using Stokes law. It is a classical method that has long been used for particle characterization. Sedimentation of particles and flocs is governed by their size, density and viscosity of the fluid. The use of this method is well established for solid spheres. However, there are some complications associated with floc sedimentation, since they are far from spherical and have non-negligible permeability. Considering a shape factor can solve the first problem, but the second problem is challenging because of the variable density of aggregates (Bushell et al., 2002). The use of the floc sedimentation technique is becoming more popular as a complementary characterization method to light scattering (Bushell et al., 2002; Gregory et al., 2009). Stokes law can be used to describe a spherical particle and its terminal velocity (Jarvis et al., 2005):

$$v_s = \frac{(\rho_p - \rho_l)gd^2}{18\mu} \quad (2.7)$$

where

v_s : terminal settling velocity, m/s

ρ_p : the density of the particle, kg/m³

ρ_l : the density of the liquid, kg/m³

d : floc diameter, m

μ : viscosity of the suspending medium, m/s

g : acceleration due to gravity, m/s

However, Stokes law does not work well in describing settling of a floc. Hence, a shape factor and a drag coefficient correction are typically added (Wu et al., 2002):

$$v_s = \frac{4d^{D_f-1}C_pg}{3A(\beta)\mu} \quad (2.8)$$

where

v_s : terminal settling velocity, m/s

d : diameter of floc, m

D_f : fractal dimension, $1 \leq D_f \leq 3$

C_p : proportionality constant, kg.m^{-D_f}

ρ_l : density of the liquid, kg/m³

$A(\beta)$: correction factor accounting for advection flow through the floc

μ : viscosity of the suspending medium, Pa.s

g: acceleration due to gravity, m/s^2

Michaels and Bolger (1962) used the sedimentation method to calculate the floc sizes of different kaolinite suspensions. Settling velocity was determined by measuring the change of height of the interface between the slurry and supernatant with time. Nasser and James (2006) also utilized this technique to study the settling behavior and gel point of kaolinite suspensions in un-networked and fully networked states.

This method requires a large amount of sample and is time consuming. Furthermore, it provides a mean floc size that may not be representative of a broad size range or irregularly shaped samples. Due to the shape of clay particles, they settle more slowly than spherical particles of the same volume. In this way, the size of the particles is underestimated. Therefore, this method is not a suitable one for validating the FPIA performance.

2.3.2 Individual Particle Sensors (Sensing Zone Techniques)

In this method single particles pass through an orifice into an electric field (electrical sensing) or through a light beam (optical sensing) and are measured by individual particle sensors (Jarvis et al., 2005).

In the electro-zone sensing (electric field) method, the particles, suspended in a dilute electrolyte solution, pass through an electric field which is created by applying voltage across the orifice. The particles cause resistance in the field that is proportional to the particle volume. The resulting measurement is a number distribution of the equivalent volume sphere diameter. More than one particle at a

time passing through the aperture will cause errors; therefore, diluted suspensions should be used. The most common instrument utilizing this method is called the Coulter Counter (Jarvis et al., 2005; Rhodes, 2008). Leentvaar and Rebhun (1983) stated that compared with optical analysis, the Coulter Counter underestimates the floc size, since it just measures the volume of the solid in the floc, ignoring the pores and water. Yuan et al. (2009) confirmed this conclusion by comparing the sludge floc size distributions obtained using a Coulter Counter and optical microscopy.

In the photo-zone (optical sensing) method, particles attenuate a part of the light beam while passing through the orifice. The amount of attenuated light is proportional to the particle size. This method can measure particles larger than 10 μm . However, the use of this technique is limited and few examples of floc size measurement with this method exist, because the narrow aperture leads to an artificially narrow size distribution (Jarvis et al., 2005). Therefore, this method is not considered for floc size measurements in the present study.

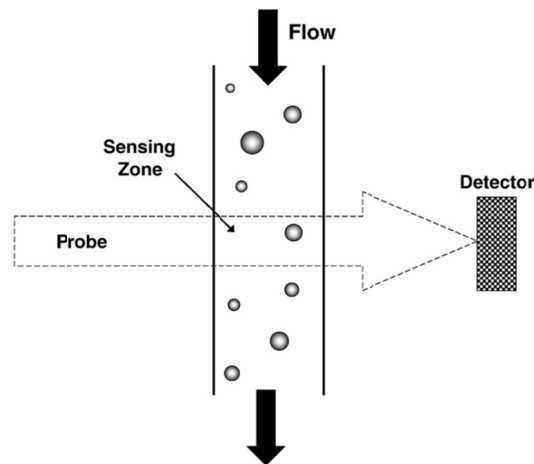


Figure 2.3 Illustration of particle counting and sizing by electrical or optical sensing zone method (Gregory, 2009)

2.3.3 Microscopy (Direct Optical Methods)

Microscopy allows individual particles to be viewed and analyzed. It gives a better indication of the shape and irregularity of the flocs under investigation (Jarvis et al., 2005). However, it is still very much operator dependent (Jarvis et al., 2005).

This method is usually combined with image analysis to allow for more rapid measurement of a large number of flocs. The basic stages of image processing and analysis are presented in Figure 2.4 (Jarvis et al., 2005). The combination of microscopy and image analysis is one of the techniques used for floc size measurement in the present study. After the images are taken, the other steps are done manually through software. The Flow Particle Image Analyzer (FPIA), utilized in this project, also uses the automated combined method of microscopy and image analysis. All the steps are done automatically before the data can be exported.

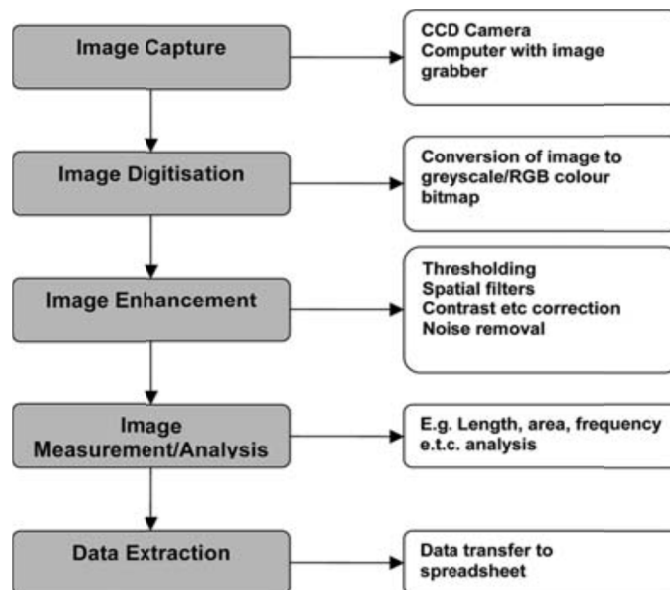


Figure 2.4 The stages of digital image analysis (Jarvis et al., 2005)

The microscopy method can be further divided into the categories of light microscopy and electron microscopy.

Light Microscopy

Light microscopy is one of the earliest and most commonly used methods for particle size measurement. It can capture images of many particles with resolution limited by light wavelength. The convenience, flexibility and economy promote the use of this method. A small depth of field does not always allow an entire three dimensional structure of flocs or particles to be in focus. In some cases a cover slide is used on top of the floc sample to resolve the depth of field problems. It is possible that the compression from the cover slide changes the structure of flocs. The other problem, which is common between all ex-situ measurement techniques, is that the flocs may settle onto one another and not be distinguished as different particles (Jarvis et al., 2005). Yuan et al. (2009) used optical microscopy to study floc sizes and obtained floc size distribution curves. This method combined with image analysis is employed to measure kaolinite floc sizes and generate floc size distribution curves in this study.

Electron Microscopy

In electron microscopes, electron beams replace the light beam of a conventional microscope. Transmission electron microscopy (TEM) and scanning electron microscopy (SEM) are the two branches of EM. Electron microscopes can measure particle sizes from 1 nm to 5 μm (Berg, 2010). The increased magnification and resolution help better understand floc microstructure as well as the interactions between primary particles. The disadvantages of electron

microscopy are time and expense required both for preparation and capturing images of a limited number of flocs. Moreover, flocs may be damaged because of drying, coating, freezing and resin embedding (Jarvis et al., 2005).

Delago and Matijevic (1991), Cheetham et al. (2008), Zbik et al. (2008) and Nemati et al. (2010) used SEM as a size measurement method for different samples of particles and flocs. Delago and Mitijevic (1991) and Dur et al. (2004) reported the use of TEM as their size measurement method. However, due to the disadvantages mentioned this method is not chosen for floc size measurements in this study.

2.3.4 Light Scattering

When light passes through a suspension, some of it is adsorbed by the particles of the suspension, some is scattered, and the rest passes through the mixture. The light scattering pattern differs depending on particle size, nature of particles and suspending medium (Gregory, 2009). In this technique, the predicted scattering pattern from an optical model is compared with the measured one to generate the particle size (Bushell et al., 2002). The most popular devices (such as Malvern Mastersizer) use light scattering to measure particle size. In these instruments a laser beam passes through the suspension where size of the particles is inversely related to the angle of scattered light (diffraction angle). The intensity of the scattered light is then recorded by the array of detectors and sizes are calculated with the help of an optical model (Mastersizer-2000 Operators Guide, 1999; Jarvis et al., 2005). The amount of lost light is controlled by the size and concentration of the particles in the mixture. It is measured as laser obscuration in

the instrument and is recommended to be between 10-30% (Jarvis et al., 2005). Light scattering is fast, easy and inexpensive, and has been widely used for particle and floc size measurement by researchers (Delago and Matijevic, 1991; Wen et al., 2002; Wu et al., 2002; Cheetham et al., 2008; Govoreanu et al., 2009). However, it requires very dilute samples to avoid multiple scattering. The laser diffraction based Mastersizer technique is utilized in this study to be compared with the FPIA.

2.4 Particle Size Measurements in the Oil Sands Industry

In order to characterize oil sands deposits and optimize the extraction process condition, PSD measurements are conducted (Sanford, 1983; Cowles, 2003; Masliyah et al., 2011). As reported by Liu (1989), concerns regarding the particle size measurement come from the significant impact of fine solids on the extraction process and the fact that these particles are the most difficult to remove from the produced oil.

In the following sections, the role of clays in different stages of oil sands mining and bitumen extraction, as well as tailings management is described. Also, the current PSD measurement method used in industry is explained. The advantages of the FPIA, used in the present research for floc size measurement, are also discussed.

2.4.1 Role of Clays in Oil Sands Mining and Bitumen Extraction

Clay minerals affect the deposition velocity and pressure drop in hydrotransport pipelines, flotation efficiency in separation processes (gravity separation,

mechanical flotation and hydrocyclones), tailings settling behaviour and dewatering (Scott et al., 1985; Kotlyar et al., 1993; Mercier et al., 2008; Kaminsky et al., 2009). Role of clays and their sizes in different stages of bitumen extraction process and tailings management are described in this section.

Effect of Clay on Design and Operation of Hydrotransport Pipelines

Deposition velocity, which is the minimum velocity that prevents coarse solid deposition in the pipeline, and pressure gradient are two key parameters in design and maintenance of hydrotransport pipelines (Sanders and Gillies, 2013). The particle size distribution affects the deposition velocity and pressure drop (Sanders et al., 2004; Masliyah et al., 2011). Pipeline performance is also a function of fines content (Sanders et al., 2004). Increasing the fines content of the slurry decreases the deposition velocity (Masliyah, 2011). The carrier fluid (fines + water) viscosity is also a significant parameter used in the prediction of pressure loss and deposition velocity by the SRC (Saskatchewan Research Council) Two-Layer model (Gillies et al., 2004; Sanders and Gillies, 2013). The viscosity of the carrier fluid, in turn, is influenced by fine non-settling particles (Shook et al., 2002; Asadi, 2012). It is best to operate hydrotransport pipelines just above the deposition velocity. If the pipeline is operated under the deposition velocity unexpected pipeline failures can occur. On the other hand, velocities higher than the deposition velocity can cause high frictional energy loss and pipe wear (Wilson et al., 2006).

Effect of Clay on Primary (Gravity) Separation

Separation of aerated bitumen from coarse particles mainly takes place in a primary separation vessel (PSV). The density difference between aerated bitumen and the carrier fluid leads to rise of bitumen globules. Similarly, density difference and particle size governs the fall of coarse solids through the carrier fluid. Depending on the amount of fine clays in the carrier fluid, its viscosity can increase and hinder the rise of aerated bitumen resulting in decreased flotation efficiency and oil recovery (Schramm, 1989; Adeyinka et al., 2009). A thick, highly viscous suspension is occasionally formed in the vessel that inhibits the flotation of aerated bitumen and settling of solids. This operational condition is called sludging of the separation vessel (Tu et al., 2005; Adeyinka et al., 2009).

Effect of Clay on Mechanical Flotation

The middlings stream from the PSV, containing recoverable bitumen and clay-containing carrier fluid goes through mechanically agitated flotation cells. Reaerated bitumen from the flotation cells recirculates to the primary separation vessel. Residual bitumen is recovered and clay fractions are disposed of (Masliyah, 2011). Fine clays are present in flotation cells and affect the bitumen recovery by altering the viscosity of the suspension. As Ding et al. (2006) report, oil sands bitumen recovery decreases in the presence of clays and divalent cations. Kasongo et al. (2000) also confirms the same result for montmorillonite clay. A flotation test in a Denver flotation cell showed a significant difference in bitumen recovery for two types of good processing ore (containing 4% fine solids) and poor processing ore (containing 40% fine solids) (Zhou et al., 2004).

Effect of Clay on Hydrocyclones

The hydrocyclone is another device used for separation processes, combining shear and gravity separation. It is utilized to produce consolidated tailings by removing coarse solids from the tailings stream and forming a high-concentration underflow (Mikhail et al., 1997). Clay particles are present in the feed stream of the hydrocyclones. As stated by Bradley (1965), variables such as solid concentration, particle size and liquid medium viscosity influence the performance of hydrocyclones. High solid concentration hinders the settling and changes the character of the underflow stream, as well as pressure drop and capacity of the hydrocyclone. High medium viscosity (to which clay particles contribute significantly) also results in lower separation efficiency (Bradley, 1965).

Effect of Clay on Conventional Tailings

Tailings are an inevitable outcome of the current extraction processes (Sobkowicz, 2011). Generally, three streams of oil sands tailings end up in the tailings ponds: coarse tailings from the primary separation vessel, fine tailings from secondary and tertiary bitumen recovery, and tailings from the froth treatment unit (Kasperski, 1992; Mikula et al., 2008). The coarser particles settle in tailings ponds and form beaches. Mature fine tailings (MFT) are produced after a few years and will remain for decades (Powter et al., 2011). This material contains approximately 62% water, 3% residual organics (bitumen and solvents) and 35% solids, of which about 97% are fine solids or clay which govern the tailings behavior (Thomas et al., 2010). Clay minerals and their

flocculation/dispersion behavior govern the sedimentation, segregation and consolidation behavior of fine tailings (Uhlik et al., 2008; Masliyah et al., 2011; Powter et al., 2011). Viscosity of the carrier fluid also influences the consolidation of fine tailings (Mihiretu et al., 2008; Masliyah et al., 2011;) which, in turn, is affected by fine particles (Shook et al., 2002; Jeeravipoolvarn et al., 2008).

Effect of Clay on Thickened Tailings

Storage of large volumes of conventional tailings is costly and poses environmental problems long-term. Thus, the goal in oil sands tailings treatment is to develop a faster way to remove water in order to provide a dry surface for further reclamation (Powter et al., 2011). In producing thickened tailings, suitable flocculants are used for flocculation of fine solids, which accelerates water separation. The warm water is recycled and reused in the extraction process and the flocculated paste-like sediment is pumped to a disposal pit and allowed to consolidate to a dry landscape (Xu and Hamza, 2003; Masliyah et al., 2011). As a result of this process, energy input, greenhouse gas emission, land disturbance and, finally, the overall costs are reduced (Chalaturnyk et al., 2002; Xu and Hamza, 2003). As described, this whole process primarily depends on flocculation of fine solids and its success is intimately related to floc size and structure (Vaezi et al., 2011).

2.4.2 How are Particle Size Measurements Currently Made?

Laser diffraction has been adopted as the standard method of PSD measurement in the industry because of the rapid, reproducible measurements, the capability to handle large numbers of samples and wide range of detectable sizes (Liu, 1989;

Cowles, 2000). During the sample preparation procedure the samples are sonicated and dispersed. Clay flocs are broken down to primary particles with an ultrasonic probe and chemical dispersants (Bulmer and Star, 1979; Cowles, 2003). In this way the size measurement would not be affected by the sample preparation procedure prior to the measurement (Cowles, 2003).

2.4.3 Anticipated Advantages of Utilizing the FPIA in Oil Sands Mining and Bitumen Extraction

The use of the Sysmex FPIA-3000 for floc size measurement can offer advantages over other sizing and characterization methods. The device measures and analyzes large number of images and particles in a short time. It can measure up to 360,000 particles in less than 3 minutes. Also, it just needs a small amount of sample (1-5 mL). The FPIA can measure not only the particle size distribution but also shape parameters. This technique can measure multiple parameters of a large number of particles/flocs simultaneously. Moreover, the FPIA is capable of orienting particles with their larger face towards the camera, while other devices lack this option. With the consistent (less random) particle orientation, more reliable and accurate measurements are determined. All particle images are stored and are accessible through the FPIA software. Therefore, further visual understanding of the measurements is provided by the analyzed pictures of particles. Finally, and perhaps most importantly, it allows measurement of particles in their natural aggregated state without intentionally trying to break down the flocs to primary particles.

2.5 Selection of Kaolinite for This Project

The significance of kaolinite as a main component of oil sands clay has made it a good option for this study. Moreover, it had been used in previous studies to represent the clay fine solids with reproducible results (Kasongo et al., 2000; Vaezi, et al., 2011; Asadi, 2012).

2.5.1 Composition of Oil Sands Fine Clays

Clay minerals in the oil sands are comprised mainly of kaolinite and illite, as well as trace amounts of smectite and montmorillonite (Dusseault and Scafe, 1979; Ignasiak et al., 1983; Schramm, 1989; Chalatrunk et al., 2002; Kaminsky et al., 2009; Masliyah et al., 2011;). Their composition is illustrated in Figure 2.5.

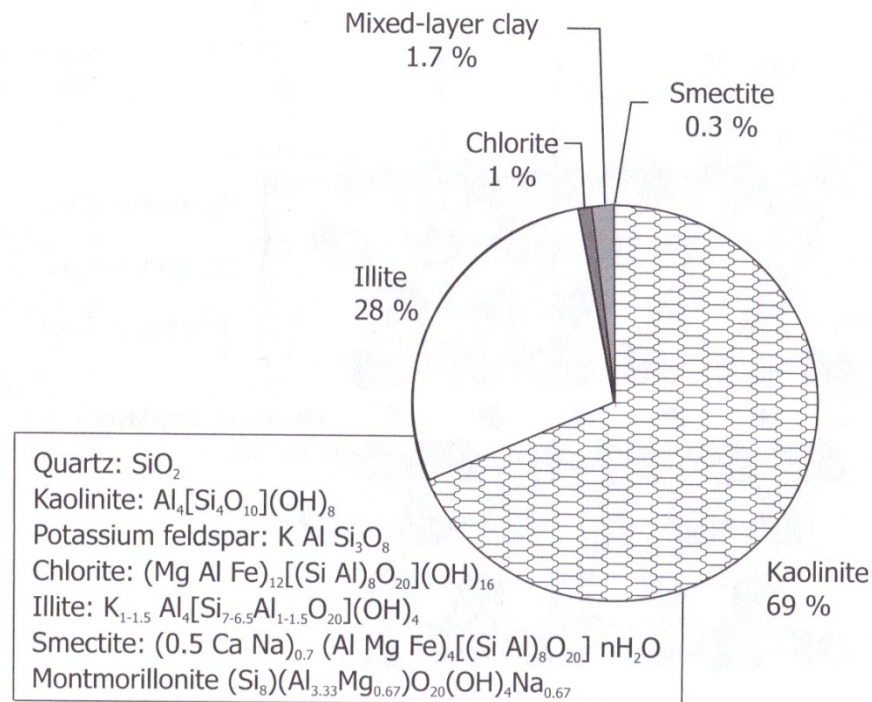


Figure 2.5 Characterization of clay minerals in oil sands ore (Masliyah et al., 2011)

2.5.2 Previous Experience with Kaolinite

Several researchers (Zbik et al., 2008; Mihiretu et al., 2008; Mohamedelhassan, 2008) utilized kaolinite as clay fine solids in their studies. Mihiretu et al. (2008) showed that a kaolinite suspension is representative of an actual oil sands clay slurry by comparing the flow characteristics of kaolinite slurry with those of tailings samples. Kaolinite suspensions are well-characterized by researchers working in the NSERC Industrial Research Chair in Pipeline Transport Processes (e.g. Vaezi et al., 2011; Rahman, 2011; Asadi, 2012; Marefatallah, 2013).

2.5.3 Properties of Kaolinite

Kaolinite has thin, roughly hexagonal (as shown in the SEM image in Figure 2.6) platelet primary particles. It is a hydrous aluminum silicate with $\text{Al}_2\text{O}_3 \cdot 2\text{SiO}_2 \cdot 2\text{H}_2\text{O}$ composition (Michaels and Bolger, 1962). The length-to-thickness ratio of the primary particles is between 10:1 and 30:1, with the largest dimension of 0.1-2 μm (Nasser and James, 2006). The faces (basal surfaces) of the kaolinite plate carry a permanent negative charge, while the charge on the edge surfaces depends on the pH of the suspension (van Olphen, 1977).

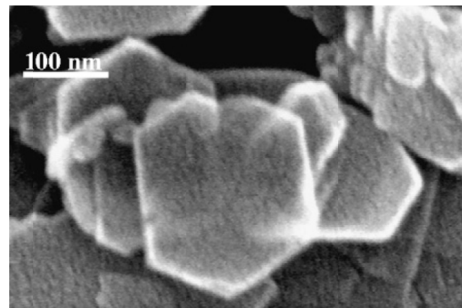


Figure 2.6 High resolution SEM micrographs of kaolinite (Zbik et al., 2008)

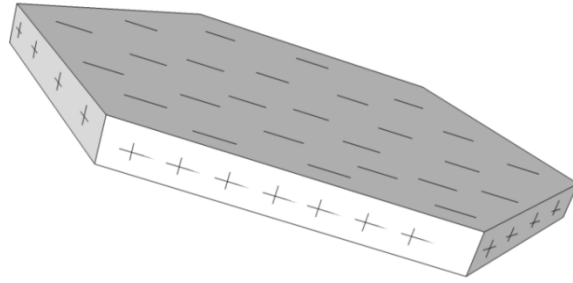


Figure 2.7 Kaolinite charge distribution at low pH (Nasser and James, 2006)

Three different modes of particle association can occur: face-to-face (F-F), edge-to-face (E-F), and edge-to-edge (E-E), caused by different combinations of the electric double layer interactions and different van der Waals forces. The different modes of particle association are illustrated in Figure 2.8. It is notable that only E-E and E-F types of particle-particle association modes are considered as "flocs" and the ones with F-F association are, in some instances, referred to as "aggregates" (van Olphen, 1977).

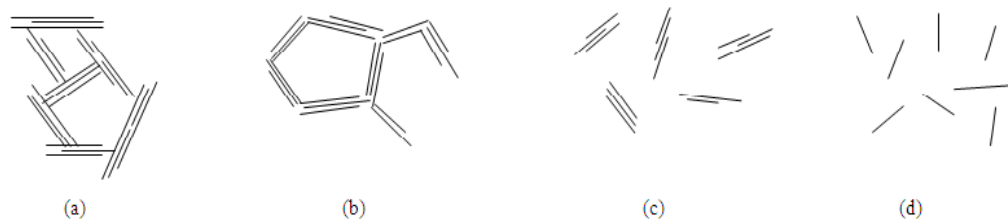


Figure 2.8 Modes of particle association (a) E-F flocculated and aggregated (b) E-E flocculated and aggregated (c) aggregated but deflocculated (F-F) (d) dispersed and deflocculated (van Olphen, 1977)

Acidic conditions cause alumina at the edges of the plate to bind to hydrogen ions in the environment and become positively charged. Therefore, there would be electrostatic attraction between edges and faces that results in a highly expanded floc structure, called "card-house" (Michaels and Bolger, 1962).

Alkaline conditions, on the other hand, cause the edges to become neutral or negatively charged, and in the case where the electrolyte concentration is low, the particles deflocculate in the absence of an attractive force to hold them together.

At high electrolyte concentrations, regardless of pH, primary particle platelets attach to each other with their basal surfaces, forming a face-to-face floc structure, called "card-pack". This adherence is due to electric double layer compression and, thus, electrostatic repulsion reduction (Michaels and Bolger, 1962).

The presence of cations such as Ca^{2+} and Na^{+} in the environment of suspensions will increase the settling rates owing to particle segregation (Zbik et al, 2008). Electrolyte addition leads to compression of electric double layer and flocculation, which is directly related to and governed by concentration and valence of the ions (van Olphen, 1977). Calcium chloride (CaCl_2) is used as a coagulant in the present study.

2.5.4 Parameters Affecting Kaolinite Floc Size Distribution

Sample concentration, sample pH and addition of coagulant (electrolyte) affect kaolinite floc size distribution. These factors are discussed in the following sections.

As concentration increases the distance between particles decreases, resulting in stronger interactions (Adeyinka et al., 2009). As the distance between particles decreases, more collisions occur meaning an increased frequency of “successful” collisions that lead to large floc formation (Masliyah and Bhattacharjee, 2006). Therefore, higher solids concentration results in a larger number of large flocs.

Sample pH and electrolyte concentration also affect kaolinite particle size distribution. In acidic condition, regardless of electrolyte concentration, particles flocculate, while in basic pH range, particles can be found in dispersed form in the absence of added salts, or in flocculated form at high electrolyte concentrations. Depending on the magnitude of attractive or repulsive electrostatic interaction, which is governed by the chemistry of the mixture, and attractive van der Waals forces between particles, different types of associations are formed (as also previously described in Section 2.5.3) (Nasser and James, 2006).

As a result of increasing the pH of the mixture, kaolinite particles edges become neutral or negatively charged and deflocculation occurs (Nasser and James, 2006). Nasser and James (2006) also reported that at pH 9 all the flocs are broken down. At high pH ranges (low electrolyte concentration), there are mostly primary kaolinite particles present in the suspension and a small number of face-to-face flocs (Nasser and James, 2006).

By adding HCl to the suspension, the pH decreases and "card-house" flocs are formed.

Coagulant addition typically causes "card-pack" flocs to form, regardless of the pH. Because of addition of coagulant (CaCl_2 in this study), the thickness of the electric double layer decreases and the electrostatic repulsion between particles decreases. Consequently, particles stick to each other along their basal surfaces forming face-to-face floc types (Nasser and James, 2006).

Face-to-face floc types are thicker and denser, whereas edge-to-face and edge-to-edge associations make larger and lighter (less dense) flocs (Nasser and James, 2006).

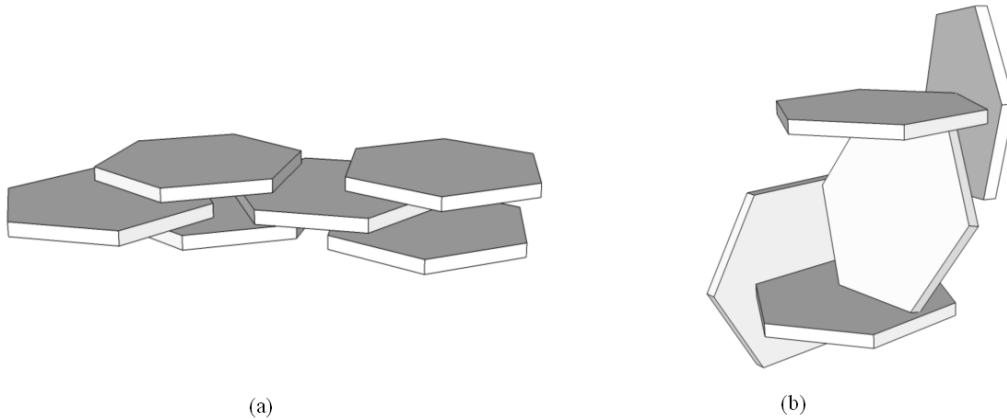


Figure 2.9 Kaolinite flocs in (a) card-pack structure (b) card-house structure (Nasser and James, 2006)

3 Experimental Method

3.1 Materials

The kaolinite used in this study to prepare suspensions comes from Dry Branch Kaolin Clay Company, Georgia, USA. In order to ensure consistency, a single bag of kaolinite is used as the source for all samples used in all the experiments. The inherent density of the kaolinite is 2560 kg/m^3 as reported by the supplier.

Silica flour (Sil 325) is provided by SIL Industries. It is used as non-flocculating irregular-shaped particle for comparing particle size measurements obtained with different instruments/methods. Table 3.1 presents the information regarding the properties of the sand. The Andreasen pipette technique was used to measure the particle size distribution (Gillies, 2012).

Table 3.1 Properties of silica flour (Asadi, 2012)

Particle size, $< 3 \mu\text{m}$	6 %
Particle size, $> 42 \mu\text{m}$	34 %
d_{50}	20 μm
Silica suspension pH at 20% concentration	8.0-8.5
Particle density	2650 kg/m^3

De-ionized (DI) water freshly produced using the “Elix Advantage Water Purification System” (Millipore, France) was used as the dispersing medium for all suspensions. The specifications of the de-ionized water, as reported by Asadi (2012), are presented in Table 3.2.

Table 3.2 Properties of de-ionized water (Asadi, 2012)

pH	6.02
Conductivity/Resistivity	2.35 $\mu\text{S}/\text{cm}$
Salinity	0.01 psu
TDS	1.6 mg/L

Additives are used to prepare the desired conditions in suspensions for making different types of flocs. Hydrochloric acid, HCl, (0.1 M solution) is used to adjust the pH and produce highly expanded F-E (card-house) flocs. Sodium hydroxide, NaOH, (0.1 M solution) is used to set the alkaline pH for some of the samples, to fully disperse the particles. Calcium chloride, CaCl_2 , (0.1 M solution) is used as coagulant in some cases to make highly coagulated suspensions.

The FPIA sheath fluid is an electrolytic solution composed of surfactant (0.6 g/L), sodium chloride (7.1 g/L), Tris buffer (2.0 g/L), and EDTA-2K (0.2 g/L) (Sysmex FPIA-3000 Operator's Manual, 2006). It is used in the FPIA-3000 to orient the particles. It is also used as rinse fluid.

Polymer microspheres from Duke Scientific Corporation are used for FPIA instrument calibration. The mono-sized polystyrene latex beads (Model 5200A) are 2 μm in diameter. The suspension characteristics are presented in Table 3.3 as provided by the supplier. The suspension also contains a trace amount of surfactant to inhibit agglomeration and promote stability. These particles are also used for size measurement results comparison using the FPIA, Mastersizer and microscope, since they are spherical, mono-sized and non-flocculating particles.

Table 3.3 Polymer microsphere suspension properties

Mean particle diameter	2 μm
Specific gravity	1.05
Refractive index	1.59
Suspension concentration	10 wt%
Material	Polystyrene
Shape	True sphere

3.2 Apparatus

The Sysmex FPIA (Flow Particle Image Analyzer) is used in this study to measure floc size distributions. As discussed in the objectives, in order to validate its performance it is compared with other techniques. The Malvern Mastersizer and Carl Zeiss microscope are chosen for this purpose. The three devices are described in Sections 3.2.1 to 3.2.3.

3.2.1 Sysmex Flow Particle Image Analyzer (FPIA)

A FPIA-3000 (Malvern Instruments Ltd, UK) was utilized for floc size measurement. The results from the instrument are then compared with results from other devices (Malvern Mastersizer and Carl Zeiss microscope). Since the FPIA has rarely been used for clay floc size measurements, it is important to study the accuracy of the instrument and the extent of changes it produces in the flocs during measurement.

The FPIA-3000 combines flat sheath flow formation and image processing technologies. It is used in the field of medical, chemistry, physicochemistry and general industry. It can automatically analyze up to 360,000 particles in a short

amount of time. Each run takes approximately 170 seconds. It measures size ranges from 0.8 to 300 μm (Sysmex FPIA-3000 Operator's Manual, 2006).

A dilute suspension of particles that is introduced to the sample chamber is transferred to a transparent flat sheath flow cell by the sample aspiration syringe (jet nozzle). The sample forms a flat laminar flow surrounded by the sheath fluid. In this way, all particles are placed in the same focusing plane so that focused images of all particles can be captured. Also, the sheath flow orients all particles with their largest surface facing the camera. Approximately 130 mL of sheath fluid is used during each test to rinse the flow cell and to guide the flow of the sample through the chamber (Sysmex FPIA-3000 Operator's Manual, 2006). Introduction of the suspension to the measurement cell and its alignment by the sheath fluid is illustrated in Figure 3.1.

A strobe light flashes every 1/60 second. The duration of the pulse light irradiation is 2 μs . Therefore, moving particles can be captured in focus as still images. The images are captured with a charged couple device (CCD) camera (Sysmex FPIA-3000 Operator's Manual, 2006).

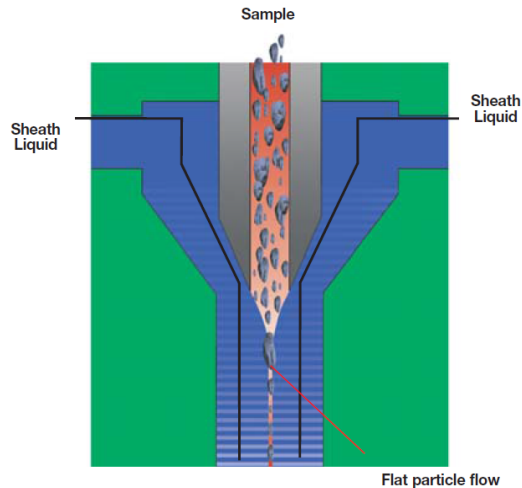


Figure 3.1 Illustration of flat particle flow (Sysmex FPIA-3000 Brochure, 2013)

The images are then digitized, measurement noise is reduced by applying a smoothing filter, the shades are corrected, the particle edges are sharpened, the images are binarized and, finally, the edges of the particles are traced and particle sizes are determined (Sysmex FPIA-3000 Operator's Manual, 2006). Thresholding and edge definition are two important steps of image extraction. Particle pixels are separated from background pixels using the difference in gray scale levels. Pixels darker than the threshold value (usually around 90% of the background value) are considered as particle, and pixels lighter than the threshold value are determined as background. For edge definition, the particle perimeter is traced by assigning a value to each pixel depending on the surrounding pixels. The technique of assigning different values to outer pixels is known as chain code, and gives a more precise perimeter value (Sysmex FPIA-3000 Brochure, 2013).

The images are then sent to the image analysis unit to calculate particle size and form parameters. Morphological parameters such as circle equivalent diameter,

circularity, convexity, and their statistical distributions help fully characterize the particles. All images along with all other sizing and morphological information are saved and are accessible through the FPIA-3000 software (Sysmex FPIA-3000 Brochure, 2013).

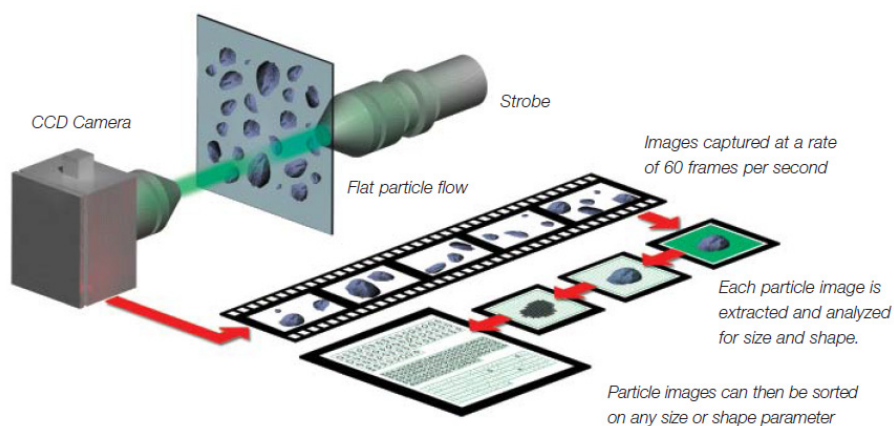


Figure 3.2 Mechanism of capturing, extracting and analyzing the images (Sysmex FPIA-3000 Brochure, 2013)

The required sample volume for testing with the FPIA-3000 is 1 to 5 mL. Since the device cannot measure more than 36,000 particles per μL , the samples should be fairly dilute for the system (Sysmex FPIA-3000 Operator's Manual, 2006). Some examples of suspension concentrations tested in the FPIA include 1 g/L mineral trioxide aggregate (Komabayashi and Spangberg, 2008), 0.67 g/L calcium hydroxide (Komabayashi and Spangberg, 2009), 40 g/L kaolinite (Marefatallah, 2013) and 0.007 g/L sipernat powder (Zeilina, 2011).

The FPIA-3000 is built with a 10x objective lens. It also has optional 5x and 20x objective lenses. Each lens can be used in high power field (HPF) and low power field (LPF) mode. The range of sizes detectable by each lens is described in Table 3.4.

A mixing rotor can be found in the sample dispersion unit. The speed of the mixer can be set from 50 to 750 RPM. There is also an ultrasonic probe in the sample chamber whose intensity can be adjusted to disperse the particles (Sysmex FPIA-3000 Operator's Manual, 2006).

Table 3.4 FPIA-300 measuring range with high or low magnification lens unit (Sysmex FPIA-3000 Operator's Manual)

Magnification unit	Particle size, HPF mode (μm)	Particle size, LPF mode (μm)
20x (high magnification unit)	0.8-20	4.0-80
10x (standard unit)	1.5-40	8.0-160
5x (low magnification unit)	3.0-80	16.0-300

Standard Operation Procedures (SOPs) determine and manage measurement conditions, analysis conditions, hardware settings, and other setting information related to the measurement such as mixing speed, sonication intensity, threshold value and power field (Sysmex FPIA-3000 Operator's Manual, 2006). In the SOP used for all FPIA experiments in this study, the high power field mode of the 10x lens is chosen, the mixing speed is set to 300 RPM, and the internal sonication is turned off in order to prevent floc breakage.

Finally, the raw data from image processing stage is extracted, statistically analyzed and calculated to obtain particle diameters and number-based frequency distributions. An Octave code by J.S. Kroll-Rabotin is used to convert the particle area data to equivalent circle diameter. It divides flocs into defined bins, and, finally, produces cumulative and frequency size distributions as the output. The

code is presented in Appendix A. The FPIA data were not directly used. In order to compare the FPIA results to other devices measurements, the Mastersizer bin sizes were utilized for PSD generation with all devices. The results are presented in form of frequency ratio versus particle size (Equation 3.1) and its cumulative form (as reported in Chapters 4 and 5).

$$Frequency\ Ratio = \frac{n_i}{\sum n_i} = \frac{n_i}{n_T} \quad (3.1)$$

where:

i: bin number

n_i : number of particles in bin ‘i’

n_T : total number of particles

3.2.2 Malvern Mastersizer

The Mastersizer (Malvern Instruments Ltd, UK) is another instrument utilized in this study. The floc size distribution measurements from this technique are compared with the FPIA results. It is a laser diffraction based device. As described in the Mastersizer operators guide and brochure:

“The Mastersizer has been designed to measure the size of particles – or more specifically, the distribution of different sizes within a sample.”

“The Mastersizer 2000 is a practical, reliable solution to the everyday particle sizing needs of industry. It is a flexible and modular, but fully integrated, particle sizing system with assured measurement performance from submicron to

millimeter, wet or dry, from milligram quantities of precious pharmaceuticals to the measurement of bulk chemicals and minerals.”

The Mastersizer-2000 and its accessory dispersant Hydro 2000SM are utilized in the present study. It can measure particles in size range of 0.02 – 2000 μm . This technique is frequently used by researchers for particle size distribution measurements (Wu et al., 2002; Cheetham et al., 2008; Govoreanu et al., 2009; Vdovic et al., 2010).

Measuring a sample with the Mastersizer includes three procedures. Sample preparation, dispersion and dilution is the first stage, accomplished in the sample dispersion unit. Next is the measurement stage where the scattering pattern of the sample is captured with an array of detectors. Finally, the raw data obtained from the measurement are analyzed by the Malvern Mastersizer software.

Mastersizer measurements are made using Standard Operating Procedures (SOPs), which are defined by the user and are easily programmed into the software in order to ensure measurement consistency. The SOPs control the accessories and prompt the operator to perform tasks (Mastersizer-2000 Operators Guide, 1999). They are used to set or specify the dispersion unit type, dispersion settings, number of measurement runs, time gap between runs, use of dispersing agents or ultrasonication, measured materials and their optical properties, measurement time, dispersant medium and its optical properties (Sperazza et al., 2004; Mastersizer Brochure, 2013).

When the sample is ready and the SOP is started, the SOP dialog asks to rinse the system and fill the tank of the accessory. Then, it will measure the background and align the optical system. Next, it will ask for introduction of the sample to the tank. Specific quantity of the sample should be added until the laser obscuration bar is in the green section i.e. between 10-20 % obscuration level. After pressing the start button, the measurement stage begins. When the particles get to the laser in the optical unit, they scatter the light at an angle inversely proportional to their size. As particle size decreases, the diffracted angle increases logarithmically (Storti and Balsamo, 2010). The intensity and energy of the scattered light is directly related to the particle size. Thus, distribution of the diffracted light intensity captured by the detectors is connected with the particle size distribution (Goossens, 2008; Sochan et al., 2012). The detectors take snap-shots of the scattering pattern of particles passing through the beam at that particular time. There are different detectors employed to detect the scattering light from a range of angles. Since only one snap-shot may not be a good representative of the scattering pattern, the Mastersizer takes over 2000 snap-shots for one measurement (each taking 1 ms) and averages the outcome. The raw data that are used for particle size calculation are collected in the optical unit, and finally analyzed by the Malvern software. The Malvern software governs the instrument during a measurement, processes the collected raw data and transforms it to a size distribution. A schematic illustration of the optical unit is shown in Figure 3.3.

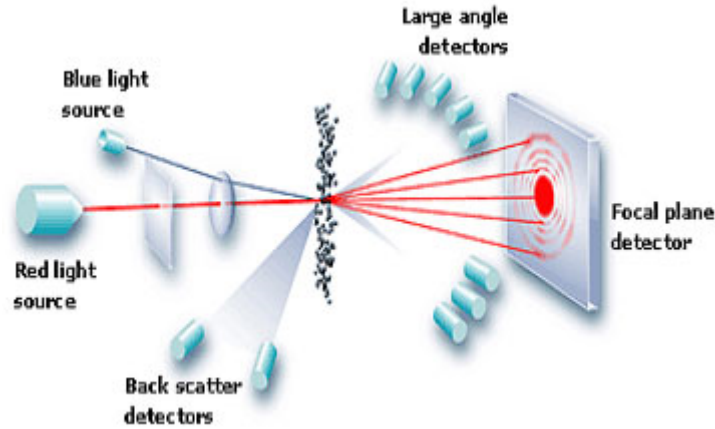


Figure 3.3 Mechanism of laser diffraction operation inside the Mastersizer (Mastersizer Brochure, 2013)

Mie theory is used to convert the light scattering data into particle size distribution. It is an accepted theory for accurate prediction of light scattering behavior of all materials under all conditions. If the size of a particle and its detailed structure is given, the way it scatters light can be predicted. The Mastersizer uses the above theory by capturing the actual scattering pattern from the particles. Provided that the refractive index and absorption of the floc material and the refractive index of the dispersing medium are known, the size of the particles that created the pattern can be calculated (Storti and Balsamo, 2010; Mastersizer-2000 Operators Guide, 1999).

The reported result is in the form of volume percent versus particle size (in terms of equivalent spheres). The particles are divided into 100 size fraction bins. The results are volume based; the corresponding y-value for a specific size range indicates the percentage of total volume of all particles with diameters in that range in total volume of all particles in the distribution:

$$Volume (\%) = \left(\frac{V_i}{\sum V_i} \right) \times 100 \quad (3.2)$$

In order to be able to compare the Mastersizer's results with the results obtained from the FPIA, they must be converted to same diameter basis. Thus, the particle size distribution information is exported and an Octave code is used to convert the volume percent to frequency ratio and produce cumulative and frequency size distribution graphs. The code is presented in Appendix A.

Suppose there is a specific volume (V_i) within any bin 'i'. The volume of a single "representative" particle in that bin is $V_{p,i}$. The number of particles in that bin is thus:

$$n_i = \frac{V_i}{V_{p,i}} \quad (3.3)$$

By combining Equations 3.1 and 3.3, the frequency ratio can be calculated using:

$$\text{Frequency ratio} = \frac{n_i}{\sum n_i} = \frac{\frac{V_i}{V_{p,i}}}{\sum (\frac{V_i}{V_{p,i}})} \quad (3.4)$$

where:

n_i : number of particles in bin 'i'

$V_{p,i}$: volume of a single "representative" particle in bin 'i'

V_i : volume of particles in bin 'i'

Values of V_i are available from the Mastersizer data and $V_{p,i}$ can be calculated using the mean particle size for each bin.

Light scattering data and consequently size distribution information can be affected by a number of factors. Mixing inside the sample dispersion unit can

affect the flocs (Storti and Balsamo, 2010). The range of stirrer speed in the sample chamber for this system is 400-3000 RPM. The impeller speed is set to 400 RPM for these tests. This choice is discussed in the next chapter. Another important parameter is dilution with dispersion medium (usually de-ionized water) inside the sample dispersion unit (Storti and Balsamo, 2010). In this study, in an attempt to prevent floc breakdown, the sample chamber is filled with the filtrate of the same sample that is being tested. In this way, the water chemistry of the sample does not change and floc breakage due to change of chemistry is avoided. However, the sample is still diluted. To overcome this problem and ensure consistency between the tests conducted with different devices, the FPIA samples are also diluted with the same volume of filtrate, just before the measurement is made.

3.2.3 Carl Zeiss Microscope

The microscope, Axio Scope.A1 (Carl Zeiss, Germany), used in this research is a universal microscope designed especially for biological, medical and material studies applications.

The transmitted light/bright-field microscopy is the most common method of all optical microscopy methods. With this method, high contrast or tinted samples can be examined easily and quickly. In order to get the best performance, condenser, field diaphragm and aperture diaphragm should be adjusted according to the Köhler illumination principle (Axio Scope.A1 Operating Manual, 2008).

The microscope has three lenses (10x, 40x and 100x). Together with the built-in 10x lens, it is possible to see the particles with 100, 400 and 1000 times magnification. The light is irradiated to the stage where the sample is held. The transmitted light then creates a picture of the object that can be seen via eyepieces or live view on the connected monitor. Some adjustments and calibrations need to be done, as described step by step in Section 3.3.4, in order to obtain clear pictures. A list of the components that are mentioned in this thesis is introduced in Table 3.5 and indicated in the sketch of the microscope, provided here as Figure 3.4.

The captured images are analyzed using AxioVision software. After loading the images and choosing the corresponding scaling depending on the lens used, the outline (boundary) of each particle is determined manually by tracing the outline around each particle. Once all particles in an image have been identified and their boundaries traced, a customized data table can be created and extracted for further analysis. In this case, the area of the particles is the parameter that is obtained and saved.

A minimum number of particle size measurements is required to represent a population, i.e., an appropriate sample size is needed to obtain a reliable PSD. The process of determining the sample size is presented in Appendix B.

After image analysis, an array of particle areas is available for data analysis, done using an Octave code that converts the area arrays to cumulative and frequency

size distribution graphs, as explained in Section 3.2.1. This is the same code as the one used to analyze the FPIA data (Appendix A).

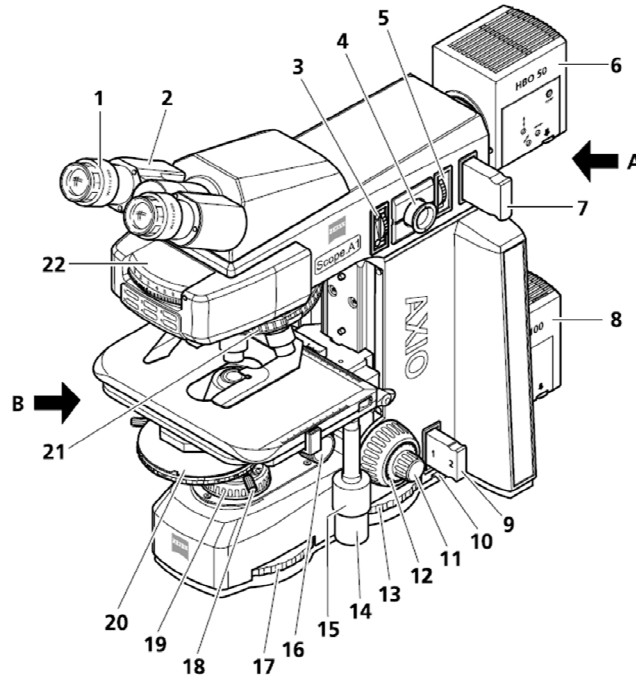


Figure 3.4 Identification of controls and functional elements on the Carl Zeiss Microscope (Axio Scope.A1 Operating Manual, 2008)

Table 3.5 Legend of Figure 3.4

1	Eyepieces
5	Aperture diaphragm
6	Reflected light lamp
11	Focusing drive – fine adjustment
12	Focusing drive – rough adjustment
14	Gera knob for adjusting the mechanical stage in direction X
15	Gera knob for adjusting the mechanical stage in direction Y
19	Field diaphragm
20	Condenser with aperture diaphragm

3.3 Procedures

3.3.1 Mixture Preparation

Experiments are conducted using four types of mixtures: suspensions of latex beads, silica particles, primary kaolinite flocs and kaolinite flocs in various conditions.

Latex suspensions are prepared using 2 μm polystyrene microspheres in DI water. They are prepared by adding 0.2 mL of the 10 wt% latex suspension to 20 mL of DI water in a 50 mL beaker. Silica samples are 2.5 g/L aqueous mixtures that are prepared by adding 0.5 g of the silica flour to 200 mL of DI water. Kaolinite samples are divided into two categories, described in the following sections.

Primary Kaolinite Flocs Mixture

After testing standard and non-flocculating irregular particles, suspensions containing a type of rigid and narrowly sized flocs, called primary flocs, are tested.

The steps followed to prepare the primary flocs suspension, as described by Vaezi (2011), are as follows:

1. Weigh 60 g of kaolinite.
2. Disperse the kaolinite in 450 mL of DI water in a 500 mL beaker. Stir the mixture using a mechanical stirrer at around 600 RPM.
3. Add NaOH solution (0.1 M) to adjust the pH to 8.70 in order to fully disperse the particles.
4. Stir the slurry for 25-30 minutes.

5. Check the pH and adjust it to 8.70.
6. Transfer the slurry to a 500 mL graduated cylinder.
7. Adjust the volume to 500 mL using DI water.
8. Let the cylinder stand overnight, around 18-22 hours.
9. Decant the supernatant (the top part of the slurry) from the cylinder to a 500 mL beaker (the transferred volume should be around 400 mL). In this way, the particles would have a fine narrow size distribution.
10. Stir the slurry in the beaker for 5 minutes to ensure that the slurry is dispersed completely.
11. Measure the slurry temperature with an accurate thermometer.
12. Measure the slurry density using Pycnometer (Figure 3.5) and then calculate the clay concentration (usually 50-60 g/L) using:

$$C = \rho_K \cdot \frac{(\rho_{Slurry} - \rho_{Water})}{(\rho_K - \rho_{Water})} \quad (3.5)$$

where

C: concentration of the concentrated clay slurry, g/L

ρ_K : kaolinite density, 2560 kg/m³

ρ_{Water} : water density at the slurry temperature, g/L

ρ_{Slurry} : measured slurry density by Pycnometer, g/L

13. To prepare the dilute suspension (5 g/L), calculate the required volume of concentrated stock slurry using:

$$V_{Concentrated} = \frac{V_{Dilute} \times C_{Dilute}}{C_{Concentrated}} \quad (3.6)$$

where

$C_{Concentrated}$: concentration of the concentrated kaolinite slurry, g/L

C_{Dilute} : concentration of the dilute kaolinite suspension, =5 g/L

V_{Dilute} : volume of the dilute suspension, = 400 mL

14. In a 50 mL graduated cylinder, measure $V_{Concentrated}$, then fill it up with DI water to have 50 mL of slurry.
15. Transfer the slurry to a 500 mL beaker and add 300 mL of DM water. Stir the magnetic stirrer and check the pH.
16. In a 50 mL graduated cylinder, mix 2 mL of 0.1 M CaCl_2 solution with DM water and adjust the volume to 50 mL.
17. Add the dilute CaCl_2 solution to the clay suspension gradually while the suspension is stirred. This creates a 0.5 mM Ca^{2+} solution. Final volume of the clay suspension is 400 mL.
18. Check the pH and adjust it to 8.0 with NaOH solution.
19. Monitor the pH during the preparation and also during the experiments.



Figure 3.5 Pycnometer used for slurry density measurement

Kaolinite Mixture

The kaolinite suspensions (including natural, acidic and alkaline mixtures) are prepared as follows:

1. Calculate the weight of kaolinite required for the desired concentration in a suspension whose total volume will be 400 mL. Put a clean paper on the scale. Zero the scale and weigh the required amount of kaolinite using a stainless steel spatula.
2. Add the kaolinite powder to a clean dry 500 mL beaker.
3. Use a graduated cylinder to add 400 mL of de-ionized water to the beaker.

The amount of DI water is different for coagulated alkaline samples depending on the concentration of CaCl_2 . In these cases, the amount of water is calculated using:

$$V_{\text{DI water}} (\text{mL}) = 400 (\text{mL}) - V_{\text{CaCl}_2 \text{ solution}} (\text{mL}) \quad (3.7)$$

4. Place the beaker under the mixer and adjust the mixer shaft height so that the bottom of the impeller is half an impeller diameter distant from the bottom of the beaker.
5. Turn on the mixer and slowly increase the speed to 400 RPM.
6. Start the stop-watch. Mix the slurry for 45 minutes.
7. Place the pH meter probe in the beaker to measure the pH of the suspension.
8. Adjust the pH of the sample to the desired value (3 or 9) using either NaOH or HCl solution. Add the solution drop by drop when near the desired pH. Wait until the pH becomes stable before adding more. Note: this step does not apply to natural samples.
9. For the case of coagulated alkaline samples, add the required amount of CaCl_2 solution (either 4 or 40 mL).



Figure 3.6 Sample preparation set up

3.3.2 FPIA Tests

As previously mentioned, in order to compare the results obtained from the FPIA and Mastersizer, the samples that go through the testing unit of the devices should be as similar as possible. The samples are diluted in the Mastersizer dispersion unit. Thus, the FPIA samples should also be diluted with the same volume of liquid that the Mastersizer sample chamber holds. The dispersant fluid should have similar chemistry to the original suspension. Therefore, to keep the dilution effect on floc size distribution at the minimum, filtrate is used for sample dilution both in Mastersizer sample dispersion unit and for sample dilution just before introduction to the FPIA. However, other samples that are going to be compared with the microscope measurements do not need dilution.

The following procedure explains the filtrate preparation steps:

1. In a 500 mL beaker, prepare 400 mL mixture of the same sample that is going to be tested as described in Section 3.3.1.
2. Stop the mixer and let the particles settle for a few minutes.
3. Meanwhile, take a side arm flask and attach the ventilation tube to the vacuum system.
4. Put filter paper (Millipore 0.22 μm GSMP membrane) in a dry clean Büchner funnel. The pore size of the filter paper is 0.22 μm and it retains particles larger than this size.
5. Adhere the filter paper to the funnel by wetting the whole filter paper area using de-ionized water.

6. Put the funnel on the flask and fix it using a stopper to seal all openings.

The filtration set up is now ready. It is shown here as Figure 3.7.

7. Take the beaker and decant the supernatant into the funnel. When there is no more suspension left in the funnel, disassemble the flask and the funnel, collect the filtrate, and dispose of the filter paper and the kaolinite solid cake.

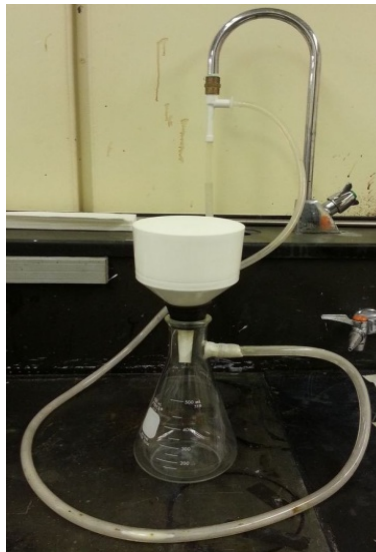


Figure 3.7 Filtration set up

Before each measurement the FPIA needs to be prepared. A background check and calibration is essential before running a sample.

The procedure for testing a sample with the FPIA whether diluted (samples to be compared with the Mastersizer's measurements) or not (samples to be compared with the microscope measurements) is as follows:

1. Start the FPIA.
2. Open the FPIA software. Open the "Test Setting" window.

3. Run “Background Check” to ensure that particles are not adhered to the flow cell inside the FPIA from previous tests. Background images are collected and the number of particles present are counted. According to the FPIA operator’s manual this number should not be more than 10. If so, this step should be repeated.
4. Run “Auto Focus” to make sure the lens is placed properly for optical image clarity (focus adjustment).
5. Add 5 mL of 2 μm polystyrene latex microsphere dilute mixture to complete the focus adjustment step.
6. Adjust the testing parameters, such as sample name, mixing speed (set as 300 RPM), magnification mode (set as HPF), and sonication power (set as “not applied”) in the “Test Setting” window.
7. Click the start button, sample chamber lid opens in 10 seconds.
8. For diluted samples only: Use 110 mL of the filtrate in a 200 mL beaker and add the appropriate amount of the sample.
9. Use a disposable plastic pipette to take 1-5 mL of the sample and inject it into the sample chamber. A large-tip opening transfer pipette from Fisher Scientific is used and the tip is cut off, as shown in Figure 3.8, to reduce the shear exerted on the flocs.
10. The measurement is completed in less than 3 minutes. For a new test, repeat from Step 6.



Figure 3.8 Large tip opening transfer pipette

3.3.3 Mastersizer Tests

Stages of running a test with the Mastersizer for the first time is as follows:

1. Start the Mastersizer.
2. Run the Mastersizer 2000 software.
3. Create a unique SOP for each type of sample. The sample handling unit (Hydro 2000SM), material, dispersant, material and dispersant's refractive indices, measurement time and snaps, number of repeated measurements, etc. are determined in a SOP.
4. Start the related SOP with respect to the sample type (latex, silica or kaolinite).
5. Flush the system with de-ionized water three times to thoroughly rinse the system.
6. Fill the tank with either the filtrate (prepared as described in Section 3.3.2) for kaolinite samples or de-ionized water for latex and silica samples.
7. Set the stirrer speed to 400 RPM.
8. Click the start button. The background is then automatically measured.
9. Add an adequate amount of sample such that the laser obscuration level is in the green section (10-15 %).

10. For the next measurements of the same sample type, repeat from Step 5, otherwise, start from Step 4.

3.3.4 Microscopy Tests

The procedure of testing a sample with the microscope is as follows:

1. Turn on the microscope.
2. Set the microscope lens to 10x.
3. Close the field diaphragm to the smallest diameter.
4. While looking through the eyepieces, centre and focus the diaphragm by turning the focus knob to make it take the shape of a red hexagonal.
5. Adjust the aperture to cover 2/3 of the area seen through the eyepieces.
6. After the microscope is calibrated, open the field diaphragm to the desired size.
7. Start the AxioVision software and open the live feed.
8. Perform white balance with a white piece of paper on the sampling platform.
9. Perform shading correction with an empty microscope slide.
10. Adjust the naming settings via the software.
11. Place a drop of the sample on a slide with a disposable pipette (tip removed).
12. Gently cover the sample with a top slide.
13. Put the slide on the sample stage, change the lens and use coarse and fine focus knobs to bring the particles into focus.
14. Take a picture by clicking the snap button.
15. Move the slide in X and Y directions on the sample stage using the gear knobs and take pictures of the sample. In order to ensure that the image of one

particle is not captured multiple times, start from one corner and trace in a spiral path.

16. For a new sample slide, start from Step 10.

4 Evaluation of Operating Conditions and Development of Test Procedures

In this chapter, the results of a series of experiments conducted to assess parameters affecting kaolinite FSD are presented. The effect of equipment configuration and operating conditions on kaolinite FSD measurements is also evaluated. In Section 4.1, the effects of sample pH, kaolinite concentration and addition of coagulant on kaolinite FSD are assessed. The results provide information regarding the conditions that create the smallest and largest flocs, which in turn allows selection of suitable sample preparation and test conditions.

Floc sizes can also be altered and modified due to the sample preparation procedure and equipment performance. In Section 4.2, the effect of mixer speed on floc size distribution in the sample preparation stage is tested. The FPIA conditions (effect of mixing time and mixing speed inside the instrument) are evaluated as well. The Mastersizer performance (effect of dilution and mixing speed in the sample dispersion unit) is also studied, and microscope magnification is determined. Based on these results, appropriate SOPs and test conditions are developed for experiments to ensure consistency of the feed sample.

All size distribution data used to plot the frequency FSD graphs are presented in Appendix C.

4.1 Evaluation of Suspension Properties Affecting Kaolinite FSD

Factors including solid concentration, sample pH and addition of coagulant affect the size and structure of kaolinite flocs by governing inter-particle electrostatic

interactions (Michaels and Bolger, 1962; Nasser and James, 2006; Masliyah and Bhattacharjee, 2006; Zbik et al., 2008; Adeyinka et al., 2009). As described in Chapter 2, increasing the kaolinite concentration results in larger floc sizes. Reducing the sample pH increases the size of flocs, while a pH increase causes deflocculation and floc size reduction. With addition of a coagulant such as calcium chloride (CaCl_2), large highly flocculated entities are formed and the number of larger particles increases (Michaels and Bolger, 1962; Michaels and Bolger, 1964; Nasser and James, 2008).

Since these factors are important in developing test procedure conditions, the effect of these parameters on kaolinite floc size distribution was studied by conducting a set of experiments. Measurements were carried out using aqueous kaolinite mixtures prepared under various conditions to investigate the changes in FSDs obtained from the FPIA. The results are presented in Sections 4.1.1 through 4.1.3.

The FPIA results are then compared with available reports in the literature studying the effect of suspension properties on floc size and structure. The qualitative agreement of the results obtained here with the literature justifies the use of the FPIA for the measurements reported in this chapter, i.e. qualitative comparisons of FSDs.

4.1.1 Kaolinite Concentration

Solid concentration is one of the main factors that can change the kaolinite floc size distribution (Michaels and Bolger, 1962; Adeyinka et al., 2009). To study this

factor, five kaolinite-water suspensions with concentrations of 1, 5, 15, 25 and 35 g/L were prepared and their corresponding FSDs were measured with the FPIA. The samples have approximately the same pH of 4.9, which is referred to as “natural” pH. The floc size distribution results are presented in Figure 4.1 and Figure 4.2. In the figures, frequency ratio is the ratio of number of particles in each bin to the total number of measured particles (Equation 3.1) and cumulative frequency ratio at a specific particle size is the ratio of summation of the number of all smaller particles to the total number of measured particles.

Compared with all other sample concentrations, the 1 g/L sample has the highest number of particles in primary floc range ($< 2 \mu\text{m}$) and lowest number of particles in the larger flocs range (Figure 4.2). On the other hand, the 35 g/L sample has the larger particles ($> 7 \mu\text{m}$). For the other three samples, the FSDs fall between those of the lowest and highest concentration mixtures (Figures 4.1 and 4.2). As clearly shown in Figure 4.1, as concentration increases, the cumulative size distribution graphs shift to larger particle sizes, confirming the fact that having more particles in the suspension leads to more collisions and thus to floc formation. This growth is depicted in Figure 4.3 by assessing the effect of solid concentration on number-based mean and d_{50} . As a quantitative comparison, number-based mean diameter, d_{10} , d_{50} and d_{90} for the five samples are provided in Table 4.1. With no exception, all parameters increase with increasing concentration.

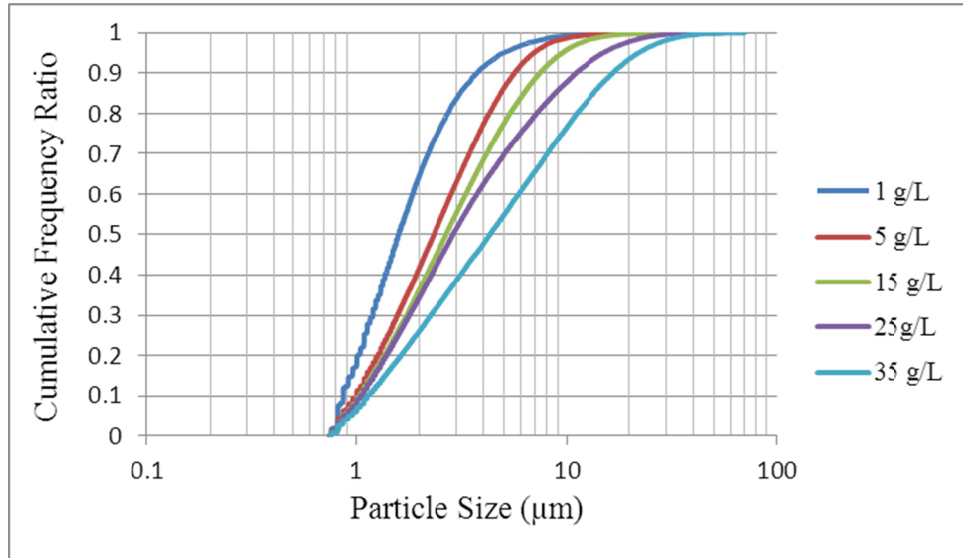


Figure 4.1 Effect of solid concentration on kaolinite cumulative FSD (natural pH, no coagulant)

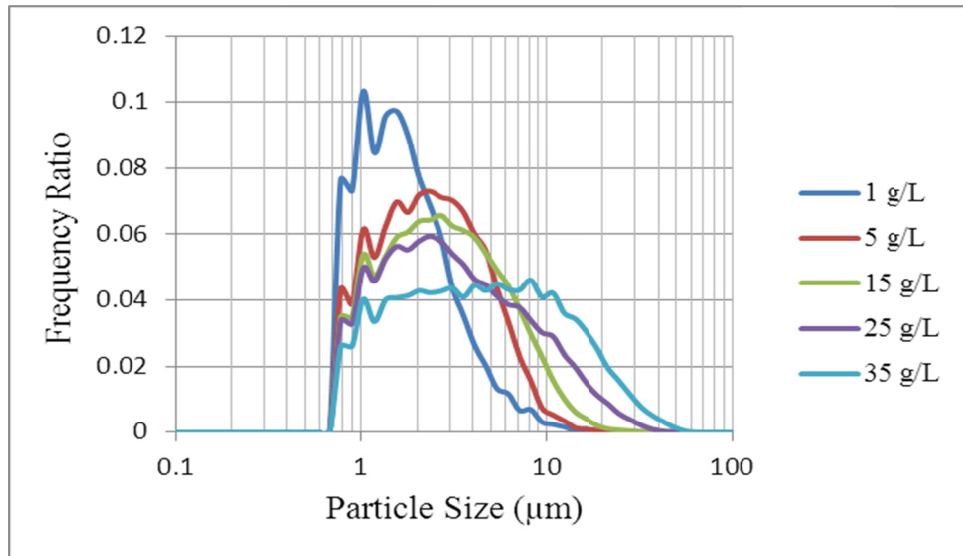


Figure 4.2 Effect of solid concentration on kaolinite frequency FSD (natural pH, no coagulant)

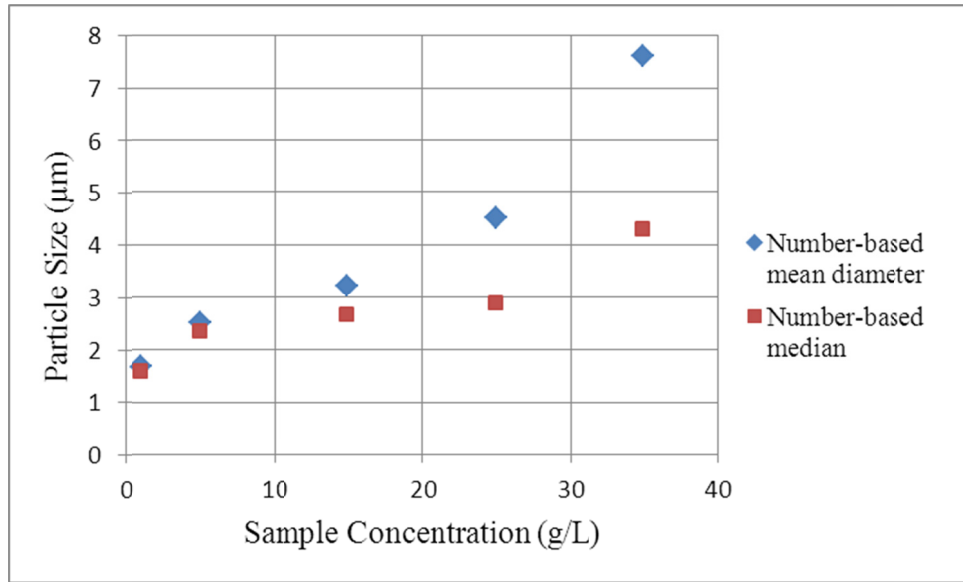


Figure 4.3 Effect of sample concentration on number-based mean and median

Table 4.1 Quantitative comparison of samples with different solid concentration

Sample concentration (g/L)	Mean diameter (μm)	d ₁₀ (μm)	d ₅₀ (μm)	d ₉₀ (μm)
1	1.7	0.9	1.6	3.7
5	2.5	1.0	2.3	5.6
15	3.2	1.0	2.7	7.4
25	4.5	1.0	2.9	11.0
35	7.6	1.1	4.3	16.6

The results from these experiments are in qualitative agreement with results found in the literature. Higher concentration leads to decreased distance between particles (Adeyinka et al., 2009). When distances are smaller, more collisions occur, increasing the chance of successful collisions and formation of larger flocs (Michaels and Bolger, 1962; Masliyah and Bhattacharjee, 2006).

The 5 g/L sample (and more concentrated ones) seem to be good options, since they have balanced numbers of particles in different size ranges and are dilute enough for the FPIA. However, Mastersizer test conditions are a limiting factor. Based on the experiments performed here, for samples more concentrated than 5 g/L, Mastersizer reached the obscuration level with very little amount of the injected sample. Using very small amount of sample would increase the probability of subsampling errors. Therefore, the 5 g/L kaolinite suspension was chosen. This sample is also dilute enough for the microscopy tests to provide clear images.

4.1.2 Suspension pH

Mixture pH affects the kaolinite floc size distribution (Nasser and James, 2008; Zbik et al., 2008). Addition of sodium hydroxide (NaOH) or hydrochloric acid (HCl) can increase or decrease the sample pH, respectively. To study the effect of pH on kaolinite floc size distribution, three samples were prepared at different pH values (3, 5 and 9) as described in Section 3.3.1. The natural sample consists of only kaolinite and de-ionized water. Acidic and alkaline samples were prepared by adding HCl and NaOH to the natural sample, respectively. The samples were then tested with the FPIA.

Figure 4.4 and Figure 4.5 compare the natural and acidic kaolinite samples. The particle sizes increase when the pH changes from natural to acidic. The median size increases from 2.0 μm to 4.0 μm (Figure 4.4). Size growth in the acidic sample appears as an increase in the number of particles larger than 4 μm . The natural sample has more particles that are smaller than 4 μm . Therefore, the

population of larger particles increases with addition of HCl (i.e. at low suspension pH).

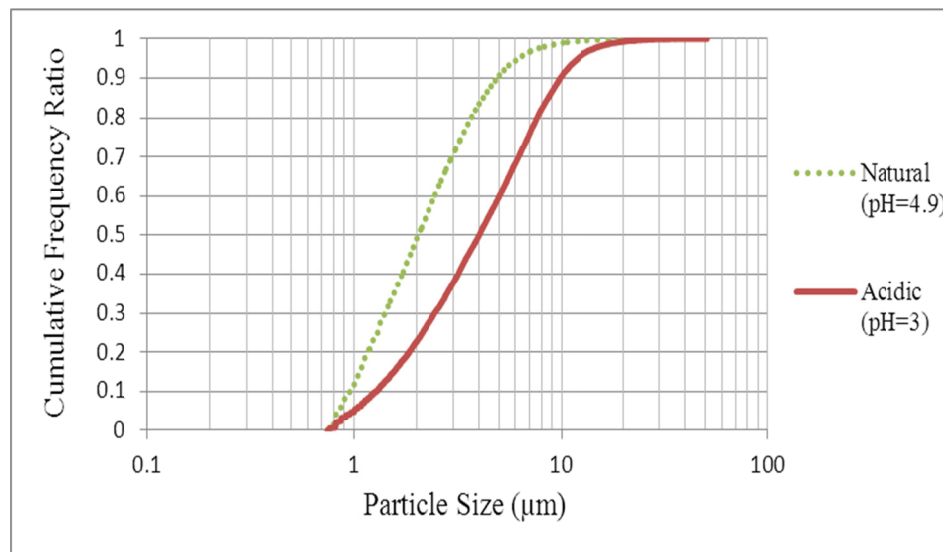


Figure 4.4 Kaolinite cumulative FSD at natural and low pH (c=5 g/L, no coagulant)

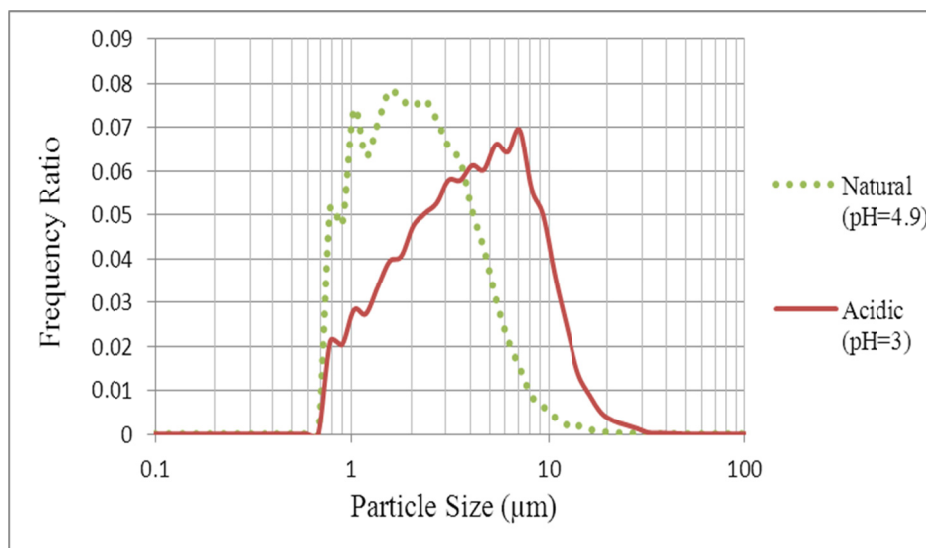


Figure 4.5 Kaolinite frequency FSD at natural and low pH (c=5 g/L, no coagulant)

Figures 4.6 and 4.7 demonstrate the differences between alkaline and natural kaolinite flocs. The number-based d_{50} changes from 2.0 μm in the natural sample to 1.5 μm in the alkaline sample (Figure 4.6). There are more particles smaller than 2 μm in the alkaline sample and the natural sample has more particles that are larger than 2 μm . This is expected since flocs break down at higher pH values to produce smaller flocs and particles.

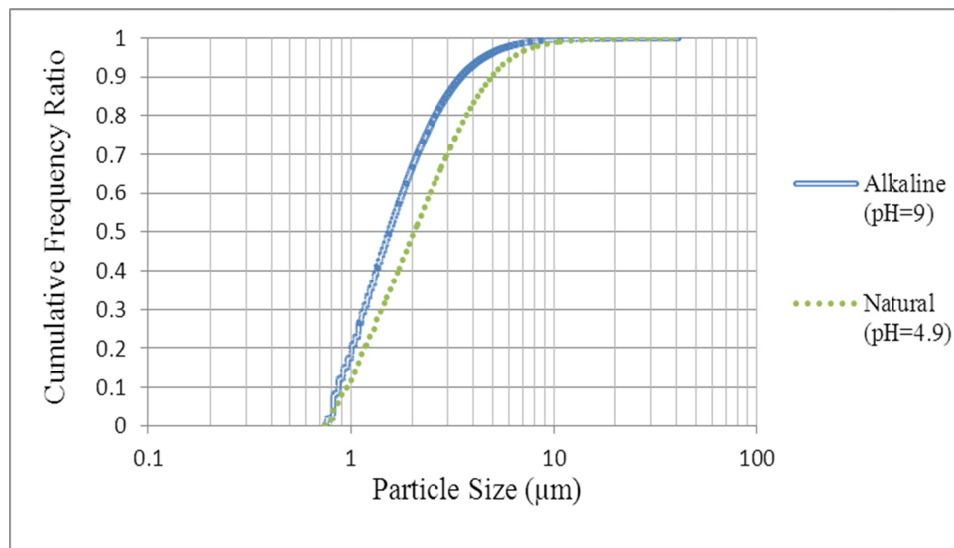


Figure 4.6 Kaolinite cumulative FSD at natural and high pH ($c=5$ g/L, no coagulant)

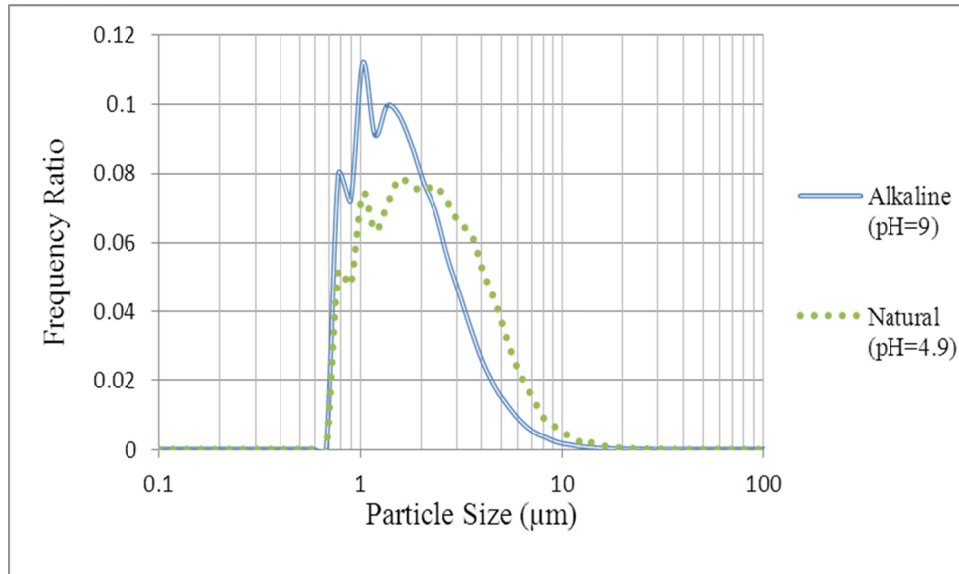


Figure 4.7 Kaolinite frequency FSD at natural and high pH (c=5 g/L, no coagulant)

The kaolinite FSDs for three suspension pH values are shown together in Figure 4.8 and Figure 4.9. As shown on the graphs, a pH increase results in decreased particle size and increased number of small flocs and particles. This can also be inferred from the data of Table 4.2 and from Figure 4.10. The particle size and suspension pH are inversely related, i.e., all representative diameters (mean, d_{10} , d_{50} , d_{90}) decrease with increasing pH.

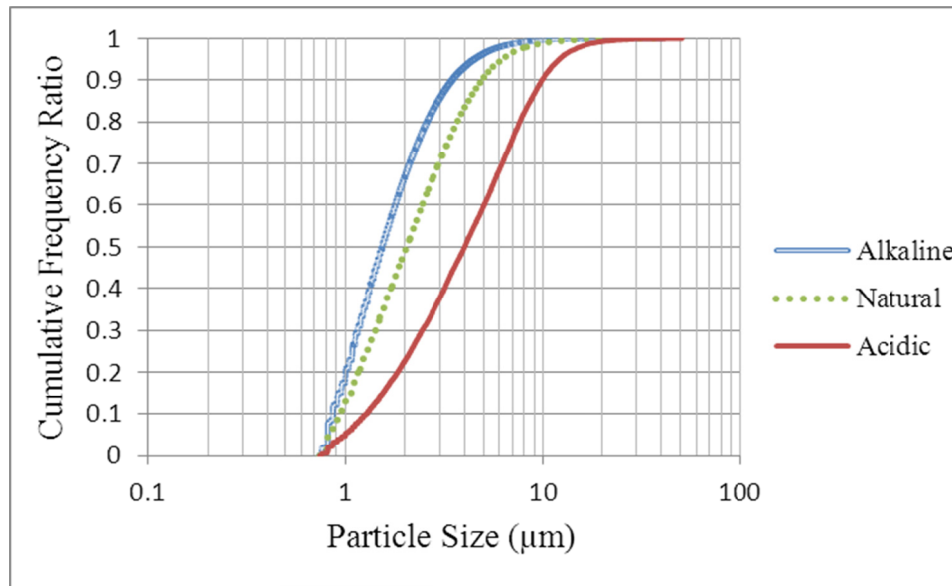


Figure 4.8 Effect of pH on kaolinite cumulative FSD ($c=5$ g/L, no coagulant)

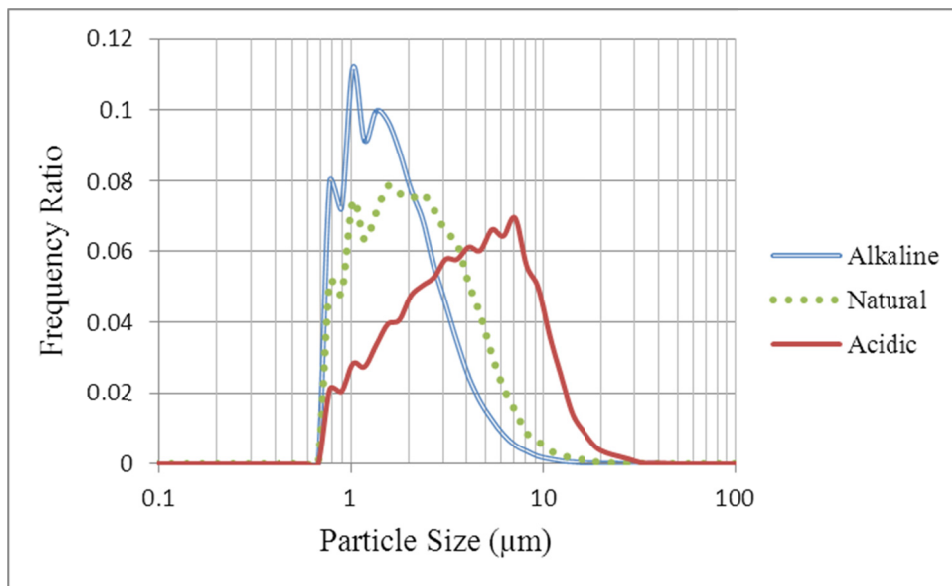


Figure 4.9 Effect of pH on kaolinite frequency FSD ($c=5$ g/L, no coagulant)

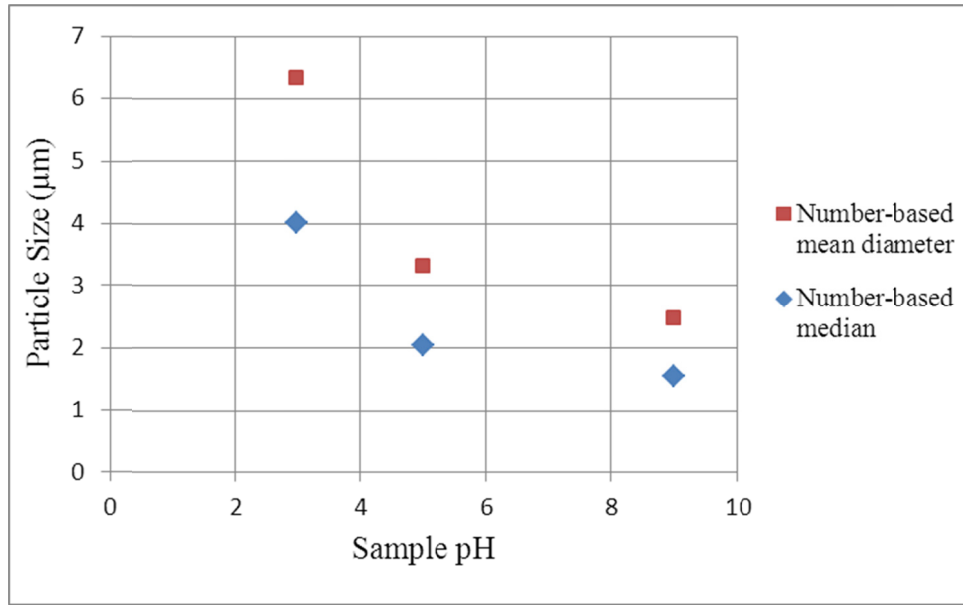


Figure 4.10 Effect of suspension pH on number-based mean and median

Table 4.2 Quantitative comparison of samples with different pH values

Sample pH	Mean diameter (μm)	d ₁₀ (μm)	d ₅₀ (μm)	d ₉₀ (μm)
3	4.6	1.3	4.0	9.8
5	2.2	1.0	2.0	4.9
9	1.6	0.9	1.5	3.5

As reported in the literature, at acidic pH values, the edges of kaolinite particles become positively charged and attracted to the negatively charged faces to form card-house flocs (Michaels and Bolger, 1962; Nasser and James, 2006). Flocs formed under these conditions are typically larger. Under alkaline conditions, however, the edges of the kaolinite particles become neutral or negatively charged by adsorbing OH⁻ ions. Therefore, floc restructuring and size reduction occur. Both are related to the stronger electrostatic repulsion. At this condition, particles are mostly present as individual primary kaolinite particles and a few card-pack

(face-to-face) flocs (Michaels and Bolger, 1962; Nasser and James, 2006). According to Nasser and James (2006), all flocs are broken down at pH 9, although this will depend on clay type.

With changing the pH parameter (along with coagulant addition, discussed in the next section), different structures of flocs can be obtained. In order to test the FPIA with different floc structures, samples of different pH values are made and tested with both the FPIA and Mastersizer. For microscopy experiments, due to the fact that the analysis is a very time-consuming process, only samples at alkaline pH were utilized. It should be noted that the dispersed particles at alkaline pH need the presence of a coagulant to produce face-to-face flocs. The process is described in detail in the next section.

4.1.3 Coagulant Addition

Coagulant addition can also affect kaolinite particle size distribution (Nasser and James, 2008; Zbik et al., 2008). The floc size distribution of a 5 g/L aqueous kaolinite mixture at pH 9 with and without the addition of 0.01 M of CaCl_2 is measured with the FPIA. The results are presented in Figures 4.11 and 4.12. The coagulant addition caused the dispersed particles to form flocs and the distribution was shifted to the right, i.e., to larger sizes. In size range larger than approximately 2 μm , the coagulated sample contains more particles, which are assumed to be flocs. More primary flocs smaller than 2 μm are present in the non-coagulated sample. At the alkaline pH, as discussed in the last section, particles exist in their dispersed state, and addition of coagulant causes face-to-face flocs to form (according to Michaels and Bolger, 1962; Nasser and James, 2006).

Formation of other associations such as edge-to-edge or face-to-edge flocs might be possible as well. Table 4.3 summarizes the differences between the two systems. Again it is shown that the particle size increases when coagulant is added to the mixture.

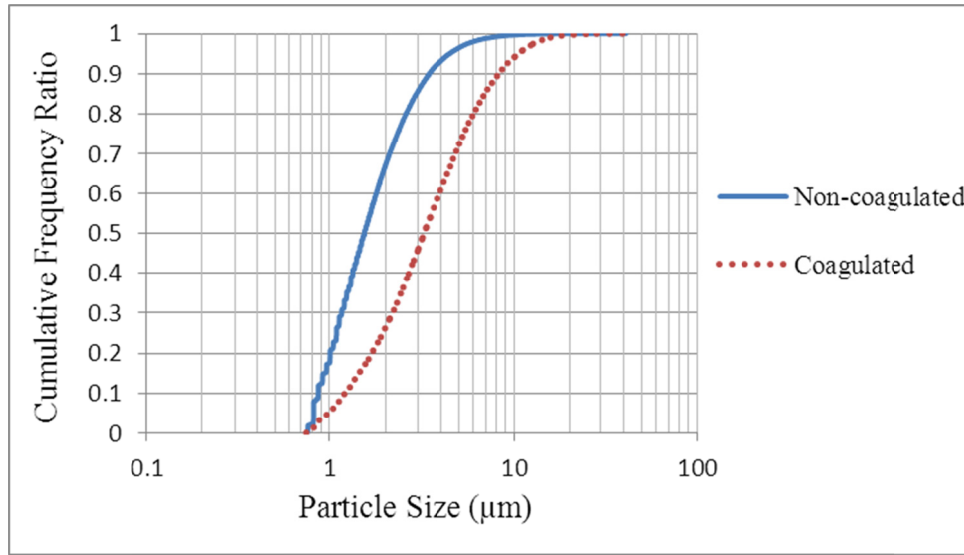


Figure 4.11 Effect of coagulant addition on kaolinite cumulative FSD (pH=9; c=5 g/L)

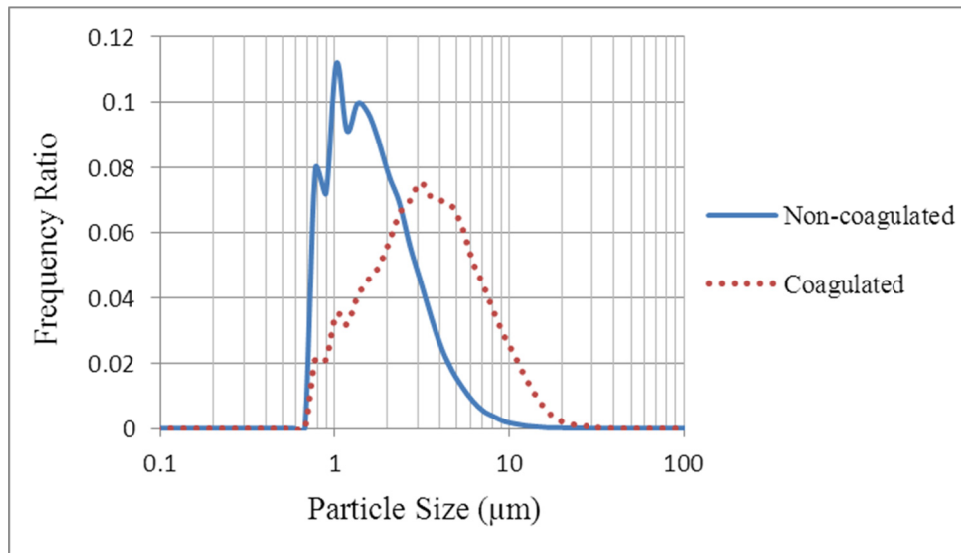


Figure 4.12 Effect of coagulant addition on kaolinite frequency FSD (pH=9; c=5 g/L)

Table 4.3 Quantitative comparison of samples with or without coagulant

Samples	Mean diameter (μm)	d_{10} (μm)	d_{50} (μm)	d_{90} (μm)
Coagulated	3.8	1.2	3.2	8.3
Non-coagulated	1.6	0.9	1.5	3.5

As stated in previous studies, when CaCl_2 is added to the alkaline suspension, the electric double layer is compressed and a card-pack floc structure would be expected because of the electrostatic repulsive force reduction between faces of the kaolinite particles (Michaels and Bolger, 1962; Nasser and James, 2006). Changes in surface charge can also result, through specific adsorption of Ca^{2+} ions onto kaolinite surfaces.

Since the objective in this study is to validate the floc size measurements, the coagulated card-pack flocs were chosen to be used as one of the floc structures to be tested. Dispersed particles at alkaline pH were coagulated using CaCl_2 and the resulting flocs were measured with the FPIA, Mastersizer and microscope.

4.2 Evaluation of Equipment Configuration and Operating Conditions

In this section, experimental setups and their effect on kaolinite floc size distribution are studied to develop appropriate and repeatable test conditions. This step involves evaluation of the effects of sample mixing, effect of the FPIA internal mixing speed and mixing time, and the effect of the Mastersizer mixing speed and dilution. In the sample preparation stage, aqueous kaolinite mixtures are mixed with a mixer. The duration of mixing can influence floc size

distribution. There is also a mixer inside sample chamber of the FPIA. The effect of the mixer speed and mixing time is also studied. The Mastersizer also has a mixer in its sample dispersion unit. Both dilution and stirring speed can affect floc size distribution. At the end of this section, the selection of the proper magnification for the microscopy is discussed.

4.2.1 Sample Mixing

Sample preparation necessarily includes mixing, and this step is likely to impact the measured floc size distributions. To identify the appropriate mixing time for sample preparation, the effect of mixing time on floc size distribution was investigated. A 10 g/L aqueous kaolinite mixture is utilized for the experiment. While the suspension was being mixed, samples were taken at different times and size analyses were conducted using the FPIA. The mixing time was varied from 1 to 120 minutes. In order to keep the experiment consistent, all samples are mixed at a stirrer speed of 400 RPM. This speed is high enough to keep the mixture suspended. The cumulative floc size distribution results are provided in Figure 4.13. The quantitative information of the size distributions shown in the graphs is reported in Table 4.4. To clarify the effect of mixing time on number-based mean diameter and median of the samples a separate graph is presented (Figure 4.14).

Based on the results presented here, one can see that floc mean diameter changes dramatically during the first 25 minutes; thereafter the mean diameter and median do not change, i.e., they become relatively stable and the rate of floc formation and breakage is in equilibrium. The cumulative FSDs for samples collected at $t \geq 45$ min

fall on top of each other (see Figure 4.13). Thus, the mixing time for sample preparation was set to $t = 45$ min.

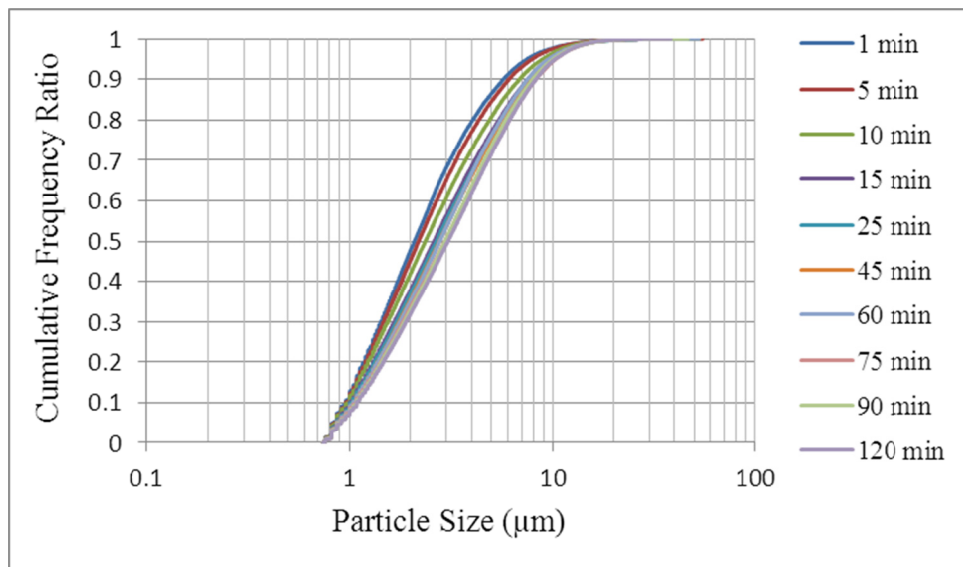


Figure 4.13 Effect of sample mixing time on kaolinite cumulative FSD ($c=10\text{g/L}$, $\text{pH}=4.9$)

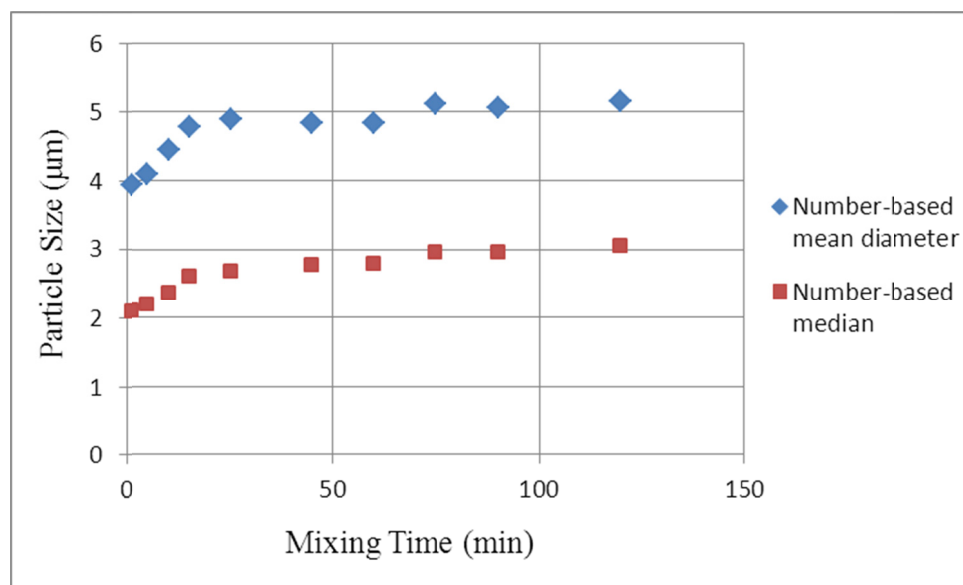


Figure 4.14 Effect of mixing time on representative particle size ($c=10\text{g/L}$, $\text{pH}=4.9$)

Table 4.4 Quantitative comparison of samples with different mixing times

Mixing time (min)	Mean diameter (μm)	d_{10} (μm)	d_{50} (μm)	d_{90} (μm)
1	2.5	1.0	2.1	5.7
5	2.6	1.0	2.2	6.0
10	2.9	1.0	2.4	6.8
15	3.2	1.0	2.6	7.5
25	3.3	1.0	2.7	7.7
45	3.3	1.0	2.8	7.7
60	3.3	1.0	2.8	7.5
75	3.6	1.1	2.9	8.2
90	3.5	1.1	3.0	8.0
120	3.6	1.1	3.1	8.2

4.2.2 Effect of FPIA Operating Parameters

In this section the performance of the FPIA is evaluated. Specifically, the effect of FPIA mixing speed and mixing time on kaolinite mixture FSDs is evaluated. The sample is mixed in the FPIA sample chamber before it goes through the flow cell. The stirrer speed can be set from 50 to 750 RPM. Samples are tested with five different rotor speeds to assess the effect on the kaolinite floc size distribution measurements. The sample mixing time is also tested.

Effect of Mixing Speed

In the FPIA a mixer and an ultrasonic probe are used to disperse samples and prevent solids from settling inside the sample chamber. Both sonication power and mixer speed can be adjusted by the operator. These two parameters can affect the floc size distribution.

It was shown by Marefatallah (2013) that sonication disperses kaolinite flocs and increases the number of smaller particles in the suspension. Since in this study the objective is to minimize floc damage or breakage, sonication is not used for this experimental program.

The mixer speed can be adjusted between 50 to 750 RPM. In order to study the effect of the internal mixing speed on the FPIA floc size measurements, a 5 g/L aqueous natural kaolinite suspension was prepared (as described in Section 3.3.1) and size measurements were made after mixing at 50, 150, 300, 500 and 750 RPM. The mixing time inside the sample chamber was kept to a minimum (“zero seconds”) (0 s, see the following section). The measured floc size distributions for the 5 tests are presented in Figure 4.15 and Figure 4.16. As illustrated in both graphs, the 5 curves overlap and show almost no change in floc size distribution. In order to be able to compare the graphs quantitatively, the mean diameter and number-based d_{10} , d_{50} and d_{90} for all experiments were calculated. These are presented in Table 4.5. It can be concluded from the graphs and the table that the kaolinite FSD does not change with FPIA sample chamber mixing speed.

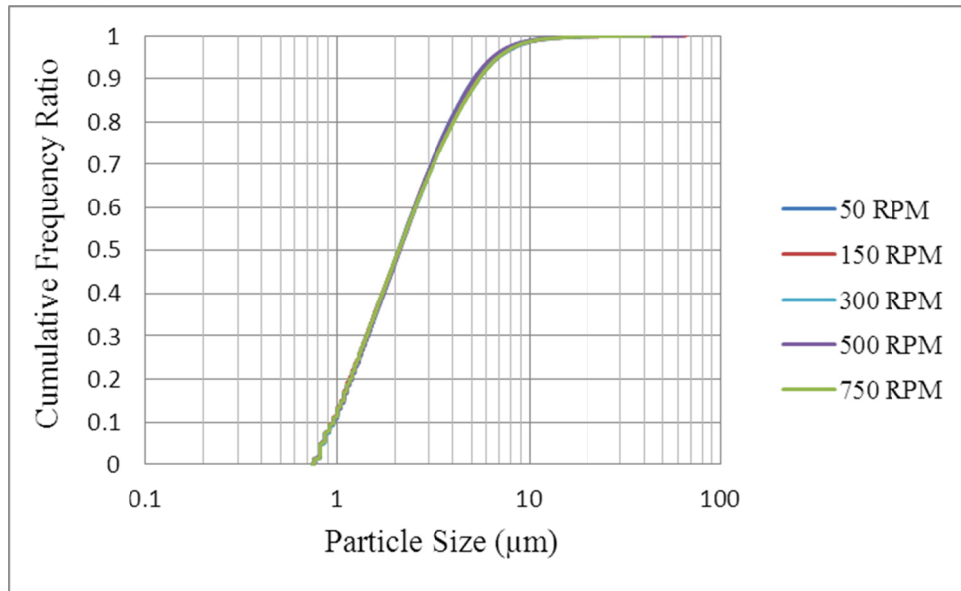


Figure 4.15 Effect of FPIA mixing speed on kaolinite cumulative FSD (c=5g/L, pH=4.9)

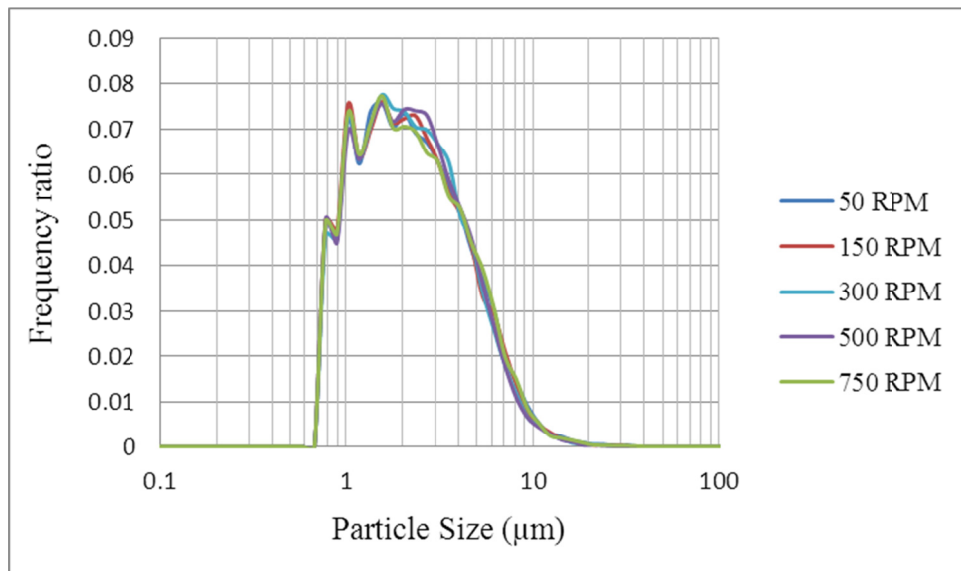


Figure 4.16 Effect of FPIA mixing speed on kaolinite frequency FSD (c=5g/L, pH=4.9)

Table 4.5 Quantitative comparison of samples with different FPIA mixing speeds

FPIA stirrer speed (RPM)	Mean diameter (μm)	d_{10} (μm)	d_{50} (μm)	d_{90} (μm)
50	2.4	1.0	2.1	5.5
150	2.4	1.0	2.1	5.4
300	2.3	1.0	2.1	5.2
500	2.3	1.0	2.1	5.2
750	2.4	1.0	2.1	5.5

A FPIA mixing speed of 300 RPM was selected for all experiments, as this speed is high enough to prevent solid sedimentation in the sample chamber and clogging. It is also the mixing speed recommended in the FPIA standard SOP.

Effect of Mixing Time

As previously mentioned, the sample injected to the FPIA is mixed in the sample chamber before passing through the flow cell. It is therefore necessary to evaluate the effect of mixing time within the FPIA sample chamber on floc size distribution. An aqueous natural kaolinite mixture with 5 g/L concentration (Section 3.3.1) was used. The sample was introduced to the FPIA and mixed for different amounts of time before starting the measurement process. This experiment was repeated 5 times with 0 seconds, 30 seconds, 1 minute, 5 minutes and 15 minutes mixing time. The resulting FSDs obtained with the FPIA are depicted in Figure 4.17 and Figure 4.18. As demonstrated in both figures, the sizes do not change significantly. In fact, the differences (clearer on Figure 4.18) are very small. Calculated parameters describing the FSDs are presented in Table

4.6. It is evident that the FPIA internal mixing time does not have any significant effect on the kaolinite FSD. Thus, for all experiments the sample is introduced immediately to the flow cell (i.e. mixing time, $t = 0$ s).

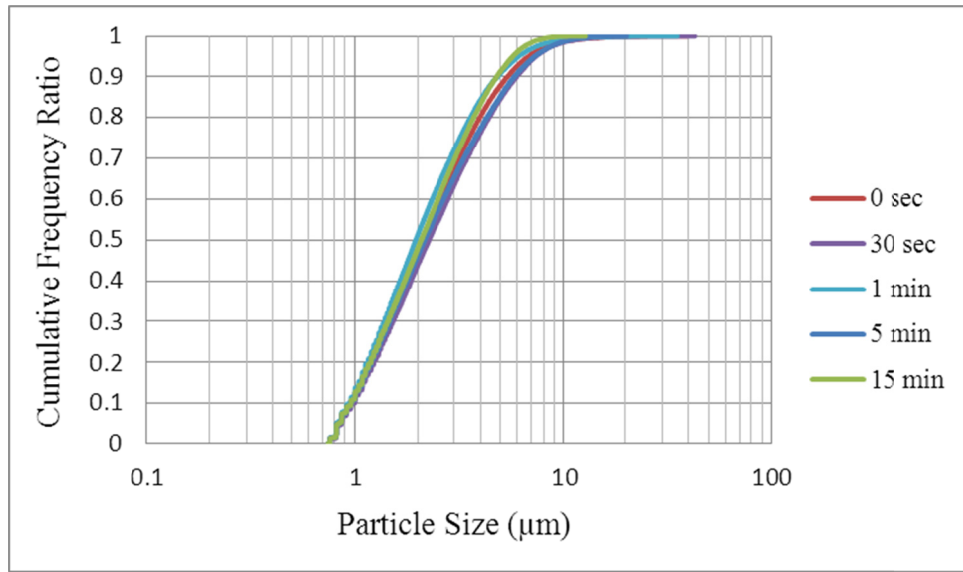


Figure 4.17 Effect of FPIA mixing time on kaolinite cumulative FSD ($c=5\text{g/L}$, $\text{pH}=4.9$)

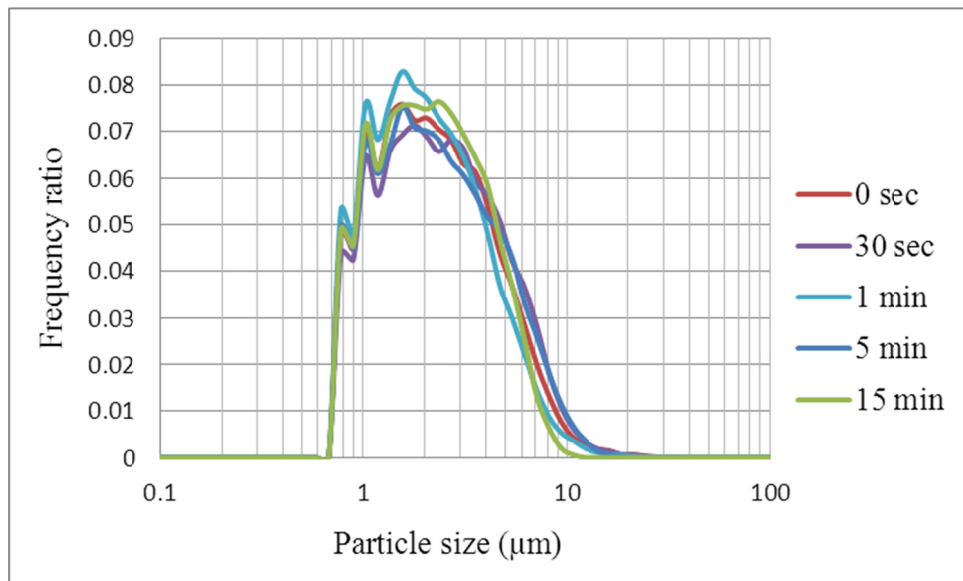


Figure 4.18 Effect of FPIA mixing speed on kaolinite frequency FSD ($c=5\text{g/L}$, $\text{pH}=4.9$)

Table 4.6 Quantitative comparison of samples with different FPIA mixing times

Mixing time in the FPIA (min)	Mean diameter (μm)	d_{10} (μm)	d_{50} (μm)	d_{90} (μm)
0	2.4	1.0	2.1	5.4
0.5	2.6	1.0	2.3	5.9
1	2.1	0.9	2.0	4.8
5	2.4	1.0	2.2	5.8
15	2.1	1.0	2.1	4.8

4.2.3 Mastersizer Performance Tests

In this section the performance of the Mastersizer is evaluated. As described in Chapter 3, the Mastersizer dispersant accessory Hydro 2000SM was used for the experiments of the present study. The sample dispersion unit is equipped with a mixing rotor and should be filled with a dispersing medium for each test. Since mixing the suspension, diluting it and/or changing the continuous phase chemistry can affect the flocs, the effects of these operating conditions on kaolinite floc size distribution were studied. The samples were tested using different dispersion unit mixing speeds. Samples were diluted with either DI water or filtrate, and the Mastersizer size distribution measurements were then compared.

Effect of Mixing Speed

The Malvern Mastersizer sample dispersion unit is fitted with a mixer, which is used for dispersing the sample and preventing solids sedimentation and blockage. However, it may affect floc sizes. In order to study the effect of mixing speed on the Mastersizer measurements, a sample of aqueous kaolinite mixture was tested at different mixing speeds. The stirrer speed can be adjusted from 400 to 3000

RPM. Experiments were conducted at mixer speeds of 400, 1000, 2000 and 3000 RPM. The kaolinite floc size distributions for the four experiments are presented in Figure 4.19 and Figure 4.20, as reported by the Malvern Mastersizer software. The volume-based distribution descriptors (d_{10} , d_{50} , d_{90}) are reported in Table 4.7. The graphs clearly show that the Mastersizer stirrer speed influences the kaolinite FSD. The effect can also be seen in the numbers reported in Table 4.7. Generally, larger particles can be found in the mixture when lower mixing speeds are used. It seems that a mixing speed of 3000 RPM causes flocs to break down to primary particles and primary flocs, as indicated by the FSD shown in Figure 4.19. The FSD measured after mixing at 3000 RPM has the highest volume per cent in the 0.15 to 0.6 μm size range. The increase in 10-20 μm size range can be due to more collisions that occur at this speed and simultaneous formation of larger flocs.

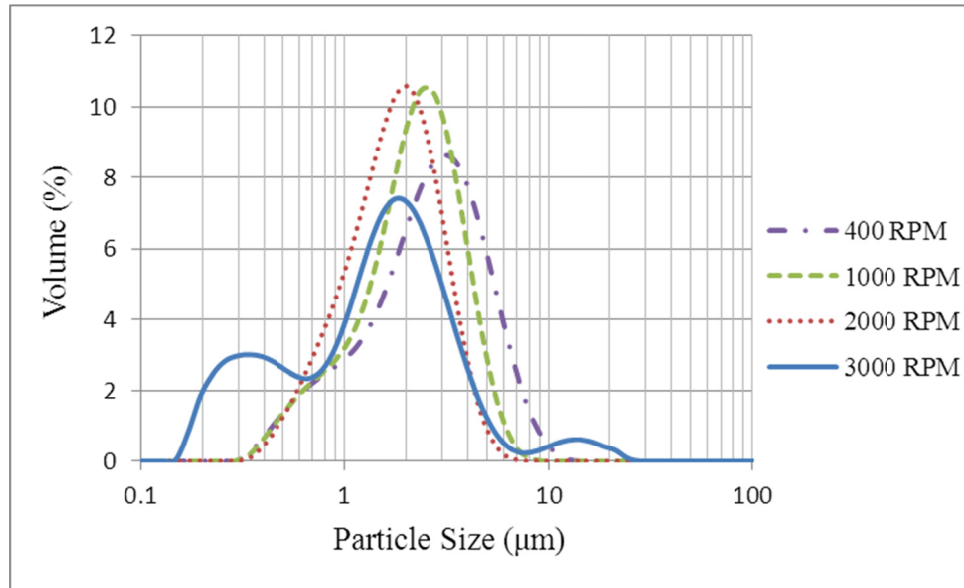


Figure 4.19 Effect of Mastersizer mixing speed on kaolinite frequency FSD

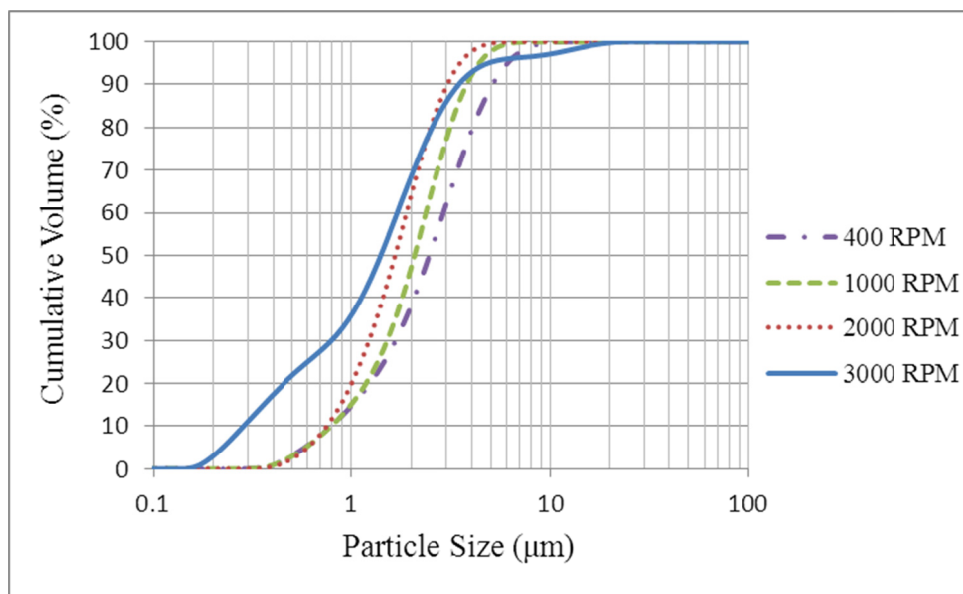


Figure 4.20 Effect of Mastersizer mixing speed on kaolinite cumulative FSD

Table 4.7 Quantitative comparison of samples with different Mastersizer mixing speeds

MS mixing speed (RPM)	d ₁₀ (μm)	d ₅₀ (μm)	d ₉₀ (μm)
400	0.8	2.6	5.4
1000	0.8	2.2	4.0
2000	0.8	1.8	3.2
3000	0.3	1.5	3.7

Based on the results demonstrated in the figures and the table, 400 RPM was chosen as the mixing speed for every Mastersizer experiment. This is the lowest stirrer speed that can be used and appears to cause the minimum floc damage. However, it is high enough to keep the sample mixed inside the dispersion unit.

Effect of Dilution

The Mastersizer dispersant accessory, Hydro 2000SM, should be filled with de-ionized water to carry the sample through the system. Dilution of the sample can

change water chemistry and, consequently, lead to changes in floc size and structure. The sample dispersion unit holds around 110 ml of DI water. In order to minimize the dilution effect, use of sample filtrate is an option since it has the same water chemistry as the sample. The effect of dilution on FSDs was assessed utilizing a 5 g/L aqueous kaolinite mixture. The sample dispersion unit was first filled with DI water. Size measurement data were then collected. Next, the filtrate from the same sample that was to be tested was used to fill the dispersion unit. Figures 4.21 and 4.22 illustrate the resulting FSDs, as reported by the Malvern Mastersizer. Larger flocs are found in the mixture when sample filtrate is used in the sample dispersion unit. The same observation is also reflected in volume-based d_{10} , d_{50} and d_{90} of the two curves (Table 4.8). It is clear that dilution of the sample with DI water changes the FSD significantly.

Based on the outcome of these experiments, filtrate was used to fill the sample dispersion unit for all Mastersizer experiments, so that the water chemistry remains constant and changes in floc size and structure associated with the use of DI dilution water are avoided.

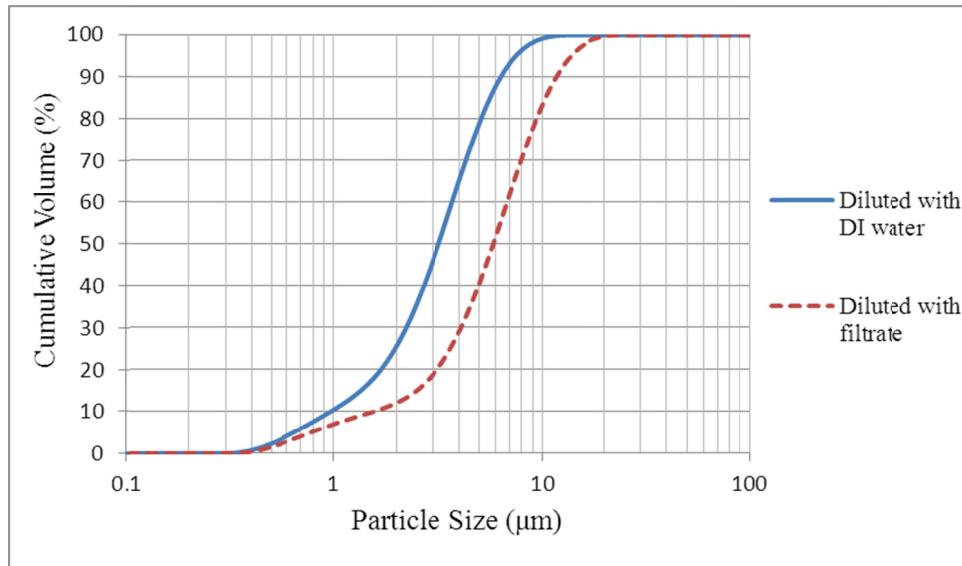


Figure 4.21 Effect of dispersing medium in the Mastersizer on kaolinite cumulative FSD

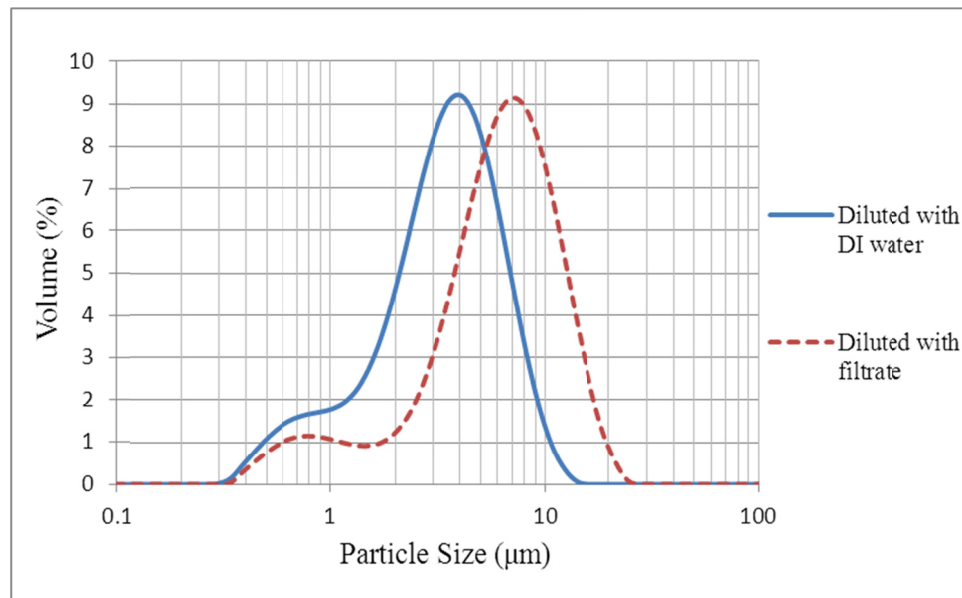


Figure 4.22 Effect of dispersing medium in the Mastersizer on kaolinite frequency FSD

Table 4.8 Quantitative comparison of samples diluted with DI water or filtrate for Malvern Mastersizer measurements

Sample	d ₁₀ (μm)	d ₅₀ (μm)	d ₉₀ (μm)
Diluted with DI water	1.0	3.4	6.8
Diluted with filtrate	1.7	6.2	12.5

Even if the sample filtrate is used so that the water chemistry does not change, the measured FSDs will still be altered because of dilution. To demonstrate the dilution effect, a 5 g/L aqueous kaolinite mixture was measured with the FPIA. The same sample diluted with 110 mL of the filtrate (which is what happens in the Mastersizer) was then tested using the FPIA. The size distribution results are presented in Figure 4.23 and 4.24. Clearly the diluted and non-diluted FSDs are somewhat different. The extent of their difference can be quantitatively obtained from Table 4.9 by comparing representative number-based diameters (mean, d₁₀, d₅₀, d₉₀). The diluted sample contains more particles that are smaller than 2 μm. The fraction of particles larger than 2 μm is greater in the original (undiluted) sample. Hence, diluting a kaolinite sample results in smaller floc sizes. Recall also that this effect was demonstrated in Section 4.1.

In order to obtain conditions for direct FSD comparison between the Mastersizer and the FPIA, samples are diluted with 110 ml of filtrate just before injection to the FPIA sample chamber.

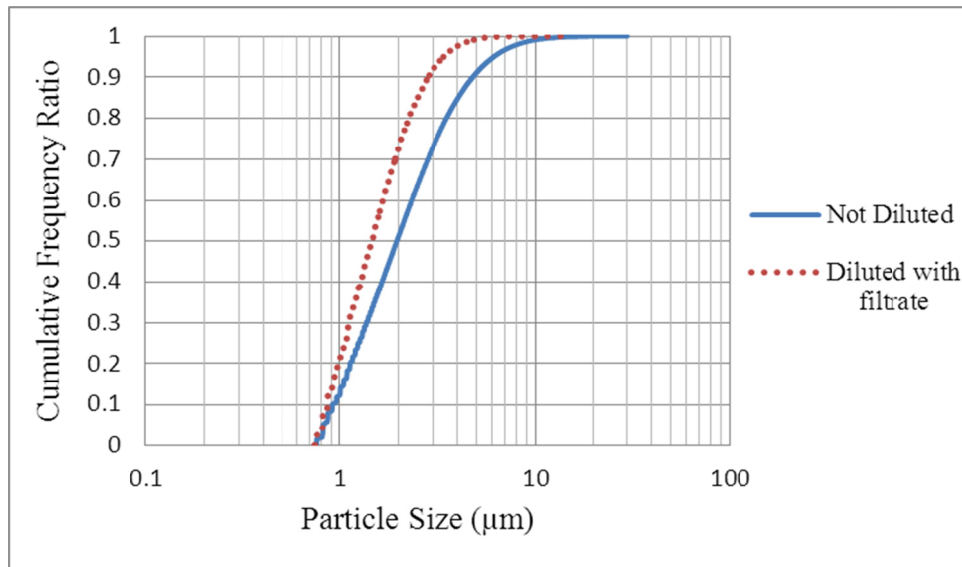


Figure 4.23 Effect of dilution on kaolinite cumulative FSD

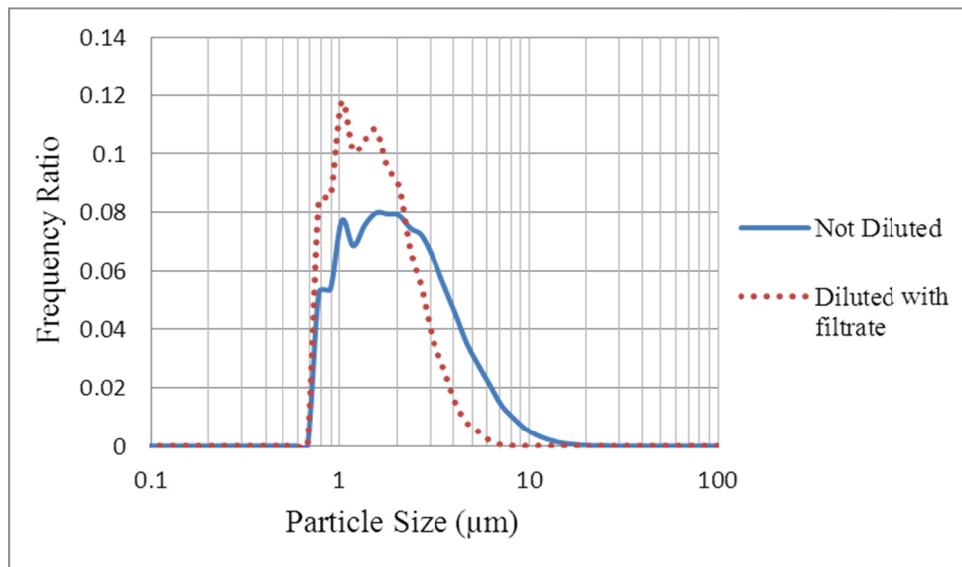


Figure 4.24 Effect of dilution on kaolinite frequency FSD

Table 4.9 Quantitative comparison of diluted and non-diluted samples for Malvern Mastersizer measurements

Samples	Mean diameter (μm)	d_{10} (μm)	d_{50} (μm)	d_{90} (μm)
Not diluted	2.1	0.9	2.0	4.8
Diluted with filtrate	1.3	0.9	1.5	2.8

4.2.4 Microscope Settings

The microscope used in this study had 100, 400 and 1000x magnification options. In order to choose the suitable magnification, samples of kaolinite flocs were viewed under the microscope. A magnification of 1000x results in a very small field of view, which means only a few flocs could be detected. Many pictures would be required in order to get enough particles to produce a reliable FSD. On the other hand, the 100x magnification could fit many flocs in the field of view. However, the images of the flocs were too small and not clear enough for detailed size measurement. The 400x magnification seemed to be the appropriate choice, since it allowed for a reasonable number of particles in one capture and enlarged particles to a suitable size for size measurement analysis.

5 Results and Discussion

5.1 Measurements Repeatability

In this section, the repeatability of the experimental particle/floc size distribution results from two of the devices (FPIA and Mastersizer) tested here are investigated. The repeatability of the measurements is tested by comparing three size distributions of the same sample with each technique.

Due to the fact that the microscope analysis is very time-consuming the microscopy method size distribution repeatability tests were only conducted for kaolinite flocs (not latex and silica particles).

All size distribution data used to plot the graphs (except the cumulative FSDs that had very large amount of data) are presented in Appendix D.

5.1.1 Latex and Sand Particles

In this section, the repeatability of the FPIA and Mastersizer measurements for non-flocculating particles (latex and sand) is tested. A dilute suspension of polystyrene latex particles (0.1 wt%) and a 2.5 g/L suspension of silica flour with DI water was prepared. Three particle size measurements for each sample were made with both devices. The PSDs obtained with both techniques are presented in Figures 5.1 through 5.4.

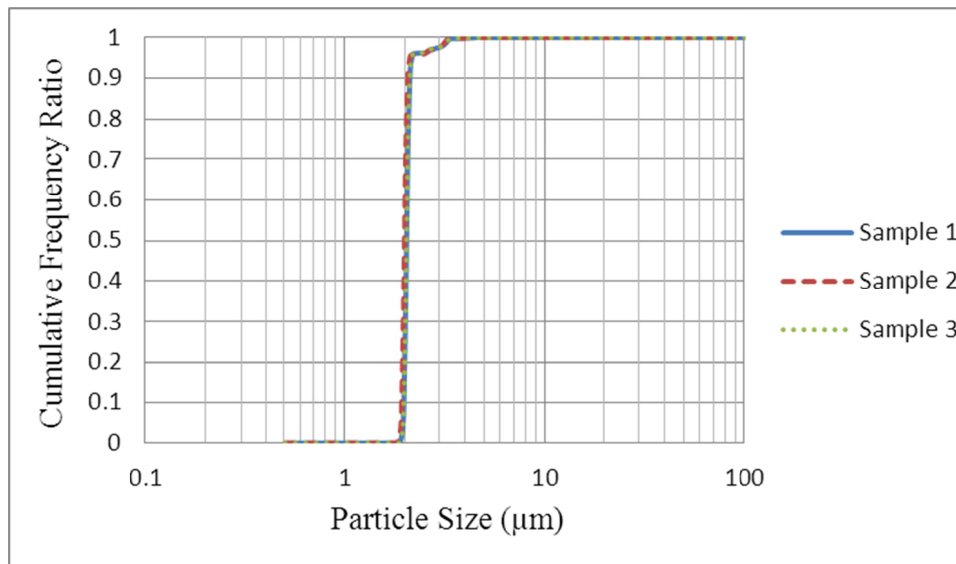


Figure 5.1 Repeatability of FPIA measurements (cumulative latex PSD, 0.1 wt% aqueous suspension)

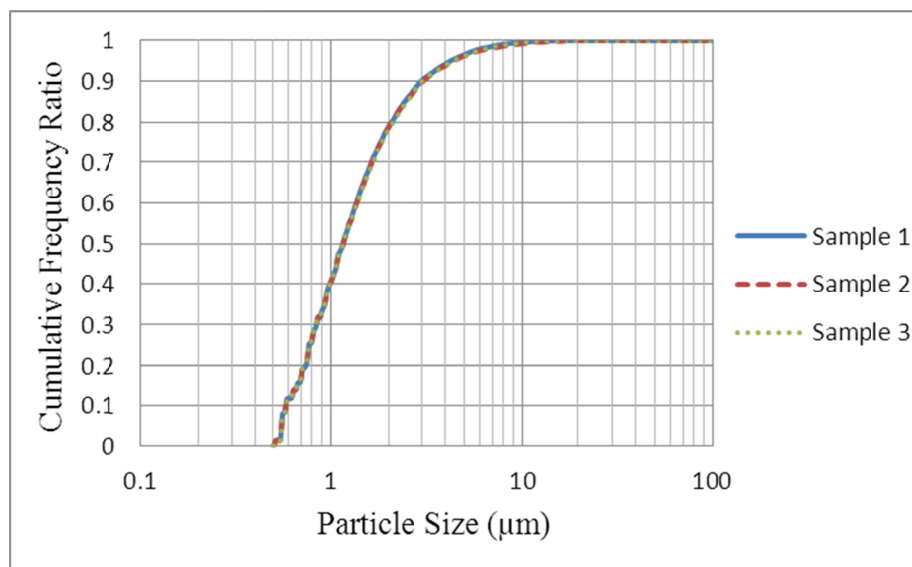


Figure 5.2 Repeatability of FPIA measurements (cumulative silica PSD, $c = 2.5 \text{ g/L}$)

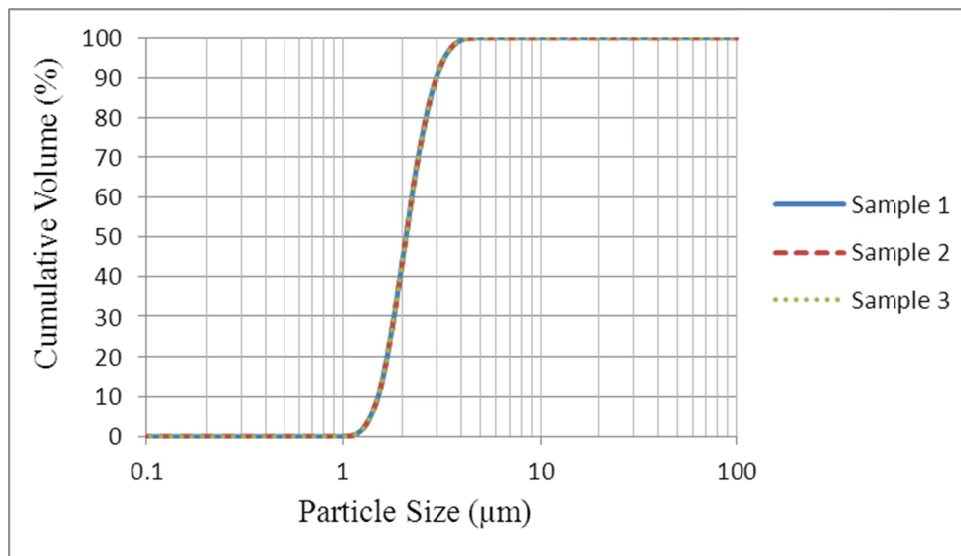


Figure 5.3 Repeatability of Mastersizer measurements (cumulative latex PSD, 0.1 wt% aqueous suspension)

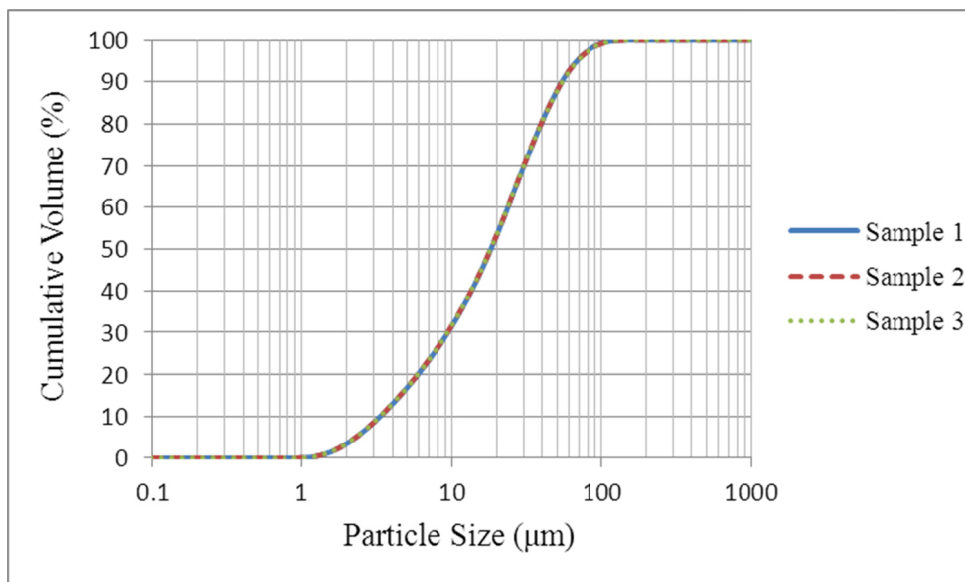


Figure 5.4 Repeatability of Mastersizer measurements (cumulative silica PSD, $c = 2.5$ g/L)

As shown in the graphs, all three latex PSD measurements obtained with the FPIA and Mastersizer are identical. It is the same for the sand PSD measurements. No quantitative analysis of repeatability was undertaken as both instruments are designed for measurements of this type. The figures, above, demonstrate the high degree of repeatability obtained for PSD measurements of these non-flocculating particles.

5.1.2 Kaolinite Flocs

FPIA Measurements

To test the repeatability of the FPIA measurements, three floc size measurements from a single kaolinite suspension are compared. The result for a 5 g/L aqueous kaolinite mixture at pH 9, with 0.01 M CaCl₂ concentration is presented in Figure 5.5 and Figure 5.6. Quantitative descriptions of the FSDs are also calculated and reported in Table 5.1. The mean diameter, number based d_{10} , d_{50} and d_{90} for the three FPIA measurements can be compared in the table.

As indicated in the graphs and table, the FSD curves are very similar and the size measurements are repeatable. Minor variations should be expected because of the colloidal nature of the kaolinite suspension.

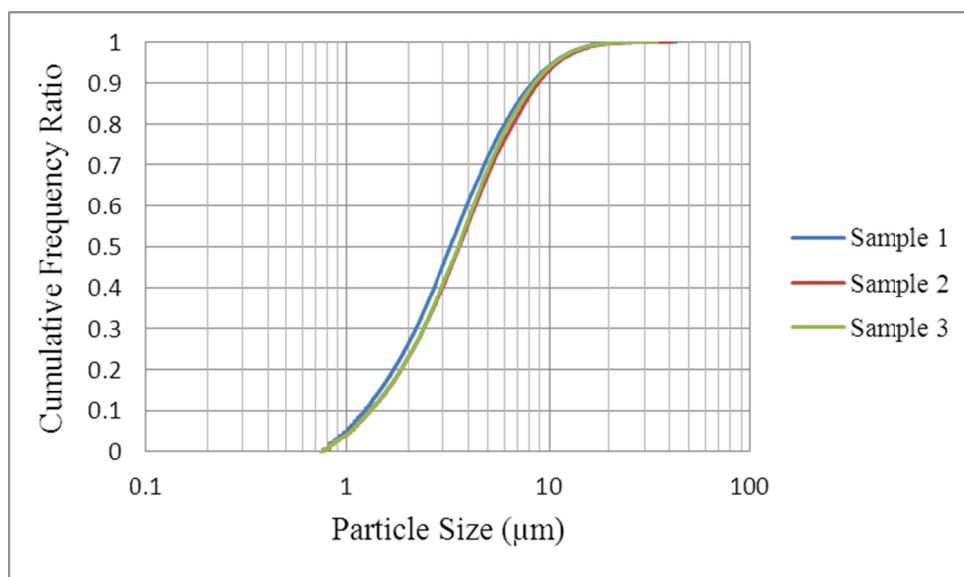


Figure 5.5 Repeatability of FPIA measurements (cumulative kaolinite FSD, $c = 5$ g/L, 0.01 M CaCl_2 , pH 9)

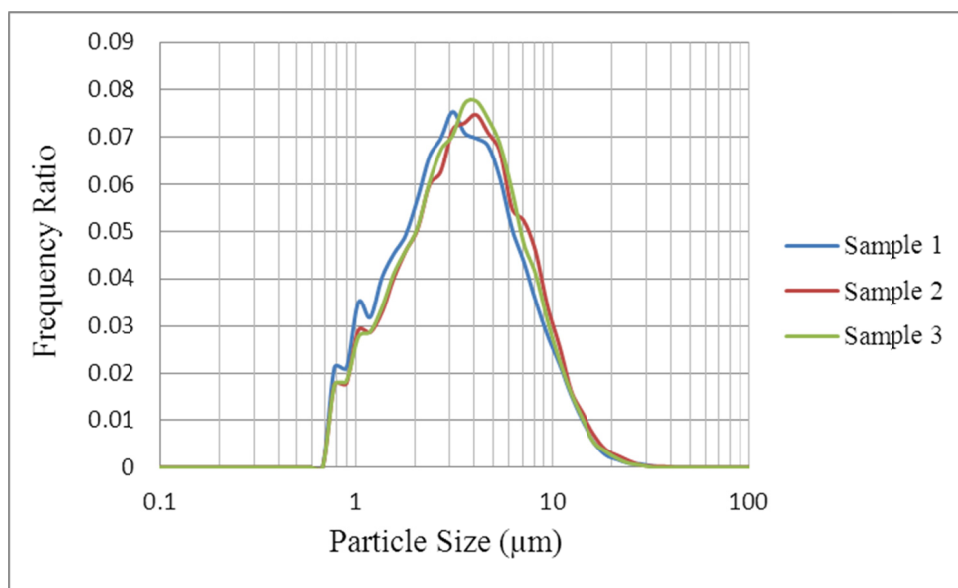


Figure 5.6 Repeatability of FPIA measurements (frequency kaolinite FSD, $c = 5$ g/L, 0.01 M CaCl_2 , pH 9)

Table 5.1 Quantitative comparison of the FPIA repeatability measurements

Samples	Mean diameter (μm)	d_{10} (μm)	d_{50} (μm)	d_{90} (μm)
1	3.8	1.2	3.2	8.3
2	4.1	1.3	3.6	8.8
3	3.9	1.3	3.6	8.5

In order to compare the distributions in a more quantitative manner, the size distribution data from the FPIA are fitted with a known distribution.

It is believed that the log-normal distribution is a common distribution for naturally occurring particle populations (Rhodes, 2008; Berg, 2010). As Niemeijer et al. (2009) state, the particle sizes in a hydrocarbon reservoir are typically distributed log-normally. Lemb et al. (1993) and Boldridge (2010) also showed that aggregates typically demonstrate a log-normal size distribution. Therefore, the log-normal distribution was used to fit and describe the data in the present study. In this way, the data can be approximated by the distribution and described by the mean and standard deviation. If these parameters are “the same” i.e. not significantly different for two or more distribution, then the repeatability of the measurements is quantified.

The best-fit curve was found by using an Octave code written by J. S. Kroll-Rabotin. The code, presented in Appendix A, uses the least squares method which minimizes the summation of the squares of the residuals of the points from the log-normal curve.

The equation of cumulative log-normal distribution, used for curve fitting, is given as:

$$F(x) = 0.5 \operatorname{erfc} \left[-\frac{\ln x - \mu_{\log x}}{\sqrt{2}\sigma_{\log x}} \right] \quad (5.1)$$

where μ ($\in \mathbb{R}$) and σ ($\in (0, \infty)$) are the mean and standard deviation of the normal distribution (logarithm of the data), respectively.

The cost function used in the code is the summation of squared differences between the real data and the fitted graph for each data point and is given by:

$$\text{Cost} = \sqrt{(F(x_i) - y_i)^2 / (n - 1)} \quad (5.2)$$

By minimizing this function the best matching cumulative log-normal graph is identified and the two distribution coefficients ($\sigma_{\log x}$ and $\mu_{\log x}$) are calculated. The results are shown in Table 5.2. The curve fitting graph from Octave software is depicted in Figure 5.7.

Employing the probability theorem results in the following equations for mean (μ), median (M) and standard deviation (σ) of the log-normally distributed data (Limpert et al., 2001):

$$\mu = e^{\mu_{\log x} + 0.5\sigma_{\log x}^2} \quad (5.3)$$

$$M = e^{\mu_{\log x}} \quad (5.4)$$

$$\sigma = \sqrt{(e^{\sigma_{\log x}^2} - 1)e^{2\mu_{\log x} + 0.5\sigma_{\log x}^2}} \quad (5.5)$$

These parameters are calculated for fitted log-normal distributions in Table 5.2.

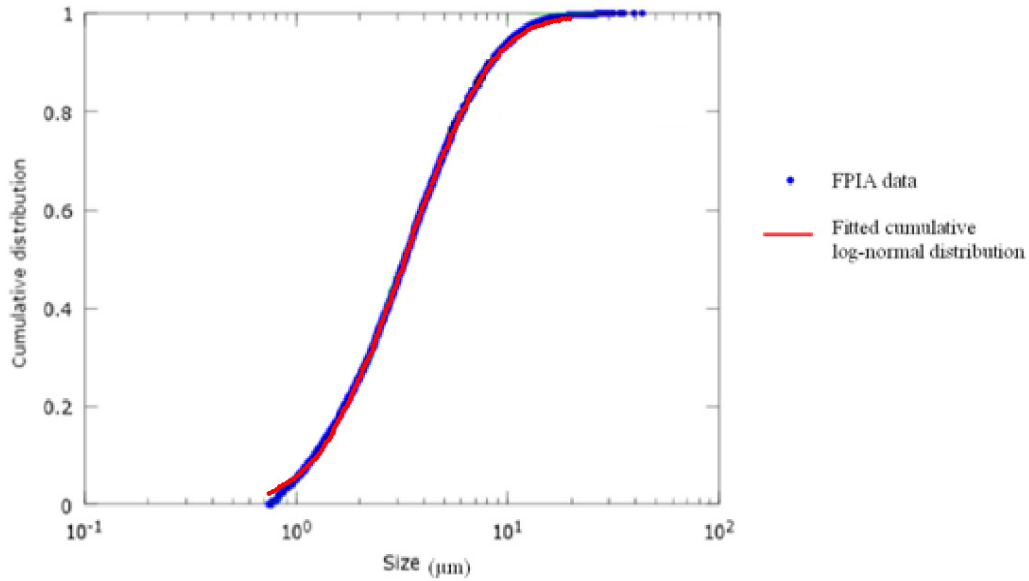


Figure 5.7 FPIA data curve fitting using Octave code

Table 5.2 Quantitative comparison of the FPIA curve fitting parameters

Sample	Cost	$\sigma_{\log x}$	$\mu_{\log x}$	μ	M	σ
1	0.004	0.7	1.2	4.3	3.2	3.7
2	0.008	0.7	1.3	4.7	3.6	4.0
3	0.008	0.7	1.3	4.5	3.5	3.7

The results of Figure 5.7, the very small amounts of residuals and the similar mean and median for the three fitted curves and the three measurements (Table 5.1 and 5.2) show how good the log-normal distribution fit the FPIA results. Moreover, the similar values of $\sigma_{\log x}$, $\mu_{\log x}$ and the log-normal distribution parameters (mean, median and standard deviation; see Table 5.2) indicate the repeatability of the FPIA size measurements.

Mastersizer Measurements

The same procedure described in the previous section was repeated to evaluate the repeatability of the Mastersizer size measurements. Three samples are taken from a 5 g/L aqueous kaolinite mixture at pH 9, with 0.01 M CaCl₂ concentration. The samples were then tested with the Mastersizer. The results of the size measurement experiments are depicted in Figures 5.8 and 5.9. Table 5.3 demonstrates the d_{10} , d_{50} and d_{90} values for the distributions shown in the aforementioned figures.

As clearly seen in the figures and the values of Table 5.3, the results are identical for the three tests, which confirms the repeatability of the Mastersizer measurements.

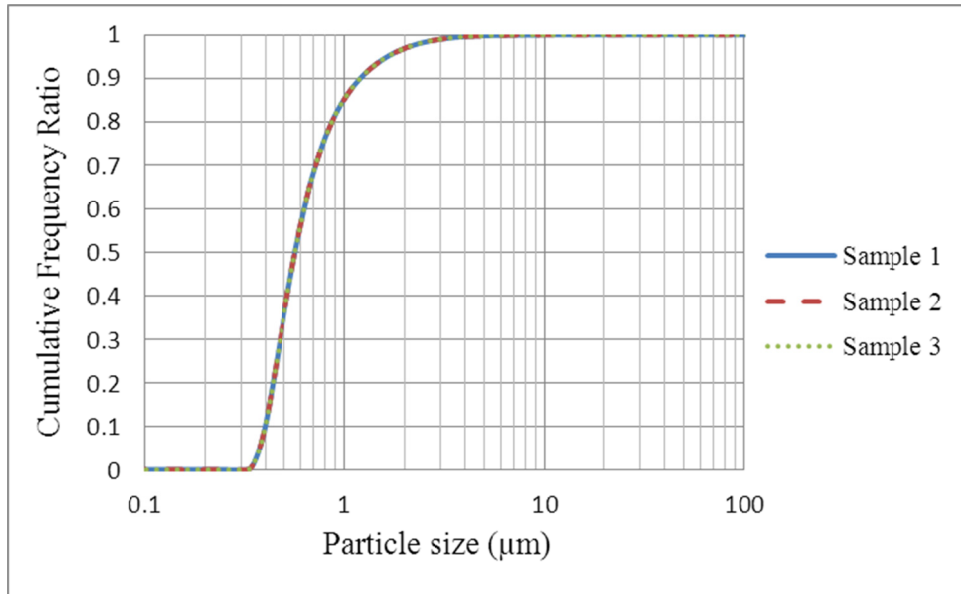


Figure 5.8 Repeatability of Mastersizer measurements (cumulative kaolinite FSD, $c = 5$ g/L, 0.01 M CaCl₂, pH 9)

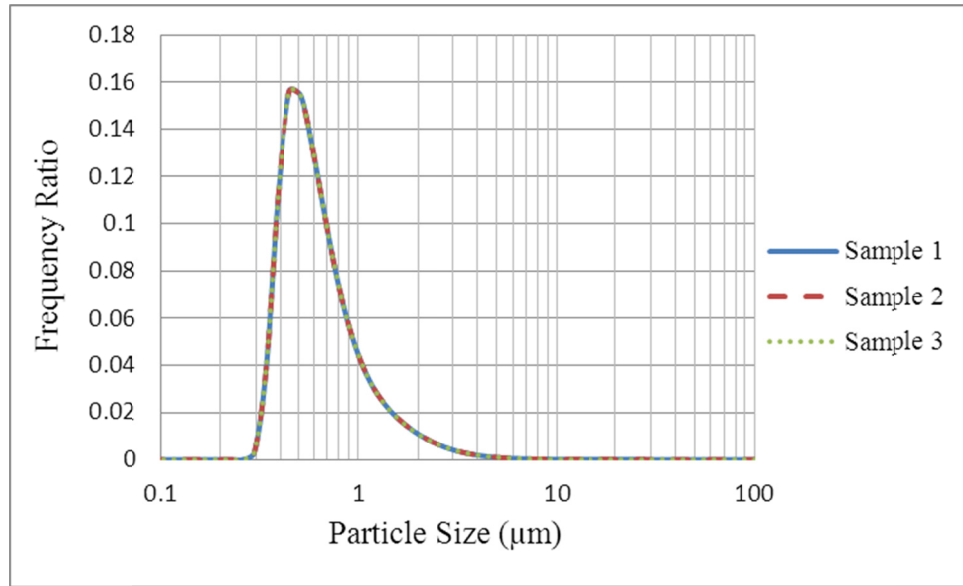


Figure 5.9 Repeatability of Mastersizer measurements (frequency kaolinite FSD, $c = 5$ g/L, 0.01 M CaCl_2 , pH 9)

Table 5.3 Quantitative comparison of the Mastersizer repeatability measurements

Samples	d_{10} (μm)	d_{50} (μm)	d_{90} (μm)
1	0.4	0.6	1.2
2	0.4	0.6	1.2
3	0.4	0.6	1.2

The curve fitting process described in the previous section is also employed here to prove the repeatability of the results. The cumulative log-normal distribution (Equation 5.1) is applied and the cost function, used for curve fitting is described in Equation 5.2. The data fitting result for one of the curves is presented in Figure 5.18. The distribution coefficients and statistical parameters calculated using Equations 5.3 to 5.5 are reported in Table 5.4. From the graph and the table it can be said that the log-normal distribution fits the data very well. The identical

values of the fitted curves (Table 5.4) and measured data (Table 5.3) indicate the same. In summary, the curve fitting results also confirm the repeatability and consistency of the sizing experiments conducted with the Mastersizer.

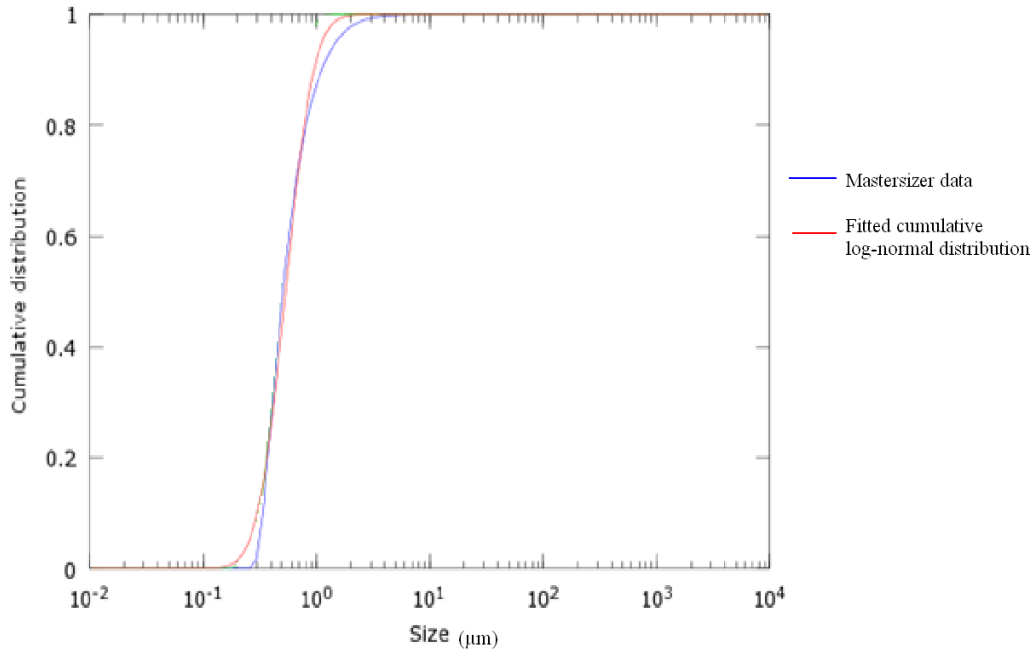


Figure 5.10 Mastersizer data curve fitting using Octave code

Table 5.4 Quantitative comparison of the Mastersizer curve fitting parameters

Sample	Cost	$\sigma_{\log x}$	$\mu_{\log x}$	μ	M	σ
1	0.03	0.4	-0.5	0.6	0.6	0.3
2	0.03	0.4	-0.5	0.6	0.6	0.3
3	0.03	0.4	-0.5	0.6	0.6	0.3

Microscope Measurements

The same experiments and analysis were repeated with the microscopy method. Again, a 5 g/L aqueous kaolinite mixture at pH 9, with 0.01 M CaCl_2 concentration was utilized for the experiment. Three samples were taken from the

suspension and floc size measurements obtained with the microscope. The graphs showing the results are presented here as Figures 5.11 and 5.12. As shown on the graphs, the three FSD curves are similar. Table 5.5 provides quantitative information describing the measured size distributions. In agreement with the graphs, the parameters presented in the table also show similar values for the three measurements. Based on the information provided by the figures and the parameters from the table, the repeatability of the measurements is confirmed.

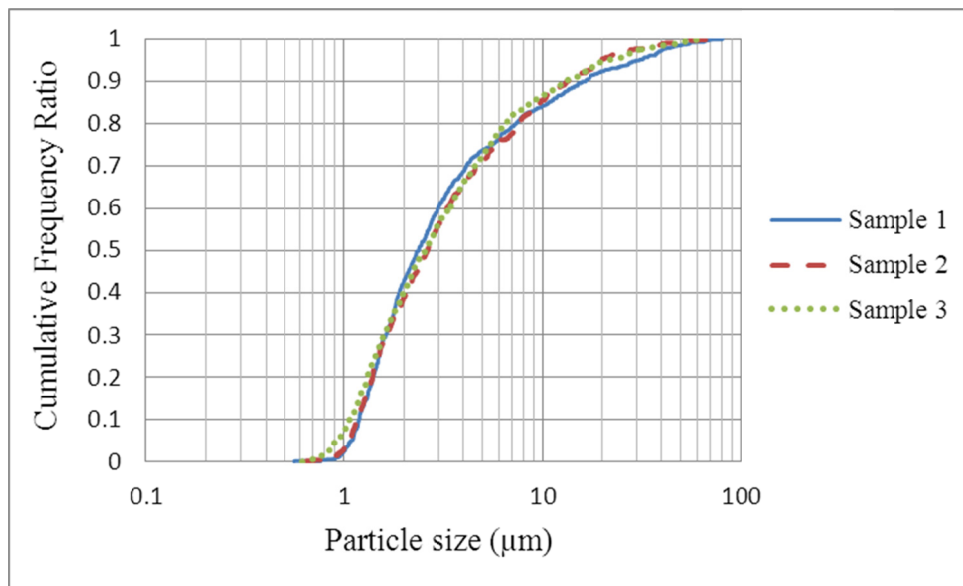


Figure 5.11 Repeatability of microscope measurements (cumulative kaolinite FSD, $c = 5$ g/L, 0.01 M CaCl_2 , pH 9)

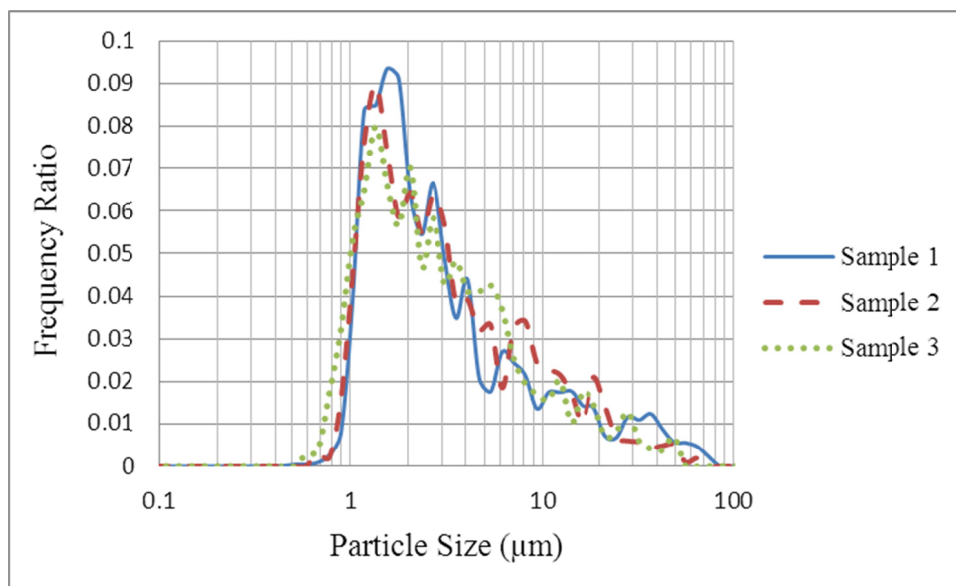


Figure 5.12 Repeatability of microscope measurements (kaolinite frequency FSD, $c=5$ g/L, 0.01 M CaCl_2 , pH 9)

Table 5.5 Quantitative comparison of the microscope repeatability measurements

Samples	Mean diameter (μm)	d_{10} (μm)	d_{50} (μm)	d_{90} (μm)
1	6.4	1.2	2.4	16.4
2	5.6	1.2	2.6	13.2
3	5.6	1.1	3.1	13.1

The curve fitting stage is also repeated for the microscope results, and the result for one of the measurements is presented in Figure 5.13. Table 5.6 provides the calculated statistical parameters for further comparison of the three measurements. Low values of the cost function and the curve fitting graph both show good agreement. The difference, however, can be attributed to operator and manual image analysis errors. By comparing the statistical data for the three curves in Table 5.6, it can be concluded that the microscope measurements are repeatable.

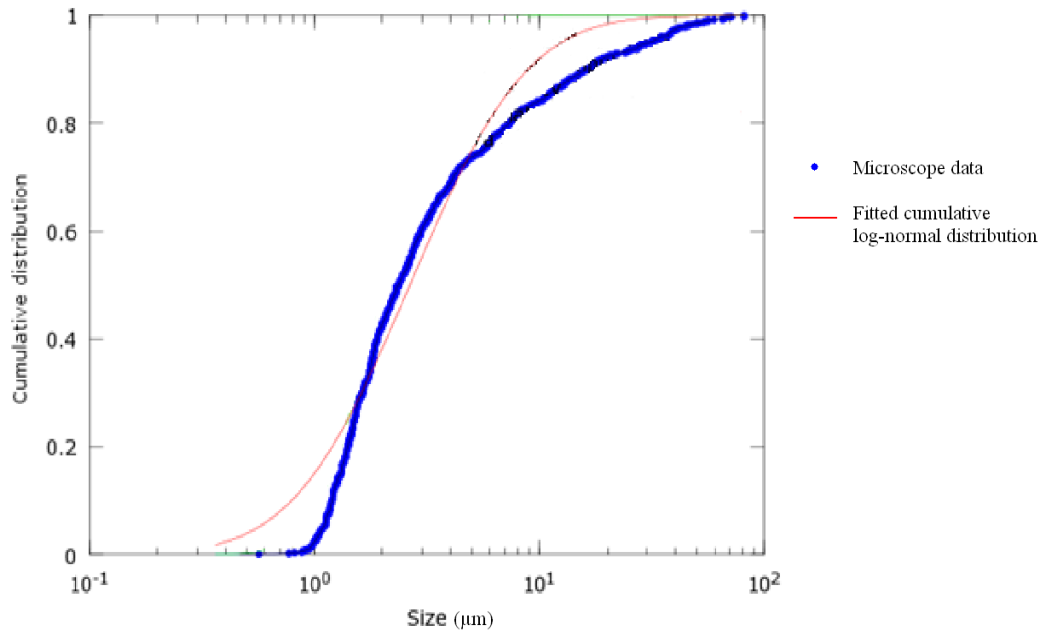


Figure 5.13 Microscope data curve fitting using Octave code

Table 5.6 Quantitative comparison of the microscope curve fitting parameters

Samples	Cost	$\sigma_{\log x}$	$\mu_{\log x}$	μ	M	σ
1	0.04	1.0	1.0	4.4	2.7	5.5
2	0.07	0.9	1.0	4.1	2.6	5.0
3	0.05	1.0	1.0	4.6	2.8	5.8

The similar FSDs and their mean and distribution descriptor values, as well as curve fitting results (Figure 5.13 and Table 5.6) confirm the repeatability of microscope measurements.

5.2 Comparison of the FPIA and Mastersizer Measurements

As per the stated objective of this study, the particle size measurements obtained with the FPIA are compared with those of the Mastersizer. The comparison process starts with mono-dispersed regular-shaped particles. A very dilute suspension of latex particles was utilized for this purpose. Then, non-flocculating irregular-shaped particle size distributions are compared. Silica flour in a suspension represents this type of particle. Finally, the comparison is made with different types of kaolinite flocs, including primary flocs and flocs formed in mixtures with different conditions (natural, acidic, basic with coagulant). Primary flocs are smaller, more rigid and less sensitive structures than the other types of flocs. Various conditions and flocs are used to validate the FPIA with different types of floc size and structure.

5.2.1 Latex Suspension

In order to compare the size distribution of standard particles, a suspension of latex particles was used. A 10 wt% latex suspension was prepared and then diluted 100 times with de-ionized water. The polystyrene latex particles are spherical and are essentially mono-sized, with a particle diameter of 2 μm . The particle size distribution of the dilute latex suspension was then measured with the FPIA and the Mastersizer. In order for the results to be comparable, some changes need to be made to directly compare the PSDs. As previously described in Chapter 3, Mastersizer volume-based results are converted to number-based particle size distributions. Additionally, the particle sizes reported by the FPIA are

divided into the same bins defined in the Mastersizer. In this way, both the frequency and cumulative particle size distributions can be compared.

The PSDs obtained from the FPIA and Mastersizer are illustrated in Figure 5.14 and Figure 5.15. As expected, both graphs are centered at 2 μm . Figure 5.14 shows identical number-based d_{50} for the two distributions and accordingly, the mean/median values reported in Table 5.7 are identical. Figure 5.15 also shows that the most frequent size of particle in the suspension is $\sim 2 \mu\text{m}$. The only difference is the deviation around the center or size range in the two distributions. The FPIA has a sharper distribution and shows a better indication of a suspension of mono-sized particles. The Mastersizer results show a broader distribution. Figure 5.16 shows some of the particles detected by the FPIA. Although almost all particles are 2 μm in size, note that a few multiplets can be seen. These multiplets are the reason for the small frequency increase around 3 μm in the FPIA graph.

Based on the values in the results presented here, it can be concluded that both techniques are very good for narrowly sized, spherical particles.

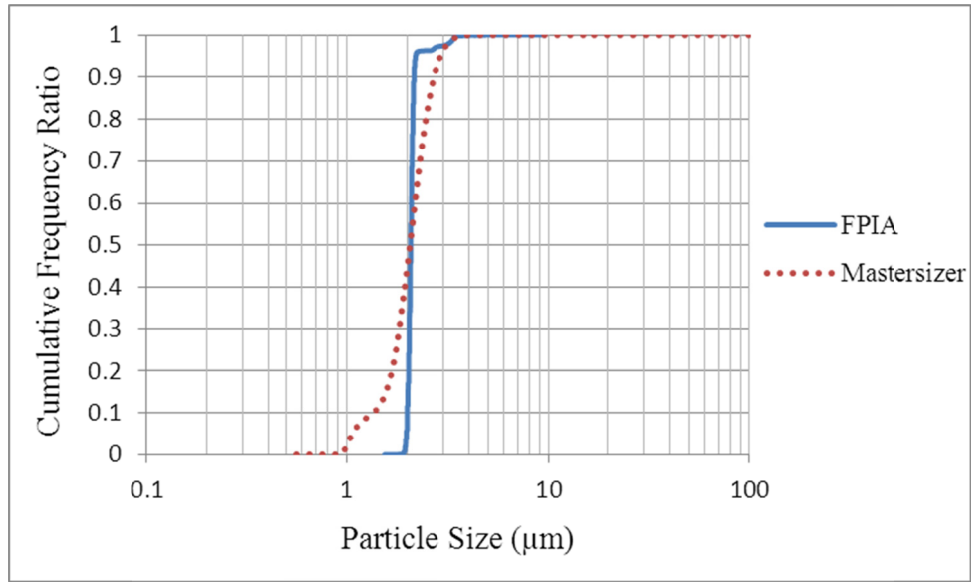


Figure 5.14 Cumulative particle size distributions for the 2 μm latex particles obtained using the FPIA and Mastersizer

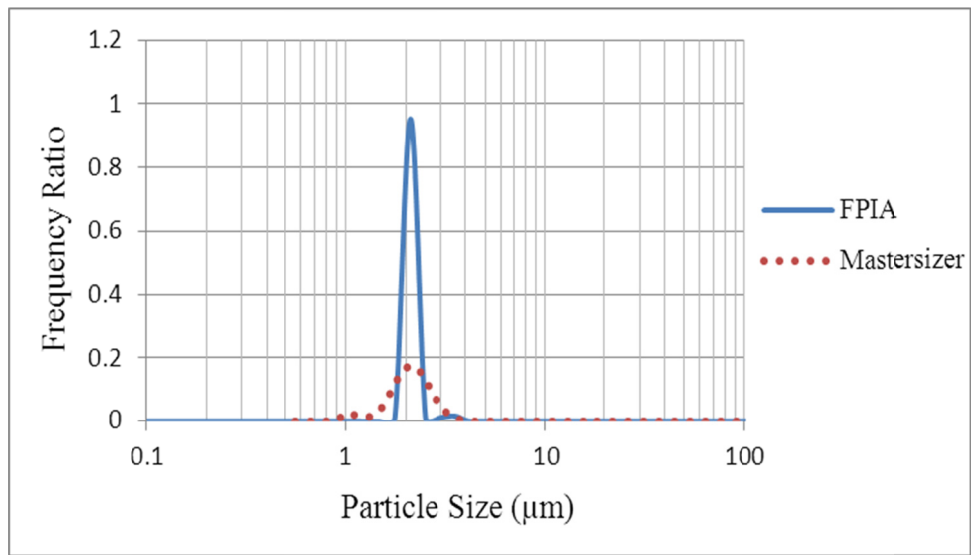


Figure 5.15 Frequency particle size distributions for the 2 μm latex particles obtained using the FPIA and Mastersizer

Table 5.7 Comparison of latex measurements with the FPIA and Mastersizer

	Mean diameter (μm)	d_{50} (μm)
FPIA	2.1	2.1
Mastersizer	2.1	2.1

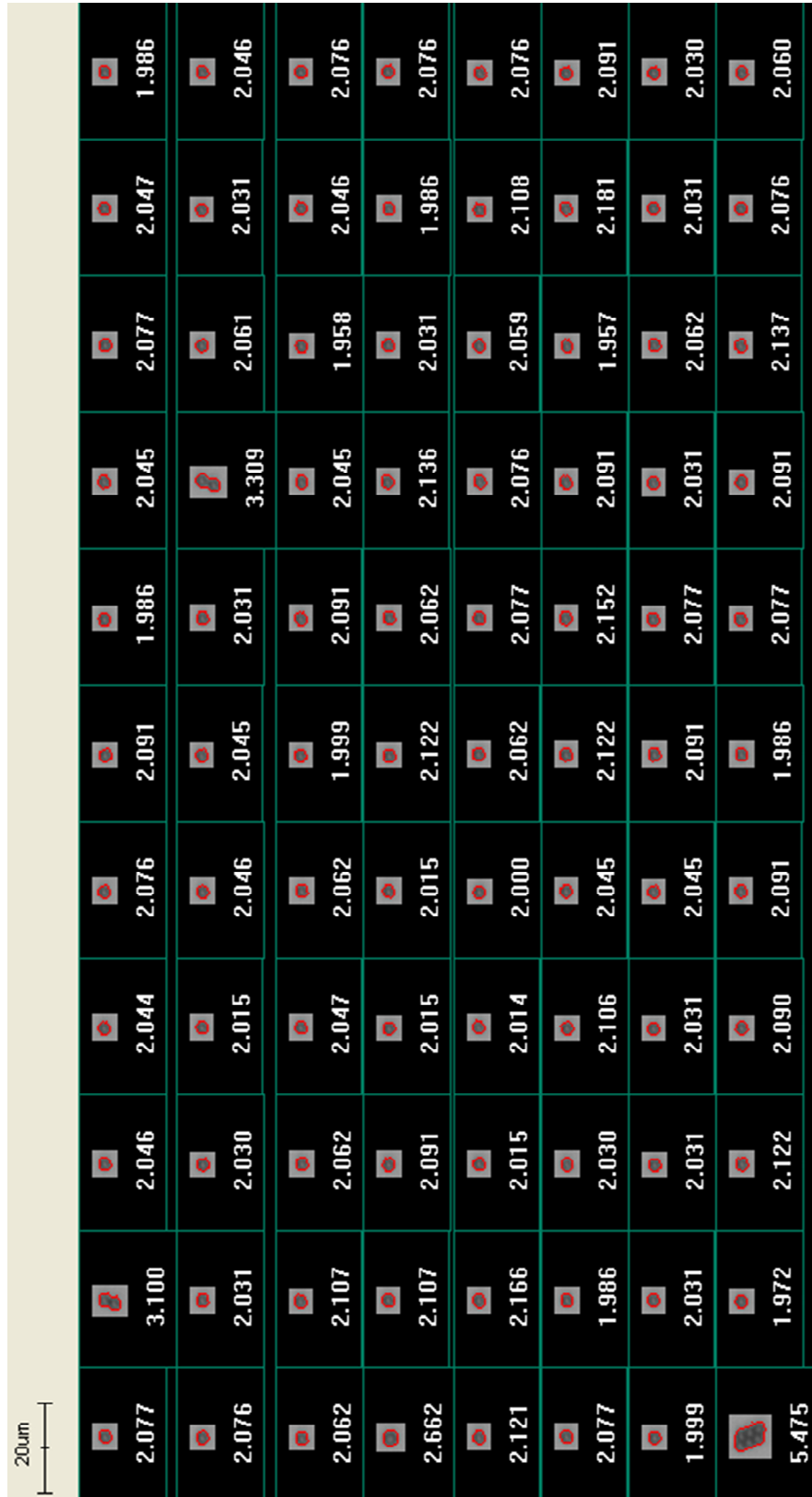


Figure 5.16 Some latex particles detected by the FPIA

5.2.2 Silica Flour Suspension

The next step was to obtain the results for non-flocculating irregular-shaped particles. A suspension of 2.5 g/L silica flour was prepared for this purpose. The mixture size distribution was measured using the FPIA and Mastersizer. The PSDs are illustrated in Figures 5.17 and 5.18. The images of some silica articles exported from the FPIA software are also shown in Figure 5.19. The graphs look similar except the small variations that are more visible in the frequency PSD graph. This difference may be due to the fact that the two apparatus measure particle size based on different principles. The FPIA is an image analysis based method while the Mastersizer utilizes laser diffraction. Also, the theory that is utilized in the Mastersizer assumes particles as spheres, while the silica particles, as seen in Figure 5.19, are far from spherical. This may be another reason that contributes to the differences between the two PSDs.

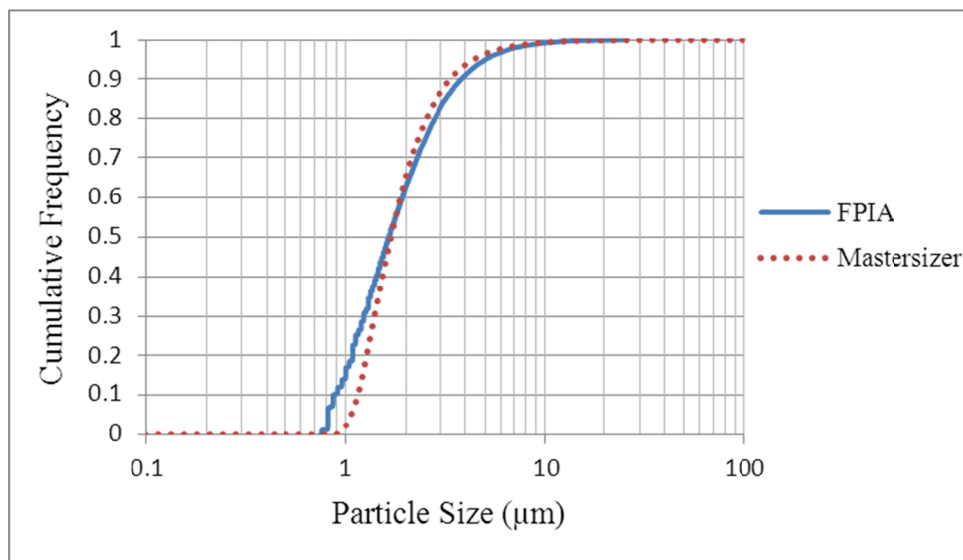


Figure 5.17 Cumulative particle size distributions for the silica particles obtained using the FPIA and Mastersizer

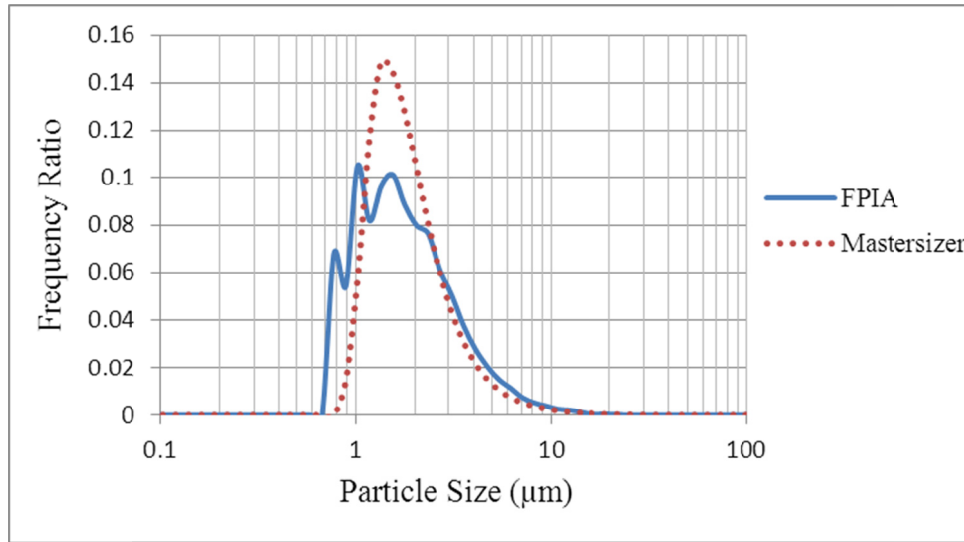


Figure 5.18 Frequency particle size distributions for the silica particles obtained using the FPIA and Mastersizer

For a more quantitative comparison of the two PSDs, Table 5.8 and Figure 5.20 are provided. The information in the table is obtained from the cumulative PSD data. Figure 5.20 compares the frequency of particles in different size ranges for the two devices. The results of Figure 5.18 are used to produce the information for Figure 5.20. In the graph on the left, for a specific bin size, X coordinate of the point in that graph is adopted from the frequency of particles in that bin from the FPIA and Y coordinate is the frequency of particles in the same bin from the Mastersizer. The graph on the right shows the difference of the two measurements for different bin sizes. The representative diameters of both PSDs can be compared in the table. Note that the d_{50} values are very similar. In Figure 5.20, it can be seen that most of the points fall on or near the $y=x$ line which means that distribution of the particles in many of the bin sizes is the same for both measurements.

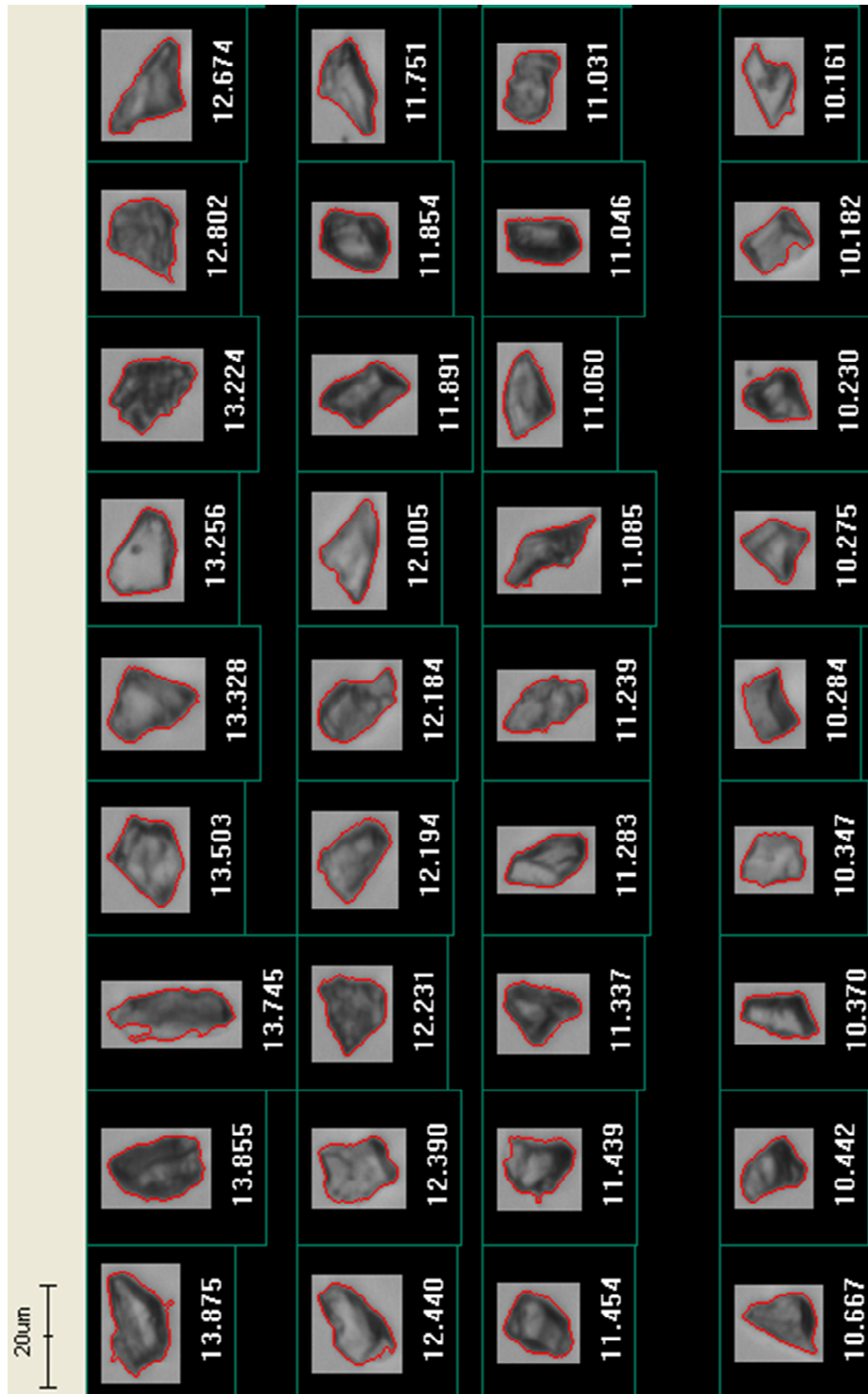


Figure 5.19 Some silica particles detected by the FPIA

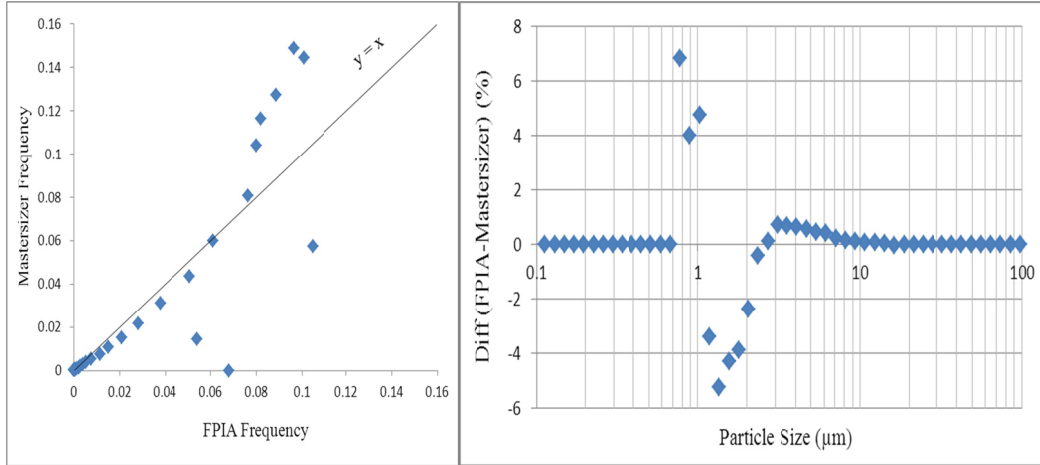


Figure 5.20 Comparison of the FPIA and Mastersizer frequency for silica particles

Table 5.8 Comparison of silica flour measurements with the FPIA and Mastersizer

	Mean diameter (μm)	d ₁₀ (μm)	d ₅₀ (μm)	d ₉₀ (μm)
FPIA	1.7	0.9	1.6	3.8
Mastersizer	2.1	1.1	1.7	3.2

Thus, the silica flour PSDs generated with the FPIA and Mastersizer are in good agreement.

5.2.3 Kaolinite Flocs

In order to compare FSDs obtained from the FPIA and Mastersizer, four types of flocs (primary, natural, acidic and coagulated basic) are utilized. Suspensions with different conditions can produce flocs with different sizes and structures, as discussed previously. Primary flocs are produced through a procedure adopted from Vaezi et al. (2011). These flocs are smaller and more rigid and have a narrower size range than the other types of flocs. A suspension of kaolinite-water produces so called natural flocs. The mixture of kaolinite and water with addition

of HCl forms more expanded E-F structure flocs (acidic flocs). Finally, addition of NaOH and CaCl₂ to the kaolinite-water suspension generates denser F-F flocs (coagulated basic flocs). Suspensions containing these different floc types are analyzed with the FPIA and Mastersizer, and the PSDs are compared.

Primary Flocs

Primary flocs are smaller in size and have a more rigid structure that are much less sensitive to shear than the other types of flocs. Thus, before carrying out experiments with natural, acidic and alkaline coagulated flocs, primary flocs are measured and compared. These flocs are prepared in a two-day process as described in Section 3.3.1. The FSDs measured with the FPIA and Mastersizer are presented in Figure 5.21 (cumulative) and Figure 5.22 (frequency). Some quantitative information from the cumulative FSDs is presented in Table 5.9. Some of the larger flocs detected by the FPIA are depicted in Figure 5.23. The differences between the measurements can be clearly seen in Figure 5.21. The differences in frequency ratios for different sizes are also shown on Figure 5.22. Generally, the FSD reported by the Mastersizer shows smaller sizes than the FPIA. Only over the range of 0.7 to 4 μm do both instruments show particles. The FPIA shows more particles that are larger than 0.7 μm , and the Mastersizer shows a much greater proportion of flocs/particles that are smaller than 0.7 μm . As indicated in Table 5.9, 90 percent of the particles measured by the Mastersizer are smaller than 1.1 μm , while this number is 2.8 μm for the FPIA. Therefore, most of the particles detected by the Mastersizer appear to fall in the primary particle size range.

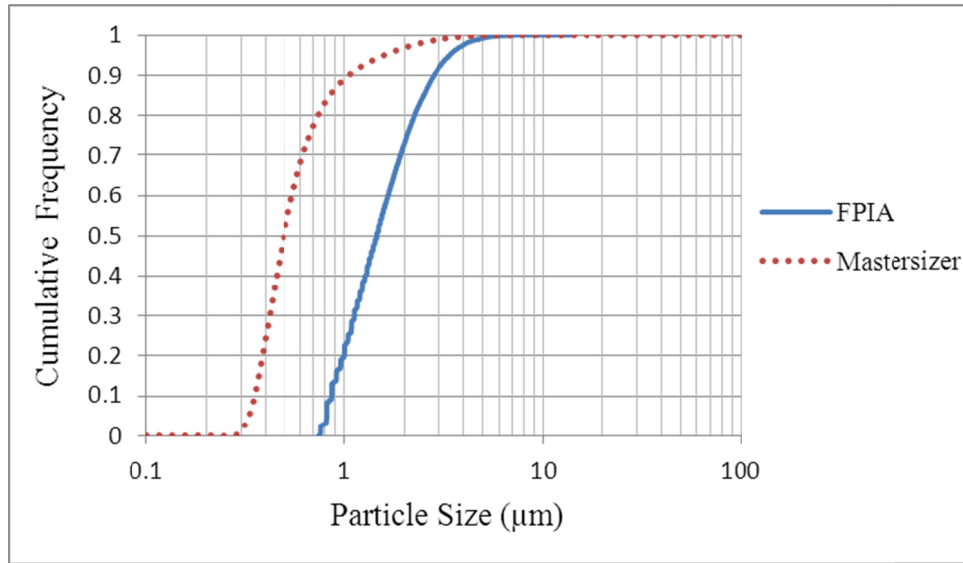


Figure 5.21 Cumulative floc size distributions for kaolinite primary flocs obtained using the FPIA and Mastersizer

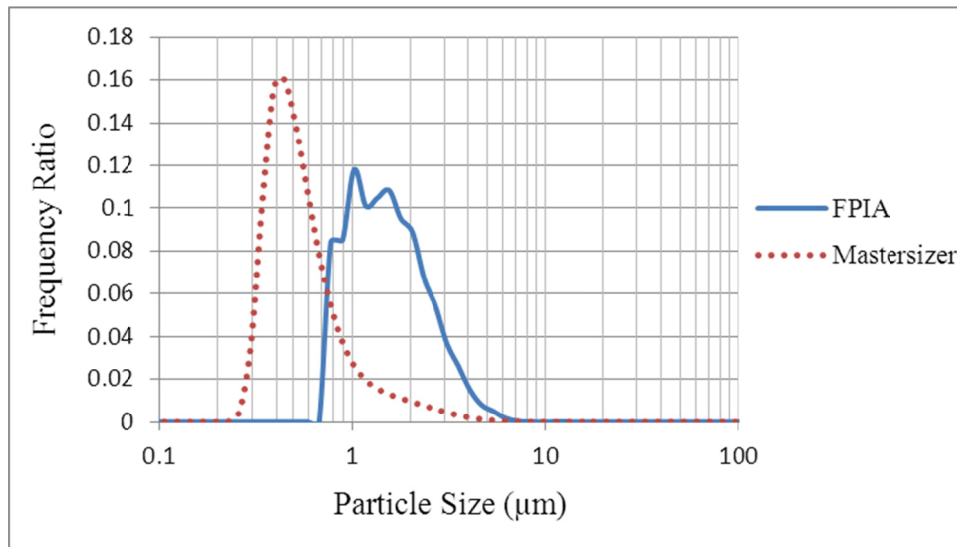


Figure 5.22 Frequency floc size distributions for kaolinite primary flocs obtained using the FPIA and Mastersizer

Table 5.9 Comparison of primary flocs measurements with the FPIA and Mastersizer

	Mean diameter (μm)	d ₁₀ (μm)	d ₅₀ (μm)	d ₉₀ (μm)
FPIA	1.3	0.9	1.5	2.8
Mastersizer	0.7	0.3	0.5	1.1

For a further comparison of the FSDs from the two instruments, Figure 5.24 is presented. Regarding the graph on the left, since the coordinate of each point is (FPIA frequency, Mastersizer frequency) for a specific defined bin size, the nearer each point is to the $y=x$ line the more similar are the measurements. For most of the bin sizes there are flocs available only with one of the measurements and zero or almost zero for the other one (this difference is specified with respect to the particle sizes in the graph on the right). Only a few points fall near the parity line. Therefore, it can be concluded that measurements of floc size distributions from the two devices do not match.

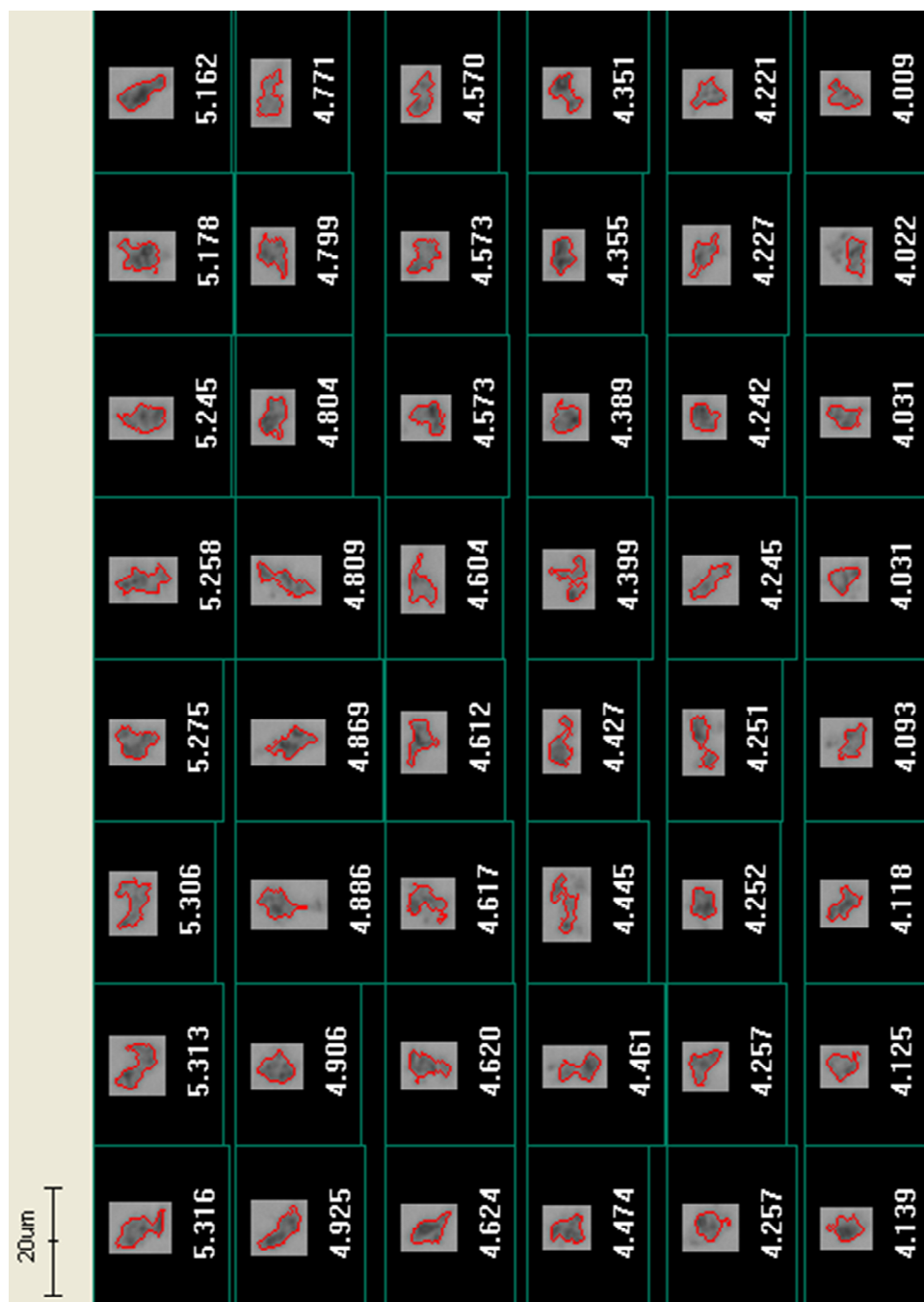


Figure 5.23 Some of the largest primary kaolinite floccs detected by the FPIA

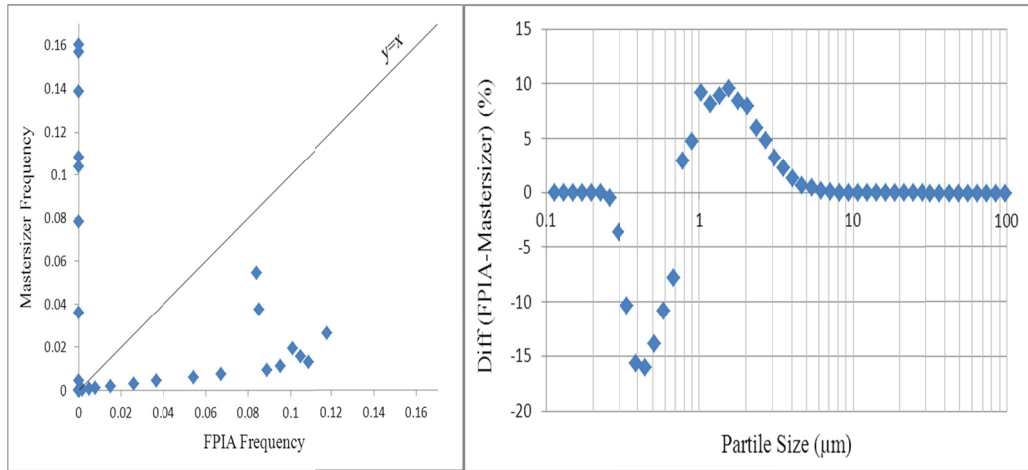


Figure 5.24 Comparison of the FPIA and Mastersizer frequency for kaolinite primary flocs

Natural Flocs

Natural flocs are made by adding DI water to kaolinite. A 5 g/L aqueous kaolinite suspension with pH 4.9 was produced. Once the sample is prepared as described in Chapter 3, floc size measurements are made with the FPIA and Mastersizer. The resulting FSDs are illustrated in Figure 5.25 and Figure 5.26. Some quantitative information for a better comparison of the graphs is reported in Table 5.10. Some of the flocs detected by the FPIA are also presented in Figure 5.27.

Similar to the primary flocs results, measurements of the natural floc suspension FSDs obtained with the two instruments are not in agreement. The only common size range is 0.7 μm to 4 μm , and even in that size range the frequency of the particles differ greatly. For sizes larger than 0.7 μm , the FPIA shows a greater proportion of flocs, and the Mastersizer measurements show that small particles (or flocs) dominate the FSD. As demonstrated in Table 5.10, 90 percent of the flocs detected by the FPIA are smaller than 4.0 μm , while the number-based d_{90}

from the Mastersizer is $1.0\ \mu\text{m}$. This suggests that most of the entities measured by the Mastersizer are individual kaolinite particles rather than flocs.

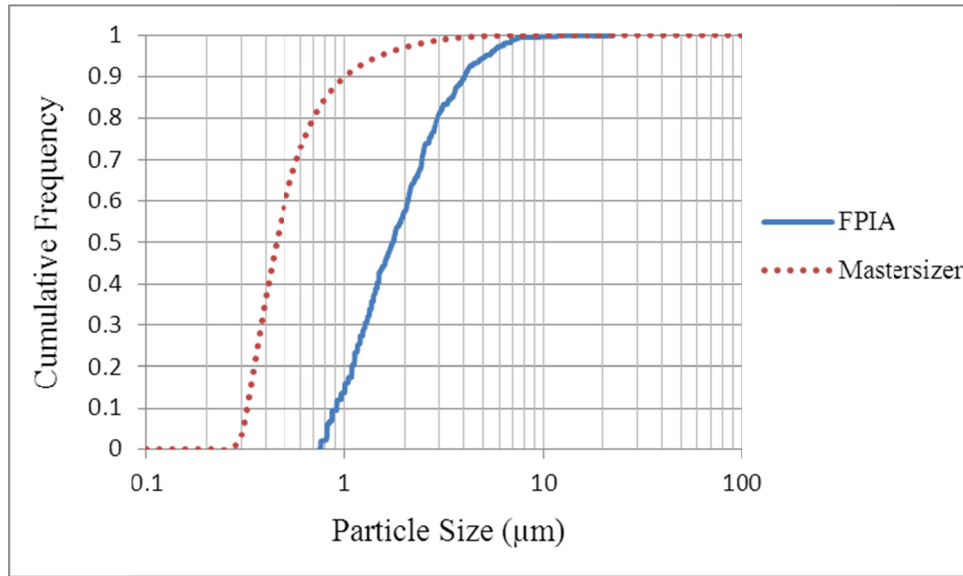


Figure 5.25 Cumulative floc size distributions for kaolinite natural flocs obtained using the FPIA and Mastersizer

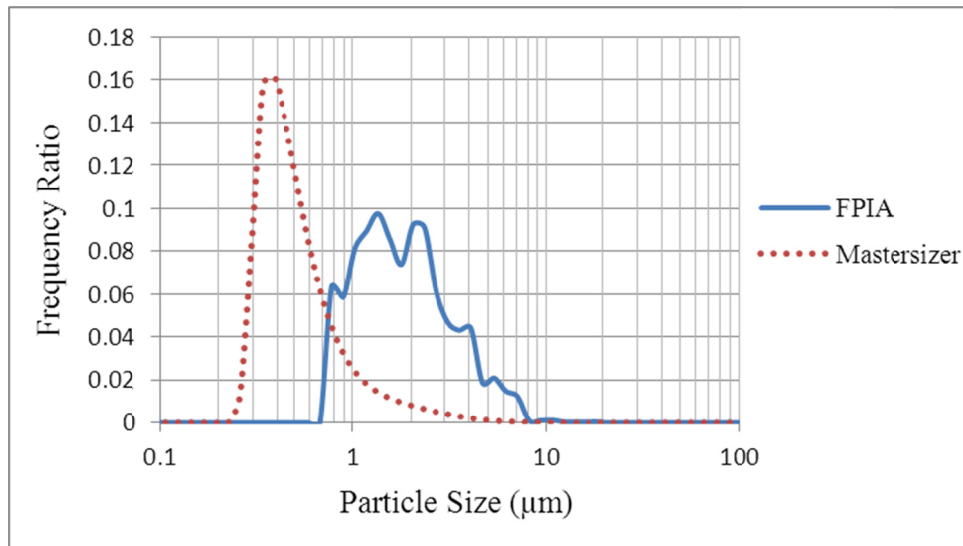


Figure 5.26 Frequency floc size distributions for kaolinite natural flocs obtained using the FPIA and Mastersizer

Table 5.10 Comparison of natural flocs measurements with the FPIA and Mastersizer

	Mean diameter (μm)	d_{10} (μm)	d_{50} (μm)	d_{90} (μm)
FPIA	1.8	0.9	1.7	4.0
Mastersizer	0.6	0.3	0.4	1.0

Figure 5.28 presents Mastersizer frequency versus FPIA frequency and the difference of the two measurements for all bin sizes. In the graph on the left, there are only a few data points that are near the line. In many cases, the frequency is zero in a given size range for at least one of the measurements. The discrepancy is also clear from Figure 5.28 (right).

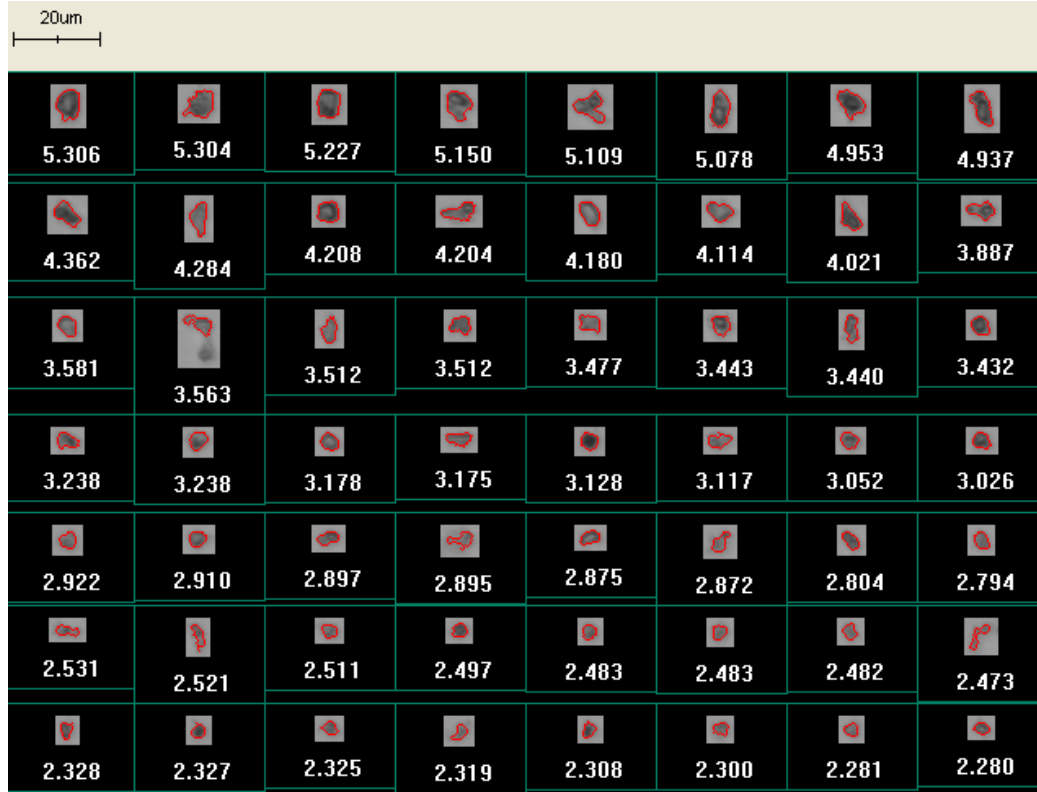


Figure 5.27 Some natural kaolinite flocs detected by the FPIA

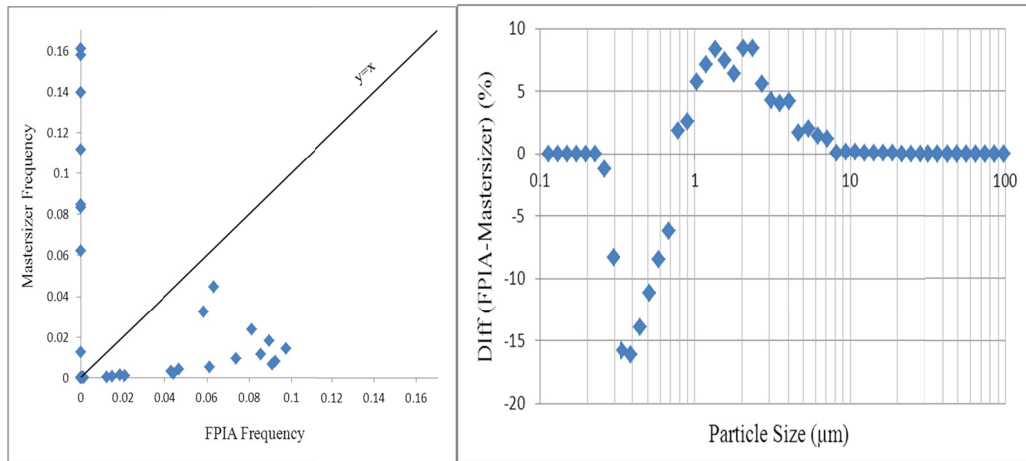


Figure 5.28 Comparison of the FPIA and Mastersizer frequency for kaolinite natural flocs

Based on the results presented in this section, the natural FSDs from the FPIA and Mastersizer are dissimilar. The Mastersizer shows most particles fall into the primary particle size range while particles detected by the FPIA are larger, i.e. in the floc/aggregate size range.

Acidic Flocs

The so-called acidic flocs are produced by adding HCl to the kaolinite-water suspension. The pH of the mixture is set to 3. In this way, highly expanded (F-E) flocs are formed (Michaels and Bolger, 1962; Nasser and James, 2006). The samples are run through both the FPIA and Mastersizer. The results are again presented in the form of cumulative and differential (frequency) FSDs and are depicted in Figures 5.29 and 5.30. Some of the largest flocs of the suspension, as reported by the FPIA, are also shown here as Figure 5.31.

As in the aforementioned graphs of primary and natural flocs, the acidic floc size distribution measurements obtained with the FPIA and Mastersizer are not in

agreement. The only common size range between the two measurements is $0.7 - 2 \mu\text{m}$. For sizes larger than $0.9 \mu\text{m}$ the FPIA size distribution demonstrates a greater proportion. The particles detected by the Mastersizer mostly fall in the primary particle size range.

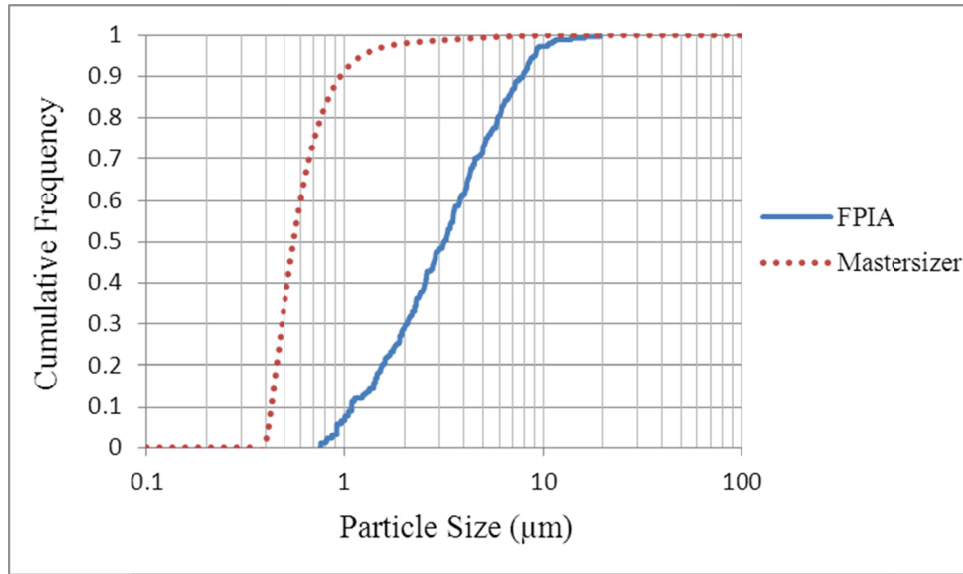


Figure 5.29 Cumulative floc size distributions for kaolinite acidic flocs obtained using the FPIA and Mastersizer

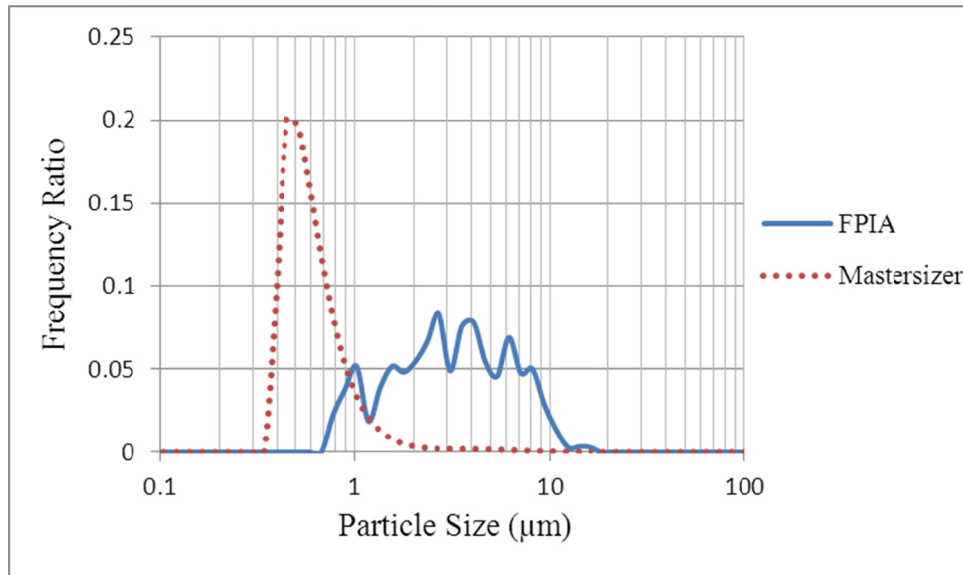


Figure 5.30 Frequency floc size distributions for kaolinite acidic flocs obtained using the FPIA and Mastersizer

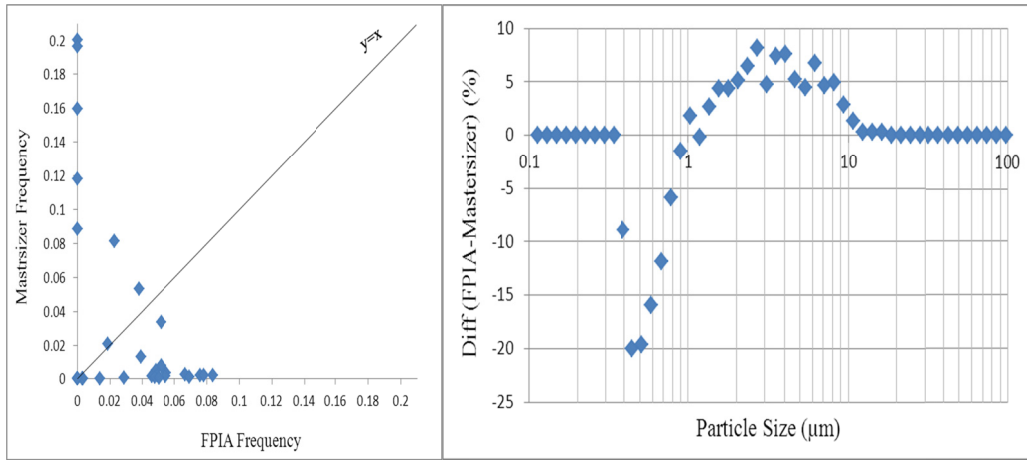


Figure 5.31 Some acidic kaolinite flocs detected by the FPIA

In order to further compare the results, Figure 5.32 and Table 5.11 are provided. A few points in Figure 5.32 (left graph) are located on or around the $y=x$ line. However, most of the points are scattered far from the line, which again shows the discrepancy of the results. The percentage of the frequency ratio difference between the FPIA and Mastersizer is also presented in Figure 5.32 (right graph). As described in Table 5.11, the distribution descriptors differ substantially between the two measurements. The d_{90} for the sample measured with the Mastersizer is $1.0 \mu\text{m}$, which suggests that most of the particles measured using the Mastersizer are broken down to primary particles through floc breakage.

Table 5.11 Comparison of acidic flocs measurements with the FPIA and Mastersizer

	Mean diameter (μm)	d_{10} (μm)	d_{50} (μm)	d_{90} (μm)
FPIA	3.4	1.1	3.1	7.9
Mastersizer	0.7	0.4	0.6	1.0

**Figure 5.32 Comparison of the FPIA and Mastersizer frequency for kaolinite acidic flocs**

Based on the information provided by the figures and table in this section, it can be concluded that the two measurements are not in agreement. The Mastersizer show mostly primary particles while the FPIA shows that particles fall into the floc size range.

Coagulated Alkaline Flocs

The coagulated alkaline samples were prepared as described in Chapter 3. A 5 g/L aqueous kaolinite suspension with 0.01 M CaCl_2 at pH 9 was measured with both the FPIA and Mastersizer. The FSDs are presented in Figures 5.33 and 5.34. Table 5.12 provides the mean diameter and distribution descriptors for the

measurements. Some of the kaolinite flocs captured by the FPIA are also shown in Figure 5.35.

The differences between the two measurements can clearly be seen in the figures. Only within the size range of 0.7 to 3 μm do both devices detect particles. The FPIA shows a greater proportion of sizes larger than 1 μm and the Mastersizer detects many more particles smaller than 1 μm . As reported in the Table 5.12, 90 % of the particles in the Mastersizer graph are smaller than 1.1 μm , indicating that most of the particles measured with the Mastersizer are primary particles.

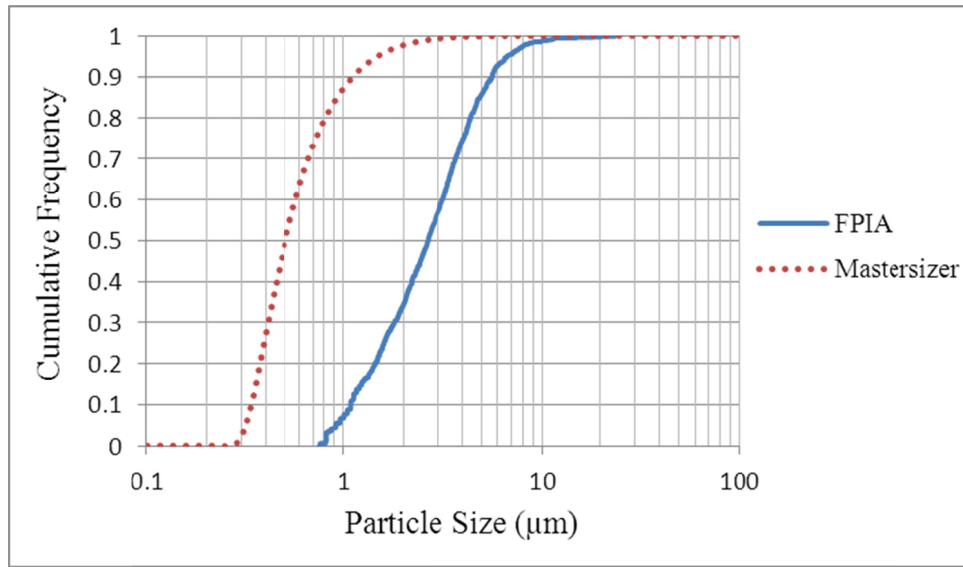


Figure 5.33 Cumulative floc size distributions for kaolinite coagulated alkaline flocs obtained using the FPIA and Mastersizer

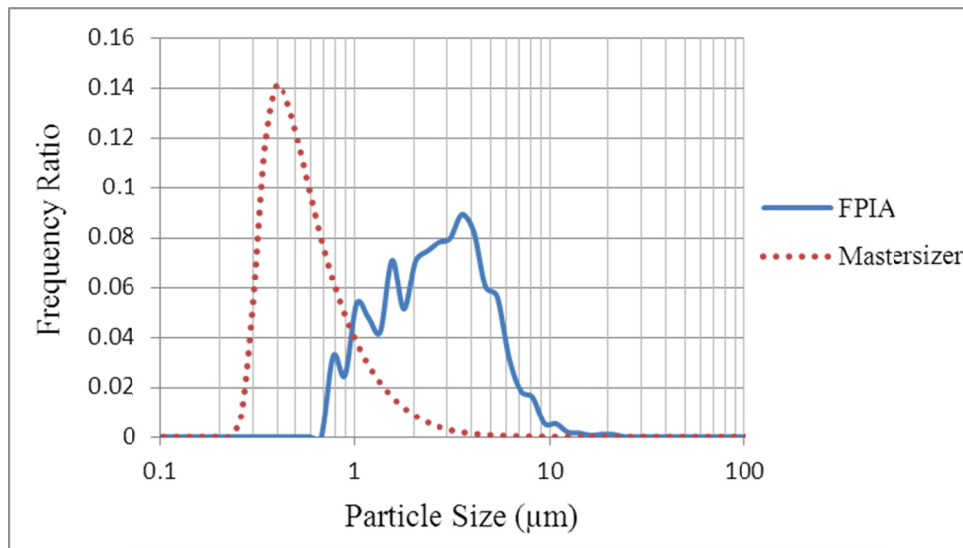


Figure 5.34 Frequency floc size distributions for kaolinite coagulated alkaline flocs obtained using the FPIA and Mastersizer



Figure 5.35 Some coagulated alkaline kaolinite flocs detected by the FPIA

Figure 5.36 further compares the FSDs obtained with the Mastersizer and FPIA. Only a few points fall near the parity line, which confirms the discrepancy of the two measurements (left graph). According to the right graph in Figure 5.36, the two devices frequency ratios differ up to 15% depending on the particle size range.

Table 5.12 Comparison of basic coagulated flocs measurements obtained with the FPIA and Mastersizer

	Mean diameter (μm)	d ₁₀ (μm)	d ₅₀ (μm)	d ₉₀ (μm)
FPIA	2.7	1.1	2.7	5.6
Mastersizer	0.7	0.3	0.5	1.1

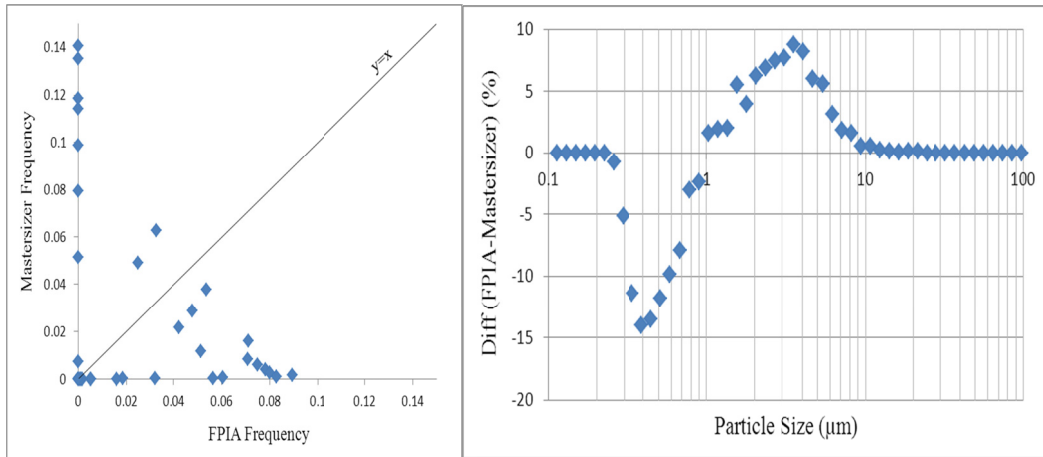


Figure 5.36 Comparison of the FPIA and Mastersizer frequency for kaolinite alkaline coagulated flocs

Therefore, the measured FSDs for basic coagulated kaolinite flocs by the FPIA and Mastersizer are not in agreement. The two measurements demonstrate very different sizes. The Mastersizer detects particles that are mostly in primary particle size range, while flocs are present in the FPIA distribution.

5.2.4 Comparison of Different Types of Flocs

In this section, the FSD of primary, natural, acidic and coagulated basic flocs from the FPIA are compared in one graph. The same procedure is done for the Mastersizer as well. This is done so that the four types of kaolinite flocs that were studied in Section 5.2.3 are compared by instrument in order to see the trends and differences of the distributions detected separately by the FPIA and Mastersizer. From this comparison, the way each device has responded to the change of floc types can be inferred.

FPIA Floc Size Measurements

The FSDs obtained with the FPIA that were described in Section 5.2.3 are compared in one graph. These FSDs are presented in Figures 5.37 (cumulative) and 5.38 (frequency). Primary, natural, acidic and coagulated basic flocs are compared in the figures. The floc sizes generally increase in size in the following order: primary, natural, coagulated basic and acidic flocs. The acidic sample has the greatest number of particles that are larger than 6 μm , and the primary floc sample has the largest number of particles that are smaller than 2 μm . The natural and coagulated alkaline floc size distributions fall between the primary and acidic FSDs. The mean diameters and distribution descriptors for the samples are listed in Table 5.13. All values in the table, as expected, increase in the order mentioned previously (primary, natural, coagulated alkaline and acidic flocs).

If the sample introduced to the FPIA changes because of flow through the FPIA, the changes are at least in qualitative agreement with the literature discussed in Chapter 2. Primary flocs will be the smallest of the four types, according to Vaezi et al. (2011). If the pH of the suspension changes from natural to acidic the flocs grow and larger flocs (card-house) would form. In the case that the pH of the mixture is increased and coagulant is added, larger card-pack flocs than those found under natural conditions are formed. Based on these results, it can be said that the FPIA FSDs respond in a qualitatively appropriate way.

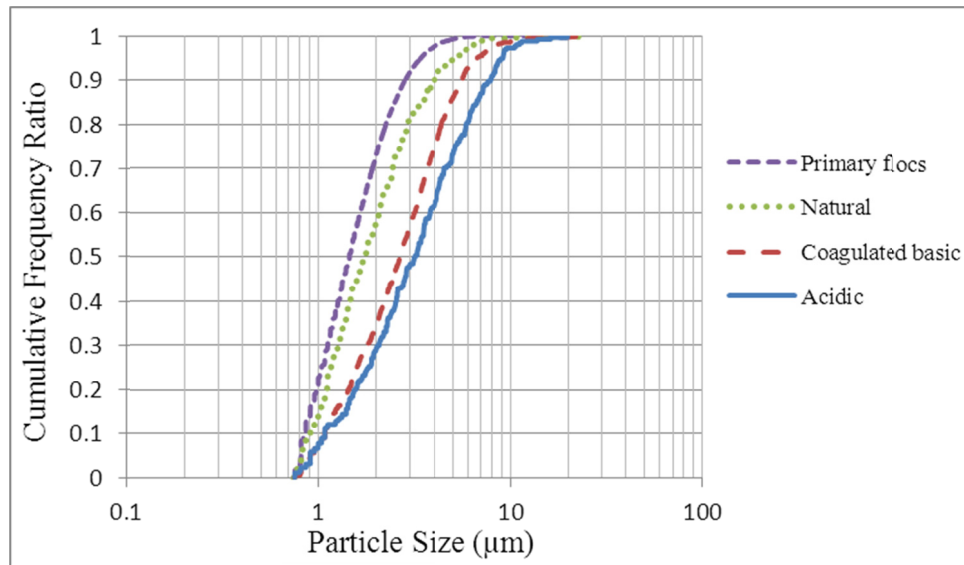


Figure 5.37 Cumulative FSDs for different types of kaolinite flocs measured using the FPIA

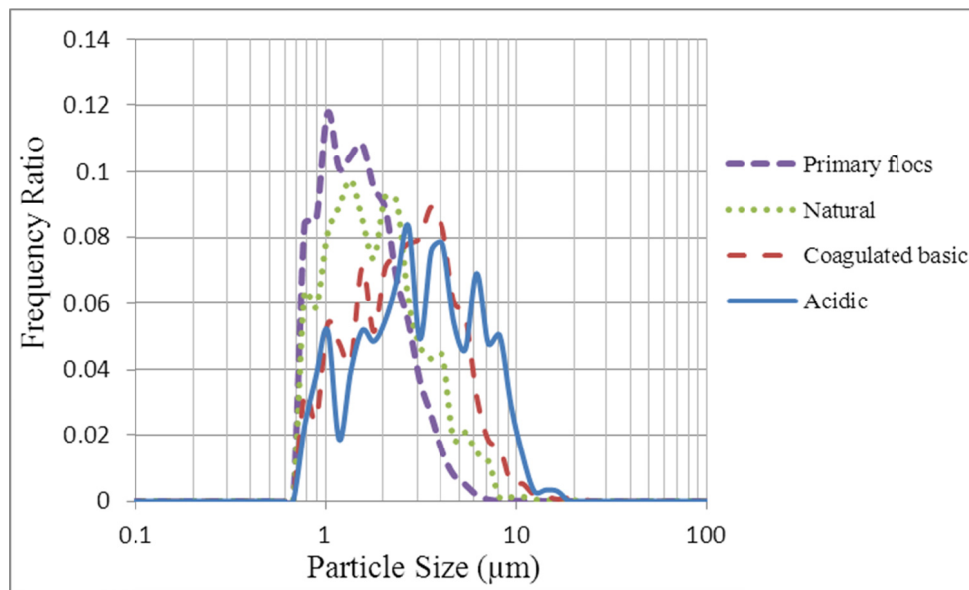


Figure 5.38 Frequency FSDs for different types of kaolinite flocs measured using the FPIA

Table 5.13 Comparison of different kaolinite floc measurements with the FPIA

FPIA samples	Mean diameter (μm)	d_{10} (μm)	d_{50} (μm)	d_{90} (μm)
Primary flocs	1.3	0.9	1.5	2.8
Natural	1.8	0.9	1.7	4.0
Coagulated basic	2.7	1.1	2.7	5.6
Acidic	3.4	1.1	3.1	7.9

Mastersizer Floc Size Measurements

In this section, the four FSDs that were measured with the Mastersizer and reported in Section 5.2.3 are collected and compared. The comparison of different types of flocs is used to assess the Mastersizer's response to changes in suspension characteristics and associated floc structures. The cumulative and differential FSDs obtained from the Mastersizer are depicted in Figure 5.39 and Figure 5.40. As shown on the graphs, regardless of the type of input sample the output is nearly identical for all floc types. The distribution descriptors for the four curves are reported in Table 5.14. Very similar values of d_{10} , d_{50} and d_{90} indicate the similarity of the FSDs during the measurement even though the inlet sample conditions should produce flocs of different sizes. Therefore, the results confirm that the Mastersizer breaks down the injected flocs to primary particles regardless of their initial sizes.

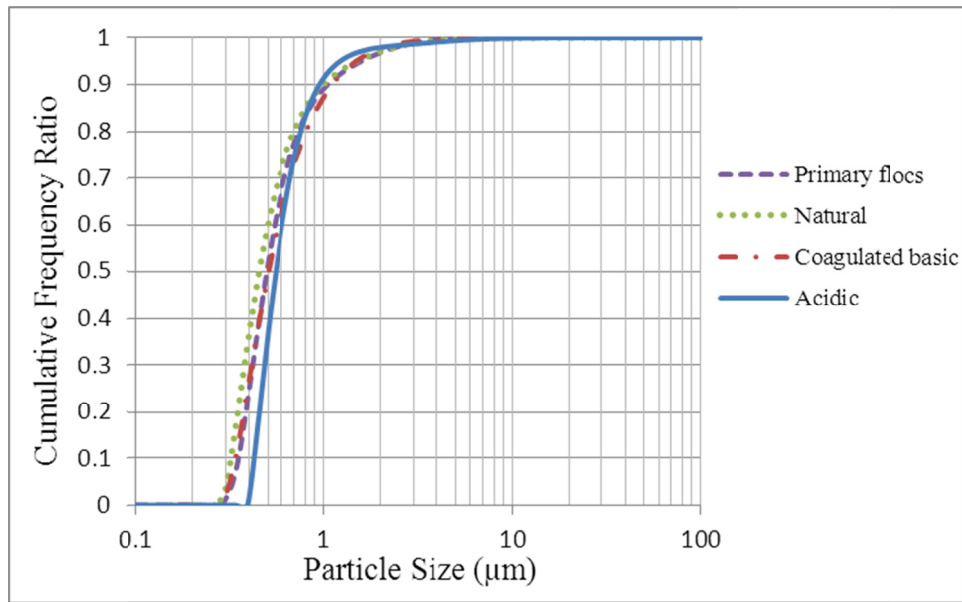


Figure 5.39 Cumulative FSDs for different types of kaolinite flocs obtained using the Mastersizer

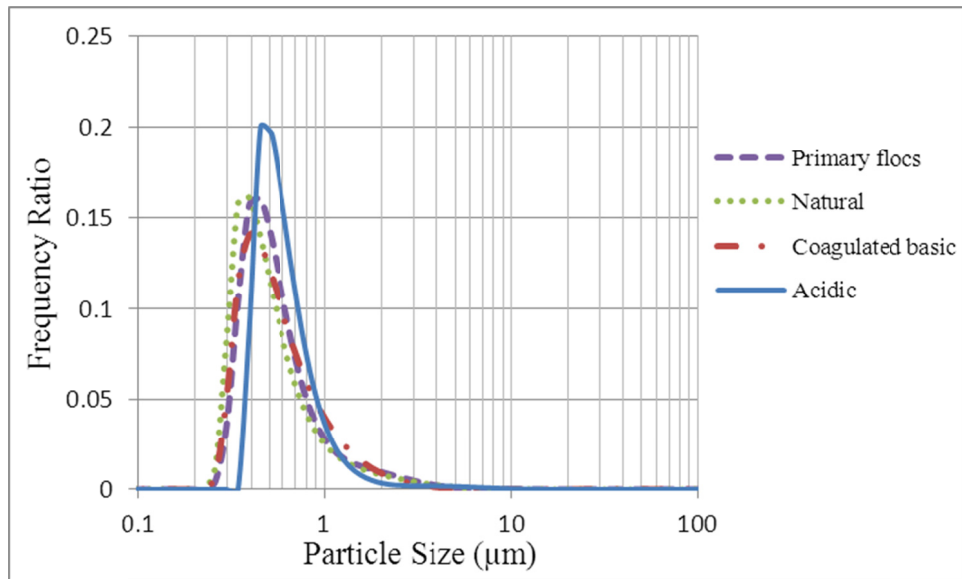


Figure 5.40 Frequency FSDs for different types of kaolinite flocs obtained using the Mastersizer

Table 5.14 Comparison of different kaolinite floc measurements with the Mastersizer

Mastersizer samples	d ₁₀ (μm)	d ₅₀ (μm)	d ₉₀ (μm)
Primary flocs	0.3	0.5	1.1
Natural	0.3	0.4	1.0
Coagulated basic	0.3	0.5	1.1
Acidic	0.4	0.6	1.0

5.3 Comparison of FPIA and Microscopy Measurements

As part of the second objective of this study, PSDs and FSDs are measured with the FPIA and microscope and the results are compared. As was the case for comparison of the FPIA and Mastersizer measurements, the process starts with measurements made for standard spherical latex particles. Then a suspension of irregular shaped non-flocculating silica particles are compared, and finally kaolinite flocs are measured using the two techniques.

5.3.1 Latex Particles

The very dilute latex suspension was prepared (as described in Chapter 3) and measured with both the FPIA and microscope. The results are presented in Figure 5.41 and Figure 5.42. The graphs show two perfectly matching curves showing 2 μm as the dominant particle diameter (as expected). A sample image taken during analysis of the microscope measurements is depicted in Figure 5.43. The data of Table 5.15 also confirm the essentially identical PSDs. The curves overlap each other, they are centered at the same size, and their average particle size, d₁₀ and

d_{90} are also very similar. Thus, the results for standard spherical particles are in excellent agreement.

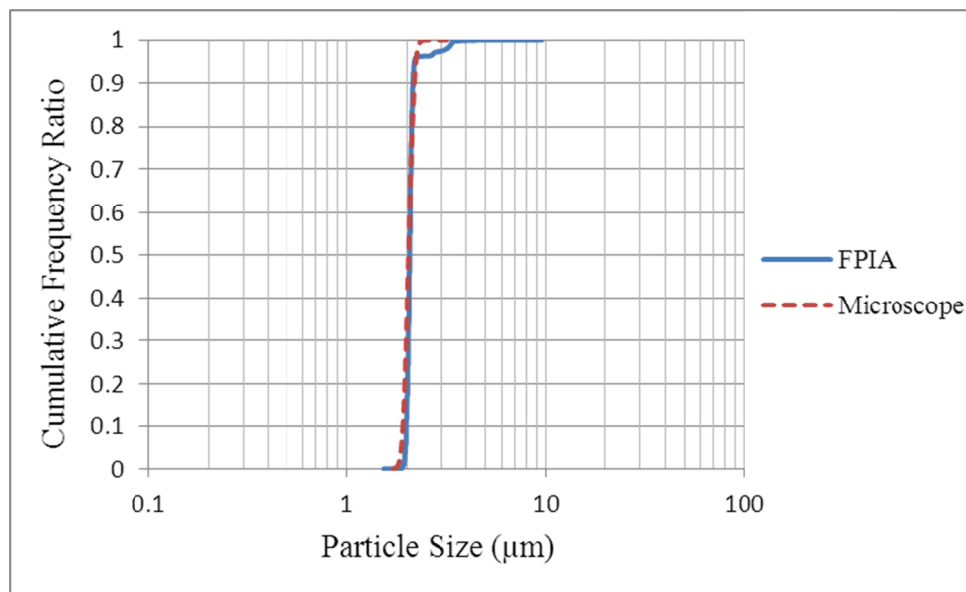


Figure 5.41 Cumulative particle size distributions for the 2 μm latex particles obtained using the FPIA and microscope

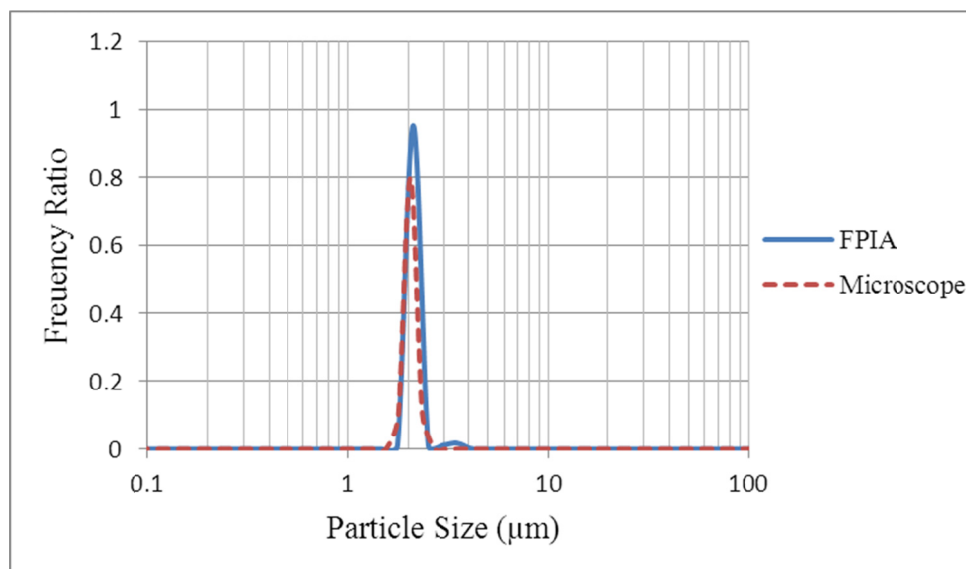


Figure 5.42 Frequency particle size distributions for the 2 μm latex particles obtained using the FPIA and microscope

Table 5.15 Comparison of latex measurements with the FPIA and microscope

	Mean diameter (μm)	d_{10} (μm)	d_{50} (μm)	d_{90} (μm)
FPIA	2.1	2.0	2.1	2.1
Microscope	2.0	1.9	2.0	2.2

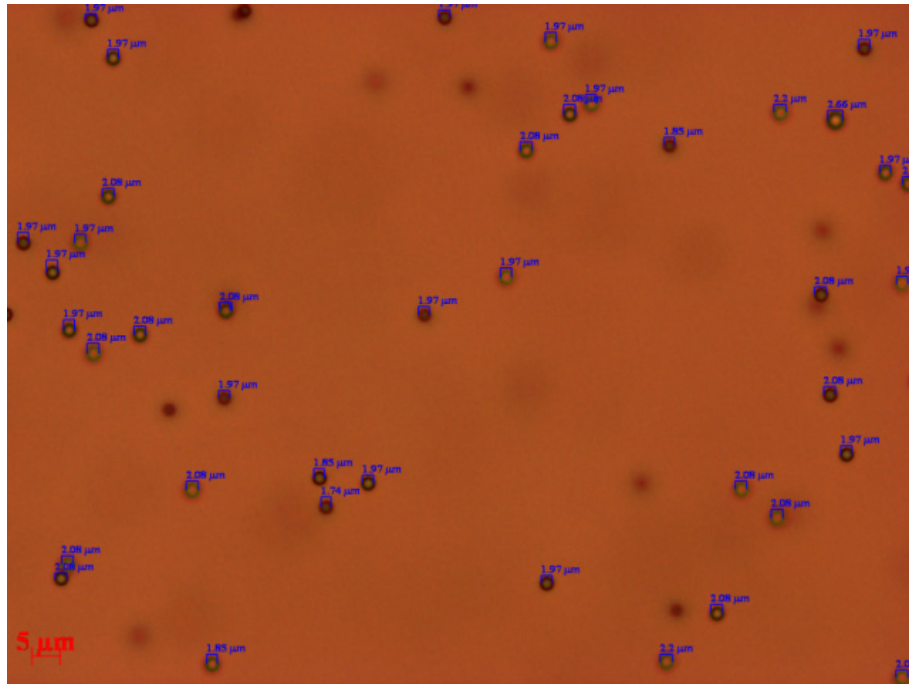


Figure 5.43 A micrograph of latex particles (0.1 wt% aqueous suspension, 400x magnification)

5.3.2 Silica Flour

In this section, mixtures of silica flour in water are measured with both devices. The results are illustrated in Figure 5.44 and Figure 5.45. It can be seen from the graphs that the two curves are qualitatively similar. Their overall size range as well as frequencies in many size ranges are similar. Since the particles are not of a standard, isometric shape (as shown in a microscope image in Figure 5.46), their orientation is likely the main reason why the PSDs from the two devices differ. It should be mentioned, though, that the difference between the two PSDs is small.

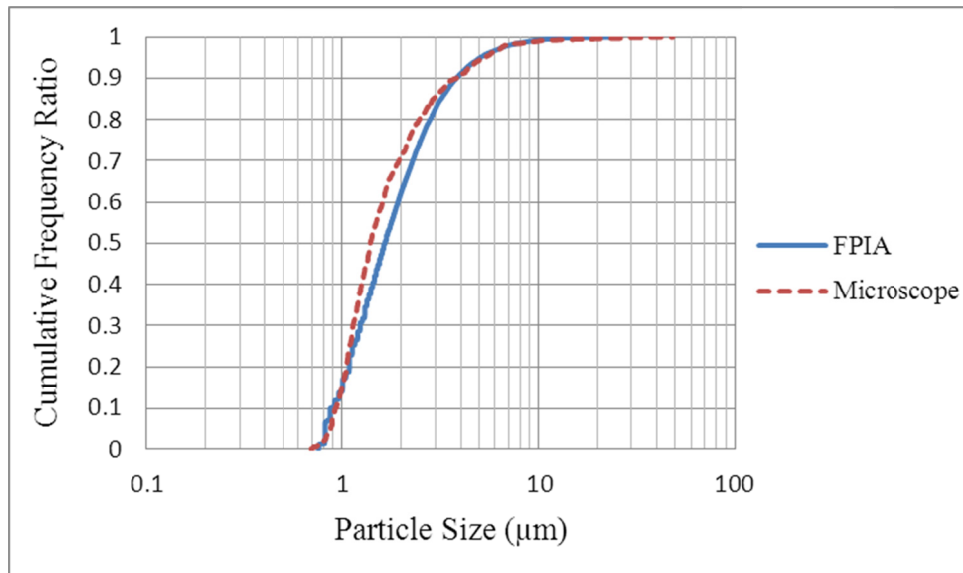


Figure 5.44 Cumulative particle size distributions for the silica particles obtained using the FPIA and microscope

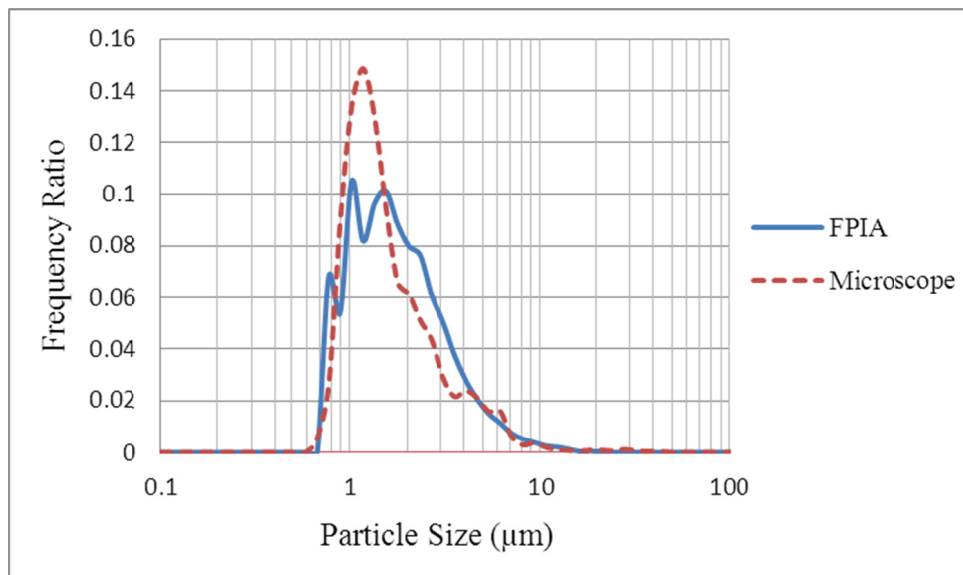


Figure 5.45 Frequency particle size distributions for the silica particles obtained using the FPIA and microscope

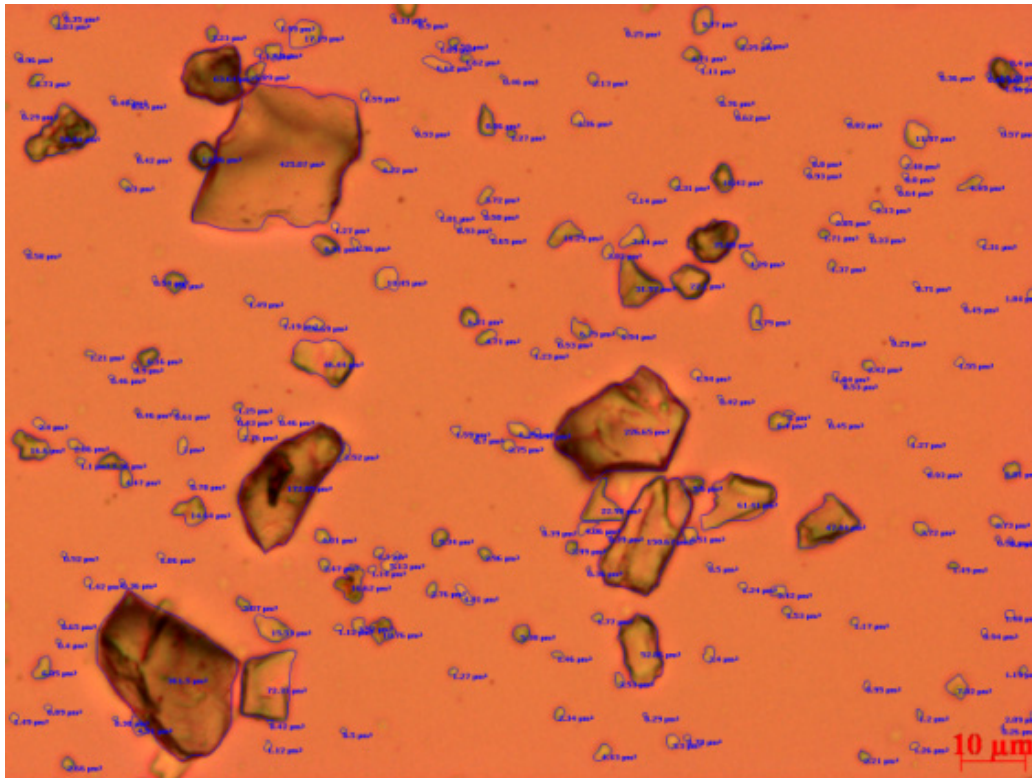


Figure 5.46 A micrograph of silica particles (2.5 g/L silica in DI water, 400x magnification)

Figure 5.47 compares microscope frequency versus FPIA frequency for different bin sizes as well as the difference of the frequency ratios obtained with the two devices. In this figure, the majority of the points are either on the line or near the line, which shows that the two measurement techniques provide similar results. On the right graph, it can be seen that how different the measurements are for each bin size. Table 5.16 provides information regarding the PSDs. The values in the table are also similar for both measurements.

It can be concluded that the size measurement of irregular shaped non-flocculating particles using the FPIA and microscope provides similar results.

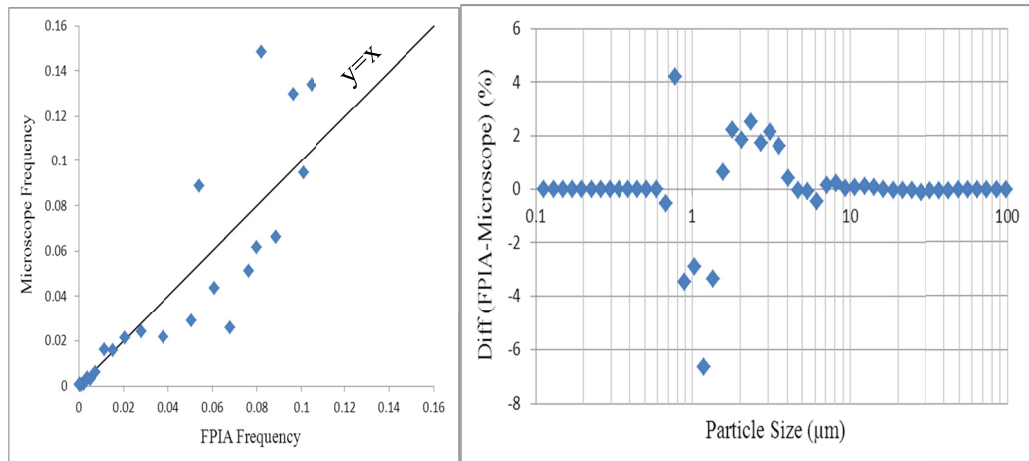


Figure 5.47 Comparison of the FPIA and microscope frequency for silica particles

Table 5.16 Comparison of silica measurements with the FPIA and microscope

	Mean diameter (μm)	d_{10} (μm)	d_{50} (μm)	d_{90} (μm)
FPIA	1.7	0.9	1.6	3.8
Microscope	2.0	0.9	1.4	3.8

5.3.3 Kaolinite Flocs

Basic coagulated flocs have been chosen for the comparison. The sample was made (as explained in Section 3.3.1), and FSDs were measured using both the microscopy method and the FPIA. The data were analyzed and converted into FSDs reported in Figures 5.48 and 5.49. Generally, the two curves are quite similar. However, there are some differences in the FSDs, including larger flocs from 10 to 50 μm in the FSD produced from the microscope measurement, more flocs in 2-10 μm size range reported by the FPIA, and a higher frequency of 0.8-2 μm flocs in the microscope sample. A processed image from the microscopy as well as of the some largest flocs detected by the FPIA are presented in Figure 5.50

and Figure 5.51, respectively. A more quantitative comparison of FSDs is available through Figure 5.52 and Table 5.17. The table provides the mean and distribution descriptors of the measurements from the two techniques. Figure 5.52 (left graph) demonstrates a narrow distribution of points around the $y=x$ line, which confirms the overall similarity of the two techniques. It is also demonstrated that the measurements are at most 4 % different for some ranges (Figure 5.52, right graph).

The slight differences can be explained by reviewing the measurement principles of the two methods. Regarding the large particles detected by the microscope, on the microscope slide flocs are next to one another in a static condition. In this way, two separate flocs that are very close or even overlap in the image can be counted as one large floc in the analysis of microscope images. Additionally, these same large but loose flocs on the microscope slide could easily be separated by the flow that is carrying the flocs through the FPIA. Another point is the orientation of the particles in the FPIA flow cell. Also, placing a top slide to help with the focus plane may cause some damage. It is also notable that in a manual measurement, operator error can play an important role.

Considering all these aspects it can be concluded that the comparison of FSD measurements made using the FPIA and the microscope is acceptable, which suggests the kaolinite floc size measurements made using the FPIA are representative of the sample's actual FSD.

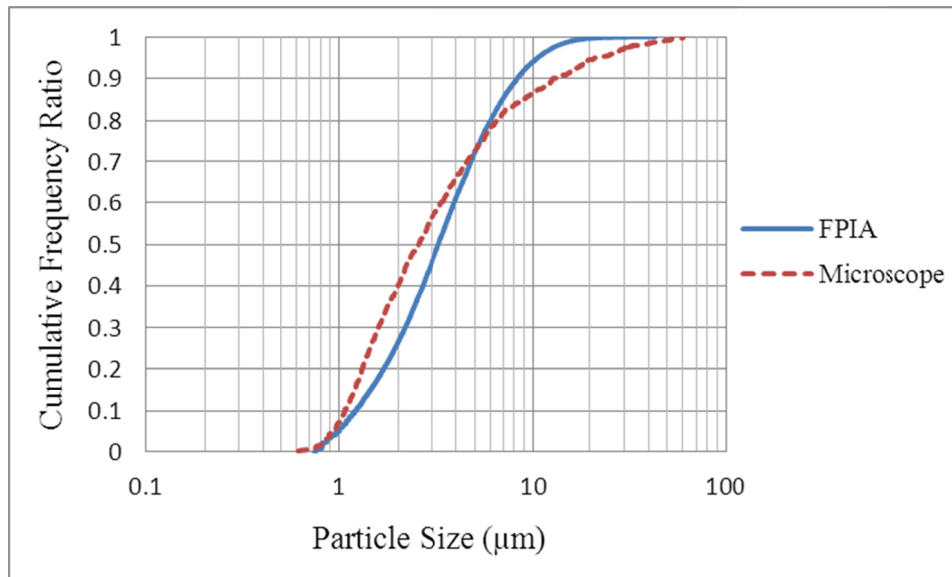


Figure 5.48 Cumulative floc size distributions for the kaolinite flocs obtained using the FPIA and microscope

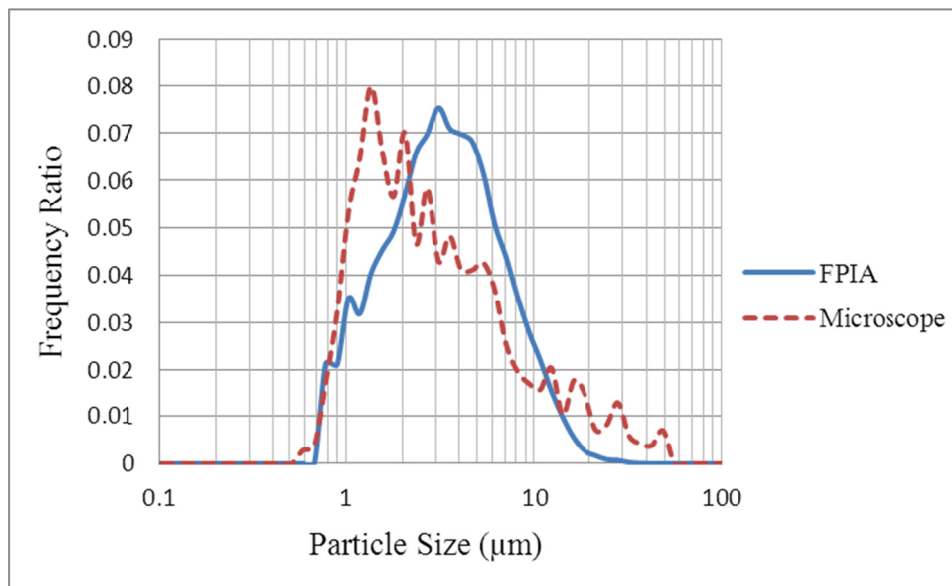


Figure 5.49 Frequency floc size distributions for the kaolinite flocs obtained using the FPIA and microscope

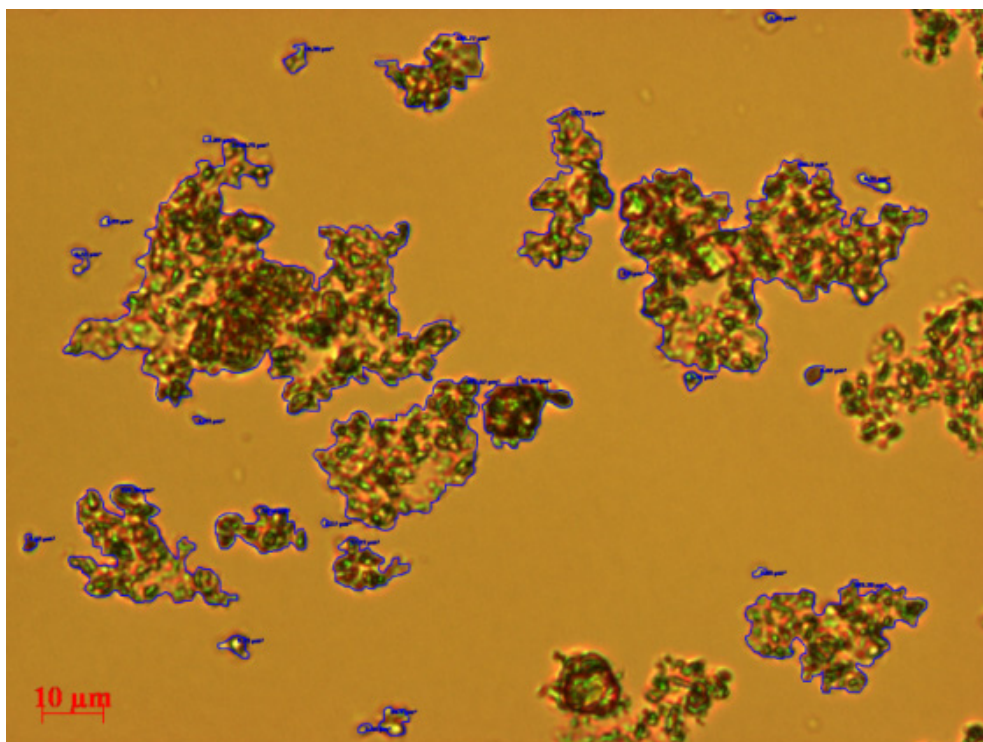


Figure 5.50 A micrograph of kaolinite flocs ($c = 5$ g/L, 0.01 M CaCl_2 , pH 9, 400x magnification)

Table 5.17 Comparison of basic coagulated flocs measurements with the FPIA and microscope

	Mean diameter (μm)	d_{10} (μm)	d_{50} (μm)	d_{90} (μm)
FPIA	3.8	1.2	3.2	8.3
Microscope	5.6	1.1	2.6	12.6

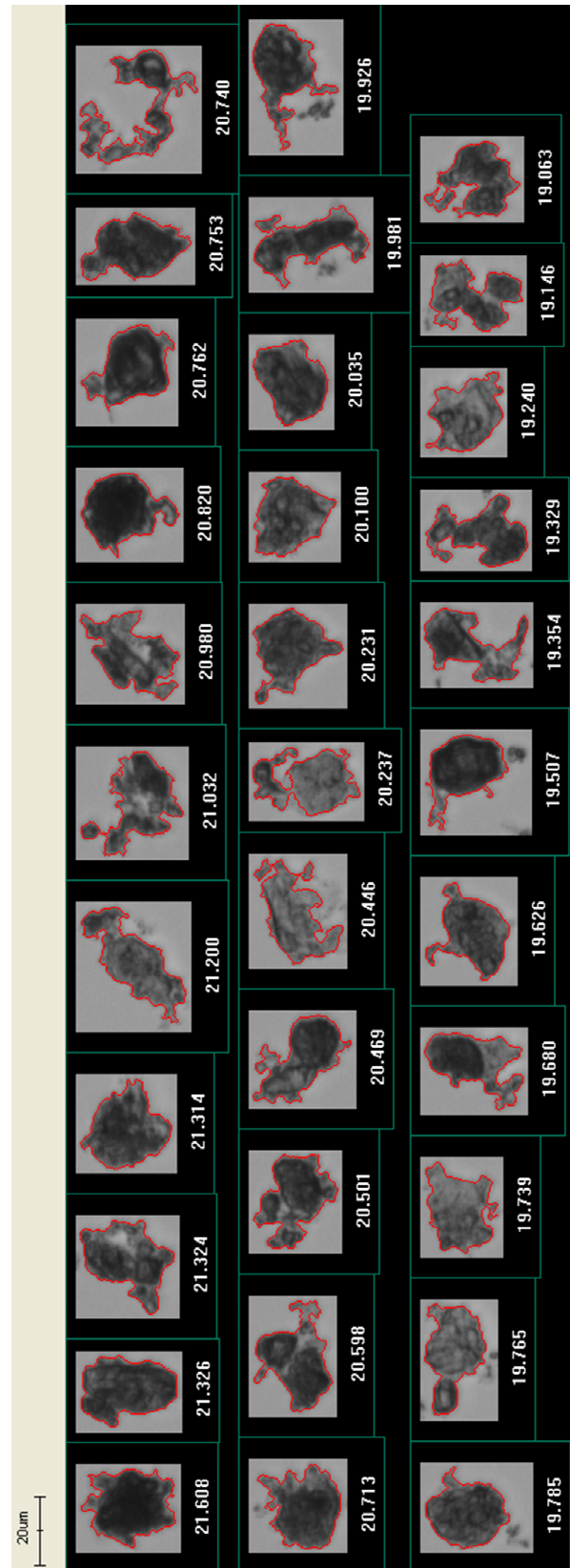


Figure 5.51 Some of the largest coagulated basic kaolinite floccs detected by the FPIA

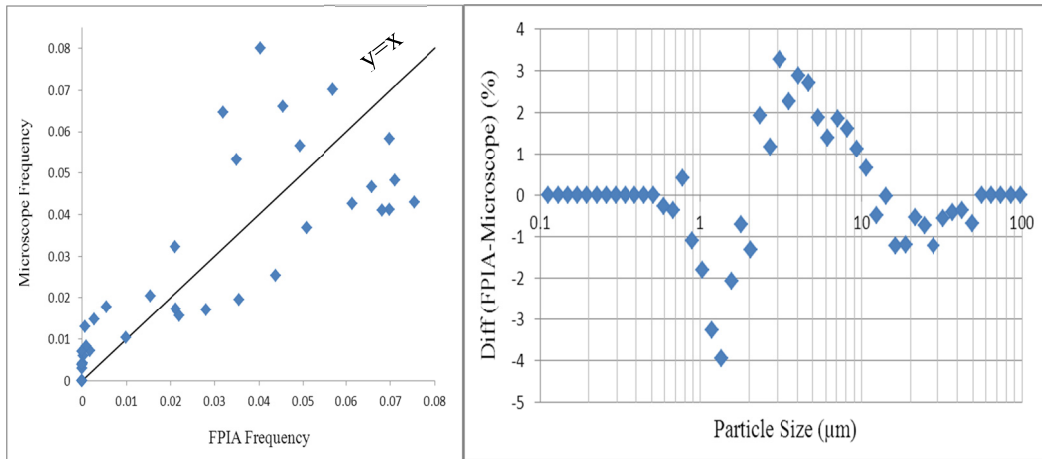


Figure 5.52 Comparison of the FPIA and microscope frequency for kaolinite flocs

6 Conclusions and Recommendations for Future Work

6.1 Conclusions

- Samples of kaolinite suspensions with different solid concentrations, different pH values and in presence or absence of coagulant (CaCl_2) were studied. Their FSDs were measured with the FPIA. The generated results were in agreement with the previous studies in the literature and confirmed the reliability of the results (i.e. qualitative validation).
- The three devices showed repeatable measurements for different types of particles and flocs.
- The PSDs of standard 2 μm latex spheres in very dilute suspensions were measured by the FPIA, Mastersizer and microscope. The resulting PSDs were in agreement for the three size measurement devices.
- The PSDs of irregular-shaped silica particles were measured by the three instruments (FPIA, Mastersizer and microscope). The results of PSD measurements were in agreement for the three size measurement apparatus used in this study.
- In order to evaluate the performance of the FPIA and determine the SOP, the effect of mixing speed and mixing time inside FPIA sample chamber on the produced kaolinite FSDs were studied. The results demonstrated that neither of the parameters had a significant effect on the floc sizes.

- Through comparison of the FSD measurement results obtained with the FPIA and Mastersizer, it was found that the Mastersizer is not a good option for size measurement of flocs and aggregates, as it breaks the flocs down to individual (primary) particles and primary flocs. The size measurement experiments were conducted on four different types of kaolinite flocs and the resulting FSDs were almost the same regardless of the feed. Mixing and dilution of the samples inside the Mastersizer sample dispersion unit were also studied, and their important role in altering floc sizes was demonstrated. The size of particles reduced due to the floc breakage caused by increasing the stirrer speed. Dilution also caused size reduction.
- The kaolinite FSDs obtained with the FPIA were fitted accurately with log-normal distributions. The fact that the FPIA FSDs can fit log-normal distributions is in agreement with reports in the literature that state aggregate sizes are log-normally distributed.
- Based on the comparison of size distribution of different floc types obtained with the FPIA, it is concluded that the device is sensitive to feed conditions.
- Dilute samples of kaolinite flocs were measured using the microscope. The floc size distributions obtained with the microscopy method were in good agreement with the FPIA results.

- Finally, it is concluded that FPIA measurements provide size distributions of in situ flocs, at least for the dilute slurries studied in the present project.

6.2 Recommendations for Future Work

- Idealized kaolinite-water suspensions were used in this study to represent clay slurries. Clays consist of different types of minerals other than kaolinite. Besides, during the oil sands extraction process they are exposed to bitumen, process water and natural surfactants that can modify them. Therefore, additional experiments should be performed to study the floc size distribution of real industrial slurries from different process streams and tailing ponds. The industrial samples should be treated to remove coarse particles and bitumen before size measurement experiments.
- Additional studies should be performed to evaluate FPIA performance and confirm the results of this study against an instrument that can measure floc size distributions during flow (e.g. Particle Vision and Measurement, PVM or Focused Beam Reflectance Measurement, FBRM).
- A separate study should be conducted (not using FPIA) to determine the relationship between concentration and floc size over a broad range of suspension concentrations.

References

- Adeyinka, O. B., Samiei, S., Xu, Z., & Masliyah, J. H. (2009). Effect of particle size on the rheology of Athabasca clay suspensions. *Canadian Journal of Chemical Engineering*, 87(3), 422-434.
- Arnold, G., Garche, J., Hemmer, R., Ströbele, S., Vogler, C., & Wohlfahrt-Mehrens, M. (2003). Fine-particle lithium iron phosphate LiFePO₄ synthesized by a new low-cost aqueous precipitation technique. *Journal of Power Sources*, 119-121, 247-251.
- Asadi, A. (2012). *The effect of fine flocculating particles and fine inerts on carrier fluid viscosity*. Edmonton, Alberta. MSc Thesis, University of Alberta.
- Axio scope.A1 operating manual (2008). (6th ed.). Goettingen, Germany: Carl Zeiss MicroImaging GmbH.
- Benouali, D., Kacha, S., Kherici, S., & Benabadji, N. (2010). Study of the flocculated particles sedimentation assisted by microcomputer. *The Open Hydrology Journal*, (4), 14-18.
- Berg, J. C. (2010). *An introduction to interfaces & colloids : The bridge to nanoscience* World Scientific.
- Besendörfer, G., & Roosen, A. (2008). Particle shape and size effects on anisotropic shrinkage in tape-cast ceramic layers. *Journal of the American Ceramic Society*, 91(8), 2514-2520.
- Boldridge, D. (2010). Morphological characterization of fumed silica aggregates. *Aerosol Science and Technology*, 44(3), 182-186.

Borm, P. J. A., Robbins, D., Haubold, S., Kuhlbusch, T., Fissan, H., Donaldson, K., Schins, R., Stone, V., Keyling, W., Lademann, J., Krutmann, J., Warheit, D., Oberdorster, E. (2006). The potential risks of nanomaterials: A review carried out for ECETOC. *Particle and Fibre Toxicology*, 3.

Bradley, D. (1965). *The hydrocyclone* (First ed.). Oxford: Pergamon Press.

Brugger, B., & Richtering, W. (2007). Magnetic, thermosensitive microgels as stimuli-responsive emulsifiers allowing for remote control of separability and stability of oil in water-emulsions. *Advanced Materials*, 19(19), 2973-2978.

Bulmer, J. T., & Starr, J. (1979). *Syn crude analytical methods for oil sand and bitumen processing* Alberta Oil Sands Technology and Research Authority.

Bushell, G. C., Yan, Y. D., Woodfield, D., Raper, J., & Amal, R. (2002). On techniques for the measurement of the mass fractal dimension of aggregates. *Advances in Colloid and Interface Science*, 95(1), 1-50.

Chalaturnyk, R. J., Scott, J. D., & Özüm, B. (2002). Management of oil sands tailings. *Petroleum Science and Technology*, 20(9-10), 1025-1046.

Cheetham, M. D., Keene, A. F., Bush, R. T., Sullivan, L. A., & Erskine, W. D. (2008). A comparison of grain-size analysis methods for sand-dominated fluvial sediments. *Sedimentology*, 55(6), 1905-1913.

Chong, J., Ng, S., Chung, K. H., Sparks, B. D., & Kotlyar, L. S. (2003). Impact of fines content on a warm slurry extraction process using model oilsands. *Fuel*, 82(4), 425-438.

Collins, L., Kaszuba, M., & Fabre, J. W. (2004). Imaging in solution of (lys)₁₆-containing bifunctional synthetic peptide/DNA nanoparticles for gene delivery. *Biochimica Et Biophysica Acta - General Subjects*, 1672(1), 12-20.

Costanzo, P. M. (2001). Baseline studies of the clay minerals society source clays: Introduction. *Clays and Clay Minerals*, 49(5), 372-373.

Cowles, R. J. H. (2000). Particle characterization for oil and sand processing 2: Particle size measurements by laser diffraction. *Petroleum Science and Technology*, 18(1), 203-220.

Cowles, R. J. H. (2003). Particle characterization for oil sand processing. III. sample preparation. *Petroleum Science and Technology*, 21(7-8), 1241-1252.

Cowles, R. J. H. (2003). Particle characterization for oil sand processing. III. sample preparation. *Petroleum Science and Technology*, 21(7-8), 1241-1252.

Delgado, A., & Matijevic, E. (1991). Particle size distribution of inorganic colloidal dispersions. A comparison of different techniques. *Particle & Particle Systems Characterization*, 8(2), 128-135.

Ding, X., Repka, C., Xu, Z., & Masliyah, J. (2006). Effect of illite clay and divalent cations on bitumen recovery. *Canadian Journal of Chemical Engineering*, 84(6), 643-650.

Dur, J. C., Elsass, F., Chaplain, V., & Tessier, D. (2004). The relationship between particle-size distribution by laser granulometry and image analysis by transmission electron microscopy in a soil clay fraction. *European Journal of Soil Science*, 55(2), 265-270.

Dusseault, M. B., & Scafe, D. (1979). Mineralogical and engineering index properties of the basal McMurray formation clay shales. *Canadian Geotechnical Journal*, 16, 285-294.

Gillies, D. P. (2013). Particle contributions to kinematic friction in slurry pipeline flow. Edmonton, Alberta. MSc, University of Alberta.

Gillies, R. G., Shook, C. A., & Xu, J. (2004). Modelling heterogeneous slurry flows at high velocities. *Canadian Journal of Chemical Engineering*, 82(5), 1060-1065.

Goossens, D. (2008). Techniques to measure grain-size distributions of loamy sediments: A comparative study of ten instruments for wet analysis. *Sedimentology*, 55(1), 65-96.

Govoreanu, R., Saveyn, H., Van Der Meeren, P., Nopens, I., & Vanrolleghem, P. A. (2009). A methodological approach for direct quantification of the activated sludge floc size distribution by using different techniques. *Water Science and Technology*, 60(7), 1857-1867.

Gray, M., Xu, Z., & Masliyah, J. (2009). Physics in the oil sands of Alberta. *Physics Today*, 62(3), 31-35.

Gregory, J. (2009). Monitoring particle aggregation processes. *Advances in Colloid and Interface Science*, 147-148(C), 109-123.

Ignasiak, T. M., Kotlyar, L., Longstaffe, F. J., Strausz, O. P., & Montgomery, D. S. (1983). Separation and characterization of clay from athabasca asphaltene. *Fuel*, 62(3), 353-362.

James, A. E., & Williams, D. J. A. (1982). Particle interactions and rheological effects in kaolinite suspensions. *Advances in Colloid and Interface Science*, 17(1), 219-232.

Jarvis, P., Jefferson, B., & Parsons, S. A. (2005). Measuring floc structural characteristics. *Reviews in Environmental Science and Biotechnology*, 4(1-2), 1-18.

Jarvis, P., Jefferson, B., & Parsons, S. A. (2005). Measuring floc structural characteristics. *Reviews in Environmental Science and Biotechnology*, 4(1-2), 1-18.

Jassby, D. (2011). *Impact of particle aggregation on nanoparticle reactivity*. Durham, United States. PhD, Duke University-Department of Civil and Environmental Engineering.

Jeeravipoolvum, S., Scott, J. D., Donahue, R., & Ozum, B. (2008). Characterization of oil sands thickened tailings. *Proceedings of the First International Oil Sands Tailings Conference*, Edmonton, Alberta, 132-142.

Jiang, J., Oberdörster, G., & Biswas, P. (2009). Characterization of size, surface charge, and agglomeration state of nanoparticle dispersions for toxicological studies. *Journal of Nanoparticle Research*, 11(1), 77-89.

Kaminsky, H. A. W., Etsell, T. H., Ivey, D. G., & Omotoso, O. (2009). Distribution of clay minerals in the process streams produced by the extraction of bitumen from Athabasca oil sands. *Canadian Journal of Chemical Engineering*, 87(1), 85-93.

Kasongo, T., Zhou, Z., Xu, Z., & Masliyah, J. (2000). Effect of clays and calcium ions on bitumen extraction from athabasca oil sands using flotation. *Canadian Journal of Chemical Engineering*, 78(4), 674-681.

Kasperski, K. L. (1992). A review of properties and treatment of oil sands tailings. *AOSTRA Journal of Research*, (8), 11-53.

Keller, A. A., Wang, H., Zhou, D., Lenihan, H. S., Cherr, G., Cardinale, B. J., Miller, R., & Zhaoxia, J. I. (2010). Stability and aggregation of metal oxide nanoparticles in natural aqueous matrices. *Environmental Science and Technology*, 44(6), 1962-1967.

Komabayashi, T., & Spångberg, L. S. W. (2008a). Comparative analysis of the particle size and shape of commercially available mineral trioxide aggregates and portland cement: A study with a flow particle image analyzer. *Journal of Endodontics*, 34(1), 94-98.

Komabayashi, T., & Spångberg, L. S. W. (2008b). Particle size and shape analysis of MTA finer fractions using portland cement. *Journal of Endodontics*, 34(6), 709-711.

Komabayashi, T., D'souza, R. N., Dechow, P. C., Safavi, K. E., & Spångberg, L. S. W. (2009). Particle size and shape of calcium hydroxide. *Journal of Endodontics*, 35(2), 284-287.

Kotlyar, L. S., Deslandes, Y., Sparks, B. D., Kodama, H., & Schutte, R. (1993). Characterization of colloidal solids from Athabasca fine tails. *Clays & Clay Minerals*, 41(3), 341-345.

Krause, B., Petzold, G., Pegel, S., & Pötschke, P. (2009). Correlation of carbon nanotube dispersability in aqueous surfactant solutions and polymers. *Carbon*, 47(3), 602-612.

Langlet, J., Gaboriaud, F., & Gantzer, C. (2007). Effects of pH on plaque forming unit counts and aggregation of MS2 bacteriophage. *Journal of Applied Microbiology*, 103(5), 1632-1638.

Leentvaar, J., & Rebhun, M. (1983). Strength of ferric hydroxide flocs. *Water Research*, 17(8), 895-902.

Lemb, M., Oei, T. H., Eifert, H., & Gunther, B. (1993). Technegas: A study of particle structure, size and distribution. *European Journal of Nuclear Medicine*, 20(7), 576-579.

Limpert, E., Stahel, W. A., & Abbt, M. (2001). Log-normal distributions across the sciences: Keys and clues. *Bioscience*, 51(5), 341-352.

Liu, J., Xu, Z., & Masliyah, J. (2004). Role of fine clays in bitumen extraction from oil sands. *AIChE Journal*, 50(8), 1917-1927.

Liu, J.K. (1989). Analytical Methods. In L.G. Hepler & C. Hsi (Eds.) *AOSTRA Technical Handbook on Oil Sands, Bitumens and Heavy Oils*. Edmonton, AB: Alberta Oil sands Technology and Research Authority.

Marefatallah, M. (2013). *Effect of sonication on the particle size of kaolinite clays*. Edmonton, Alberta. MSc Thesis, University of Alberta.

Masliyah, J. (2011) *Course Notes - ChE 534 Fundamentals of Oilsands Extraction*. Department of Chemical and Materials Engineering, University of Alberta: Edmonton, AB.

Masliyah, J., & Bhattacharjee, S. (2006). *Electrokinetic and colloid transport phenomena* John Wiley and Sons.

Masliyah, J., Czarnecki, J., & Xu, Z. (2011). *Handbook on theory and practice of bitumen recovery from Athabasca oil sands, volume 1: Theoretical basis* Kingsley Publishing Services.

Masliyah, J., Zhou, Z., Xu, Z., Czarnecki, J., & Hamza, H. (2004). Understanding water-based bitumen extraction from Athabasca oil sands. *Canadian Journal of Chemical Engineering*, 82(4), 628-654.

Mastersizer-2000 Brochure. (2013). Retrieved, 2013, from <http://www.malvern.com/common/downloads/MRK501.pdf>

Mastersizer-2000 Operators Guide (1999). (2nd ed.). United Kingdom: Malvern Instruments.

Mercier, P. H. J., Le Page, Y., Tu, Y., & Kotlyar, L. (2008). Powder X-ray diffraction determination of phyllosilicate mass and area versus particle thickness distributions for clays from the athabasca oil sands. *Petroleum Science and Technology*, 26(3), 307-321.

Michaels, A. S., & Bolger, J. C. (1962). Settling rates and sediment volumes of flocculated kaolin suspensions. *Industrial & Engineering Chemistry Fundamentals*, 1(1), 24-33.

Michaels, A. S., & Bolger, J. C. (1962). Settling rates and sediment volumes of flocculated kaolin suspensions. *Industrial & Engineering Chemistry Fundamentals*, 1(1), 24-33.

Michaels, A. S., & Bolger, J. C. (1964). Particle interactions in aqueous kaolinite dispersions. *Industrial & Engineering Chemistry Fundamentals*, 3(1), 14-20.

Mihiretu, Y., Chalaturnyk, R., & Scott, D. (2008). Tailings segregation fundamentals from flow behaviour perspectives. *Proceedings of the First International Oil Sands Tailings Conference*, Edmonton, Alberta. 112-120.

Mikhail, M. W. (1997). Fine particles removal from oil sand tailings by hydrocyclone. *CIM Bulletin*, (1015), 86-90.

Mikula, R. J., Omotoso, O., & Kasperski, K. L. (2008). The chemistry of oil sands tailings: Production to treatment. *Proceedings of the First International Oil Sands Tailings Conference*, Edmonton, Alberta. 23-33.

- Mitsumoto, K., Yabusaki, K., & Aoyagi, H. (2009). Classification of pollen species using autofluorescence image analysis. *Journal of Bioscience and Bioengineering*, 107(1), 90-94.
- Mohamedelhasan, E. (2008). Electrokinetic sedimentation and dewatering of clay slurries. *Proceedings of the First International Oil Sands Tailings Conference*, Edmonton, Alberta. 153-160.
- Murray, H. H. (1991). Overview - clay mineral applications. *Applied Clay Science*, 5(5-6), 379-395.
- Nasser, M. S., & James, A. E. (2006). Settling and sediment bed behaviour of kaolinite in aqueous media. *Separation and Purification Technology*, 51(1), 10-17.
- Nasser, M. S., & James, A. E. (2008). Degree of flocculation and viscoelastic behaviour of kaolinite-sodium chloride dispersions. *Colloids and Surfaces A: Physicochemical and Engineering Aspects*, 315(1-3), 165-175.
- Nasser, M. S., & James, A. E. (2009). The effect of electrolyte concentration and ph on the flocculation and rheological behaviour of kaolinite suspensions. *Journal of Engineering Science and Technology*, 4(4), 430-446.
- Nemati, A., Goharian, P., Shabanian, M., & Afshar, A. (2010). Effects of nucleation agent particle size on properties, crystallisation and microstructure of glass-ceramics in TiO₂-ZrO₂-li₂O-CaO- Al₂O₃-SiO₂ system. *Advances in Applied Ceramics*, 109(6), 318-323.
- Niemeijer, A., Elsworth, D., & Marone, C. (2009). Significant effect of grain size distribution on compaction rates in granular aggregates. *Earth and Planetary Science Letters*, 284(3-4), 386-391.

Van Olphen, H. (1977). *An introduction to clay colloid chemistry* John Wiley & Sons.

Pialy, P., Nkoumbou, C., Villi  ras, F., Razafitianamaharavo, A., Barres, O., Pelletier, M., Ollivier, G., Bihannic, I., Njopwouo, D., Yvon, J., Bonnet, J.- P. (2008). Characterization for industrial applications of clays from lembo deposit, mount bana (cameroon). *Clay Minerals*, 43(3), 415-435.

Powter, C. B., Biggar, K. W., Silva, M. J., McKenna, G. T., & Scordo, E. B. (2011). Review of oil sands tailings technology options. Paper presented at the *Tailings and Mine Waste'10 - Proceedings of the 14th International Conference on Tailings and Mine Waste*, 381-391.

Promeyrat, A., Gatellier, P., Lebret, B., Kajak-Siemaszko, K., Aubry, L., & Sant  -Lhoutellier, V. (2010). Evaluation of protein aggregation in cooked meat. *Food Chemistry*, 121(2), 412-417.

Rahman, M. H. (2011). *Yield Stresses of Mixtures with Bimodal Size Distributions*. Edmonton, Alberta. MSc Thesis, University of Alberta.

Rhodes, M. J. (2008). *Introduction to particle technology* (2nd ed.) John Wiley & Sons.

Saigo, K., Hashimoto, M., Kumagai, S., Tanaka, C., & Imoto, S. (2005). Usefulness of particle image analyzer for evaluation of fragmented red cells. *Transfusion and Apheresis Science*, 33(1), 71-73.

Sanders, R. S., Schaan, J., Hughes, R., & Shook, C. (2004). Performance of sand slurry pipelines in the oil sands industry. *Canadian Journal of Chemical Engineering*, 82(4), 850-857.

Sanders, R.S. & Gillies, R.G. (2012). Hydrotransport. In J. Czarnecki, et al. (Eds.) *Handbook on Theory and Practice of Bitumen Recovery from Athabasca Oil Sands, Volume II: Industrial Practice*. Cochrane, AB: Kingsley Knowledge Publishing.

Sanford, E. C. (1983). Processibility of athabasca oil sand: Interrelationship between oil sand fine solids, process aids, mechanical energy and oil sand age after mining. *Canadian Journal of Chemical Engineering*, 61(4), 554-567.

Scales, P. J., Johnson, S. B., Healy, T. W., & Kapur, P. C. (1998). Shear yield stress of partially flocculated colloidal suspensions. *AIChE Journal*, 44(3), 538-544.

Schramm, L. L. (1989). The influence of suspension viscosity on bitumen rise velocity and potential recovery in the hot water flotation process for oil sands. *Journal of Canadian Petroleum Technology*, 28(3), 73-80.

Scott, D. J., Dusseault, M. B., & David Carrier III, W. (1985). Behaviour of the clay/bitumen/water sludge system from oil sands extraction plants. *Applied Clay Science*, 1(1-2), 207-218.

Shook, C. A., Gillies, R. G., & Sanders, R. S. (2002). *Pipeline hydrotransport with applications in the oil sands industry*. SRC Publication.

Silva-Valenzuela, M. G., Matos, C. M., Shah, L. A., Carvalho, F. M. S., Sayeg, I. J., & Valenzuela-Diaz, F. R. (2013). Engineering properties of kaolinitic clay with potencial use in drugs and cosmetics. *International Journal of Modern Engineering Research*, 3(1), 163-165.

Smith, J. (2013). *Measurement of carrier fluid viscosities for oil sand extraction and tailings slurries*. Edmonton, Alberta. MSc Thesis, University of Alberta.

Sobkowicz, J. C. (2011). History and developments in the treatment of oil sands fine tailings. Paper presented at the *Tailings and Mine Waste'10 - Proceedings of the 14th International Conference on Tailings and Mine Waste*, 11-30.

Sochan, A., Bieganski, A., Ryzak, M., Dobrowolski, R., & Bartmiski, P. (2012). Comparison of soil texture determined by two dispersion units of mastersizer 2000. *International Agrophysics*, 26(1), 99-102.

Sparks, B. D., Kotlyar, L. S., O'Carroll, J. B., & Chung, K. H. (2003). Athabasca oil sands: Effect of organic coated solids on bitumen recovery and quality. *Journal of Petroleum Science and Engineering*, 39(3-4), 417-430.

Sperazza, M., Moore, J. N., & Hendrix, M. S. (2004). High-resolution particle size analysis of naturally occurring very fine-grained sediment through laser diffractometry. *Journal of Sedimentary Research*, 74(5), 736-743.

Stone, M., & Krishnappan, B. G. (2003). Floc morphology and size distributions of cohesive sediment in steady-state flow. *Water Research*, 37(11), 2739-2747.

Storti, F., & Balsamo, F. (2010). Particle size distributions by laser diffraction: Sensitivity of granular matter strength to analytical operating procedures. *Solid Earth*, 1(1), 25-48.

Sysmex FPIA-3000 Brochure. Retrieved, 2013, from <http://www.malvern.com/common/downloads/MRK652.pdf>

Sysmex FPIA-3000/FPIA-3000S operator's manual. (2006). Kobe, Japan: Sysmex Corporation.

Tanaka, M., Komagata, M., Tsukada, M., & Kamiya, H. (2008). Fractal analysis of the influence of surface roughness of toner particles on their flow properties and adhesion behavior. *Powder Technology*, 186(1), 1-8.

Thomas, T., Afacan, A., Masliyah, J., Xu, Z., Wang, Y., & Liu, J. (2010). Recovery of hydrocarbons from mature fine tailings of oil sands extraction, *Proceedings of the 2nd International Oil Sands Tailings Conference*, Edmonton, Alberta. 141-148.

Tripathy, T., & Ranjan De, B. (2006). Flocculation : A new way to treat the waste water. *Journal of Physical Sciences*, 10, 93-127.

Tu, Y., O'Carroll, J. B., Kotlyar, L. S., Sparks, B. D., Ng, S., Chung, K. H., & Cuddy, G. (2005). Recovery of bitumen from oilsands: Gelation of ultra-fine clay in the primary separation vessel. *Fuel*, 84(6 SPEC. ISS.), 653-660.

Uhlik, P., Hooshlar, A., Kaminsky, H. A. W., Etsell, T. H., Ivey, D. G., & Liu, Q. (2008). Cation exchange capacity of clay fractions from oil sands process streams. *Proceedings of the First International Oil Sands Tailings Conference*, Edmonton, Alberta, 64-72.

Vaezi G., F., Sanders, R. S., & Masliyah, J. H. (2011). Flocculation kinetics and aggregate structure of kaolinite mixtures in laminar tube flow. *Journal of Colloid and Interface Science*, 355(1), 96-105.

Vaezi, F. (2011). Description of the experimental step to study the effect of shearing on the flocculated kaolin slurry.

Vdovic, N., Obhodaš, J., & Pikelj, K. (2010). Revisiting the particle-size distribution of soils: Comparison of different methods and sample pre-treatments. *European Journal of Soil Science*, 61(6), 854-864.

Waite, T. D. (1999). Measurement and implications of floc structure in water and wastewater treatment. *Colloids and Surfaces A: Physicochemical and Engineering Aspects*, 151(1-2), 27-41.

- Wen, B., Aydin, A., & Duzgoren-Aydin, N. S. (2002). A comparative study of particle size analyses by sieve-hydrometer and laser diffraction methods. *Geotechnical Testing Journal*, 25(4), 434-442.
- Wilson, K. C., Addie, G. R., Sellgren, A., & Clift, R. (2006). *Slurry transport using centrifugal pumps* (3rd ed.). New York, USA: Springer.
- Wilson, K. C., Addie, G. R., Sellgren, A., & Clift, R. (2006). *Slurry transport using centrifugal pumps* (3rd ed.). New York, USA: Springer.
- Wu, R. M., Lee, D. J., Waite, T. D., & Guan, J. (2002). Multilevel structure of sludge flocs. *Journal of Colloid and Interface Science*, 252(2), 383-392.
- Xu, Y., & Hamza, H. (2003). Thickening and disposal of oil sand tailings. *Mining Engineering*, 55(11), 33-39.
- Yuan, Y., Ndoutoumve, J. F., Siew, M., Vo, O., & Farnood, R. (2009). Sizing of wastewater particles using the electrozone sensing technique. *Particulate Science and Technology*, 27(1), 50-56.
- Zbik, M. S., Smart, R. S. C., & Morris, G. E. (2008). Kaolinite flocculation structure. *Journal of Colloid and Interface Science*, 328(1), 73-80.
- Zhou, Z., Kasongo, T., Xu, Z., & Masliyah, J. (2004). Assessment of bitumen recovery from the athabasca oil sands using a laboratory denver flotation cell. *Canadian Journal of Chemical Engineering*, 82(4), 696-703.
- Zielina, M. (2011). Particle shapes in the drinking water filtration process. *Clean - Soil, Air, Water*, 39(11), 941-946.

Appendix A: Octave code used for size distribution calculations

```
%%% Define the kind of distribution to be fitted:

% 0 = number; 1 = length; 2 = area; 3 = volume based

distkind = 0;

%%% Define log-normal distribution and "first guess" coefficients

% Log-normal distribution: c = sigma, mu

cumdist = @(c, x) .5 * erfc(-(log(x) - c(2))/(c(1) * sqrt(2)));

c = [.001, 0];

%%% Load array of particle sizes from a csv file

% For loading the FPIA and microscope particle areas

areadata = load('file name.csv');

sizedata = sqrt(areadata/pi)*2;

% For loading the Mastersizer size distribution data

binboundsms = sizedata(1:end,1);

sizems = sizedata(2:end,3);

volpct = sizedata(2:end,2);

volpct = volpct./sum(volpct);

freqpct = volpct./(sizems.^3);

freqpct = freqpct/sum(freqpct);

cumfreqpct = cumsum(freqpct);
```

```

fx = cumfreqpct;

sx = sizedata(2:end,3);

%% Generate a cumulative distribution from an array of sizes:

% First output (su) is an array of sizes to be used as abscissa for the second output
(fu), which is the number-based cumulative distribution.

% Third and fourth outputs are the same as first and second, but with only one
point per stair, so that the resulting curve does not have staircases.

function [su, fu, sx, fx] = mkCumDistFromSizeArray (s)

s = sort(s);

[su, iu] = unique(s);

fu = reshape([[0; iu(1:end-1)] iu]', 2 * numel(iu), 1);

fu = fu/fu(end);

su = reshape([su su]', 2 * numel(su), 1);

sx = .5 * (su(1:end-1)+su(2:end));

sx = [2*sx(1) - sx(2); sx];

sx = [2*sx(1) - sx(2); sx];

fx = .5 * (fu(1:end-1)+fu(2:end));

fx = [0; fx];

fx = [0; fx];

%% Make number based cumulative distribution

[su, fu, sx, fx] = mkCumDistFromSizeArray(sizedata);

```



```

%% If necessary, turn number based distribution into another distribution.

fxs = fx(2:end);

sxd = .5 * (sx(1:end-1)+sx(2:end));

dfx = diff(fx)./diff(sx).*sxd.^(distkind);

fx = cumsum(dfx .* diff(sx));

dfx = dfx / fx(end);

fx = [0; fx] / fx(end);

sxds = .5 * (sxs(1:end-1)+sxs(2:end));

dfxs = diff(fxs)./diff(sxs).*sxds.^(distkind);

fxs = cumsum(dfxs .* diff(sxs));

dfxs = dfxs / fxs(end);

fxs = [0; fxs] / fxs(end);

%% Fit cumulative distribution with the data using "least square" cost function.

function c = Cost(coeffs, dist, x, y)

c = sum((dist(coeffs(1), coeffs(2), coeffs(3), x) - y).^2);

c = minimize("lsqCost", {c, dist, sxd, dfx});

cumc = minimize("lsqCost", {c, cumdist, sx, fx});

%% Save the cost value for the best fit (estimation of the error to compare
several distributions)

cost = [lsqCost(c, dist, sxd, dfx) lsqCost(cumc, cumdist, sx, fx)];

cost = sqrt(cost ./ (numel(sizedata)-1))

```

```

coeffs = [c; cumc]

%%% Plot the results

% Cumulative distribution

Figure(1);

semilogx(su, fu, 'b', sx, cumdist(cumc, sx), '-r');

xlabel('Size');

ylabel('Cumulative distribution');

switch distkind

case 0

    str = 'Number based ';

case 1

    str = 'Length based ';

case 2

    str = 'Area based ';

case 3

    str = 'Volume based ';

otherwise

    str = 'Unknown ';

end

legend('Number based raw data', 'Fitted with cumulative distribution');

```

Appendix B: Microscopy sample size determination

A well known formula for sample size determination is called Cochran's formula (Cochran, W. G. (1977). *Sampling techniques*. New York: John Wiley & Sons).

The values calculated with this equation considering different population size, confidence level and degree of accuracy is presented in Table B.1.

Table B.1 Sample size determination using Cochran's formula (The Research Advisors (research-advisors.com), 2006)

Population Size	Confidence = 95 %				Confidence = 99 %			
	Degree of Accuracy							
	0.05	0.035	0.025	0.01	0.05	0.035	0.025	0.01
10	10	10	10	10	10	10	10	10
20	19	20	20	20	19	20	20	20
30	28	29	29	30	29	29	30	30
50	44	47	48	50	47	48	49	50
75	63	69	72	74	67	71	73	75
100	80	89	94	99	87	93	96	99
150	108	126	137	148	122	135	142	149
200	132	160	177	196	154	174	186	198
250	152	190	215	244	182	211	229	246
300	169	217	251	291	207	246	270	295
400	196	265	318	384	250	309	348	391
500	217	306	377	475	285	365	421	485
600	234	340	432	565	315	416	490	579
700	248	370	481	653	341	462	554	672
800	260	396	526	739	363	503	615	763
900	269	419	568	823	382	541	672	854
1,000	278	440	606	906	399	575	727	943
1,200	291	474	674	1067	427	636	827	1119
1,500	306	515	759	1297	460	712	959	1376
2,000	322	563	869	1655	498	808	1141	1785
2,500	333	597	952	1984	524	879	1288	2173
3,500	346	641	1068	2565	558	977	1510	2890
5,000	357	678	1176	3288	586	1066	1734	3842
7,500	365	710	1275	4211	610	1147	1960	5165
10,000	370	727	1332	4899	622	1193	2098	6239
25,000	378	760	1448	6939	646	1285	2399	9972
50,000	381	772	1491	8056	655	1318	2520	12455
75,000	382	776	1506	8514	658	1330	2563	13583
100,000	383	778	1513	8762	659	1336	2585	14227
250,000	384	782	1527	9248	662	1347	2626	15555
500,000	384	783	1532	9423	663	1350	2640	16055
1,000,000	384	783	1534	9512	663	1352	2647	16317

2,500,000	384	784	1536	9567	663	1353	2651	16478
10,000,000	384	784	1536	9594	663	1354	2653	16560
100,000,000	384	784	1537	9603	663	1354	2654	16584
264,000,000	384	784	1537	9603	663	1354	2654	16586

For 95% confidence and 5% degree of accuracy the sample size is constant (384) for populations larger than 250,000.

However, the sample size was not determined only based on the information in the table. The other method is to check the changes of the distribution when a particle is added to the sample. If the addition of the extra particle does not have a significant effect on the size distribution, the sample size is considered large enough.

A code was used to take subsamples of the randomly sorted particle areas from microscopy method. In order to eliminate the errors, the array of sizes is randomly ordered and the code is run several times for each sample (i.e. with different orders of particles). Suppose a sample with 800 particles. Subsamples of 1-800 particles were taken. Then the mean and variance of each subsample was calculated, as well as variance of the mean and variance of the variance. If the mean and variance are constant (which results in decrease of the variance of these values) for a reasonable number of particles, the size of the sample used to run the code is acceptable. For the example of 800-particle sample, if the mean and variance of the 400 to 800 subsample size is constant, a sample of 800 particles is considered large enough and a good representative of the population. If this result is constant for most of times that the code runs, the number of the particles (sample size) is fixed. The code is as following:

```

%%%%%%%% Read the file from the source

num = load('microscopy.csv');

%%%%%%%% Separate the area column

AreaList = num(:,1);

AreaList = AreaList(randperm(length(AreaList)));

%%%%%%%% Define parameterers

MaxRange = numel(AreaList);  %%%% Maximum Range of data used for
calculations

NRepeats = 1; %%%% Number of times each range is repeated

%%%%%%%% Initializations

Data_mean = zeros(MaxRange, NRepeats);

Data_var = zeros(MaxRange, NRepeats);

Data_volmean = Data_mean;

Data_volvar = Data_var;

Data_varofmean = zeros(MaxRange, 1);

Data_varofvar = zeros(MaxRange, 1);

for Range = 1:MaxRange

    for Repeat = 1:NRepeats

```

```

        %%% Extract random sub-sample

        %%% Diameter = AreaList(randperm(length(AreaList),Range));

        Area = AreaList(1:Range);

        Diameter = 2*(Area/pi)^0.5;

        %%% Calculate statistical quantities

        Data_mean(Range, Repeat) = mean(Diameter);

        Data_var(Range, Repeat) = var(Diameter);

    end

    Data_varofmean(Range) = var(reshape(Data_mean(1:Range,:), Range *
NRepeats, 1));

    Data_varofvar(Range) = var(reshape(Data_var(1:Range,:), Range *
NRepeats, 1));

end

Ranges = 1:MaxRange;

Figure(1);

plot(Ranges, Data_mean, 'k');

Figure(2);

plot(Ranges, Data_var, 'k');

```

Figure(3);

```
plot(Ranges, Data_varofmean, '-k', Ranges, Data_varofvar, '-r');
```

Two graphs of variance versus number of particles and number-based mean area versus number of the particles are presented in Figures B.1 and B.2. A sample of 821 alkaline coagulated kaolinite flocs were used to produce these graphs. As proved by the graphs the sample was considered large enough to produce a reliable floc size distribution. The variance and mean diameter of the samples are almost constant for subsamples larger than 200 particles.

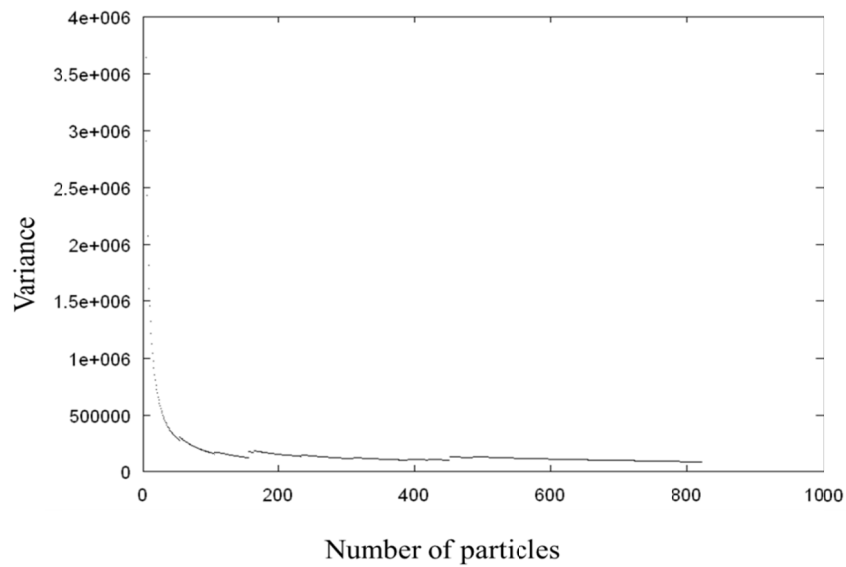


Figure B.1 Changes of the variance with different subsample sizes of kaolinite flocs

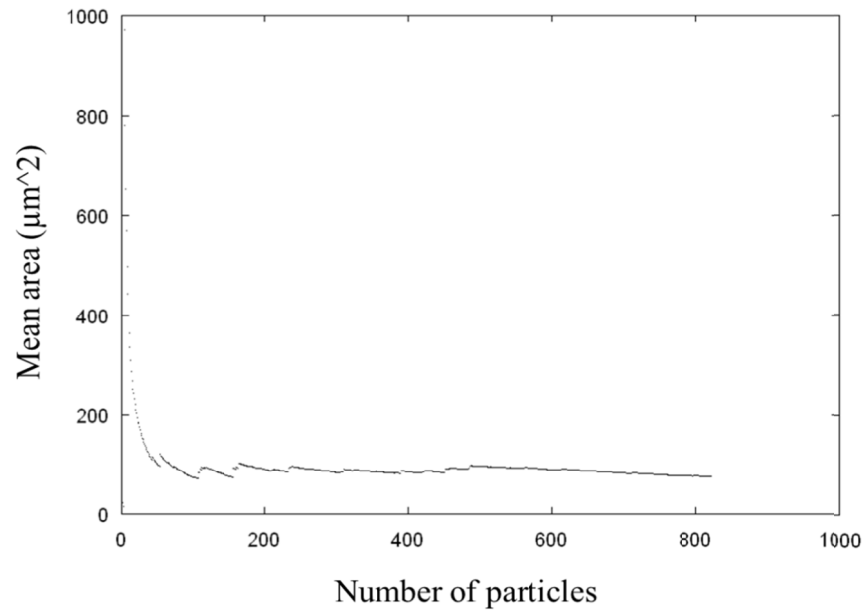


Figure B.2 Changes of the number-based mean diameter with different subsample sizes of kaolinite flocs

Appendix C: Size distribution data used for plotting the graphs in

Chapter 4

Table C.1 Effect of concentration on kaolinite floc size distribution (Figure 4.2)

Particle Size (μm)	Frequency Ratio				
	1 g/L	5 g/L	15 g/L	25 g/L	35 g/L
0.11247	0	0	0	0	0
0.129132	0	0	0	0	0
0.148264	0	0	0	0	0
0.17023	0	0	0	0	0
0.19545	0	0	0	0	0
0.224407	0	0	0	0	0
0.257653	0	0	0	0	0
0.295826	0	0	0	0	0
0.339653	0	0	0	0	0
0.389974	0	0	0	0	0
0.44775	0	0	0	0	0
0.514086	0	0	0	0	0
0.590249	0	0	0	0	0
0.677697	0	0	0	0	0
0.7781	0.076443	0.043292	0.034814	0.033716	0.025873
0.893379	0.073054	0.038842	0.034765	0.032725	0.025988
1.025736	0.103369	0.061478	0.053828	0.049733	0.040266
1.177702	0.084691	0.05304	0.047242	0.045836	0.033485
1.352183	0.095825	0.062387	0.053346	0.052647	0.040082
1.552514	0.097354	0.069771	0.059139	0.056367	0.040828
1.782524	0.089913	0.06662	0.060764	0.055336	0.041394
2.046612	0.077226	0.071884	0.064009	0.057985	0.042928
2.349824	0.068623	0.072983	0.064397	0.059457	0.042269
2.697959	0.058783	0.071166	0.065674	0.05776	0.042799
3.097671	0.043922	0.070229	0.062583	0.054036	0.043721
3.556603	0.035325	0.066712	0.061245	0.050835	0.041028
4.083526	0.026323	0.060079	0.059039	0.046334	0.044555
4.688515	0.020214	0.055039	0.054246	0.044693	0.042954
5.383136	0.013323	0.043694	0.04908	0.041242	0.045026
6.180667	0.011742	0.033519	0.04446	0.038716	0.043321
7.096355	0.006728	0.023087	0.037453	0.037863	0.043074
8.147706	0.006971	0.015721	0.029785	0.033912	0.046144
9.354818	0.003147	0.007473	0.022971	0.030179	0.041047
10.74077	0.002421	0.005301	0.01579	0.028973	0.042164

12.33205	0.001653	0.003533	0.010221	0.023592	0.036107
14.15909	0.000664	0.0014	0.006217	0.019742	0.034303
16.25681	0.000847	0.001023	0.004077	0.015046	0.03052
18.66532	0.000552	0.000603	0.002143	0.011395	0.025529
21.43065	0.000409	0.000416	0.001084	0.008719	0.019599
24.60568	0.000431	0.000165	0.000731	0.005732	0.015665
28.2511	0	0.00019	0.000437	0.003861	0.011504
32.4366	0	9.47E-05	0.000183	0.002165	0.007659
37.2422	0	0.000109	0.000176	0.000939	0.005095
42.75977	0	0.000132	4.61E-05	0.000309	0.003171
49.09478	0	0	4.3E-05	0.000132	0.001467
56.36835	0	0	0	0	0.000379
64.71953	0	0	0	0	2.21E-05
74.30796	0	0	0	0	0
85.31695	0	0	0	0	0
97.95697	0	0	0	0	0

Table C.2 Effect of pH on Kaolinite floc size distribution (Figure 4.9)

Particle Size (μm)	Frequency Ratio		
	Acidic (pH=3)	Alkaline (pH=9)	Natural (pH=4.9)
0.11247	0	0	0
0.129132	0	0	0
0.148264	0	0	0
0.17023	0	0	0
0.19545	0	0	0
0.224407	0	0	0
0.257653	0	0	0
0.295826	0	0	0
0.339653	0	0	0
0.389974	0	0	0
0.44775	0	0	0
0.514086	0	0	0
0.590249	0	0	0
0.677697	0	0	0
0.7781	0.021134	0.079679	0.051568
0.893379	0.020352	0.072053	0.047768
1.025736	0.028264	0.111921	0.074178
1.177702	0.027366	0.091366	0.063417
1.352183	0.033475	0.099668	0.070861

1.552514	0.0394	0.096901	0.078457
1.782524	0.04059	0.088427	0.076388
2.046612	0.047472	0.077497	0.074892
2.349824	0.050373	0.06909	0.076351
2.697959	0.05269	0.055855	0.071831
3.097671	0.057844	0.045139	0.065633
3.556603	0.057851	0.034291	0.062329
4.083526	0.061297	0.024601	0.051009
4.688515	0.060353	0.017697	0.042218
5.383136	0.066157	0.012594	0.030832
6.180667	0.064424	0.008331	0.021593
7.096355	0.069443	0.005315	0.015226
8.147706	0.056034	0.003638	0.008724
9.354818	0.049779	0.002151	0.006327
10.74077	0.036026	0.001406	0.003837
12.33205	0.024569	0.00084	0.00213
14.15909	0.013983	0.000558	0.001968
16.25681	0.008968	0.000294	0.00104
18.66532	0.004889	0.000229	0.000579
21.43065	0.003094	0.000138	0.000377
24.60568	0.002166	0.000129	0.000148
28.2511	0.001306	7.61E-05	0.000163
32.4366	0.000299	2.82E-05	8.6E-05
37.2422	0.000185	6.36E-05	0
42.75977	0.000156	0	0
49.09478	0	0	0
56.36835	0	0	0
64.71953	0	0	0
74.30796	0	0	0
85.31695	0	0	0
97.95697	0	0	0

Table C.3 Effect of coagulant addition on kaolinite floc size distribution (Figure 4.12)

Particle Size (μm)	Frequency Ratio	
	Non-coagulated	Coagulated
0.11247	0	0
0.129132	0	0
0.148264	0	0
0.17023	0	0

0.19545	0	0
0.224407	0	0
0.257653	0	0
0.295826	0	0
0.339653	0	0
0.389974	0	0
0.44775	0	0
0.514086	0	0
0.590249	0	0
0.677697	0	0
0.7781	0.079679	0.021242
0.893379	0.072053	0.02099
1.025736	0.111921	0.035015
1.177702	0.091366	0.031864
1.352183	0.099668	0.040378
1.552514	0.096901	0.045378
1.782524	0.088427	0.049303
2.046612	0.077497	0.056947
2.349824	0.06909	0.065813
2.697959	0.055855	0.069869
3.097671	0.045139	0.075465
3.556603	0.034291	0.070989
4.083526	0.024601	0.069806
4.688515	0.017697	0.068174
5.383136	0.012594	0.061353
6.180667	0.008331	0.050758
7.096355	0.005315	0.043765
8.147706	0.003638	0.035449
9.354818	0.002151	0.028082
10.74077	0.001406	0.022074
12.33205	0.00084	0.015457
14.15909	0.000558	0.0099
16.25681	0.000294	0.005502
18.66532	0.000229	0.002752
21.43065	0.000138	0.001708
24.60568	0.000129	0.000879
28.2511	7.61E-05	0.000714
32.4366	2.82E-05	0.00025
37.2422	6.36E-05	8.04E-05
42.75977	0	0
49.09478	0	0

56.36835	0	0
64.71953	0	0
74.30796	0	0
85.31695	0	0
97.95697	0	0

Table C.4 Effect of mixing time on kaolinite floc size distribution (frequency form of Figure 4.13)

Particle Size (μm)	Frequency Ratio									
	1 min	5 min	10 min	15 min	25 min	45 min	60 min	75 min	90 min	120 min
0.11247	0	0	0	0	0	0	0	0	0	0
0.129132	0	0	0	0	0	0	0	0	0	0
0.148264	0	0	0	0	0	0	0	0	0	0
0.17023	0	0	0	0	0	0	0	0	0	0
0.19545	0	0	0	0	0	0	0	0	0	0
0.224407	0	0	0	0	0	0	0	0	0	0
0.257653	0	0	0	0	0	0	0	0	0	0
0.295826	0	0	0	0	0	0	0	0	0	0
0.339653	0	0	0	0	0	0	0	0	0	0
0.389974	0	0	0	0	0	0	0	0	0	0
0.44775	0	0	0	0	0	0	0	0	0	0
0.514086	0	0	0	0	0	0	0	0	0	0
0.590249	0	0	0	0	0	0	0	0	0	0
0.677697	0	0	0	0	0	0	0	0	0	0
0.7781	0.04 9093	0.04 6441	0.04 3993	0.03 8964	0.03 7309	0.03 4777	0.03 3803	0.03 227	0.03 144 8	0.02 967 6

0.893379	0.04 4733	0.04 2303	0.04 2446	0.03 6998	0.03 4362	0.03 2798	0.03 3896	0.03 118 8	0.02 935 9	0.02 909 6
1.025736	0.07 2932	0.06 9788	0.06 2775	0.05 664	0.05 5184	0.05 0057	0.05 077	0.04 789 8	0.04 612 6	0.04 441 4
1.177702	0.06 3921	0.05 905	0.05 5727	0.04 9691	0.04 7825	0.04 6634	0.04 4969	0.04 380 2	0.04 299 8	0.04 079 4
1.352183	0.07 0864	0.07 0147	0.06 3534	0.05 6696	0.05 4613	0.05 1814	0.05 2514	0.04 828 9	0.05 056 3	0.04 890 3
1.552514	0.07 478	0.07 0982	0.06 4014	0.05 9596	0.05 8384	0.05 883	0.05 5758	0.05 575	0.05 252 8	0.05 290 7
1.782524	0.07 5364	0.07 0934	0.06 5751	0.06 0326	0.06 0644	0.05 8741	0.05 8325	0.05 646 1	0.05 507 4	0.05 492
2.046612	0.07 095	0.06 9926	0.06 5865	0.06 1377	0.06 1353	0.06 0862	0.05 8438	0.05 756 3	0.05 903 7	0.05 616 2
2.349824	0.07 2594	0.06 8033	0.06 3825	0.06 3768	0.06 2766	0.06 1729	0.06 3748	0.05 930 2	0.05 947 6	0.05 755 5
2.697959	0.06 8644	0.06 5073	0.06 1854	0.06 2605	0.06 165	0.06 2039	0.06 4503	0.05 787 8	0.06 179 5	0.06 122 4
3.097671	0.06 0315	0.06 271	0.06 2246	0.05 9945	0.05 9874	0.06 237	0.06 3874	0.05 951 6	0.06 450 5	0.05 973
3.556603	0.05 4632	0.05 6825	0.05 6201	0.05 9307	0.05 6853	0.06 027	0.06 3401	0.05 870 3	0.06 153 2	0.06 239 5
4.083526	0.04 7324	0.05 0718	0.05 2564	0.05 5064	0.05 6153	0.05 7228	0.06 3276	0.05 915 3	0.06 156 2	0.06 087
4.688515	0.04 0621	0.04 4859	0.04 8196	0.05 1532	0.05 3426	0.05 6323	0.05 6754	0.05 528 4	0.06 109 9	0.05 969 7
5.383136	0.03 5163	0.03 8854	0.04 5573	0.04 8879	0.05 0112	0.05 3416	0.05 1421	0.05 637 7	0.05 665 5	0.05 583 1
6.180667	0.02 886	0.03 2788	0.03 7277	0.04 4007	0.04 5943	0.04 8122	0.04 7891	0.05 224 8	0.04 936 5	0.05 497 7
7.096355	0.02 1755	0.02 4391	0.03 1361	0.03 7416	0.03 9028	0.04 1433	0.03 9698	0.04 583 1	0.04 298 5	0.04 728 1
8.147706	0.01 4662	0.01 8795	0.02 3514	0.03 0528	0.03 3076	0.03 4459	0.03 1682	0.03 684	0.03 627	0.03 885

								2	4	2
9.354818	0.01 0211	0.01 31	0.01 9016	0.02 3099	0.02 5601	0.02 4404	0.02 2428	0.03 053	0.02 721 1	0.03 076 4
10.74077	0.00 7288	0.00 7843	0.01 3344	0.01 5946	0.01 6756	0.01 7702	0.01 6276	0.02 219 6	0.01 954 8	0.02 012 3
12.33205	0.00 5416	0.00 6165	0.00 8554	0.01 1839	0.01 177	0.01 0528	0.01 0703	0.01 406 1	0.01 241 2	0.01 496 9
14.15909	0.00 3301	0.00 3614	0.00 4468	0.00 6805	0.00 7596	0.00 6717	0.00 6673	0.00 848 2	0.00 814 8	0.00 905 5
16.25681	0.00 2239	0.00 2722	0.00 2741	0.00 356	0.00 4065	0.00 3644	0.00 3767	0.00 524 5	0.00 451	0.00 462 1
18.66532	0.00 1485	0.00 1198	0.00 245	0.00 2554	0.00 2225	0.00 231	0.00 2487	0.00 278	0.00 277 5	0.00 238 1
21.43065	0.00 0864	0.00 1223	0.00 1027	0.00 1097	0.00 1537	0.00 156	0.00 1232	0.00 119 4	0.00 125 5	0.00 137 3
24.60568	0.00 0822	0.00 0488	0.00 0533	0.00 0574	0.00 0924	0.00 0647	0.00 0652	0.00 059 4	0.00 075 3	0.00 095 8
28.2511	0.00 0508	0.00 0503	0.00 0654	0.00 061	0.00 0417	0.00 0296	0.00 0575	0.00 032 5	0.00 057	0.00 022 1
32.4366	0.00 0379	0.00 023	0.00 0206	0.00 037	0.00 0208	0.00 0195	0.00 0329	0.00 015 6	0.00 030 3	0.00 015
37.2422	0.00 0159	0.00 0168	0.00 0228	0.00 0123	0.00 0313	6.93 E-05	4.6E- 05	0	8.32 E- 05	0
42.75977	0	8.39 E-05	3.47 E-05	0	0	0	5.81 E-05	0	4.14 E- 05	0
49.09478	0	3.36 E-05	2.64 E-05	0	0	0	5.23 E-05	0	0	0
56.36835	0	0	0	0	0	0	0	0	0	0
64.71953	0	0	0	0	0	0	0	0	0	0
74.30796	0	0	0	0	0	0	0	0	0	0
85.31695	0	0	0	0	0	0	0	0	0	0

97.95697	0	0	0	0	0	0	0	0	0	0
----------	---	---	---	---	---	---	---	---	---	---

Table C.5 Effect of FPIA mixing speed on kaolinite floc size distribution (Figure 4.16)

Particle Size (μm)	Frequency Ratio				
	50 RPM	150 RPM	300 RPM	500 RPM	750 RPM
0.11247	0	0	0	0	0
0.129132	0	0	0	0	0
0.148264	0	0	0	0	0
0.17023	0	0	0	0	0
0.19545	0	0	0	0	0
0.224407	0	0	0	0	0
0.257653	0	0	0	0	0
0.295826	0	0	0	0	0
0.339653	0	0	0	0	0
0.389974	0	0	0	0	0
0.44775	0	0	0	0	0
0.514086	0	0	0	0	0
0.590249	0	0	0	0	0
0.677697	0	0	0	0	0
0.7781	0.049679	0.050039	0.046908	0.050072	0.049648
0.893379	0.045825	0.047748	0.045716	0.044966	0.046917
1.025736	0.072159	0.075527	0.073052	0.06954	0.073635
1.177702	0.062266	0.063706	0.063552	0.063254	0.064307
1.352183	0.073904	0.06979	0.070799	0.070995	0.071257
1.552514	0.075889	0.076077	0.077538	0.075572	0.077321
1.782524	0.070426	0.071413	0.074578	0.071604	0.070207
2.046612	0.073411	0.072279	0.07381	0.074367	0.070549
2.349824	0.069085	0.072896	0.070462	0.074016	0.069339
2.697959	0.066986	0.067914	0.06977	0.073034	0.064726
3.097671	0.062822	0.062837	0.066582	0.066453	0.062744
3.556603	0.057352	0.05575	0.062584	0.058644	0.055138
4.083526	0.051941	0.051418	0.050925	0.052557	0.052542
4.688515	0.043582	0.044508	0.045534	0.046052	0.04499
5.383136	0.037101	0.033216	0.034316	0.035922	0.039318
6.180667	0.030176	0.029372	0.025791	0.026697	0.030623
7.096355	0.019645	0.021	0.017891	0.017845	0.019907
8.147706	0.014335	0.01381	0.011807	0.010914	0.014953
9.354818	0.009036	0.007672	0.006564	0.006489	0.008472
10.74077	0.005224	0.004852	0.004714	0.004325	0.00529

12.33205	0.002956	0.00323	0.002614	0.002839	0.002461
14.15909	0.002313	0.001773	0.001796	0.001545	0.001973
16.25681	0.001341	0.001077	0.000828	0.001056	0.001441
18.66532	0.000925	0.000687	0.000651	0.00034	0.000862
21.43065	0.000517	0.000313	0.000478	0.000379	0.000407
24.60568	0.000494	0.000447	0.000384	0.000231	0.000334
28.2511	0.000212	0.000289	0.000155	9.49E-05	0.000233
32.4366	0.0003	0.00017	0.000127	6.44E-05	0.000226
37.2422	6.89E-05	2.87E-05	4.69E-05	4.12E-05	0.000119
42.75977	1.72E-05	7.24E-05	0	1.59E-05	0
49.09478	0	5.71E-05	0	5.93E-05	0
56.36835	0	2.04E-05	0	1.43E-05	0
64.71953	0	0	0	0	0
74.30796	0	0	0	0	0
85.31695	0	0	0	0	0
97.95697	0	0	0	0	0

Table C.6 Effect of FPIA mixing time on kaolinite floc size distribution (Figure 4.18)

Particle Size (μm)	Frequency Ratio				
	0 sec	30 sec	1 min	5 min	15 min
0.11247	0	0	0	0	0
0.129132	0	0	0	0	0
0.148264	0	0	0	0	0
0.17023	0	0	0	0	0
0.19545	0	0	0	0	0
0.224407	0	0	0	0	0
0.257653	0	0	0	0	0
0.295826	0	0	0	0	0
0.339653	0	0	0	0	0
0.389974	0	0	0	0	0
0.44775	0	0	0	0	0
0.514086	0	0	0	0	0
0.590249	0	0	0	0	0
0.677697	0	0	0	0	0
0.7781	0.048791	0.044166	0.053193	0.049537	0.049042
0.893379	0.044808	0.042486	0.047648	0.045014	0.045496
1.025736	0.070052	0.064564	0.07596	0.067685	0.071536
1.177702	0.061889	0.056239	0.068299	0.060895	0.061754
1.352183	0.073366	0.065924	0.076475	0.067104	0.072571
1.552514	0.075949	0.06927	0.082854	0.075369	0.075611

1.782524	0.072491	0.071383	0.079301	0.070916	0.075656
2.046612	0.072961	0.068906	0.077218	0.070167	0.074861
2.349824	0.070509	0.065727	0.072923	0.068261	0.076525
2.697959	0.068256	0.068196	0.069537	0.063629	0.073973
3.097671	0.063044	0.066429	0.064634	0.06066	0.069455
3.556603	0.061289	0.059403	0.057518	0.056394	0.064316
4.083526	0.053863	0.056104	0.04818	0.051537	0.05835
4.688515	0.043863	0.050761	0.036943	0.048556	0.046803
5.383136	0.03676	0.042182	0.029839	0.042899	0.036757
6.180667	0.028447	0.036532	0.022129	0.033162	0.025151
7.096355	0.020002	0.028218	0.014567	0.025904	0.013134
8.147706	0.013201	0.018094	0.008783	0.018038	0.006398
9.354818	0.00775	0.010837	0.005409	0.011478	0.002
10.74077	0.00433	0.006154	0.003659	0.006682	0.00058
12.33205	0.002993	0.003502	0.001992	0.003635	0
14.15909	0.001893	0.001907	0.001115	0.001524	0
16.25681	0.001519	0.001399	0.000726	0.000713	0
18.66532	0.000698	0.00064	0.000584	0.000229	0
21.43065	0.000665	0.000601	0.000265	0	0
24.60568	0.000365	0.000183	0.000155	0	0
28.2511	0.000108	6.48E-05	6.78E-05	0	0
32.4366	8.32E-05	2.49E-05	2.59E-05	0	0
37.2422	0	7.45E-05	0	0	0
42.75977	0	0	0	0	0
49.09478	0	0	0	0	0
56.36835	0	0	0	0	0
64.71953	0	0	0	0	0
74.30796	0	0	0	0	0
85.31695	0	0	0	0	0
97.95697	0	0	0	0	0

Table C.7 Effect of Mastersizer mixing speed on kaolinite floc size distribution (Figure 4.19)

Particle Size (μm)	Volume (%)			
	400 RPM	1000 RPM	2000 RPM	3000 RPM
0.11247	0	0	0	0
0.129132	0	0	0	0
0.148264	0	0	0	0.046564
0.17023	0	0	0	0.827056

0.19545	0	0	0	1.850026
0.224407	0	0	0	2.460736
0.257653	0	0	0	2.827512
0.295826	0.009419	0.019582	0.00767	2.974553
0.339653	0.24894	0.188422	0.08677	3.008406
0.389974	0.621595	0.57723	0.388617	2.956563
0.44775	1.051819	1.013032	0.82175	2.799919
0.514086	1.468897	1.449315	1.371687	2.575224
0.590249	1.846745	1.84938	2.029623	2.383939
0.677697	2.156718	2.18264	2.757654	2.344834
0.7781	2.415901	2.489899	3.581894	2.576653
0.893379	2.652135	2.826824	4.499564	3.152859
1.025736	2.931611	3.301752	5.566406	4.07364
1.177702	3.321597	4.018298	6.778259	5.18489
1.352183	3.89835	5.085351	8.11341	6.264609
1.552514	4.688547	6.497312	9.390968	7.051264
1.782524	5.67025	8.112264	10.32661	7.4032
2.046612	6.723547	9.569484	10.5649	7.271775
2.349824	7.683174	10.44834	9.901409	6.706421
2.697959	8.367817	10.43795	8.418766	5.79837
3.097671	8.628191	9.479303	6.443047	4.693612
3.556603	8.375772	7.764598	4.376557	3.53297
4.083526	7.616836	5.689213	2.595693	2.452006
4.688515	6.441206	3.659742	1.290998	1.539701
5.383136	5.038136	2.025608	0.519585	0.867658
6.180667	3.592018	0.925417	0.137376	0.442806
7.096355	2.31856	0.306977	0.030785	0.25501
8.147706	1.311023	0.082067	0	0.249936
9.354818	0.635533	0	0	0.355903
10.74077	0.237342	0	0	0.495326
12.33205	0.048322	0	0	0.594675
14.15909	0	0	0	0.615359
16.25681	0	0	0	0.555542
18.66532	0	0	0	0.424334
21.43065	0	0	0	0.307749
24.60568	0	0	0	0.0784
28.2511	0	0	0	0
32.4366	0	0	0	0
37.2422	0	0	0	0
42.75977	0	0	0	0
49.09478	0	0	0	0
56.36835	0	0	0	0

64.71953	0	0	0	0
74.30796	0	0	0	0
85.31695	0	0	0	0
97.95697	0	0	0	0

Table C.8 Effect of dispersing medium in the Mastersizer on kaolinite floc size distribution (Figure 4.22)

Particle size (μm)	Volume (%)	
	Diluted with DI water	Diluted with filtrate
0.11247	0	0
0.129132	0	0
0.148264	0	0
0.17023	0	0
0.19545	0	0
0.224407	0	0
0.257653	0	0
0.295826	0.014206	0
0.339653	0.14205	0.038568
0.389974	0.483849	0.310705
0.44775	0.827651	0.572326
0.514086	1.142123	0.807804
0.590249	1.396484	0.995824
0.677697	1.562731	1.110274
0.7781	1.659517	1.15285
0.893379	1.717769	1.129267
1.025736	1.796907	1.060918
1.177702	1.965253	0.980122
1.352183	2.301805	0.922667
1.552514	2.868284	0.927316
1.782524	3.707682	1.032388
2.046612	4.794061	1.278209
2.349824	6.043942	1.711851
2.697959	7.303065	2.375199
3.097671	8.374192	3.284757
3.556603	9.057571	4.416905
4.083526	9.194058	5.681951
4.688515	8.719712	6.960591
5.383136	7.692928	8.068443
6.180667	6.256417	8.848668
7.096355	4.666761	9.143899

8.147706	3.125695	8.88182
9.354818	1.856362	8.083107
10.74077	0.918573	6.828439
12.33205	0.354409	5.334778
14.15909	0.055943	3.773428
16.25681	0	2.385993
18.66532	0	1.273528
21.43065	0	0.542772
24.60568	0	0.084634
28.2511	0	0
32.4366	0	0
37.2422	0	0
42.75977	0	0
49.09478	0	0
56.36835	0	0
64.71953	0	0
74.30796	0	0
85.31695	0	0
97.95697	0	0

Table C.9 Effect of dilution on kaolinite floc size distribution measured using the FPIA (Figure 4.24)

Particle Size (μm)	Frequency Ratio	
	Not diluted	Diluted
0.11247	0	0
0.129132	0	0
0.148264	0	0
0.17023	0	0
0.19545	0	0
0.224407	0	0
0.257653	0	0
0.295826	0	0
0.339653	0	0
0.389974	0	0
0.44775	0	0
0.514086	0	0
0.590249	0	0
0.677697	0	0
0.7781	0.052682	0.084109
0.893379	0.053599	0.085033

1.025736	0.077113	0.117965
1.177702	0.068443	0.101059
1.352183	0.07547	0.104805
1.552514	0.079751	0.10831
1.782524	0.079359	0.095192
2.046612	0.078928	0.088844
2.349824	0.074522	0.067304
2.697959	0.072059	0.054284
3.097671	0.064497	0.036666
3.556603	0.054684	0.025995
4.083526	0.045252	0.014866
4.688515	0.035242	0.007925
5.383136	0.027897	0.005017
6.180667	0.021087	0.001859
7.096355	0.014213	0.00045
8.147706	0.0099	9.02E-05
9.354818	0.006306	4.94E-05
10.74077	0.003984	5.77E-05
12.33205	0.002385	9.05E-05
14.15909	0.001251	0
16.25681	0.000719	0
18.66532	0.000358	0
21.43065	0.000174	0
24.60568	9.49E-05	0
28.2511	0	0
32.4366	0	0
37.2422	0	0
42.75977	0	0
49.09478	0	0
56.36835	0	0
64.71953	0	0
74.30796	0	0
85.31695	0	0
97.95697	0	0

Appendix D: Size distribution data used for plotting the graphs in Chapter 5

Table D.1 Repeatability of FPIA measurements for latex particles (Figure 5.1)

Particle Size (μm)	Cumulative Frequency Ratio		
	Sample 1	Sample 2	Sample 3
1.0095	0	0	0
1.0365	0	0	0
1.0645	0	0	0
1.0935	0	0	0
1.1225	0	0	0
1.1525	0	0	0
1.1835	0	0	0
1.215	0	0	0
1.248	0	0	0
1.282	0	0	0
1.316	0	0	0
1.351	0	0	0
1.3875	0	0	0
1.425	0	0	0
1.4635	0	0	0
1.5025	0	0	0
1.5425	0	0	0
1.584	0	0.0001	0
1.6265	0	0.0001	0
1.6705	0	0.0001	0
1.7155	0	0.0001	0.0001
1.7615	0.0001	0.0001	0.0001
1.809	0.0002	0.0002	0.0002
1.8575	0.0005	0.0005	0.0005
1.9075	0.0087	0.0074	0.0083
1.959	0.0582	0.048	0.0552
2.0115	0.339	0.3025	0.3288
2.0655	0.7325	0.701	0.7257
2.121	0.9228	0.9113	0.9211
2.178	0.9581	0.9544	0.9587
2.2365	0.9607	0.9575	0.9616
2.2965	0.9615	0.9583	0.9623
2.358	0.9618	0.9586	0.9625
2.421	0.9619	0.9588	0.9627

2.486	0.9621	0.9591	0.9629
2.553	0.963	0.9598	0.9638
2.622	0.9672	0.964	0.968
2.6925	0.971	0.9679	0.9719
2.7645	0.9721	0.9694	0.9728
2.8385	0.973	0.9706	0.974
2.915	0.9743	0.9718	0.975
2.9935	0.976	0.9737	0.9769
3.074	0.9788	0.9765	0.9794
3.1565	0.9823	0.9798	0.9831
3.241	0.9878	0.9859	0.9886
3.328	0.9948	0.9939	0.9951
3.4175	0.9973	0.997	0.9976
3.5095	0.9977	0.9974	0.9979
3.604	0.9978	0.9976	0.9981
3.701	0.9981	0.9978	0.9984
3.8	0.9983	0.9981	0.9985
3.902	0.9986	0.9983	0.9988
4.007	0.9988	0.9985	0.9989
4.1145	0.999	0.9989	0.9991
4.225	0.9992	0.9992	0.9993
4.3385	0.9994	0.9994	0.9995
4.455	0.9995	0.9996	0.9996
4.575	0.9996	0.9996	0.9996
4.698	0.9996	0.9996	0.9997
4.824	0.9996	0.9997	0.9997
4.9535	0.9997	0.9997	0.9997
5.0865	0.9997	0.9998	0.9998
5.2235	0.9997	0.9998	0.9998
5.364	0.9998	0.9998	0.9998
5.508	0.9998	0.9999	0.9999
5.656	0.9998	0.9999	0.9999
5.808	0.9999	0.9999	0.9999
5.964	0.9999	0.9999	0.9999
6.124	0.9999	0.9999	0.9999
6.2885	0.9999	0.9999	1
6.4575	0.9999	0.9999	1
6.631	0.9999	1	1
6.809	0.9999	1	1
6.992	0.9999	1	1
7.18	1	1	1

7.373	1	1	1
7.571	1	1	1
7.774	1	1	1
7.983	1	1	1
8.1975	1	1	1
8.4175	1	1	1
8.644	1	1	1
8.8765	1	1	1
9.1145	1	1	1
9.3595	1	1	1
9.611	1	1	1
9.869	1	1	1

Table D.2 Repeatability of FPIA measurements for sand particles (Figure 5.2)

Particle Size (μm)	Cumulative Frequency Ratio		
	Sample 1	Sample 2	Sample 3
0.5065	0.0015	0.0016	0.0009
0.52	0.0133	0.0137	0.0128
0.534	0.015	0.0148	0.0134
0.5485	0.0155	0.0151	0.0136
0.5635	0.0807	0.0809	0.0808
0.5785	0.0848	0.0844	0.0848
0.594	0.1177	0.1183	0.1167
0.61	0.1195	0.1194	0.1189
0.6265	0.1198	0.1198	0.1198
0.6435	0.1388	0.1408	0.1395
0.6605	0.1401	0.1418	0.141
0.678	0.1581	0.1592	0.1601
0.6965	0.1592	0.1603	0.1612
0.7155	0.191	0.1925	0.1959
0.7345	0.195	0.1962	0.1995
0.754	0.2084	0.211	0.2124
0.7745	0.2527	0.2575	0.2574
0.7955	0.2543	0.2591	0.2587
0.8165	0.2818	0.2844	0.2839
0.8385	0.2943	0.2968	0.2973
0.861	0.315	0.3188	0.3177
0.884	0.3175	0.3211	0.3193
0.908	0.337	0.3415	0.3394
0.9325	0.3483	0.3507	0.3496

0.9575	0.3801	0.3802	0.3788
0.983	0.3976	0.3967	0.3967
1.0095	0.4103	0.4087	0.4099
1.0365	0.4261	0.4232	0.4246
1.0645	0.4385	0.4354	0.4362
1.0935	0.472	0.4667	0.4695
1.1225	0.4816	0.4751	0.479
1.1525	0.4971	0.4908	0.4946
1.1835	0.5168	0.5122	0.5151
1.215	0.5304	0.5249	0.5275
1.248	0.5505	0.5468	0.5479
1.282	0.5615	0.5581	0.5592
1.316	0.5798	0.5766	0.5743
1.351	0.5956	0.5928	0.5893
1.3875	0.6107	0.6081	0.6032
1.425	0.6271	0.6235	0.6201
1.4635	0.6423	0.6382	0.636
1.5025	0.6564	0.6515	0.6469
1.5425	0.671	0.6698	0.6631
1.584	0.683	0.6807	0.6739
1.6265	0.6989	0.6953	0.6892
1.6705	0.7129	0.7091	0.7021
1.7155	0.7227	0.7205	0.7135
1.7615	0.7367	0.7333	0.73
1.809	0.7478	0.7462	0.742
1.8575	0.7584	0.7565	0.7524
1.9075	0.7716	0.7692	0.7651
1.959	0.7805	0.7784	0.7732
2.0115	0.7898	0.789	0.7837
2.0655	0.7983	0.7994	0.7934
2.121	0.8059	0.8068	0.7994
2.178	0.8156	0.8165	0.8099
2.2365	0.8247	0.8236	0.8176
2.2965	0.8332	0.8324	0.8268
2.358	0.8413	0.839	0.8337
2.421	0.8494	0.8463	0.8427
2.486	0.8557	0.8525	0.8486
2.553	0.8632	0.8595	0.8561
2.622	0.8694	0.8654	0.8637
2.6925	0.8766	0.8727	0.8721
2.7645	0.8832	0.8782	0.8791

2.8385	0.8893	0.8852	0.8865
2.915	0.8952	0.891	0.8933
2.9935	0.9013	0.8965	0.8988
3.074	0.9055	0.9017	0.9036
3.1565	0.9101	0.9059	0.9074
3.241	0.9137	0.9105	0.9125
3.328	0.918	0.9144	0.916
3.4175	0.921	0.9183	0.9198
3.5095	0.9253	0.9224	0.9234
3.604	0.9295	0.9267	0.9267
3.701	0.9332	0.9305	0.9291
3.8	0.9364	0.933	0.9328
3.902	0.9399	0.9357	0.9358
4.007	0.9426	0.9384	0.9389
4.1145	0.9461	0.9422	0.9424
4.225	0.9497	0.9454	0.9459
4.3385	0.9525	0.9485	0.9488
4.455	0.9549	0.951	0.9514
4.575	0.957	0.9536	0.9541
4.698	0.96	0.9563	0.9565
4.824	0.9619	0.9592	0.9588
4.9535	0.9643	0.9615	0.9606
5.0865	0.9667	0.9633	0.963
5.2235	0.9687	0.9658	0.9662
5.364	0.9712	0.9679	0.9686
5.508	0.9733	0.9699	0.97
5.656	0.9751	0.9711	0.9716
5.808	0.9772	0.9729	0.9735
5.964	0.9787	0.9746	0.9752
6.124	0.9801	0.976	0.9769
6.2885	0.9813	0.9771	0.9781
6.4575	0.9825	0.9778	0.9795
6.631	0.9833	0.9795	0.9808
6.809	0.9847	0.9802	0.9821
6.992	0.9858	0.981	0.9841
7.18	0.987	0.9821	0.9854
7.373	0.9883	0.9832	0.986
7.571	0.9895	0.9841	0.9875
7.774	0.99	0.9851	0.9882
7.983	0.991	0.9861	0.9889
8.1975	0.9917	0.9867	0.9895

8.4175	0.9925	0.9878	0.9903
8.644	0.9931	0.9885	0.9915
8.8765	0.9937	0.9889	0.992
9.1145	0.9946	0.9901	0.9927
9.3595	0.9952	0.9906	0.9929
9.611	0.9954	0.9913	0.9933
9.869	0.9959	0.9918	0.9942
10.135	0.996	0.9924	0.9948
10.405	0.9964	0.9932	0.9953
10.685	0.9967	0.9941	0.9961
10.975	0.9971	0.9947	0.9968
11.27	0.9976	0.9951	0.9969
11.57	0.9979	0.9954	0.9973
11.88	0.9984	0.9957	0.9975
12.2	0.9987	0.9959	0.9978
12.525	0.9987	0.9962	0.9979
12.865	0.9989	0.9963	0.9981
13.215	0.999	0.9966	0.9985
13.57	0.999	0.9966	0.9986
13.93	0.9992	0.9972	0.9989
14.3	0.9994	0.9975	0.9992
14.685	0.9995	0.9977	0.9996
15.08	0.9995	0.9981	0.9996
15.485	0.9998	0.9984	0.9996
15.905	0.9998	0.9987	0.9996
16.335	0.9998	0.9988	0.9997
16.77	0.9998	0.9989	0.9998
17.22	0.9998	0.9994	0.9999
17.685	0.9998	0.9994	0.9999
18.16	0.9998	0.9995	0.9999
18.645	0.9999	0.9995	1
19.145	0.9999	0.9996	1
19.66	0.9999	0.9997	1
20.19	0.9999	0.9997	1
20.735	1	0.9997	1
21.29	1	0.9998	1
21.86	1	0.9999	1
22.45	1	1	1
23.055	1	1	1
23.675	1	1	1
24.31	1	1	1

24.96	1	1	1
25.63	1	1	1
26.32	1	1	1
27.03	1	1	1
27.755	1	1	1
28.5	1	1	1
29.265	1	1	1
30.05	1	1	1
30.86	1	1	1
31.69	1	1	1
32.54	1	1	1
33.415	1	1	1
34.31	1	1	1
35.23	1	1	1
36.18	1	1	1
37.15	1	1	1
38.145	1	1	1
39.17	1	1	1
40.225	1	1	1
41.305	1	1	1
42.415	1	1	1
43.555	1	1	1
44.725	1	1	1
45.93	1	1	1
47.165	1	1	1
48.43	1	1	1
49.73	1	1	1
51.065	1	1	1
52.435	1	1	1
53.845	1	1	1
55.29	1	1	1
56.775	1	1	1
58.305	1	1	1
59.87	1	1	1
61.475	1	1	1
63.13	1	1	1
64.825	1	1	1
66.565	1	1	1
68.355	1	1	1
70.19	1	1	1
72.075	1	1	1

74.01	1	1	1
76	1	1	1
78.045	1	1	1
80.14	1	1	1
82.29	1	1	1
84.5	1	1	1
86.77	1	1	1
89.105	1	1	1
91.5	1	1	1
93.955	1	1	1
96.48	1	1	1
99.08	1	1	1

Table D.3 Repeatability of Mastersizer measurements for latex particles (Figure 5.3)

Particle Size (μm)	Cumulative Volume (%)		
	Sample 1	Sample 2	Sample 3
0.11247	0	0	0
0.129132	0	0	0
0.148264	0	0	0
0.17023	0	0	0
0.19545	0	0	0
0.224407	0	0	0
0.257653	0	0	0
0.295826	0	0	0
0.339653	0	0	0
0.389974	0	0	0
0.44775	0	0	0
0.514086	0	0	0
0.590249	0	0	0
0.677697	0	0	0
0.7781	0	0	0
0.893379	0	0	0
1.025736	0.071465	0.072975	0.073217
1.177702	0.739496	0.744067	0.744348
1.352183	4.298476	4.295021	4.293252
1.552514	12.48356	12.45406	12.44814
1.782524	27.9358	27.86101	27.85208
2.046612	47.71301	47.59816	47.59179
2.349824	67.20075	67.07162	67.07266
2.697959	82.57118	82.45802	82.46612

3.097671	92.50478	92.42663	92.43727
3.556603	97.61499	97.57366	97.5821
4.083526	99.56491	99.55074	99.5547
4.688515	99.95074	99.94767	99.94869
5.383136	100	100	100
6.180667	100	100	100
7.096355	100	100	100
8.147706	100	100	100
9.354818	100	100	100
10.74077	100	100	100
12.33205	100	100	100
14.15909	100	100	100
16.25681	100	100	100
18.66532	100	100	100
21.43065	100	100	100
24.60568	100	100	100
28.2511	100	100	100
32.4366	100	100	100
37.2422	100	100	100
42.75977	100	100	100
49.09478	100	100	100
56.36835	100	100	100
64.71953	100	100	100
74.30796	100	100	100
85.31695	100	100	100
97.95697	100	100	100

Table D.4 Repeatability of Mastersizer measurements for sand particles (Figure 5.4)

Particle Size (μm)	Cumulative Volume (%)		
	Sample 1	Sample 2	Sample 3
0.11247	0	0	0
0.129132	0	0	0
0.148264	0	0	0
0.17023	0	0	0
0.19545	0	0	0
0.224407	0	0	0
0.257653	0	0	0
0.295826	0	0	0
0.339653	0	0	0
0.389974	0	0	0

0.44775	0	0	0
0.514086	0	0	0
0.590249	0	0	0
0.677697	0	0	0
0.7781	0	0	0
0.893379	0	0	0
1.025736	0.040585	0.04099	0.041517
1.177702	0.221551	0.223347	0.225636
1.352183	0.691011	0.6949	0.699524
1.552514	1.414012	1.420953	1.428478
1.782524	2.422352	2.433579	2.444456
2.046612	3.701852	3.718708	3.733107
2.349824	5.230314	5.254097	5.271843
2.697959	6.97715	7.008967	7.029607
3.097671	8.911815	8.952486	8.97548
3.556603	11.01009	11.06008	11.08503
4.083526	13.25331	13.31273	13.33953
4.688515	15.63125	15.6998	15.72882
5.383136	18.14047	18.21748	18.24964
6.180667	20.79221	20.87675	20.91357
7.096355	23.60794	23.69894	23.74238
8.147706	26.62411	26.72046	26.77269
9.354818	29.87922	29.97994	30.0428
10.74077	33.42141	33.52568	33.60003
12.33205	37.28731	37.39452	37.47951
14.15909	41.51274	41.62241	41.71479
16.25681	46.1069	46.21846	46.31225
18.66532	51.06166	51.17418	51.26062
21.43065	56.32765	56.43942	56.50791
24.60568	61.82107	61.92923	61.96866
28.2511	67.41577	67.51613	67.51705
32.4366	72.95524	73.04226	72.99907
37.2422	78.26605	78.33346	78.2464
42.75977	83.17662	83.21828	83.09442
49.09478	87.53791	87.54917	87.40196
56.36835	91.24129	91.22036	91.06757
64.71953	94.22556	94.17474	94.03511
74.30796	96.49159	96.41791	96.30696
85.31695	98.08869	98.0035	97.93009
97.95697	99.11272	99.03104	98.99426
112.4696	99.70011	99.63577	99.62782

129.1324	99.93294	99.90555	99.90624
148.2639	100	100	100
170.2297	100	100	100
195.4498	100	100	100
224.4065	100	100	100
257.6531	100	100	100
295.8253	100	100	100
339.6529	100	100	100
389.9737	100	100	100
447.7497	100	100	100
514.0855	100	100	100
590.2491	100	100	100
677.6967	100	100	100
778.0999	100	100	100
893.3782	100	100	100

Table D.5 Repeatability of FPIA measurements for kaolinite flocs (Figure 5.6)

Particle Size (μm)	Frequency Ratio		
	Sample 1	Sample 2	Sample 3
0.11247	0	0	0
0.129132	0	0	0
0.148264	0	0	0
0.17023	0	0	0
0.19545	0	0	0
0.224407	0	0	0
0.257653	0	0	0
0.295826	0	0	0
0.339653	0	0	0
0.389974	0	0	0
0.44775	0	0	0
0.514086	0	0	0
0.590249	0	0	0
0.677697	0	0	0
0.7781	0.021242	0.01759	0.017538
0.893379	0.02099	0.017842	0.018317
1.025736	0.035015	0.029125	0.02771
1.177702	0.031864	0.028639	0.028738
1.352183	0.040378	0.03294	0.033966
1.552514	0.045378	0.040244	0.04118
1.782524	0.049303	0.045945	0.046032

2.046612	0.056947	0.050584	0.050892
2.349824	0.065813	0.059864	0.060344
2.697959	0.069869	0.062765	0.067364
3.097671	0.075465	0.071622	0.070479
3.556603	0.070989	0.073047	0.077147
4.083526	0.069806	0.074806	0.077703
4.688515	0.068174	0.070936	0.073918
5.383136	0.061353	0.066968	0.068513
6.180667	0.050758	0.054957	0.058848
7.096355	0.043765	0.052339	0.047624
8.147706	0.035449	0.045905	0.041136
9.354818	0.028082	0.034235	0.031202
10.74077	0.022074	0.025899	0.02284
12.33205	0.015457	0.016328	0.015851
14.15909	0.0099	0.011538	0.01029
16.25681	0.005502	0.007062	0.005406
18.66532	0.002752	0.003865	0.003475
21.43065	0.001708	0.002564	0.001914
24.60568	0.000879	0.001418	0.000859
28.2511	0.000714	0.000509	0.000514
32.4366	0.00025	0.000255	0
37.2422	8.04E-05	0.000185	0
42.75977	0	0	0
49.09478	0	0	0
56.36835	0	0	0
64.71953	0	0	0
74.30796	0	0	0
85.31695	0	0	0
97.95697	0	0	0

Table D.6 Repeatability of Mastersizer measurements for kaolinite flocs (Figure 5.9)

Particle Size (μm)	Frequency Ratio		
	Sample 1	Sample 2	Sample 3
0.11247	0	0	0
0.129132	0	0	0
0.148264	0	0	0
0.17023	0	0	0
0.19545	0	0	0
0.224407	0	0	0
0.257653	0	0	0

0.295826	0.003308	0.003317	0.003318
0.339653	0.040386	0.040473	0.040488
0.389974	0.111949	0.112012	0.112078
0.44775	0.156161	0.156067	0.156184
0.514086	0.154367	0.154231	0.154354
0.590249	0.131448	0.131334	0.131433
0.677697	0.103408	0.103337	0.103398
0.7781	0.077591	0.077565	0.077583
0.893379	0.05705	0.057058	0.057036
1.025736	0.041986	0.042014	0.041963
1.177702	0.031346	0.031382	0.031313
1.352183	0.023818	0.023854	0.02378
1.552514	0.01826	0.018292	0.018222
1.782524	0.013936	0.013961	0.013903
2.046612	0.010449	0.01047	0.010427
2.349824	0.007647	0.007666	0.007636
2.697959	0.005453	0.005471	0.005451
3.097671	0.003795	0.003812	0.003799
3.556603	0.002585	0.002602	0.002592
4.083526	0.001732	0.001746	0.001738
4.688515	0.001146	0.001157	0.00115
5.383136	0.000753	0.00076	0.000754
6.180667	0.000494	0.000497	0.000491
7.096355	0.000324	0.000325	0.00032
8.147706	0.000213	0.000212	0.000208
9.354818	0.00014	0.000138	0.000135
10.74077	9.17E-05	8.98E-05	8.81E-05
12.33205	6E-05	5.82E-05	5.73E-05
14.15909	3.89E-05	3.75E-05	3.72E-05
16.25681	2.5E-05	2.4E-05	2.4E-05
18.66532	1.58E-05	1.52E-05	1.54E-05
21.43065	9.83E-06	9.5E-06	9.69E-06
24.60568	5.94E-06	5.8E-06	5.96E-06
28.2511	3.46E-06	3.44E-06	3.54E-06
32.4366	1.93E-06	1.96E-06	2.01E-06
37.2422	1.03E-06	1.07E-06	1.08E-06
42.75977	5.17E-07	5.47E-07	5.47E-07
49.09478	2.46E-07	2.6E-07	2.56E-07
56.36835	1.09E-07	1.13E-07	1.09E-07
64.71953	4.52E-08	4.16E-08	3.94E-08
74.30796	1.7E-08	1.05E-08	9.67E-09

85.31695	5.51E-09	1.2E-09	1.09E-09
97.95697	1.58E-09	0	0

Table D.7 Repeatability of microscopy measurements for kaolinite flocs (Figure 5.12)

Particle Size (μm)	Frequency Ratio		
	Sample 1	Sample 2	Sample 3
0.11247	0	0	0
0.129132	0	0	0
0.148264	0	0	0
0.17023	0	0	0
0.19545	0	0	0
0.224407	0	0	0
0.257653	0	0	0
0.295826	0	0	0
0.339653	0	0	0
0.389974	0	0	0
0.44775	9.14E-05	0	0
0.514086	0.000432	0	0
0.590249	0.000496	5.86E-05	0.002882
0.677697	0.000934	0.003144	0.003802
0.7781	0.002705	0.002123	0.017206
0.893379	0.007922	0.01571	0.032164
1.025736	0.03857	0.044418	0.053135
1.177702	0.083681	0.075869	0.064653
1.352183	0.084894	0.089748	0.080004
1.552514	0.093519	0.073818	0.066117
1.782524	0.091099	0.058405	0.056551
2.046612	0.063861	0.064258	0.070147
2.349824	0.054546	0.054946	0.046735
2.697959	0.066483	0.063566	0.058368
3.097671	0.048914	0.056751	0.042977
3.556603	0.034907	0.038512	0.048301
4.083526	0.043903	0.03922	0.041226
4.688515	0.020926	0.031983	0.041098
5.383136	0.01769	0.033311	0.042592
6.180667	0.026977	0.018557	0.036834
7.096355	0.024422	0.032649	0.025316
8.147706	0.021409	0.034147	0.019562
9.354818	0.013666	0.024406	0.017043

10.74077	0.017517	0.022811	0.015702
12.33205	0.01752	0.021575	0.020331
14.15909	0.017768	0.017163	0.010335
16.25681	0.014365	0.010466	0.017695
18.66532	0.014	0.020975	0.014772
21.43065	0.007311	0.014437	0.00721
24.60568	0.006844	0.006982	0.008249
28.2511	0.011742	0.006105	0.012967
32.4366	0.011046	0.005772	0.005871
37.2422	0.012465	0.004473	0.004237
42.75977	0.008815	0.004906	0.003865
49.09478	0.005787	0.005166	0.00703
56.36835	0.005635	0.001013	0
64.71953	0.004724	0.00196	0
74.30796	0.002278	0	0
85.31695	0	0	0
97.95697	0	0	0

Table D.8 Frequency particle size distributions for the 2 μm latex particles obtained using the FPIA and Mastersizer (Figure 5.15)

Particle Size (μm)	Frequency Ratio	
	FPIA	Mastersizer
0.514086	0	0
0.590249	0	0
0.677697	0	0
0.7781	0	0
0.893379	0	0.000601
1.025736	0	0.025255
1.177702	0	0.015428
1.352183	1.05E-05	0.017976
1.552514	0.002664	0.053772
1.782524	0.061366	0.122007
2.046612	0.777423	0.169042
2.349824	0.388853	0.157784
2.697959	0.009468	0.095754
3.097671	0.012821	0.040197
3.556603	0.015754	0.01127
4.083526	0.001754	0.00161
4.688515	0.000415	0.000105
5.383136	0.000186	1.7E-06

6.180667	9.67E-05	0
7.096355	4.3E-05	0
8.147706	2.69E-05	0
9.354818	1.47E-05	0
10.74077	0	0
12.33205	0	0
14.15909	0	0
16.25681	0	0
18.66532	0	0

Table D.9 Frequency particle size distributions for the silica particles obtained using the FPIA and Mastersizer (Figure 5.18)

Particle Size (μm)	Frequency Ratio	
	FPIA	Mastersizer
0.11247	0	0
0.129132	0	0
0.148264	0	0
0.17023	0	0
0.19545	0	0
0.224407	0	0
0.257653	0	0
0.295826	0	0
0.339653	0	0
0.389974	0	0
0.44775	0	0
0.514086	0	0
0.590249	0	0
0.677697	0	0
0.7781	0.068076	0
0.893379	0.054129	0.014298
1.025736	0.104738	0.057212
1.177702	0.08197	0.116126
1.352183	0.096352	0.148732
1.552514	0.101052	0.144245
1.782524	0.08856	0.127305
2.046612	0.07997	0.10394
2.349824	0.076372	0.080493
2.697959	0.061048	0.059975
3.097671	0.050624	0.043498
3.556603	0.037879	0.030979

4.083526	0.027992	0.021801
4.688515	0.020686	0.015238
5.383136	0.015076	0.010629
6.180667	0.011432	0.007435
7.096355	0.007405	0.005235
8.147706	0.005194	0.003716
9.354818	0.003896	0.002658
10.74077	0.002552	0.001912
12.33205	0.002124	0.001378
14.15909	0.001243	0.000992
16.25681	0.000355	0.000709
18.66532	0.000489	0.000501
21.43065	0.000307	0.000349
24.60568	0	0.000237
28.2511	0	0.000158
32.4366	0	0.000102
37.2422	0	6.35E-05
42.75977	0	3.82E-05
49.09478	0	2.21E-05
56.36835	0	1.22E-05
64.71953	0	6.42E-06
74.30796	0	3.18E-06
85.31695	0	1.46E-06
97.95697	0	6.16E-07
112.4696	0	2.25E-07
129.1324	0	6.22E-08
148.2639	0	1.15E-08
170.2297	0	0

Table D.10 Frequency floc size distributions for kaolinite primary flocs obtained using the FPIA and Mastersizer (Figure 5.22)

Particle Size (μm)	Frequency Ratio	
	FPIA	Mastersizer
0.11247	0	0
0.129132	0	0
0.148264	0	0
0.17023	0	0
0.19545	0	0
0.224407	0	0
0.257653	0	0.004634

0.295826	0	0.035938
0.339653	0	0.104054
0.389974	0	0.156978
0.44775	0	0.160401
0.514086	0	0.138866
0.590249	0	0.108253
0.677697	0	0.078437
0.7781	0.084109	0.054505
0.893379	0.085033	0.037422
1.025736	0.117965	0.026306
1.177702	0.101059	0.019529
1.352183	0.104805	0.015501
1.552514	0.10831	0.012961
1.782524	0.095192	0.011071
2.046612	0.088844	0.009357
2.349824	0.067304	0.007658
2.697959	0.054284	0.005985
3.097671	0.036666	0.004432
3.556603	0.025995	0.003093
4.083526	0.014866	0.002024
4.688515	0.007925	0.001237
5.383136	0.005017	0.000702
6.180667	0.001859	0.000367
7.096355	0.00045	0.000175
8.147706	9.02E-05	7.52E-05
9.354818	4.94E-05	2.82E-05
10.74077	5.77E-05	8.78E-06
12.33205	9.05E-05	2E-06
14.15909	0	1.91E-07
16.25681	0	0
18.66532	0	0
21.43065	0	0
24.60568	0	0
28.2511	0	0
32.4366	0	0
37.2422	0	0
42.75977	0	0
49.09478	0	0
56.36835	0	0
64.71953	0	0
74.30796	0	0

85.31695	0	0
97.95697	0	0

Table D.11 Frequency floc size distributions for kaolinite natural flocs obtained using the FPIA and Mastersizer (Figure 5.26)

Particle Size (μm)	Frequency Ratio	
	FPIA	Mastersizer
0.11247	0	0
0.129132	0	0
0.148264	0	0
0.17023	0	0
0.19545	0	0
0.224407	0	0
0.257653	0	0.01244
0.295826	0	0.083407
0.339653	0	0.157883
0.389974	0	0.161107
0.44775	0	0.139533
0.514086	0	0.111527
0.590249	0	0.084685
0.677697	0	0.062137
0.7781	0.063293	0.044896
0.893379	0.058534	0.032443
1.025736	0.08118	0.023856
1.177702	0.089352	0.018079
1.352183	0.097505	0.014205
1.552514	0.085635	0.011512
1.782524	0.07376	0.009505
2.046612	0.09241	0.007867
2.349824	0.090838	0.006437
2.697959	0.061333	0.005148
3.097671	0.04682	0.003996
3.556603	0.043051	0.002996
4.083526	0.044106	0.002165
4.688515	0.018672	0.001507
5.383136	0.020953	0.00101
6.180667	0.014828	0.000653
7.096355	0.012279	0.000408
8.147706	0.001009	0.000247
9.354818	0.00115	0.000146

10.74077	0.001304	8.5E-05
12.33205	0.000406	4.91E-05
14.15909	0.000325	2.86E-05
16.25681	0.000373	1.69E-05
18.66532	0.000428	1.02E-05
21.43065	0	6.28E-06
24.60568	0	3.87E-06
28.2511	0	2.35E-06
32.4366	0	1.39E-06
37.2422	0	7.88E-07
42.75977	0	4.28E-07
49.09478	0	2.22E-07
56.36835	0	1.1E-07
64.71953	0	5.16E-08
74.30796	0	2.26E-08
85.31695	0	8.87E-09
97.95697	0	2.67E-09

Table D.12 Frequency floc size distributions for kaolinite acidic flocs obtained using the FPIA and Mastersizer (Figure 5.30)

Particle Size (μm)	Frequency Ratio	
	FPIA	Mastersizer
0.11247	0	0
0.129132	0	0
0.148264	0	0
0.17023	0	0
0.19545	0	0
0.224407	0	0
0.257653	0	0
0.295826	0	0
0.339653	0	0
0.389974	0	0.088786
0.44775	0	0.200449
0.514086	0	0.196406
0.590249	0	0.159529
0.677697	0	0.118178
0.7781	0.022743	0.081258
0.893379	0.037943	0.053187
1.025736	0.051656	0.033627
1.177702	0.018801	0.020881

1.352183	0.039189	0.012904
1.552514	0.051701	0.008018
1.782524	0.048358	0.005068
2.046612	0.054698	0.003361
2.349824	0.06673	0.002474
2.697959	0.083532	0.002102
3.097671	0.049088	0.001996
3.556603	0.076013	0.001968
4.083526	0.078188	0.001909
4.688515	0.054249	0.001772
5.383136	0.045852	0.00156
6.180667	0.069129	0.001299
7.096355	0.047728	0.001023
8.147706	0.050146	0.000764
9.354818	0.028794	0.000541
10.74077	0.013721	0.000365
12.33205	0.002976	0.000234
14.15909	0.003348	0.000144
16.25681	0.003011	8.52E-05
18.66532	0	4.88E-05
21.43065	0	2.73E-05
24.60568	0	1.51E-05
28.2511	0	8.43E-06
32.4366	0	4.77E-06
37.2422	0	2.77E-06
42.75977	0	1.66E-06
49.09478	0	1.01E-06
56.36835	0	6.16E-07
64.71953	0	3.73E-07
74.30796	0	2.21E-07
85.31695	0	1.27E-07
97.95697	0	7.09E-08

Table D.13 Frequency floc size distributions for kaolinite coagulated alkaline flocs obtained using the FPIA and Mastersizer (Figure 5.34)

Particle Size (μm)	Frequency Ratio	
	FPIA	Mastersizer
0.11247	0	0
0.129132	0	0
0.148264	0	0

0.17023	0	0
0.19545	0	0
0.224407	0	0
0.257653	0	0.007302
0.295826	0	0.051272
0.339653	0	0.114176
0.389974	0	0.140532
0.44775	0	0.135132
0.514086	0	0.118534
0.590249	0	0.098707
0.677697	0	0.079494
0.7781	0.032581	0.062842
0.893379	0.024855	0.049004
1.025736	0.053597	0.037843
1.177702	0.047818	0.028905
1.352183	0.04219	0.021808
1.552514	0.071055	0.016193
1.782524	0.051327	0.011808
2.046612	0.070777	0.008438
2.349824	0.074775	0.005909
2.697959	0.078216	0.004059
3.097671	0.079866	0.002741
3.556603	0.089269	0.001825
4.083526	0.082674	0.001203
4.688515	0.060411	0.000788
5.383136	0.056315	0.000515
6.180667	0.031953	0.000337
7.096355	0.018613	0.000221
8.147706	0.016069	0.000145
9.354818	0.005411	9.51E-05
10.74077	0.005244	6.23E-05
12.33205	0.001806	4.07E-05
14.15909	0.001471	2.64E-05
16.25681	0.000591	1.7E-05
18.66532	0.001036	1.08E-05
21.43065	0.000951	6.79E-06
24.60568	0	4.16E-06
28.2511	0	2.48E-06
32.4366	0	1.42E-06
37.2422	0	7.8E-07
42.75977	0	4.09E-07

49.09478	0	2.04E-07
56.36835	0	9.67E-08
64.71953	0	4.3E-08
74.30796	0	1.79E-08
85.31695	0	6.76E-09
97.95697	0	2.02E-09
112.4696	0	3.53E-10
129.1324	0	0
148.2639	0	0
170.2297	0	0

Table D.14 Frequency FSDs for different types of kaolinite flocs measured using the FPIA (Figure 5.38)

Particle Size (µm)	Frequency Ratio			
	Primary Floc	Natural Flocs	Alkaline Coagulated Flocs	Acidic Flocs
0.11247	0	0	0	0
0.129132	0	0	0	0
0.148264	0	0	0	0
0.17023	0	0	0	0
0.19545	0	0	0	0
0.224407	0	0	0	0
0.257653	0	0	0	0
0.295826	0	0	0	0
0.339653	0	0	0	0
0.389974	0	0	0	0
0.44775	0	0	0	0
0.514086	0	0	0	0
0.590249	0	0	0	0
0.677697	0	0	0	0
0.7781	0.084109	0.063293	0.032581	0.022743
0.893379	0.085033	0.058534	0.024855	0.037943
1.025736	0.117965	0.08118	0.053597	0.051656
1.177702	0.101059	0.089352	0.047818	0.018801
1.352183	0.104805	0.097505	0.04219	0.039189
1.552514	0.10831	0.085635	0.071055	0.051701
1.782524	0.095192	0.07376	0.051327	0.048358
2.046612	0.088844	0.09241	0.070777	0.054698
2.349824	0.067304	0.090838	0.074775	0.06673
2.697959	0.054284	0.061333	0.078216	0.083532

3.097671	0.036666	0.04682	0.079866	0.049088
3.556603	0.025995	0.043051	0.089269	0.076013
4.083526	0.014866	0.044106	0.082674	0.078188
4.688515	0.007925	0.018672	0.060411	0.054249
5.383136	0.005017	0.020953	0.056315	0.045852
6.180667	0.001859	0.014828	0.031953	0.069129
7.096355	0.00045	0.012279	0.018613	0.047728
8.147706	9.02E-05	0.001009	0.016069	0.050146
9.354818	4.94E-05	0.00115	0.005411	0.028794
10.74077	5.77E-05	0.001304	0.005244	0.013721
12.33205	9.05E-05	0.000406	0.001806	0.002976
14.15909	0	0.000325	0.001471	0.003348
16.25681	0	0.000373	0.000591	0.003011
18.66532	0	0.000428	0.001036	0
21.43065	0	0	0.000951	0
24.60568	0	0	0	0
28.2511	0	0	0	0
32.4366	0	0	0	0
37.2422	0	0	0	0
42.75977	0	0	0	0
49.09478	0	0	0	0
56.36835	0	0	0	0
64.71953	0	0	0	0
74.30796	0	0	0	0
85.31695	0	0	0	0
97.95697	0	0	0	0

Table D.15 Frequency FSDs for different types of kaolinite flocs obtained using the Mastersizer (Figure 5.40)

Particle Size (µm)	Frequency Ratio			
	Primary Flocs	Natural Flocs	Alkaline Coagulated Flocs	Acidic Flocs
0.11247	0	0	0	0
0.129132	0	0	0	0
0.148264	0	0	0	0
0.17023	0	0	0	0
0.19545	0	0	0	0
0.224407	0	0	0	0
0.257653	0.004634	0.01244	0.007302	0
0.295826	0.035938	0.083407	0.051272	0

0.339653	0.104054	0.157883	0.114176	0
0.389974	0.156978	0.161107	0.140532	0.088786
0.44775	0.160401	0.139533	0.135132	0.200449
0.514086	0.138866	0.111527	0.118534	0.196406
0.590249	0.108253	0.084685	0.098707	0.159529
0.677697	0.078437	0.062137	0.079494	0.118178
0.7781	0.054505	0.044896	0.062842	0.081258
0.893379	0.037422	0.032443	0.049004	0.053187
1.025736	0.026306	0.023856	0.037843	0.033627
1.177702	0.019529	0.018079	0.028905	0.020881
1.352183	0.015501	0.014205	0.021808	0.012904
1.552514	0.012961	0.011512	0.016193	0.008018
1.782524	0.011071	0.009505	0.011808	0.005068
2.046612	0.009357	0.007867	0.008438	0.003361
2.349824	0.007658	0.006437	0.005909	0.002474
2.697959	0.005985	0.005148	0.004059	0.002102
3.097671	0.004432	0.003996	0.002741	0.001996
3.556603	0.003093	0.002996	0.001825	0.001968
4.083526	0.002024	0.002165	0.001203	0.001909
4.688515	0.001237	0.001507	0.000788	0.001772
5.383136	0.000702	0.00101	0.000515	0.00156
6.180667	0.000367	0.000653	0.000337	0.001299
7.096355	0.000175	0.000408	0.000221	0.001023
8.147706	7.52E-05	0.000247	0.000145	0.000764
9.354818	2.82E-05	0.000146	9.51E-05	0.000541
10.74077	8.78E-06	8.5E-05	6.23E-05	0.000365
12.33205	2E-06	4.91E-05	4.07E-05	0.000234
14.15909	1.91E-07	2.86E-05	2.64E-05	0.000144
16.25681	0	1.69E-05	1.7E-05	8.52E-05
18.66532	0	1.02E-05	1.08E-05	4.88E-05
21.43065	0	6.28E-06	6.79E-06	2.73E-05
24.60568	0	3.87E-06	4.16E-06	1.51E-05
28.2511	0	2.35E-06	2.48E-06	8.43E-06
32.4366	0	1.39E-06	1.42E-06	4.77E-06
37.2422	0	7.88E-07	7.8E-07	2.77E-06
42.75977	0	4.28E-07	4.09E-07	1.66E-06
49.09478	0	2.22E-07	2.04E-07	1.01E-06
56.36835	0	1.1E-07	9.67E-08	6.16E-07
64.71953	0	5.16E-08	4.3E-08	3.73E-07
74.30796	0	2.26E-08	1.79E-08	2.21E-07
85.31695	0	8.87E-09	6.76E-09	1.27E-07

97.95697	0	2.67E-09	2.02E-09	7.09E-08
112.4696	0	4.66E-10	3.53E-10	3.87E-08
129.1324	0	0	0	2.07E-08
148.2639	0	0	0	1.08E-08
170.2297	0	0	0	5.65E-09
195.4499	0	0	0	2.98E-09
224.4065	0	0	0	1.65E-09
257.6531	0	0	0	9.63E-10
295.8253	0	0	0	5.84E-10
339.6529	0	0	0	3.53E-10
389.9737	0	0	0	2.05E-10
447.7497	0	0	0	1.1E-10
514.0855	0	0	0	4.62E-11
590.2491	0	0	0	1E-11
677.6967	0	0	0	0
778.0999	0	0	0	0
893.3782	0	0	0	0

Table D.16 Frequency particle size distributions for the 2 μm latex particles obtained using the FPIA and microscope (Figure 5.42)

Particle Size (μm)	Frequency Ratio	
	FPIA	Microscope
0.514086	0	0
0.590249	0	0
0.677697	0	0
0.7781	0	0
0.893379	0	0
1.025736	0	0
1.177702	0	0
1.352183	1.05E-05	0
1.552514	0.002664	0.001574
1.782524	0.061366	0.108995
2.046612	0.777423	0.786252
2.349824	0.388853	0.102238
2.697959	0.009468	0.00094
3.097671	0.012821	0
3.556603	0.015754	0
4.083526	0.001754	0
4.688515	0.000415	0
5.383136	0.000186	0

6.180667	9.67E-05	0
7.096355	4.3E-05	0
8.147706	2.69E-05	0
9.354818	1.47E-05	0
10.74077	0	0
12.33205	0	0
14.15909	0	0
16.25681	0	0
18.66532	0	0

Table D.17 Frequency particle size distributions for the silica particles obtained using the FPIA and microscope (Figure 5.45)

Particle Size (μm)	Frequency Ratio	
	FPIA	Microscope
0.11247	0	0
0.129132	0	0
0.148264	0	0
0.17023	0	0
0.19545	0	0
0.224407	0	0
0.257653	0	0
0.295826	0	0
0.339653	0	0
0.389974	0	0
0.44775	0	0
0.514086	0	0
0.590249	0	0
0.677697	0	0.005482
0.7781	0.068076	0.025949
0.893379	0.054129	0.088875
1.025736	0.104738	0.133765
1.177702	0.08197	0.148543
1.352183	0.096352	0.129756
1.552514	0.101052	0.09473
1.782524	0.08856	0.066215
2.046612	0.07997	0.06148
2.349824	0.076372	0.051215
2.697959	0.061048	0.043646
3.097671	0.050624	0.029167
3.556603	0.037879	0.021725

4.083526	0.027992	0.024
4.688515	0.020686	0.021224
5.383136	0.015076	0.015963
6.180667	0.011432	0.016108
7.096355	0.007405	0.006118
8.147706	0.005194	0.002902
9.354818	0.003896	0.003719
10.74077	0.002552	0.001982
12.33205	0.002124	0.001042
14.15909	0.001243	0.000706
16.25681	0.000355	0.000515
18.66532	0.000489	0.000891
21.43065	0.000307	0.000837
24.60568	0	0.000657
28.2511	0	0.001187
32.4366	0	0.000613
37.2422	0	0.000377
42.75977	0	0.000416
49.09478	0	0
56.36835	0	0
64.71953	0	0
74.30796	0	0
85.31695	0	0
97.95697	0	0

Table D.18 Frequency floc size distributions for the kaolinite flocs obtained using the FPIA and microscope (Figure 5.49)

Particle Size (μm)	Frequency Ratio	
	FPIA	Microscope
0.11247	0	0
0.129132	0	0
0.148264	0	0
0.17023	0	0
0.19545	0	0
0.224407	0	0
0.257653	0	0
0.295826	0	0
0.339653	0	0
0.389974	0	0
0.44775	0	0

0.514086	0	0
0.590249	0	0.002882
0.677697	0	0.003802
0.7781	0.021242	0.017206
0.893379	0.02099	0.032164
1.025736	0.035015	0.053135
1.177702	0.031864	0.064653
1.352183	0.040378	0.080004
1.552514	0.045378	0.066117
1.782524	0.049303	0.056551
2.046612	0.056947	0.070147
2.349824	0.065813	0.046735
2.697959	0.069869	0.058368
3.097671	0.075465	0.042977
3.556603	0.070989	0.048301
4.083526	0.069806	0.041226
4.688515	0.068174	0.041098
5.383136	0.061353	0.042592
6.180667	0.050758	0.036834
7.096355	0.043765	0.025316
8.147706	0.035449	0.019562
9.354818	0.028082	0.017043
10.74077	0.022074	0.015702
12.33205	0.015457	0.020331
14.15909	0.0099	0.010335
16.25681	0.005502	0.017695
18.66532	0.002752	0.014772
21.43065	0.001708	0.00721
24.60568	0.000879	0.008249
28.2511	0.000714	0.012967
32.4366	0.00025	0.005871
37.2422	8.04E-05	0.004237
42.75977	0	0.003865
49.09478	0	0.00703
56.36835	0	0
64.71953	0	0
74.30796	0	0
85.31695	0	0
97.95697	0	0